Miniaturised Dual Band High Impedance Surfaces

Rola Saad

Department of Electronic and Electrical Engineering
University of Sheffield

A thesis submitted in partial fulfilment of the requirements for the degree of
Doctor of Philosophy

March 2019

To My Adorable Daughters Hayal and Noor

“ Simplicity Is The Ultimate Sophistication ”

— Leonardo da Vinci

Acknowledgements

First, I would like to express my sincere gratitude to my supervisor Dr Lee Ford for his excellent support and outstanding supervision. Thank you for your guidance and advice throughout the course of this research project.

For all the valuable technical support many thanks to Mr Steven Marsden who effortlessly makes every technical problem manageable. Your help and advice was greatly appreciated.

To my second supervisor Prof. Jo Shen Ng, thank you so much for all the valuable discussions and great support throughout every difficulty. Your positivity and encouragement always gave me confidence going forward.

The first person I met at the university who showed me great understanding is Prof. John David. Thank you for your kindness.

To Mrs Hilary Levesley, from administration team, you have a very special place in my heart and I am very thankful for your ultimate support in every difficult moment.

To all my friends and colleagues within communication group, thank you for contributing to a friendly enjoyable workplace.

To my deeply loved grandparents. Loosing you within one year apart was extremely difficult and I wished to thank you where you are still with us. However, you deserve ultimate recognition. Thank you for parenting me with so much love and contributing to everything I am. You are greatly missed. May your souls rest in peace.

To my parents and husband; you are my support system. Thank you for baring with me and your continuous encouragement.

The most heartfelt thank you is to my daughters who hopefully will read this work “ at some point ”. I have missed precious hours of playtime! But no words can describe how grateful I am to be able to complete this research with us as one team. You have been wonderful and amazing. Every single success I have achieved is ours and is dedicated to you both.

Abstract

High Impedance Surface (HIS) is an exclusive type of artificial periodic structure defined as man-made material of peculiar properties not available in nature. HIS has found ultimate applications in the electromagnetic field community due to its unsurpassed distinctive characteristics for its ability to suppress surface waves and exhibit total in-phase reflection. Research has been ongoing for decades to optimize, design and explain the physical properties of such material. Particularly, high impedance surfaces which are electrically small, multifunctional and reliable are essential requirements to accommodate the high demand of modern technology trend towards compact, efficient and multifunctional systems.

This research project is focused on the design and characterization of miniaturised dual band high impedance surfaces with emphasis on inter unit cell mutual coupling. Two miniaturisation methods are discussed where both utilize an uncomplicated approach to realise a dual band system. The first miniaturisation technique incorporates surface mount capacitors and realises significantly miniature HIS. Nevertheless, mutual coupling encountered necessitated attention. Therefore, novel miniaturised gridded HIS has been proposed, which effectively suppressed mutual coupling and demonstrated potential to upgrade into multiband HIS. The second miniaturisation technique implements interdigital capacitors. The original analytical methodology to realise three different miniaturised single band interdigital HIS design prototypes have been discussed. Moreover, upgrading single band interdigital HIS into dual band interdigital HIS is possible provided that mutual coupling is taken into consideration. Therefore, the final part of the thesis discusses a novel methodology to develop robust models that predict the mutual coupling level in advance such that a miniaturised dual band interdigital HIS is realised from single band structures. More precisely, a multiple linear regression technique is employed, therefore, generating mathematical models that calculate percentage frequency displacement encountered as a consequence of mutual coupling. For a generic dual band HIS, regression models are verified in three novel miniaturised dual band interdigital high impedance surfaces, which differ in design complexity and polarization dependency.

List of Publications

Journal Articles

1. R.Saad and K. L. Ford (2012, April). "Miniaturised dual-band artificial magnetic conductor with reduced mutual coupling". In *Electronics Letters*, vol. 48, no. 8, p. 425, 2012.

Conference Publications

1. R.Saad and K. L. Ford (2014, April). "A miniaturised dual band artificial magnetic conductor using interdigital capacitance". In *The 8th European Conference on Antennas and Propagation (EuCAP 2014)*, pp. 25-26, 2014.
2. R.Saad and K. L. Ford (2014, November). "A triple band Artificial Magnetic Conductor surface incorporating a split ring resonator antenna". In *2014 Loughborough Antennas & Propagation Conference (LAPC)*, pp. 717-720, 2014.
3. R.Saad and K. L. Ford (2012, November). "A dual band miniaturised Artificial Magnetic Conductor design methodology". In *2012 Loughborough Antennas & Propagation Conference (LAPC)*, pp. 1-4, 2012.
4. R.Saad and K. L. Ford (2011, November). "A miniaturised dual band Artificial Magnetic Conductor using lumped components". In *2011 Loughborough Antennas & Propagation Conference (LAPC)*, pp. 1-4, 2011.

Table of contents

Abstract **vii**

List of Publications **ix**

List of figures **xvii**

List of tables **xxv**

Nomenclature **xxix**

1 Introduction **1**
- 1.1 General Overview 1
- 1.2 Research Motivation 2
- 1.3 Research Novelty and Contribution 3
- 1.4 Thesis Structure 4

2 Literature Review and Background Theory **7**
- 2.1 Introduction 7
- 2.2 Historical Review – Artificial Periodic Electromagnetic Structures 8
- 2.3 Basic Concepts of High Impedance Surfaces (HIS) 12
  - 2.3.1 HIS for surface wave suppression 13
  - 2.3.2 HIS as a perfect magnetic conductor 15
- 2.4 Miniaturised Multiband High Impedance Surfaces 18
  - 2.4.1 HIS miniaturisation techniques 18
  - 2.4.2 Multiband compact high impedance surfaces 21
  - 2.4.3 Inter-unit cell mutual coupling in dual band HIS 24
- 2.5 Measurement Techniques 25
  - 2.5.1 Antenna return loss measurements 25
  - 2.5.2 Antenna gain measurements 27

2.5.3 NRL Arch reflectivity measurements 28
2.6 Conclusion 29

3 Dual Band High Impedance Surface Miniaturised By Lumped Capacitors 31
3.1 Introduction 31
3.2 Simple Patch Miniaturised HIS 31
3.3 Lumped Component Loaded Dual Band HIS 33
3.4 Parametric Study Lumped Capacitors Dual Band HIS 35
3.4.1 Substrate permittivity (ε_r) effect 36
3.4.2 Component separation distance ($\mathrm{d_c}$) effect 37
3.4.3 Band 1 capacitance ($\mathrm{C_1}$) effect 39
3.4.4 Band 2 capacitance ($\mathrm{C_2}$) effect 41
3.4.5 Periodicity ($\mathrm{P_T}$) effect 43
3.4.6 Substrate thickness (H) effect 45
3.4.7 Comments on inter unit cell mutual coupling 47
3.5 Conclusion 47

4 Dual Band Lumped Capacitor HIS Design Accounting For Mutual Coupling 49
4.1 Introduction 49
4.2 Methodology To Reduce Mutual Coupling 50
4.2.1 Unit cell configuration effect on resonance frequency 51
4.2.2 Mutual coupling analysis comparing HIS 1, HIS 3 and HIS 5 53
4.2.3 Surface current plots comparing HIS 1 and HIS 5 56
4.3 Gridded Miniaturised Dual Band HIS Analysis 58
4.3.1 Guard conductor width (d) effect on resonance frequency 58
4.3.2 Guard conductor width (d) effect on mutual coupling 60
4.4 Gridded Miniaturised Dual Band HIS ECM 63
4.4.1 Conductor width (d) effect 65
4.4.2 Substrate thickness (H) effect 66
4.4.3 Periodicity (P) effect 67
4.5 Gridded Miniaturised HIS Experimental Study 68
4.6 Conclusion 72

5 Single Band Interdigital High Impedance Surface Design Methodology 73
5.1 Introduction 73
5.2 Single Band Interdigital HIS Design 1 Fundamentals 74
5.2.1 Unit cell structure 74

5.2.2 Interdigital capacitance ($\mathrm{C_d}$) 76
5.2.3 Interdigital inductance - approximation 1 79
5.2.4 Interdigital inductance - approximation 2 79
5.2.5 Interdigital inductance - approximation 3 80
5.3 Single Band Interdigital HIS Design 1 Parametric Study 81
5.3.1 Substrate thickness (H) effect 83
5.3.2 Unit cell periodicity (P) effect 84
5.3.3 Substrate permittivity (ε_r) effect 85
5.3.4 Interdigital number of digits ($\mathrm{N_d}$) effect 86
5.3.5 Interdigital digits length (L) effect 87
5.3.6 Interdigital digits gap/width (s = w) effect 88
5.3.7 Interdigital digits gap (s) effect 89
5.3.8 Interdigital digits width (w) effect 90
5.4 Single Band Interdigital HIS Design 1 Verification 91
5.4.1 Optimizing interdigital HIS for effective miniaturisation 91
5.4.2 Experimental verification 93
5.5 Single Band Interdigital HIS Design 2 – Dual Layer Dual Polarized 95
5.6 Single Band Interdigital HIS Design 3 – Single Layer Dual Polarized 97
5.6.1 Unit cell design methodology 97
5.6.2 Equivalent circuit model 98
5.6.3 Interdigital inductance ($\mathrm{L_{d1}}$) design equations 99
5.6.4 Interdigital inductance ($\mathrm{L_{d2}}$) design equations 100
5.6.5 Experimental verification 100
5.7 Conclusion 103

6 Dual Band Interdigital High Impedance Surface - Accounting For Mutual Coupling 105
6.1 Introduction 105
6.2 Interdigital Dual Band HIS Design Methodology 106
6.2.1 Unit cell structure 106
6.2.2 Periodicity limitation 107
6.2.3 Substrate thickness limitation 107
6.2.4 Dual band HIS design procedure summarized 107
6.3 Introduction to Dual Band Mutual Coupling 109
6.3.1 Single band to dual band interdigital HIS 109
6.3.2 Reverse engineered dual band interdigital HIS 116
6.3.3 Summary of design 119

6.4 Dual Band Interdigital HIS Mutual Coupling Analysis 121
  6.4.1 Equivalent circuit model 121
  6.4.2 Substrate permittivity effect 123
  6.4.3 Substrate electrical thickness effect 124
  6.4.4 Unit cell electrical periodicity effect 125
  6.4.5 Unit cell interelement spacing effect 126
  6.4.6 Band separation effect 127
6.5 Conclusion 128

7 Dual band Interdigital High Impedance Surface - Mutual Coupling Model 131
7.1 Introduction 131
7.2 Dual Band Interdigital HIS Generalised Mutual Coupling Model 132
  7.2.1 Stating research question 132
  7.2.2 What is regression analysis ? 135
  7.2.3 Multiple linear regression equation and assumptions 135
  7.2.4 Assessing the quality of linear regression model 137
7.3 Linear Regression In Dual Band Interdigital HIS 139
  7.3.1 Band 1 linear multiple regression model 139
  7.3.2 Band 2 linear multiple regression model 142
7.4 Transformed Regression In Dual Band Interdigital HIS 144
  7.4.1 Band 1 linear-log transformed regression model 145
  7.4.2 Band 2 log-linear transformed regression model 147
7.5 Summary Of Design Methodology 150
7.6 Mutual Coupling Model Verification In Dual Band Interdigital HIS Design . 152
  7.6.1 Interdigital HIS Design 1 - Dual Band Single Layer Single Polarized (DB-SLSP) 152
  7.6.2 Interdigital HIS Design 2 - Dual Band Dual Layer Dual Polarized (DB-DLDP) 155
  7.6.3 Interdigital HIS Design 3 - Dual Band Single Layer Dual Polarized (DB-SLDP) 158
7.7 Conclusion 161

8 Conclusion And Future Work 165
8.1 Research Project Conclusions 165
8.2 Future Work 169

References 171

Appendix A CST Microwave Studio 181
A.1 CST Microwave Studio Concepts 182
A.2 CST Microwave Studio Meshing Technique 183
A.3 Time Domain (TD) Solver 184
A.4 Frequency Domain (FD) Solver 185
A.5 Concluding Remarks 187

Appendix B Single Band Design 2 - Dual Layer Dual Polarized IDC HIS Coupling Model 189
B.1 Equivalent Circuit Model 190
B.2 Top Layer Interdigital Surface Explained 192
B.3 Lower Layer Interdigital Surface Explained 193
B.4 Parametric Analysis 194
B.5 Interlayer Coupling Factor (CF) 195

Appendix C Introduction To Multiple Linear Regression Analysis 197
C.1 Simple Linear Regression 198
C.2 Multiple Linear Regression 199
C.3 Multiple Linear Regression assumptions 199
C.4 Squared Correlation Coefficient - **R Square** 200
C.5 Analysis Of Variance (ANOVA) Table 201

List of figures

2.1 Classifications of artificial periodic electromagnetic structures. 8
2.2 Mushroom type High Impedance Surface (HIS) model. 12
2.3 Analytical dispersion diagram for mushroom-type HIS. Effective capacitance and inductance 0.03 pF and 2 nH respectively. 13
2.4 Illustrated electromagnetic wave propagation for antenna supported by a Perfect Electric Conductor (PEC) ground plane as compared to a High Impedance Surface (HIS). 15
2.5 Phase of reflection coefficient for a high impedance surface versus frequency. 16
2.6 Return loss 1-port measurement setup. 26
2.7 Gain pattern measurement setup. 27
2.8 NRL Arch reflectivity measurement setup at normal incidence. 28

3.1 Capacitive Patch HIS loaded with lumped capacitor. 31
3.2 Dual band miniaturised HIS using lumped surface mount capacitors. 33
3.3 Lumped capacitor loaded dual band miniaturised HIS simulated reflection phase. Design optimized for reduced periodicity. Unit cell parameters detailed in Table 3.1. 35
3.4 Simulated reflection phase of lumped capacitor loaded dual band HIS. Parametric study on permittivity (ε_r). Unit cell parameters are fixed as of Ref. Design, Table 3.2. 37
3.5 Simulated reflection phase of lumped capacitor loaded dual band HIS. Parametric study on separation distance ($\mathrm{d_c}$). Unit cell parameters are fixed as of Ref. Design, Table 3.2. 37
3.6 Lower band surface currents. Varying capacitors separation distance ($\mathrm{d_c}$). . 38
3.7 Upper band surface currents. Varying capacitors separation distance ($\mathrm{d_c}$). . 38
3.8 Simulated reflection phase of lumped capacitor loaded dual band HIS. Parametric study on Band 1 capacitor ($\mathrm{C_1}$). Unit cell parameters are fixed as of Ref. Design, Table 3.2. 39

3.9 Band 1 capacitance (C_1) effect on resonance frequency, band separation and fractional bandwidth. Miniaturised dual band HIS dimensions are fixed as in Table 3.2. 40
3.10 Simulated reflection phase of lumped capacitor loaded dual band HIS. Parametric study on Band 2 capacitor (C_2). Unit cell parameters are fixed as of Ref. Design, Table 3.2. 41
3.11 Band 2 capacitance (C_2) effect on resonance frequency, band separation and fractional bandwidth. Miniaturised dual band HIS dimensions are fixed as in Table 3.2. 42
3.12 Simulated reflection phase of lumped capacitor loaded dual band HIS. Parametric study on periodicity (P_T). Unit cell parameters are fixed as of Ref. Design, Table 3.2. 43
3.13 Periodicity (P_T) effect on resonance frequency, band separation and fractional bandwidth. Miniaturised dual band HIS dimensions are fixed as in Table 3.2. 44
3.14 Simulated reflection phase of lumped capacitor loaded dual band HIS. Parametric study on substrate thickness (H). Unit cell parameters are fixed as of Ref. Design, Table 3.2. 45
3.15 Miniaturised dual HIS. Effect of substrate thickness (H) on resonance frequency, band separation and fractional bandwidth. Unit cell parameters are fixed as in Table 3.2. 46
3.16 Surface current amplitude in miniaturised dual band HIS loaded with capacitors. 47

4.1 Lumped component loaded miniaturized dual band HIS designs 1 to 5 are compared. 50
4.2 Simulated reflection phase plots comparing HIS design configurations. . . . 52
4.3 Simulated reflection phase. Lower band capacitance (C_1) is reduced in HIS configurations HIS 1, HIS 3, HIS 5; all are initially designed at 430 MHz and 900 MHz. 54
4.4 Simulated reflection phase. Upper band capacitance (C_2) is increased in HIS configurations HIS 1, HIS 3, HIS 5; all are initially designed at 430 MHz and 900 MHz. 55
4.5 Simulated surface current amplitude for HIS 1 and HIS 5, observed at 430 MHz. 57
4.6 Simulated surface current amplitude for HIS 1 and HIS 5, observed at 900 MHz. 57
4.7 Gridded dual band miniaturised HIS capacitive patch loaded with lumped capacitors. 58

4.8 Simulated reflection phase. Conductor width (d) varied in lumped capacitor loaded gridded dual band HIS. Unit cell parameters and capacitors are fixed as in Table 4.5. 59
4.9 Simulated reflection phase. Lower band capacitance (C_1) is reduced in lumped capacitor loaded gridded dual band HIS while setting conductor width to 0.5 mm and 2 mm. 61
4.10 Simulated reflection phase. Upper band capacitance (C_2) is increased in lumped capacitor loaded gridded dual band HIS while setting conductor width to 0.5 mm and 2 mm. 61
4.11 Surface current amplitude observed at 430 MHz. Conductor width (d) effect in miniaturised dual band gridded capacitive patch HIS. Unit cell design parameters, Table 4.6. 62
4.12 Surface current amplitude observed at 900 MHz. Conductor width (d) effect in miniaturised dual band gridded capacitive patch HIS. Unit cell design parameters, Table 4.6. 63
4.13 Dual band gridded lumped capacitor loaded high impedance surface. 63
4.14 UWB monopole antenna 0.01λ above miniaturised gridded capacitive patch lumped capacitor loaded dual band high impedance surface. 69
4.15 Lower Band, 880 MHz, simulated and measured gain pattern for low profile UWB monopole antenna 0.01λ above dual band lumped capacitor loaded gridded HIS. 70
4.16 Upper Band, 1080 MHz, simulated and measured gain pattern for low profile UWB monopole antenna 0.01λ above dual band lumped capacitor loaded gridded HIS. 71

5.1 Single Band Single Layer Single Polarized Interdigital HIS. 74
5.2 Interdigital capacitance density versus digits width to gap ratio (X_{ws}) as effective permittivity varies ($\varepsilon_{reff} = 1,2,3,4$). Interdigital digits gap (s = 0.1 mm). 77
5.3 Interdigital capacitance density per effective permittivity versus digits width to gap ratio (X_{ws}). Interdigital digits gap varies ($s(mm) = 0.01, 0.02, 0.05, 0.1, 0.5$). 78
5.4 Interdigital capacitance density versus number of digits (N_d). Digits width to gap ratio varied ($X_{ws} = 0.25, 0.5, 1$) at a fixed interdigital digits gap of ($s = 0.1$ mm). 78
5.5 Single band interdigital capacitive surface detailed self inductance structure. 80
5.6 Miniaturised Single Band Single Layer Single Polarized (SB-SLSP) interdigital HIS. 81

5.7 Interdigital HIS substrate thickness (H) effect. 83
5.8 Interdigital HIS periodicity (P) effect. 84
5.9 Interdigital HIS substrate relative permittivity (ε_r) effect. 85
5.10 Interdigital HIS number of digits ($\mathrm{N_d}$) effect. 86
5.11 Interdigital HIS digits length (L) effect. 87
5.12 Interdigital HIS digits gap (s) and width (w) effect where (s = w). 88
5.13 Interdigital HIS digits gap (s) and digits width to gap ratio ($\mathrm{X_{ws}}$) effect. . . 89
5.14 Interdigital HIS digits gap (w) and digits width to gap ratio ($\mathrm{X_{ws}}$) effect. . . 90
5.15 Single band interdigital HIS Design 1. Optimized for reduced periodicity. . 92
5.16 Low profile UWB monopole antenna 3 mm above miniaturised interdigital HIS. 93
5.17 Monopole SB-SLSP IDC HIS system 1550 MHz E H plane radiation pattern. 94
5.18 Single Band Dual Layer Dual Polarized (SB-DLDP) interdigital HIS Design 2. 95
5.19 Single Band Single Layer Dual Polarized (SB-SLDP) interdigital HIS Design 3. 97
5.20 ECM Single Band Single Layer Dual Polarized (SB-SLDP) Interdigital HIS. 98
5.21 Low profile UWB monopole antenna 3 mm above miniaturised SB-SLDP IDC HIS 101
5.22 Monopole – SB-SLDP IDC HIS system 1500 MHz E H plane radiation pattern. 102

6.1 Miniaturised Dual Band Single Layer Single Polarized (DB-SLSP) interdigital HIS. 106
6.2 Design procedure for dual band interdigital HIS conducted through iteration. 108
6.3 Dual band interdigital high impedance surface subunit cells detailed top view. 109
6.4 900 MHz and 1800 MHz single band 300 mm × 300 mm IDC HIS fabricated on 1.6 mm FR4 ($\varepsilon_r = 4.3, \tan\delta = 0.025$), supported by 6 mm Rohacell and backed by a metal. 110
6.5 Reflectivity measurement setup using NRL Arch. 111
6.6 Single band 900 MHz IDC HIS simulated and measured reflection phase. . 112
6.7 Single band 1800 MHz IDC HIS simulated and measured reflection phase. . 112
6.8 900 - 1800 MHz dual band 300 mm × 300 mm IDC HIS fabricated on 1.6 mm FR4 substrate ($\varepsilon_r = 4.3, \tan\delta = 0.025$), supported by 6 mm Rohacell and backed by a metal plate. 113
6.9 Miniaturised 900-1800 MHz dual band interdigital HIS reflection phase. . . 114
6.10 Simulated surface current amplitude in miniaturised dual band interdigital HIS. 114
6.11 Simulated input impedance smith chart of miniaturised 900-1800 MHz interdigital dual band HIS as compared to 900 MHz and 1800 MHz single band interdigital HIS. 115

6.12 Reversed engineered miniaturised 900-1800 MHz dual band interdigital HIS simulated reflection phase plot. Design parameters, Table 6.2 117

6.13 Simulated surface current amplitude in reversed engineered miniaturised dual band interdigital HIS. 118

6.14 Reversed engineered miniaturised 900-1800 MHz dual band interdigital HIS simulated input impedance smith chart. 119

6.15 Design procedure for miniaturised dual band interdigital HIS. Structure is revered engineered though numerically estimating frequency displacement due to mutual coupling. 120

6.16 Miniaturised dual band interdigital high impedance surface model. 121

6.17 dual band interdigital HIS percentage frequency shift versus substrate permittivity. $\varepsilon_r = 1,\ 5,$ and 8 is considered in dual bands separated by 100%. Substrate thickness $0.02\lambda_{\mathrm{N}}$. Unit cell periodicity $0.08\lambda_{\mathrm{N}}$. Interelement spacing to periodicity ratio 0.05. 123

6.18 Dual band interdigital HIS percentage frequency shift versus substrate electrical thickness. Percentage band separation 100%. Permittivity $(\varepsilon_r = 1)$. Unit cell periodicity $0.08\lambda_{\mathrm{N}}$. Interelement spacing to periodicity ratio 0.05. 124

6.19 Dual band interdigital HIS percentage frequency shift versus electrical periodicity. Percentage band separation 100%. Permittivity $(\varepsilon_r = 5)$. Interelement spacing to periodicity ratio 0.05. Electrical substrate thickness $0.02\lambda_{\mathrm{N}}$. . . . 125

6.20 Dual band interdigital HIS percentage frequency shift versus interelement spacing to periodicity ratio. Percentage band separation 100%. Permittivity $(\varepsilon_r = 5)$. Electrical periodicity $0.08\lambda_{\mathrm{N}}$. Electrical substrate thickness $0.02\lambda_{\mathrm{N}}$. 126

6.21 Dual band interdigital HIS percentage frequency shift versus percentage band separation. Substrate permittivity $(\varepsilon_r = 5)$. Electrical substrate thickness $0.02\lambda_{\mathrm{N}}$. Electrical periodicity $0.08\lambda_{\mathrm{N}}$. Interelement spacing to periodicity ratio 0.05. 127

7.1 Dual band IDC HIS lower band (Band 1) percentage frequency shift versus electrical substrate thickness and periodicity. Fixed, $\frac{\mathrm{S_g}}{\mathrm{P_T}} = 0.05$, %BandSep = 100% and $\varepsilon_r = 1$. 133

7.2 Dual band IDC HIS lower band (Band 2) percentage frequency shift versus electrical substrate thickness and periodicity. Fixed, $\frac{\mathrm{S_g}}{\mathrm{P_T}} = 0.05$, %BandSep = 100% and $\varepsilon_r = 1$. 133

7.3 Band 1 linear regression model standardized residuals normality diagnostics. 141

7.4 Band 2 linear regression model standardized residuals normality diagnostics. 144

7.5 Band 1 percentage frequency shift standardized residuals normality diagnostics linear-log model plots as compared to linear-linear model. 145
7.6 Band 2 percentage frequency shift regression standardized residuals normality diagnostics log-linear model plots as compared to linear-linear model. . 149
7.7 Design procedure for miniaturised dual band interdigital HIS predicting inter unit cell mutual coupling level using multiple linear regression models. . . . 151
7.8 Miniaturised Dual Band Single Layer Single Polarized (DB-SLSP) interdigital HIS. 152
7.9 Manufactured miniaturised interdigital dual band HIS Design 1 operating at 1500 MHz and 2500 MHz. 154
7.10 NRL Arch normal incidence reflectivity measurement setup featuring manufactured Design 1 DB-SLSP interdigital HIS operated at 1500 MHz and 2500 MHz. 154
7.11 Simulated and measured reflection phase for miniaturised DB-SLSP interdigital HIS (Design 1). Unit cell design parameters,Table 7.13. 155
7.12 Miniaturised interdigital HIS Design 2 - Dual Band Dual Layer Dual Polarized (DB-DLDP) 3D prospective view. 156
7.13 Simulated reflection phase for miniaturised Dual Band Dual Layer Dual Polarized (DB-DLDP) interdigital HIS (Design 2). Unit cell parameters, Table 7.14. 158
7.14 Miniaturised interdigital HIS Design 3 - Dual Band Single Layer Dual Polarized (DB-SLDP) top view model. 159
7.15 Simulated reflection phase for miniaturised Dual Band Single Layer Dual Polarized (DB-SLDP) interdigital HIS (Design 3). Unit cell parameters, Table 7.15. 161

A.1 Overview of Computer Simulation Technology (CST) software. 181
A.2 Time Domain (TD) and Frequency Domain (FD) solvers suitability. 182
A.3 CST Suite supported mesh types. 183
A.4 Transient Solver Accuracy Checks. 184
A.5 Frequency Domain Solver Accuracy Checks. 186

B.1 Single Band Dual Layer Dual Polarized (SB-DLDP) Interdigital HIS. . . . 189
B.2 Simulated reflection phase plot for SB-DLDP interdigital HIS observed at E_1 and E_2 polarizations and compared at dielectric separation thickness ($H_d = 0.1$ mm , 1.6 mm). 194
B.3 Interlayer coupling factor as function of varying dielectric thickness (H_d). . 196

C.1 Simple linear regression model best fit line. 198

List of tables

2.1 Thesis Miniaturised Single Band HIS Designs Compared to Literature . . . 20
2.2 Thesis Miniaturised Dual Band HIS Designs Compared to Literature 23

3.1 430-900 MHz Miniaturised HIS Optimized For Reduced Periodicity 34
3.2 Dual Band Lumped Capacitor Loaded HIS - Reference Design 36

4.1 Dual Band Miniaturised Lumped Capacitor Loaded HIS 1 51
4.2 Miniaturised HIS 1, HIS 3, and HIS 5 Designed to Operate at 430-900 MHz 53
4.3 Band Separation Achieved When Band 1 Lumped Capacitor C_1 Is Reduced Comparing HIS Configurations HIS 1, HIS 3 And HIS 5 56
4.4 Band Separation Achieved When Band 1 Lumped Capacitor C_2 Is Reduced Comparing HIS Configurations HIS 1, HIS 3 And HIS 5 56
4.5 430-900 MHz Original Design Miniaturised Gridded Capacitive Patch HIS 58
4.6 430-900 MHz Miniaturised Gridded HIS Designed At Different Conductor Width 60
4.7 Conductor Width $(\mathbf{d})$ Effect – Circuit Model Elements. Gridded Miniaturised Dual Band HIS - Unit Cell: FR4 $(\varepsilon_r = 4.3, \tan\delta = 0.025)$ $\mathbf{H} = 6.4$ mm P = 15 mm $\mathbf{S_g} = 3$ mm $\mathbf{C}_1 = 48$ pF $\mathbf{C}_2 = 10.5$ pF 66
4.8 Conductor Width $(\mathbf{d})$ Effect – Resonance Frequency. Gridded Miniaturised Dual Band HIS - Unit Cell: FR4 $(\varepsilon_r = 4.3, \tan\delta = 0.025)$ $\mathbf{H} = 6.4$ mm P = 15 mm $\mathbf{S_g} = 3$ mm $\mathbf{C}_1 = 48$ pF $\mathbf{C}_2 = 10.5$ pF 66
4.9 Substrate Thickness $(\mathbf{H})$ Effect – Circuit Model Elements. Gridded Miniaturised Dual Band HIS - Unit Cell: FR4 $(\varepsilon_r = 4.3, \tan\delta = 0.025)$ P = 15 mm $\mathbf{S_g} = 3$ mm $\mathbf{d} = 1$ mm $\mathbf{g} = 1$ mm $\mathbf{C}_1 = 48$ pF $\mathbf{C}_2 = 10.5$ pF $\mathbf{C_p} = 0.53$ pF 67

4.10 Substrate Thickness (**H**) Effect – Resonance Frequency. Gridded Miniaturised Dual Band HIS - Unit Cell: FR4 ($\varepsilon_r = 4.3, \tan\delta = 0.025$) P = 15 mm $\mathbf{S_g} = 3$ mm $\mathbf{d} = 1$ mm $\mathbf{g} = 1$ mm $\mathbf{L_D} = 0.7$ nH $\mathbf{L_C} = 7.1$ nH $\mathbf{C_p} = 0.53$ pF $\mathbf{C}_1 = 48$ pF $\mathbf{C}_2 = 10.5$ pF 67
4.11 Periodicity (**P**) Effect – Resonance Frequency. Gridded Miniaturised Dual Band HIS - Unit Cell: FR4 ($\varepsilon_r = 4.3, \tan\delta = 0.025$) $\mathbf{H} = 6.4$ mm $\mathbf{C}_1 = 48$ pF $\mathbf{C}_2 = 10.5$ pF 68
4.12 Periodicity (**P**) Effect – Circuit Model Elements. Gridded Miniaturised Dual Band HIS - Unit Cell: FR4 ($\varepsilon_r = 4.3, \tan\delta = 0.025$) $\mathbf{H} = 6.4$ mm $\mathbf{C}_1 = 48$ pF $\mathbf{C}_2 = 10.5$ pF 68

5.1 Reference Design 960 MHz SB-SLSP Interdigital HIS Design 1 82
5.2 Interdigital HIS Substrate Thickness Effect - Unit Cell: FR4 ($\varepsilon_r = 4.3, \tan\delta = 0.025$) $\mathbf{P} = 12.5$ mm $\mathbf{S_g} = 1$ mm $\mathbf{W_p} = 11.5$ mm $\mathbf{L} = 11$ mm $\mathbf{N_d} = 12$ $\mathbf{s} = \mathbf{w} = 0.5$ mm 83
5.3 Interdigital HIS Periodicity Effect - Unit Cell: FR4 ($\varepsilon_r = 4.3, \tan\delta = 0.025$) $\mathbf{H} = 6.4$ mm $\mathbf{S_g} = 1$ mm $\mathbf{W_p} = 11.5$ mm $\mathbf{L} = 11$ mm $\mathbf{N_d} = 12$ $\mathbf{s} = \mathbf{w} = 0.5$ mm . 84
5.4 Interdigital HIS Substrate Relative Permittivity Effect - Unit Cell: $\mathbf{P} = 12.5$ mm $\mathbf{H} = 6.4$ mm $\mathbf{S_g} = 1$ mm $\mathbf{W_p} = 11.5$ mm $\mathbf{L} = 11$ mm $\mathbf{N_d} = 12$ $\mathbf{s} = \mathbf{w} = 0.5$ mm 85
5.5 Interdigital HIS Number of Digits Effect - Unit Cell: FR4 ($\varepsilon_r = 4.3, \tan\delta = 0.025$) $\mathbf{P} = 12.5$ mm $\mathbf{H} = 6.4$ mm $\mathbf{S_g} = 1$ mm $\mathbf{L} = 11$ mm $\mathbf{s} = \mathbf{w} = 0.5$ mm 86
5.6 Interdigital HIS Digits Length Effect-Unit Cell: FR4 ($\varepsilon_r = 4.3, \tan\delta = 0.025$) $\mathbf{P} = 12.5$ mm $\mathbf{H} = 6.4$ mm $\mathbf{S_g} = 1$ mm $\mathbf{W_p} = 11.5$ mm $\mathbf{N}_\mathrm{d} = 12$ $\mathbf{s} = \mathbf{w} = 0.5$ mm 87
5.7 Interdigital HIS Digits Gap and Width Effect at ($\mathrm{X_{ws}} = 1$) - Unit Cell: FR4 ($\varepsilon_r = 4.3, \tan\delta = 0.025$) $\mathbf{P} = 12.5$ mm $\mathbf{H} = 6.4$ mm $\mathbf{S_g} = 1$ mm $\mathbf{N}_\mathrm{d} = 12$ $\mathbf{L} = 11$ mm 88
5.8 Interdigital HIS Digits Gap Effect - Unit Cell: FR4 ($\varepsilon_r = 4.3, \tan\delta = 0.025$) $\mathbf{P} = 12.5$ mm $\mathbf{H} = 6.4$ mm $\mathbf{S_g} = 1$ mm $\mathbf{N}_\mathrm{d} = 12$ $\mathbf{L} = 11$ mm $\mathbf{w} = 0.5$ mm 89
5.9 Interdigital HIS Digits Width Effect - Unit Cell: FR4 ($\varepsilon_r = 4.3, \tan\delta = 0.025$) $\mathbf{P} = 12.5$ mm $\mathbf{H} = 6.4$ mm $\mathbf{S_g} = 1$ mm $\mathbf{N}_\mathrm{d} = 12$ $\mathbf{L} = 11$ mm $\mathbf{s} = 0.5$ mm 90
5.10 Interdigital Single Band HIS Design 1 Unit Cell and ECM Parameters. Modelled on 6.4 mm FR4 ($\varepsilon_r = 4.3, \tan\delta = 0.025$). 1550 MHz Optimized For Reduced Periodicity. 91

5.11 Single Band Dual Layer Dual Polarized (SB-DLDP) Interdigital HIS Design 2 – 900 MHz Prototype Optimized at 0.8 mm FR4, 6.8 mm Rohacell, P = 12.5 mm, $S_g = 1$ mm 96
5.12 SB-SLDP Interdigital HIS Design 3 Operated at 1500 MHz – Unit Cell and Circuit Parameters as Modelled on 6.4 mm FR4 $(\varepsilon_r = 4.3, \tan\delta = 0.025)$. 101

6.1 Dual Band Interdigital HIS Subunit Cell Design Parameters 109
6.2 Revered Engineer Dual Band Interdigital HIS Subunit Cell Design Parameters 116

7.1 Band 1 Linear Multiple Regression - Model Summary 140
7.2 Band 1 Linear Regression Model - ANOVA 140
7.3 Band 1 Linear Regression Model - Coefficients 141
7.4 Band 2 Linear Multiple Regression - Model Summary 142
7.5 Band 2 Linear Regression Model - ANOVA 142
7.6 Band 2 Linear Regression Model - Coefficients 143
7.7 Band 1 Linear-Log Multiple Regression - Model Summary 146
7.8 Band 1 Linear-Log Regression Model - ANOVA 146
7.9 Band 1 Linear-Log Regression Model - Coefficients 147
7.10 Band 2 Log-Linear Multiple Regression - Model Summary 148
7.11 Band 2 Log-Linear Regression Model - ANOVA 148
7.12 Band 2 Log-Linear Regression Model - Coefficients 150
7.13 Design 1 Dual Band Single Layer Single Polarized (DB-SLSP) Interdigital HIS Unit Cell and Equivalent Circuit Parameters 153
7.14 Design 2 Dual Band Dual Layer Dual Polarized (DB-DLDP) Interdigital HIS Unit Cell and Equivalent Circuit Parameters 157
7.15 Design 3 Dual Band Single Layer Dual Polarized (DB-SLDP) Interdigital HIS Unit Cell and Equivalent Circuit Parameters 160

B.1 Circuit Model Parameters of Single Band Dual Layer Dual Polarized Interdigital HIS. $\mathbf{f}_{\mathrm{dsn}} = 900$ MHz $\mathbf{C}_{\mathrm{d}} = 2.8$ pF $\mathbf{L}_{\mathrm{d}} = 1.7$ nH $\mathbf{C}_{\mathrm{p}} = 1.5\mathrm{e}^{-3}$ pF $\mathbf{C}_{\mathrm{Sg}} = 0.4$ pF $\mathbf{C}_{\mathrm{s}} = 0.05$ pF 191

C.1 Multiple Linear Regression ANOVA - Explained 201

Nomenclature

Symbols

$\hat{\mathrm{B}}_{\mathrm{n}}$	Least Square estimates of coefficients of observation number (n)
$\hat{\mathrm{Y}}$	Least Square predicted value of the dependent variable
$\frac{\mathrm{K}(\mathrm{k})}{\mathrm{K}'(\mathrm{k})}$	Complete elliptical integral of first kind
η	Free space impedance
$\mathrm{C}_{\mathrm{coupling}}$	Coupling capacitance between two HIS capacitive layers
$\mathrm{C}_{\mathrm{S_g}}$	Capacitance developed between HIS unit cell interelement spacing
$\mathrm{C}_{\mathrm{s_i}}$	Elementary capacitance between adjacent interdigital digits along cross polarization
$\mathrm{SS}_{\mathrm{reg}}$	Regression Sum of Squares
$\mathrm{SS}_{\mathrm{res}}$	Residual Sum of Squares
SS_{Y}	Total Sum of Squares
α	Decay constant
β	Phase constant
Γ_{in}	Input reflection coefficient
$\in$	Error term in multiple linear regression model
λ	Wavelength
λ_{g}	Guided wavelength
λ_{N}	Upper band wavelength

μ_0	Free space permeability
μ_r	Relative permeability
ω	Angular frequency
$\overline{\mathrm{X}}$	Observed independent variable sample mean
$\overline{\mathrm{Y}}$	Observed dependent variable sample mean
Φ	Input reflection phase
$\tan\delta$	Loss tangent
$\mathrm{B_n}$	Regression coefficients of number (n) in multiple linear regression model
$\mathrm{B_0}$	Intercept in multiple linear regression model
CF	Interlayer coupling factor
$\mathrm{C_0}$	First order fringing sheet capacitance
$\mathrm{C_{cc}}$	Capacitive coupling empirical series capacitance
$\mathrm{C_d}$	Interdigital capacitor capacitance
$\mathrm{C_{IDC}}$	Equivalent effective capacitance of FSS-based interdigital HIS capacitive layer
$\mathrm{C_i}$	Surface mount lumped capacitance corresponding to band number (i)
$\mathrm{C_p}$	HIS unit cell mutual capacitance
D	HIS patch width
d	HIS grid conductor width
$\mathrm{d_c}$	Distance between surface mount lumped capacitors
f	Frequency
$\mathrm{f_r}$	Resonance frequency
H	HIS unit cell substrate thickness
$\mathrm{H_d}$	Dielectric thickness
$\mathrm{H_v}$	Rohacell material thickness

k	Constant in complete elliptical integral
K_i	Correction term associated with stripline self inductance L_i
L	Interdigital capacitor digits length
L_{cc}	Capacitive coupling empirical series inductance
L_C	HIS grid conductor inductance
L_{di}	Elementary interdigital capacitor self inductance
L_D	Gridded HIS centre patch inductance
L_d	Interdigital capacitor associated inductance
L_s	HIS unit cell dielectric substrate inductance
L_{wl}	Self inductance of stripline of width (w) and length (l)
MS_{reg}	Regression Mean Square
MS_{res}	Residuals Mean Square
N	Number of bands
N_d	Interdigital capacitor number of digits
P	Periodicity
p	Top plate interdigital capacitor number of digits
P_T	Total periodicity
q	Lower plate interdigital capacitor number of digits
s	Interdigital capacitor digits side gap
S_g	HIS unit cell interelement spacing
s_p	Interdigital capacitor digits top/bottom gap
t	Copper thickness
w	Interdigital capacitor digits width
W_p	Interdigital capacitor patch width

$\mathrm{X_n}$	Independent variable of number (n) in multiple linear regression model
$\mathrm{X_{ws}}$	Interdigital capacitor digits width to digits gap ratio
Y	Dependant variable in multiple linear regression model
$\mathrm{Z_0}$	Free space impedance
$\mathrm{Z_{(TE)}}$	TE surface wave impedance
$\mathrm{Z_{(TM)}}$	TM surface wave impedance
$\mathrm{Z_{cc}}$	Dual band HIS capacitive coupling empirical impedance
$\mathrm{Z_c}$	Transmission line characteristic impedance
$\mathrm{Z_{HIS}}$	HIS effective impedance
$\mathrm{Z_{IDC}}$	Interdigital HIS equivalent FSS-based capacitive layer impedance
$\mathrm{Z_{in}}$	Input impedance
$\mathrm{Z_s}$	HIS substrate input impedance
ε_0	Free space permittivity
ε_{eff}	Effective permittivity
ε_r	Relative permittivity
c	Speed of light
k	Wave vector
k_{ij}	Magnetic coupling factor between two inductors L_i and L_j
g	Gap within HIS subunit cell centre patch and grid conductor
m	Number of observations in multiple linear regression model
F	F-Statistics
n	Number of independent variables in multiple linear regression
R	Correlation coefficient
R Square	Squared correlation coefficient

Acronyms / Abbreviations

3D	3 Dimensional
AMC	Artificial Magnetic Conductor
ANOVA	Analysis Of Variance
BPF	Band Pass Filter
BSF	Band Stop Filter
CST	Computer Simulation Technology
DB-DLDP	Dual Band Dual Layer Dual Polarized
DB-SLDP	Dual Band Single Layer Dual Polarized
DB-SLSP	Dual Band Single Layer Single Polarized
DL	Dual Layer
DNG	Double Negative
DUT	Device Under Test
DV	Dependant Variable
EBG	Electromagnetic Bandgap
ECM	Equivalent Circuit Model
E	Electric Field
ESL	Equivalent Series Inductor
ESR	Equivalent Series Resistor
FD	Frequency Domain
FSS	Frequency Selective Surface
GA	Genetic Algorithm
H	Magnetic Field
HIS	High Impedance Surface

IDC	Interdigital Capacitor
IE	Integral Equation
IV	Independent Variable
LH	Left Handed
LPF	Low Pass Filter
MRI	Magnetic Resonance Imaging
MTMs	Metamaterials
NRI	Negative Refraction Index
NRL	Naval Research Laboratory
OSM	Open Short Match
PBA	Perfect Boundary Approximation
PBG	Photonic Bandgap
PCB	Printed Circuit Board
PEC	Perfect Electric Conductor
PMC	Perfect Magnetic Conductor
RCS	Radar Cross Section
RF	Radio Frequency
RL	Return Loss
Rx	Receiver
S.C	Short Circuit
SAR	Specific Absorption Rate
SAS	Statistical Analysis System
SB-DLDP	Single Band Dual Layer Dual Polarized
SB-SLDP	Single Band Single Layer Dual Polarized

SB-SLSP	Single Band Single Layer Single Polarized
SL	Single Layer
SPSS	Statistical Package for the Social Sciences
SRR	Split Ring Resonator
TD	Time Domain
TE	Transverse Electric
TL	Transmission Line
TM	Transverse Magnetic
TST	Thin Sheet Technology
Tx	Transmitter
UWB	Ultra Wide Band
VNA	Vector Network Analyzer

Chapter 1

Introduction

1.1 General Overview

A review of the literature shows that photonic crystals are the only naturally occurring material that has been reported and experimentally analysed for its ability to manipulate propagation of light. It was first introduced by G.G. Stokes in 1885 when he observed optical light reflections and refractions within a crystal slab, and therefore, discovered that periodic arrangement of crystals allows the light to undergo total reflection as a function of the light spectrum's wavelength; a phenomena that has also been commented on by Lord Rayleigh in 1887 describing it extraordinary [1, 2]. Properties of light reflection, refraction and transmission has fascinated researchers to develop such phenomena in electromagnetic wave propagation. However, materials of such characteristics are not naturally available but made possible by introducing man-made structures. Therefore, artificial periodic structures incorporating different material combinations such as metal, dielectrics and inclusions have been developed—within which different terminologies are reported such as metamaterials, frequency selective surfaces, electromagnetic band gap structures and high impedance surfaces. All are classified according to functionality and unique characteristics, which without a doubt have been and will be under significant interest and immense investigation for many decades and to date.

Of particular interest to this thesis is High Impedance Surface (HIS) defined as an extraordinary class of artificial periodic structures that exhibit distinctive characteristics while controlling electromagnetic wave propagation. HIS has the ability to surpass material readily available in nature and prove physical properties which were only theoretically predicted. The main particularities of HIS are summarized by its ability to suppress surface waves and exhibit total reflection associated with nearly zero degrees phase reversal within a given bandwidth.

Therefore, HIS has direct analogy to perfect magnetic conductors which do not exist naturally.

On the other hand, HIS has contrary performance to perfect electric conductors which are naturally occurring materials of well known electromagnetic and electric properties; they support surface waves and exhibit a total reflection with 180° phase reversal. With respect to distinctive HIS properties, the structure initially found many applications in antenna design and performance enhancement such as reducing mutual coupling among antenna arrays, realising high gain low profile antennas, and antenna miniaturisation; extended to further widespread applications in RF, microwave and communication fields applicable for implementation in commercial, industrial and medical sectors.

1.2 Research Motivation

Research and development of High Impedance Surfaces (HIS) has been ongoing since first reported by Sievenpiper in 1999 [3], initially proposed as a general antenna ground plane with significant attention paid towards functionality and detailed principles. Nevertheless, technology development rate is always on a fast track and requirements for compact highly functional devices operating with optimum efficiency and reliability put immense pressure on engineers to improve design methods and techniques such that high standard requirements are fulfilled. Therefore, research and work is ongoing to realise multifunctional miniature devices such as antennas, filters, couplers, transmission lines and periodic structures and high impedance surfaces are not an exclusion.

Motivated by high demand for miniature systems, which are multifunctional and highly operational, the main aim of this research project is to develop a robust design methodology to realise miniaturised dual band HIS with an overall periodicity less than one tenth of the wavelength and a reasonable fractional bandwidth. From that prospective, this research deals with implementing design strategies as based on an using equivalent circuit model approach while discussing miniaturisation techniques. Moreover, significant attention is drawn towards developing methods and strategies that provide solutions to encounter and manage inter unit cell mutual coupling, which possesses considerable design constraints realising dual band to multiband HIS. Therefore, considerable work within the thesis is focused on high impedance surface design and characterization. Nevertheless, essential experimental verification and practical investigation has been carried forward as proposed miniaturised HIS designs are manufactured and incorporated with a planar antenna; therefore, design methodologies are validated for the HIS being recognised as an antenna ground plane where the term artificial magnetic conductor is widely used.

1.3 Research Novelty and Contribution

This research project is focused on realising miniaturised dual band HIS. For dual band purposes, two optimized single band subunit cells are concatenated into one structure. For miniaturisation purposes, two different techniques are employed which are focused on increasing the effective equivalent capacitance of the HIS metallic capacitive layer. The first miniaturisation method was surface mount lumped capacitor loading, while the second approach was incorporating interdigital capacitors. Nevertheless, both methodologies are hindered by inter unit cell mutual coupling possessing design challenges, which the thesis will cover. State of the art and research project contributions are summarized as follows:

- A dual band miniaturised HIS using surface mount lumped capacitors is realised.
- A novel miniaturised lumped capacitor loaded dual band HIS is designed featuring grid conductors as such that inter unit cell mutual coupling is minimized where each band is generated by the corresponding value of loaded capacitor.
- Accurate analytical design methodology to model a HIS unit cell engineered with interdigital capacitor as such that optimum miniaturisation is achieved. Comments on modelling interdigital inductance are given. The analytical circuit model is validated as three single band miniaturised interdigital HIS prototypes that are addressed and discussed in terms of design limitation, miniaturisation level and polarization dependency.
- Original straightforward design methodology is discussed to realise a miniaturised dual band interdigital HIS as based on an analytical circuit model. By combining individually designed single band interdigital HIS unit cells, a dual band system is possible and proved effective when mutual coupling is accounted for. Consequently, a comprehensive study on factors contributing to inter unit cell mutual coupling is conducted leading to a proposed generalised solution suitable for a generic dual band system.
- An unprecedented approach to manage mutual coupling is proposed. A multiple linear regression technique is implemented to interrelate frequency displacement, within each band, to all factors which contribute to inter unit cell mutual coupling. Therefore, an

effective 5-dimensional mathematical model is developed. Reliability of regression models as well as design methodology are proven through three novel miniaturised dual band interdigital HIS prototypes, which differ in polarization dependency and design complexity.

1.4 Thesis Structure

The thesis comprises of eight chapters and is structured as follows:

Chapter 1 Introduction: An introductory chapter providing a general overview to HIS and stating HIS main characteristics and applications. Research motivation is highlighted. Also, areas of contribution within the thesis are discussed.

Chapter 2 Literature Review and Background Theory: Discusses concepts and characteristics of HIS within the context of broad term artificial periodic structures. A full detailed theory of HIS principles, therefore, states its main distinctive properties and advantages as well as applications. Thereafter, a literature review of available miniaturisation techniques, as compared to work within the thesis, is presented. Then, attention is directed towards methods previously implemented to realise compact multiband HIS and also to compare these methods to work within the thesis. Moreover, being a major topic within the thesis, previously reported methodologies that have addressed inter unit cell mutual coupling are reviewed in context to the thesis work. Finally, a brief overview of measurement techniques, as related to experimental work conducted within the thesis, is given.

Chapter 3 Dual Band High Impedance Surface Miniaturised By Lumped Capacitors: Detailed design concepts to a novel miniaturised dual band HIS are presented. Methodology is based on concatenating two single band subunit cells each loaded with surface mount lumped capacitor, unequal and mechanically tuned. Design challenges are highlighted through full parametric analysis, therefore, introducing inter unit cell mutual coupling as a significant design constraint which possess limitation on HIS performance.

Chapter 4 Multiband Reduced Mutual Coupling Lumped Capacitor HIS: Presents an original design approach to suppress inter unit cell mutual coupling while maintaining significant miniaturisation. Detailed design procedure leading to novel miniaturised dual band HIS, featuring gridded concatenated lumped capacitor loaded subunit unit cells, is discussed. Novel HIS design philosophy, mechanism and principles of operation are explained through full parametric analysis and an empirical equivalent circuit model, proving the surface potential to upgrade into a multiband system. Miniaturised dual band gridded HIS design is experimentally verified as fabricated and incorporated with a planar antenna where a low profile system is possible. Design challenges are discussed addressing system losses.

Chapter 5 Single Band Interdigital High Impedance Surface Design Methodology: This chapter introduces interdigital capacitors into HIS design for the aim to achieve miniaturisation and overcome losses in the surface mount lumped capacitor technique. Detailed design methodology, based on an analytical equivalent circuit model, is developed such that fast and optimum miniaturisation implementing interdigital capacitances are achieved. Also, setting design fundamentals for consecutive chapters which discuss miniaturised dual band interdigital HIS design. In addition, this chapter introduces three different single band interdigital HIS designs; each features design contributions not only with respect to miniaturisation, but also dealing with HIS polarization suitability as well as design techniques which are superior to available literature. Design 1: Single Band Single Layer Single Polarized (SB-SLSP) interdigital HIS is the fundamental design whose unit cell parameters are analysed through complete parametric study based on an equivalent circuit model. Design 1 is manufactured and integrated with a planar monopole antenna whose performance is improved realising a low profile system. Design 2: Single Band Dual Layer Dual Polarized (SB-DLDP) interdigital HIS is proposed where design methodology is detailed with insights on interlayer coupling. Design 3: Single Band Single Layer Dual Polarized (SB-SLDP) interdigital HIS is considered with high accuracy in unit cell analytical modelling where the surface is also validated experimentally as fabricated to perform as an antenna ground plane.

Chapter 6 Dual band Interdigital High Impedance Surface - Introduction To Mutual Coupling: Design methodology to realise miniaturised dual band interdigital HIS is thoroughly discussed where novelty of the work extends in the development of a simplistic design approach for a dual band design that originates from single band interdigital HIS which are individually modelled. However, inter unit cell mutual coupling possesses significant design limitation causing displacement in both bands' resonance frequencies. Further study within this Chapter involves detailed parametric analysis on factors that affect inter unit cell mutual coupling such that a general solution can be developed.

Chapter 7 Dual band Interdigital High Impedance Surface - Mutual Coupling Model: Critiques on dual band mutual coupling are given to generalising the problem into a 5-dimensional prospective, therefore, identifying main factors involved which contribute to inter unit cell mutual coupling. Defining the research question and identifying the problem, an original methodology to overcome and handle dual band mutual coupling is proposed based on multiple linear regression analysis. From prior definition of unit cell parameters and system requirements, mathematical models are developed to estimate the percentage frequency shift in each dual band HIS system as a consequence of mutual coupling. Furthermore, regression models are assessed, analysed and optimized for improved accuracy. Methodology is verified as applied to three miniaturised dual band interdigital HIS design prototypes where each is discussed detailing their distinctive characteristics in terms of miniaturisation, stability and polarization dependency. Novel designs are: Design 1: Dual Band Single Layer Single Polarized (DB-SLSP), Design 2: Dual Band Dual Layer Dual Polarized (DB-DLDP) and Design 3: Dual Band Single Layer Dual Polarized (DB-SLDP).

Chapter 8 Conclusion And Future Work: Research project conclusions are discussed summarizing contributions and areas of novelty as well as critiques on design challenges and constraints. Suggestions for future work are given.

Appendix A CST Microwave Studio: Presents a brief introduction to commercial simulation software which has been used within the thesis.

Appendix B Single Band Design 2 - Dual Layer Dual Polarized IDC HIS Coupling Model: Describes design methodology of interlayer coupling in single band dual layer miniaturised interdigital high impedance surface design.

Appendix C Introduction To Multiple Linear Regression Analysis: Basic concepts of multiple linear regression analysis are detailed as applicable to the thesis.

Chapter 2

Literature Review and Background Theory

2.1 Introduction

This Chapter covers the background theory and provides a literature review of the design and characterization of miniaturised multiband high impedance surfaces with special attention to inter element mutual coupling.

A historical review of artificial periodic electromagnetic structures is initially provided. Therefore, introducing the reader to essential differences in the conception and properties of various periodic structure categories and highlighting the distinctive characteristics of High Impedance Surface (HIS) thesis subject matter . Thereafter, basic theoretical concepts of HIS are provided based on Sievenpiper's mushroom type model [3]. Afterwards, miniaturisation techniques available within the literature are stated and compared to the research study proposed in the thesis. Subsequently, the literature review on the methods to realise compact multiband HIS structures are outlined in comparison to thesis proposed miniaturised dual band and triple band HIS designs as with respect to miniaturisation level and fractional bandwidth. Additionally, the methodology to manage and control undesired mutual coupling between periodic elements is discussed, being a significant part of the thesis, which is subsequently compared to available reported methods. Finally, measurement techniques and setups as related to antenna and HIS characterization are discussed as applicable to experimental work conducted in the thesis.

2.2 Historical Review – Artificial Periodic Electromagnetic Structures

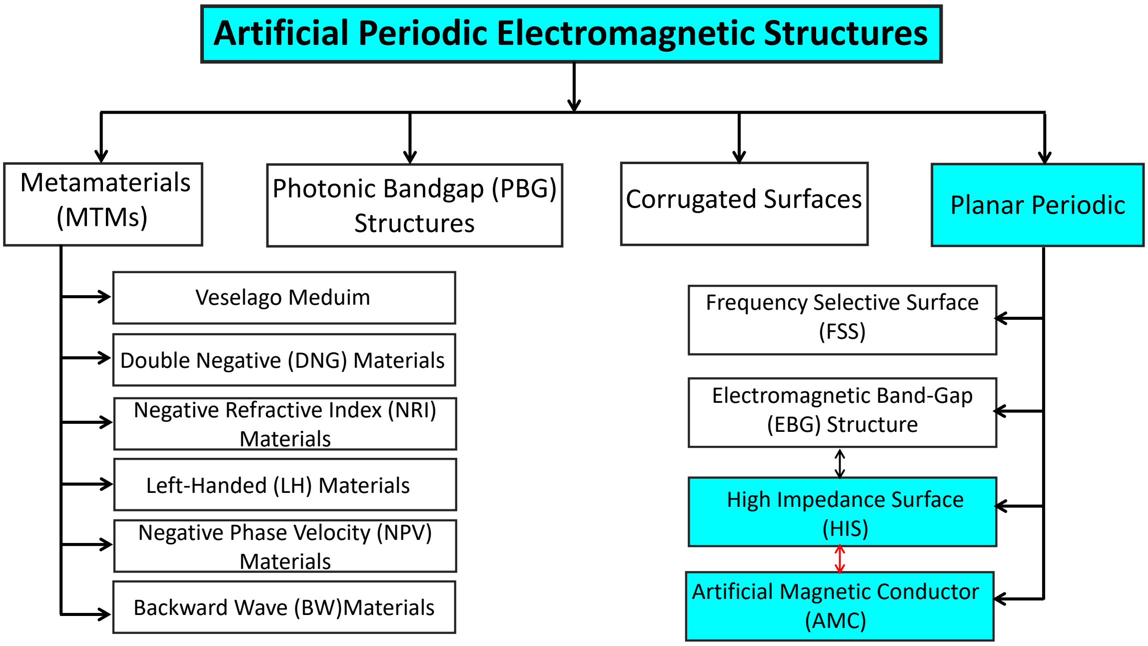

Fig. 2.1 Classifications of artificial periodic electromagnetic structures.

Artificial periodic materials are distinctive engineered structures within which electromagnetic waves are manipulated to exhibit unusual characteristics that do not exist in nature, but are mathematically, theoretically and physically possible. The first conducted which proved that light filters, transmits and reflects differently if exposed to a non-continuous surface was the experiment reported by American physicist Rittenhouse over 250 years ago. In 1768, F. Hopkinson and D. Rittenhouse observed a silk handkerchief directed to a street lamp and discovered that certain colours of the lamp light spectrum are suppressed differently as filtered through the handkerchief periodic threads [4]; an experiment believed to be the first insights on the very well-known Frequency Selective Surface (FSS). In 1895-1898, J.C. Bose reported the first experiment conducted in the microwave field as he observed the effect of “twisted structures” and proved that polarization of electromagnetic waves can be altered by implementing composite artificial material as crystals and dielectrics. Bose’s work is considered a first attempt into the development of Metamaterials (MTMs) concepts [5, 6]. Therefore, historically, these were the very early works that led to developing artificial periodic materials of unique properties. Fig. 2.1 presents the main outlook of periodic electromagnetic structures where pioneering work has been ongoing over the years, in all categories, and each will be briefly addressed.

“Meta” in Greek means “Beyond”. Metamaterials (MTMs) refers to extraordinary artificial materials constructed of inclusions having various shapes and composite media to realise negative effective permittivity and permeability which result in transmitted electromagnetic waves to propagate in the reverse direction contrary to ordinary materials such as dielectrics where waves propagate in the forward direction. Historically, these concepts were first proposed theoretically by V.G. Veselago in 1968. Veselago explained that simultaneous negative effective permittivity and permeability are possible, where the wave propagates in the backward direction and the electric and magnetic fields follow the Left Hand (LH) rule, featuring a negative index of refraction [7]. These theoretical concepts did not come to be validated experimentally until 1996 when Pendry reported the existence of thin periodic wire structures of negative permittivity properties in the GHz range [8, 9]. In 1999, Pendry et al. reported the first artificial material with negative magnetic properties in the form of Split Ring Resonator (SRR) conducting rings [10]. Later in 2000, Smith et al. demonstrated that a rectangular and ring shaped SRR can exhibit both negative permeability and permittivity which is the first practical metamaterial element with man-made composite structures that proved concepts theoretically reported by Vesalago in 1968 and defined as “Left Handed Media” where the wave propagate with negative group velocity [11, 12]. Other terminologies were implemented to describe metamaterials such as Double Negative (DNG) materials and Negative Refractive Index (NRI) materials. Metamaterials have attracted a lot of research interest to date with a wide range of applications such as the realisation of flat lenses with negative refraction index for better sharpness [13], antenna miniaturisation [14], cloaking [15, 16] and antenna beam control [17].

Photonic Bandgap (PBG) structures, first introduced by Yablonovitch in 1987 [18, 19], are generally 3-dimensional periodic elements in a lattice of infinite dielectric material as investigated in the optical range with analogy to propagation of light in photonic crystals [20, 21]. It was deduced that electromagnetic waves can be controlled within a given bandgap for a periodic lattice in multiple orders of half the operating wavelength. Further work in the field proposed a 3D PBG lattice using woodpile [22], diamond like dielectric [23] and metallic mesh elements [24] which are proved to be bulky and hard to fabricate [25, 26].

On the other hand, planar periodic structures of a 2-dimensional nature are of great importance in electromagnetic structure design being lighter, easier to fabricate and which can be engineered to meet high demand for compact and efficient devices. Frequency Selective Surface (FSS) and High Impedance Surface (HIS) are two main planar periodic structures that existed in the literature, which will be discussed next.

Frequency selective surfaces are planar periodic structures made of conducting or aperture elements mainly supported by a dielectric material and designed to alter transmission and reflection properties of electromagnetic waves offering a filtering mechanism. According to the literature, the first planar artificial periodic surface was introduced in 1919 where Marconi proposed the first patent on practical FSS used to improve the efficiency of a transmit and receive parabolic reflector implemented in wireless telegraphy and telephony [27]; even though the term FSS was not used during that time. In 1946 efficient and real work was conducted to explore the explicit principles of frequency selective surface elements when G. G. Macfarlane analysed electromagnetic fields, in capacitive and inductive diaphragms, for a normal incidence plane wave as associated with transmission lines [28]. Within the same period, the concept of "resonant grating" was introduced by H.G. Booker in 1946 when transmission and reflection characteristics of metal screens comprising of half wave dipoles and slots were analysed proving that the resonant conducting array of dipoles acts as a passive Band Stop Filter (BSF) while the slot dipole array is a Band Pass Filter (BPF) [29]. However, the clear definition of frequency selective surfaces in addition to accurate modelling theoretically and experimentally came to light in 1967 when R. Ulrich presented an accurate circuit model representation for inductive and capacitive grids and validated the concepts through measurements that inductive screens are high pass while capacitive screens are low pass [30, 31]. FSS can provide various filtering characteristics ranging from being low pass, high pass, band stop or bandpass with analogy to microwave filters. Therefore, FSS is evaluated and characterized by its element shape, which influences the surface stability to angle of incidence, operational bandwidth and polarization level. For example, square loop FSS is recognised as the most stable element with the highest cross polarization level and wider bandwidth [32]. FSS detailed design concepts are beyond this thesis, but to date the FSS is subject to intensive research and serves a range of applications such as shielding, radomes, antennas, radars, filters, absorbers, polarizers and phased arrays [33].

Another class of two-dimensional planar periodic structures of distinctive properties which significantly differ from frequency selective surfaces, is the so-called High Impedance Surface (HIS), first introduced by Sievenpiper in 1999 [3]. Sievenpiper's high impedance surface was proposed as a periodic electromagnetic surface comprised of metallic capacitive patches, supported by a thin dielectric material and backed by a metallic plane in addition to metallic vias connecting each patch to the ground plane, therefore, being "Mushroom" like structures. The HIS provided potantial to replace the antenna's conventional metallic ground plane due to the ability, within a given bandgap, to control surface waves and possesses a very high impedance. Therefore, an antenna system, which is low profile, high gain and efficiency is possible. In that sense, the HIS has been proposed with a strong analogy to corrugated structures, which were first developed in the early 1940s by H. Goldstein [34] who introduced periodic corrugated waveguide and coaxial lines. Periodic corrugations are defined as a 3-dimensional quarter wavelength deep metallic slabs, very closely spaced, and shorted by a conducting metallic slab, where analytical and experimental work has been reported in the early 1950's in [35, 36]. Corrugations are polarization dependent, while "Mushroom" type HIS are polarization independent, significantly compact and offer similar performance as compared to corrugations [3].

Sievenpiper "Mushroom" type HIS is often referred to as an Electromagnetic Bandgap (EBG) Structure for its ability to suppress surface waves with analogous properties to 3-dimensional PBG structures briefly addressed earlier [37]. Later in 2003, a via-less Uniplanar photonic bandgap structure EBG was introduced by Chang et al. [38] which demonstrated control of surface waves and has been validated in applications such as waveguides, microstrip filters, patch antennas and low profile slotted antennas. Uniplanar EBG has an edge over "Mushroom" type HIS for it is purely planar (no vias), lighter and easier to fabricate.

On the other hand, the Sievenpiper's "Mushroom" type HIS exclusive ability to develop a significantly high impedance and operate as a Perfect Magnetic Conductor (PMC), a property not present in natural material, renders the surface to earn the name Artificial Magnetic Conductor (AMC). HIS in that sense has been extensively reported in the literature to replace antenna conventional Perfect Electric Conductor (PEC) ground planes [37]. Therefore, high impedance surfaces are artificial periodic planar materials that exhibit unique and exceptional properties not readily available in nature where some in the literature has classified HIS as a special form of "Metamaterial" or "Meta-Surface" [39, 40]. Research interest into the design and optimization of HIS has been growing to date for its significant advantages in electromagnetic, antennas and microwave design fitted for a wide range of applications in every sector such as medical, commercial, military and industrial. Efforts have been made to enhance surface design where many research groups have invested in analytical modelling and optimization, performance enhancement, miniaturisation, multiband designs and surface tunability.

This research project is heavily focused on realising via-less miniaturised compact multiband HIS, validated experimentally as an antenna ground plane and discussed from the AMC point of view. Subsequent sections will detail HIS characterization, modelling, miniaturisation and multiband techniques as well as design challenges as compared to present literature.

2.3 Basic Concepts of High Impedance Surfaces (HIS)

Basic concepts and principles of Sievenpiper's "Mushroom" type HIS [3] are discussed. HIS, as originally proposed, constitute of metallic square patches supported by a dielectric material and connected to a metal plane through vias as shown in Fig. 2.2 for a 5 by 5 HIS array. The surface provides distinctive properties suppressing surface waves within a bandgap, as well as operating as a perfect magnetic conductor within a given frequency band very much desired, to coincide with the surface wave bandgap for optimum performance.

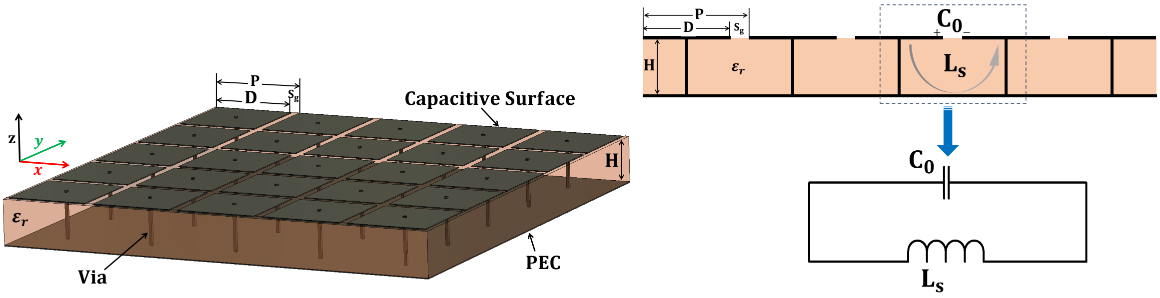

(a) 3D View (b) Side View and ECM Model

Fig. 2.2 Mushroom type High Impedance Surface (HIS) model.

For a HIS unit cell periodicity much smaller than the operating wavelength, the structure is considered as an effective medium, and analysed using an Equivalent Circuit Model (ECM), as in Fig. 2.2b. Effective sheet capacitance (C_0) developed between the gaps separating each unit cell is the result of the developed electric field component exciting the surface. Moreover, the presence of vias encourages the development of a conducting current path between patch elements and the HIS metal plane, which can be represented by inductance $(\mathrm{L_s})$. Therefore the effective HIS impedance $(\mathrm{Z_{HIS}})$ is the resulting parallel combination of LC resonant circuit model and defined as [25, 3]:

$$\mathrm{Z_{HIS}} = \frac{j\omega \mathrm{L_s}}{(1-\omega^2 \mathrm{L_s C_0})} \tag{2.1}$$

where ω is the angular frequency

First order fringing sheet capacitance, C_0, is [3]:

$$\mathrm{C}_0 \backsimeq \frac{\mathrm{D}\varepsilon_0(\varepsilon_r+\varepsilon_{r(air)})}{\pi}\cosh^{-1}\left(\frac{\mathrm{P}}{\mathrm{S_g}}\right) \tag{2.2}$$

where

P, D and $\mathrm{S_g}$ are the unit cell periodicity, patch width and interelement spacing respectively. ε_r and $\varepsilon_{r(air)}$ are the relative substrate permittivity and surrounding material (air).

For a shorted electrically thin substrate of thickness (H). Substrate inductance is:

$$\mathrm{L_s} = \mu_0 \mu_r \mathrm{H} \tag{2.3}$$

where μ_0 and μ_r are the free space and relative dielectric material permeability respectively. Based on the ECM, the HIS resonance frequency is given by:

$$\mathrm{f_r} = \frac{1}{2\pi\sqrt{\mathrm{C_0 L_s}}} \tag{2.4}$$

2.3.1 HIS for surface wave suppression

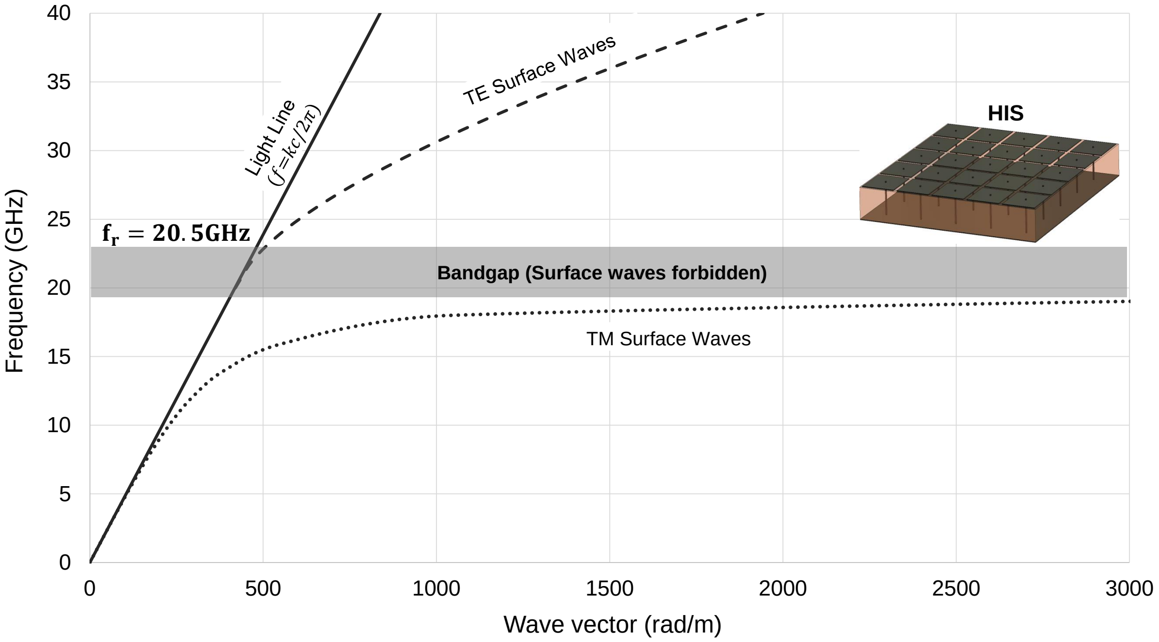

Fig. 2.3 Analytical dispersion diagram for mushroom-type HIS. Effective capacitance and inductance 0.03 pF and 2 nH respectively.

According to Eq. (2.1), HIS impedance properties are a function of frequency. The surface is capacitive above resonance frequency and supports TE surface waves while it is inductive below resonance frequency, supporting TM waves. Within a bandgap around resonance, surface waves are forbidden from propagation. However, ordinary material available in nature does not have this distinctive property, where surface waves propagate exponentially decaying within a decay constant α.

For example, metals are inductive and support TM surface waves whose impedance [25, 3]:

$$\mathrm{Z}_{(\mathrm{TM})} = \frac{j\alpha}{\omega\varepsilon} \tag{2.5}$$

On the other hand surfaces of capacitive nature such as FSS, corrugated structures and textures surfaces support TE surface waves of effective impedance [25, 3]:

$$\mathrm{Z}_{(\mathrm{TE})} = \frac{-j\omega\mu}{\alpha} \tag{2.6}$$

HIS surface wave bandgap is generally determined from dispersion diagrams which are the plot of frequency versus wave vector (k). The analytical HIS dispersion diagram, has been reported by Sievenpiper as extracted from the combined plots of TE and TM wave vectors, $k_{(\mathrm{TE})}$ and $k_{(\mathrm{TE})}$, which are defined as [3]:

$$k_{(\mathrm{TE})} = \frac{\omega}{c}\sqrt{1 - \frac{\eta^2}{\mathrm{Z}_{\mathrm{HIS}}^2}} \tag{2.7}$$

$$k_{(\mathrm{TM})} = \frac{\omega}{c}\sqrt{1 - \frac{\mathrm{Z}_{\mathrm{HIS}}^2}{\eta^2}} \tag{2.8}$$

where η and $\mathrm{Z}_{\mathrm{HIS}}$ are the free space and effective HIS impedance respectively. ω is the angular frequency. c is the speed of light.

An analytical dispersion diagram, for a mushroom type HIS of equivalent lumped capacitance and inductance of 0.03 pF and 2 nH respectively and a resonance of 20.5 GHz, is considered. The dispersion diagram, presented in Fig. 2.3, shows that below lower bandgap frequency the HIS supports TM surface waves in analogy to a metal surface, while above upper bandgap frequency the HIS is capacitive and supports TE surface waves as capacitive FSS or corrugations would do. However, within a bandgap, shown in Fig. 2.3, TE and TM wave vectors do not exist and surface waves are suppressed, where the surface behaves as a HIS.

HIS designed to suppress surface waves is technically known as an Electromagnetic Bandgap (EBG) Structure, initially presented in [3]. Within the same time planar PBG structures, which are light weight and compact, were also proposed to eliminate surface waves in patch antennas [41, 42]. EBG structures have been reported in different applications with examples stated such as noise suppression and isolation among printed circuit boards [43–45] as well as mutual coupling reduction between patch antenna array elements [46, 47]. Improvement of EBG design by reducing unit cell size and implementing via-less structures have also been considered such as uniplanar EBG designs demonstrating effective surface wave suppression while implementing less complicated EBG structures of applications in microstrip filters, power amplifiers, patch antennas, MIMO antennas, directional couplers and coupled lines [38, 48–50]. Also, examples of miniaturised EBG elements of unit cell size reduction around 40%, as compared to conventional patch elements, were reported such as fork-like structures [51] and spiral elements [52] which have effectively suppressed surface waves in microstrip antenna arrays. Finally, surface waves were utilized in [53] to introduce additional resonances within a patch antenna and improve its bandwidth and gain.

2.3.2 HIS as a perfect magnetic conductor

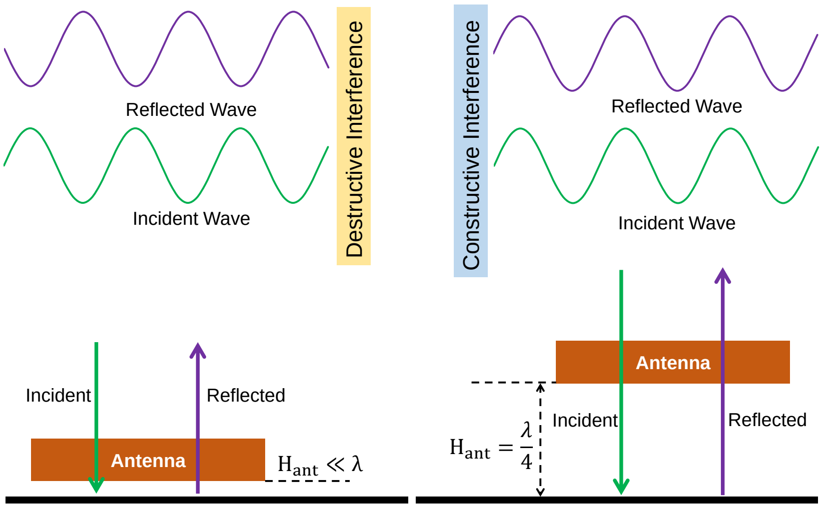

(a) Antenna $\ll \lambda$ above PEC (b) Antenna 0.25λ above PEC

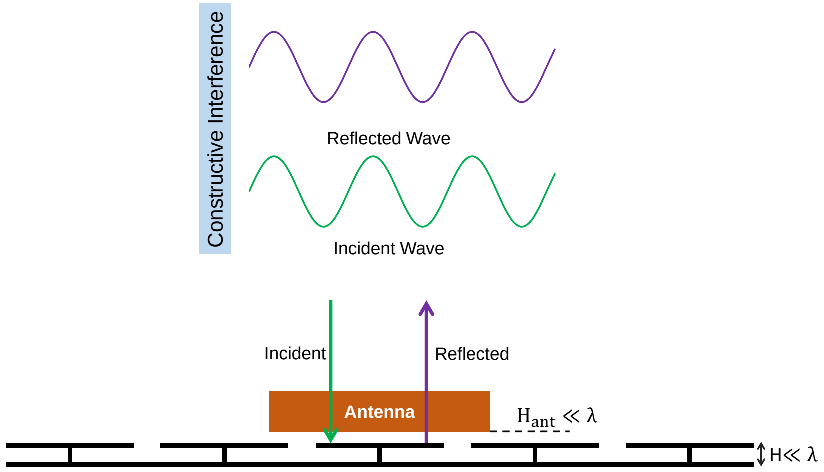

(c) Antenna $\ll \lambda$ above HIS

Fig. 2.4 Illustrated electromagnetic wave propagation for antenna supported by a Perfect Electric Conductor (PEC) ground plane as compared to a High Impedance Surface (HIS).

The HIS second distinctive feature is its ability to behave as a perfect magnetic conductor where the terminology Artificial Magnetic Conductor (AMC) is widely used. HIS as an AMC was initially reported in [3] for applications focused on realising low profile antenna systems where the mushroom-type HIS replaces the conventional antenna's metal ground plane. Metallic ground planes are typical in antennas which can improve radiation efficiency and gain only if the antenna is placed a quarter wavelength from the metal surface such that the image currents are added constructively to improve antenna radiation. Otherwise, properties of metal surfaces, being a Perfect Electric Conductor (PEC), are expected to totally reflect incident waves with a 180 degrees phase reversal resulting in destructive interference which deteriorate radiation performance if placed very close to the PEC as illustrated in Fig.2.4a and Fig.2.4b. This is quite significant considering that periodic textured metal surfaces also support surface waves which tend to radiate from metallic surface edges. However, HIS is electrically thin and its properties are particular such that the phase of input reflection coefficient is zero at resonance and if designed to match the antenna resonance, incident waves add constructively with reflected waves for the antenna to be located at a very close proximity from the surface, Fig.2.4c, where a low profile system is possible. The HIS, therefore, mimics the behaviour of a Perfect Magnetic Conductor (PMC) allowing waves to reflect at a reflection coefficient magnitude of $+1$, 0 degrees phase reversal.

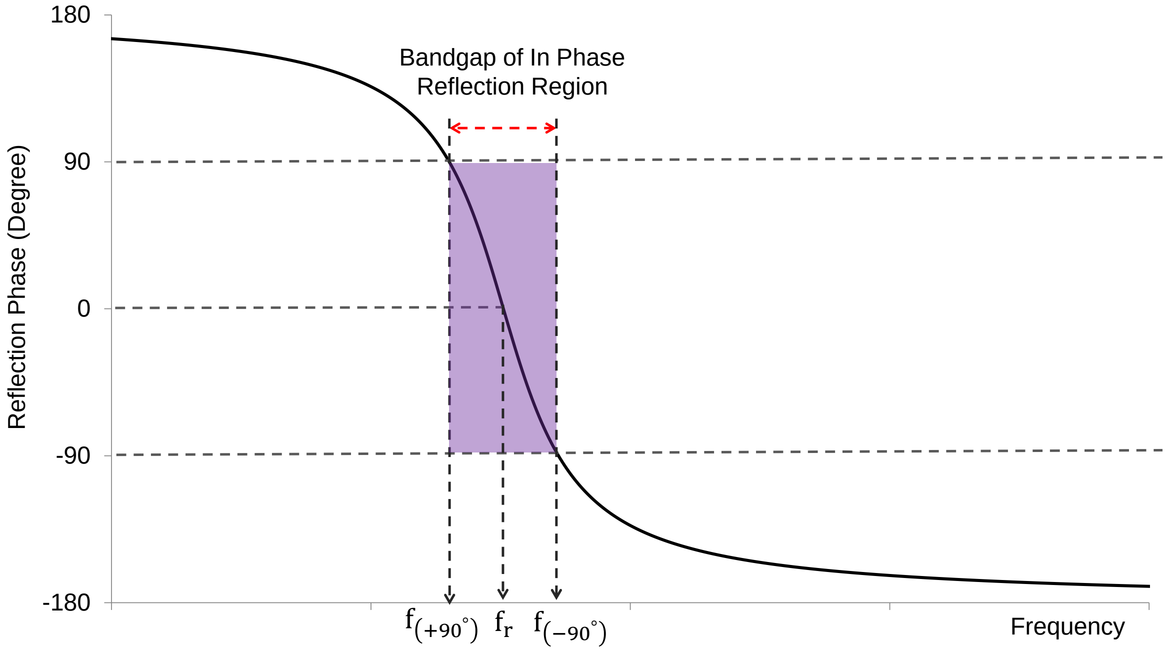

Fig. 2.5 Phase of reflection coefficient for a high impedance surface versus frequency.

However, the HIS is an engineered structure whose total impedance varies with frequency. Therefore, the input reflection phase versus frequency, at normal incidence, is [25, 3]:

$$\Phi_{\mathrm{HIS}} = \mathrm{Im}\left[\ln\left(\frac{Z_{\mathrm{HIS}} - Z_0}{Z_{\mathrm{HIS}} + Z_0}\right)\right] \tag{2.9}$$

where Z_0 is the free space impedance. Z_{HIS} is the HIS impedance, defined in Eq. (2.1).

Fig.2.5 presents the HIS reflection phase plot as a function of frequency demonstrating that the HIS is beyond a PMC. At resonance frequency (f_r), the surface has a very high impedance and reflection phase is 0°, therefore, a PMC. Below resonance frequency the surface becomes inductive and reflection phase approaches $+180°$, therefore, a PEC. Above resonance, the HIS is capacitive and reflection phase approaches $-180°$. Usable bandwidth within which the structure is of very high impedance and operates as an AMC has been reported to fall within a frequency range for the reflection phase varying between $\pm 90°$, defined as [3]:

$$\pm 90 \text{ Bandwidth Percentage} = \frac{f_{(-90°)} - f_{(+90°)}}{f_r} \times 100 \tag{2.10}$$

Since the introduction of Mushroom-type HIS, research interest has significantly intensified to explore and utilize the surface's unique properties. Reflection phase characteristics of the surface are generally analysed as a function of unit cell geometry, substrate properties and wave polarization. Early work following Sievenpiper's paper has been conducted by various research groups who successfully provided analytical conceptions analysing the surface structure design, which are carried forward to date [47]. Via-less AMC surfaces are regarded as planar FSS-based structures backed by a metal plate which exhibit reflection phase properties, as in Fig.2.5, observed in various unit cell structures such as patch elements [54], Jerusalem cross and spiral shaped elements combined with loops with significant stability to incident angles and polarization [55] and other geometries such as fractal, slotted and meanders [56, 57]. While earlier work involved parametric study provided essential insights into design guidelines such as the effect of unit cell structure, periodicity, substrate thickness, permittivity and angle of incidence on resonance frequency, fractional bandwidth and surface stability as reported in [49, 58]. Nowadays, developed work on utilizing HIS operating as an AMC which feature in-phase reflection characteristics has various applications beyond just being an antenna ground plane such as miniaturised polarization independent AMC functioning as a reflector for a circularly polarized antenna [59], a miniaturised AMC implemented in MRI systems for improved magnetic field [60, 61], flexible compact AMC integrated with microstrip antenna providing improved performance to eliminate undesired electromagnetic interference for tele-medicine applications [62], combined broadband checkboard dual band

AMC for radar cross section applications [63] and realisation of single band as well as multiband metamaterial absorbers [64–66]; just to name a few. Nevertheless, the work in this thesis is not targeted toward a specific application but very much focused on designing a miniaturised dual band FSS-based HIS in addition to special attention to inter element mutual coupling. Therefore, HIS miniaturisation techniques, multiband HIS structures and critiques on inter unit cell mutual coupling are discussed next.

2.4 Miniaturised Multiband High Impedance Surfaces

A Literature review on techniques to realise and characterize miniaturised multiband HIS are discussed and interrelated to the context of research conducted within the thesis as well as methods to manage inter unit cell mutual coupling.

2.4.1 HIS miniaturisation techniques

Miniaturisation of devices is a modern requirement based on designing smaller and compact structures of either electrical, optical or mechanical nature while maintaining functionality and is of great interest in the electromagnetic field community. As High Impedance Surface (HIS) is concerned, miniaturisation is fulfilled by designing the structure to resonate at lower design frequencies within a fixed unit cell periodicity. Therefore, miniaturisation of HIS is based on techniques to either increase effective inductance or capacitance such that design resonance frequency reduces where the structure's dimensions are maintained electrically small. Increasing HIS inductance is governed mainly by increasing substrate thickness which is highly undesirable where the surface diverts from being light, low profile and compact. On the other hand, HIS effective capacitance is mainly generated by a capacitive FSS-based surface featuring various element shapes, the simplest being a patch-like element. As for initially proposed mushroom-type HIS [3], HIS equivalent capacitance is that which is developed between patch element gaps denoted as fringe capacitance. To increase fringe capacitance and reduce resonance frequency, periodicity must be significantly increased leading to a large unit cell size, which is governed by grating lobe limit. Therefore, effective methods have been developed which aim to increase equivalent HIS sheet capacitance within a small unit cell size and are discussed below.

According to available literature, miniaturisation of periodic structures traces back to 1971 when Munk et al. discussed the concept of loading FSS dipoles to alter the surface impedance, control resonance frequency and FSS bandwidth by varying the load impedance, dipole dimensions and structure geometry [67]. Therefore, for the sake of argument, HIS is treated as an FSS-based structure in the absence of vias and miniaturisation techniques implemented in frequency selective surfaces are applicable to high impedance surfaces. Early work on HIS miniaturisation was a compact 0.14λ slotted patch HIS design operated at 12 GHz [68]. A combined approach of slotted patch and high dielectric constant material to reduce the unit cell size to less than 20mm, operating within GSM band, was reported in [69]. In [70], a magneto dielectric material of high permeability was proposed to replace mushroom type HIS substrate, therefore, increasing fractional bandwidth and reducing unit cell size by 25%; however, the design proved to be limited by material choice. Convolutions effectively increase the electrical size within a fixed unit cell, dimensions resulting in a reduction of resonance frequency, therefore, in [71] a convoluted HIS structure was reported offering a reduction in resonance frequency of 55% which was inspired by convoluted FSS discussed in [72]. A 20% reduction in resonance frequency as well as unit cell size was reported in [73] implementing edge-located vias. Also, meandering top HIS capacitive surface is a widely used technique to miniaturise HIS unit cell size such as 0.08λ uniplanar unit cell with meander inclusions [74]; meander line and spiral unit cell designs which provided reduction in resonance frequency by 30% and 50% as compared to a conventional patch [75]; and a general meander structure of unit cell 0.06λ [76].

Moreover, multilayer designs were reported within the literature benefiting from interlayer coupling to reduce resonance frequency. Examples are: complex elements featuring polarization independent tripoles combined with closely coupled layers presented for a 0.028λ EBG structure as well as loaded tripoles in the form of a single layer fractal tripoles demonstrated a 40% reduction in resonance frequency in a 0.18λ AMC unit cell [77]. Also, in [78], a multilayer design comprising of 11 stacked layers were compared to 6 shifted layers resulting in reduced periodicity to 0.027λ and 0.017λ respectively.

Furthermore, significant miniaturisation has been achieved in FSS using surface mount lumped reactive components such that resonance frequency completely depends on the value of the loaded component irrespective of periodicity [79–81]. In [82], a single band capacitor loaded HIS design featuring a miniature unit cell of 0.02λ was proposed. Additionally, the concept of loading HIS unit cell with high capacitance density elements can be realised using interdigital capacitors, which are promising to enhance HIS fractional bandwidth. Interdigital capacitors were first introduced in 1970 by Alley to reduce losses in microwave circuits [83], but early work to implement interdigital distributed elements in HIS design appeared in 2003 by Rogers et al. [84], aimed for frequencies below 3GHz, and proved effective to enhance sheet capacitance and reduce manufacturing cost by more than 50% as compared to multilayer design alternatives. A two layer compact EBG design comprising of interdigital elements was reported in [85] promoting a unit cell size reduction up to 40% but proved too complex. Other work reported the use of interdigital capacitors aiming to study HIS performance features such as sensitivity to angle of incidence [86], uniplanar and rhombic HIS loaded with interdigital elements with significant increase in sheet capacitance [87, 88], dual polarized [89, 61] as well as interdigital electrodes combined with offset vias to increase effective inductance [90]. Finally, in [91] combined methods such as a multilayer split ring resonator loaded with interdigital structure were reported, reducing resonance frequency by 35% within a unit cell of 0.056λ.

Table 2.1 Thesis Miniaturised Single Band HIS Designs Compared to Literature

Reference	Miniaturisation Technique	Substrate ε_r	Substrate Electrical Thickness	Electrical Periodicity	Single Band f_r (GHz)	Single Band %BW
[77]	Fractal Tripoles	2.2	0.034	0.18	9	6
[68]	Slotted Patch+Vias	2.2	0.04	0.12	12	17
[76]	Planar Meander	4.3	0.025	0.06	4.76	10
[71]	Convolution+Vias	3.5	0.012	0.05	1.8	5.2
[75]	Spiral+Vias	2.2	0.039	0.046	2.9	1.7
[78]	6 Layer Patch Shifted	4.3	–	0.017	1.1	10
[82]	Lumped Capacitors	4.3	0.018	0.02	1.55	10
[84]	Checkerboard IDC	4.3	0.023	0.08	2.8	11
[87]	Rohmbic IDC	2.65	0.015	0.073	3	–
[86]	Stripline+ IDC	10.2	0.018	0.06	4.15	2.4
[92]	Mid-Patch + IDC	3	0.013	0.13	2.67	7.2
[61]	2 Layer + IDC	4.3	0.01	0.011	0.064	12
Chapter 5-Design1	SB-SLSP-IDC	4.3	0.03	0.03	1.55	20
Chapter 5-Design2	SB-DLDP-IDC	4.3	0.02	0.037	0.9	15
Chapter 5-Design3	SB-SLDP + IDC	4.3	0.03	0.13	1.5	15

Where research study within the thesis is concerned, lumped and interdigital capacitors loading are the two miniaturisation techniques utilized. Dual band and triple band HIS designs are detailed in Chapter 3 and Chapter 4 employing lumped capacitor loading, an upgraded method based on [82], which is discussed in the next section. While miniaturisation of HIS using Interdigital Capacitor (IDC) has been previously reported, the novelty of work within the thesis stands out with respect to available literature as from the conception, methodological and technical point of view. In Chapter 5, a full analytical study based on an equivalent circuit model is discussed to effectively optimize miniaturised single band HIS featuring three different design prototypes. Subsequently, Chapter 6 and Chapter 7 extends the work to present three novel dual band miniaturised interdigital HIS designs.

Nevertheless, miniaturisation techniques reported in the literature discussed earlier were focused on single band high impedance surfaces. Therefore, they are compared against the single band interdigital HIS designs of Chapter 5, Table 2.1, presenting trade-off to be made between substrate thickness, periodicity and fractional bandwidth; while Chapter 5 presents three miniaturised single band interdigital HIS designs. Design 1: Single Band Single Layer Single Polarized (SB-SLSP) IDC HIS. Design 2: Single Band Dual Layer Dual Polarized (SB-DLDP) IDC HIS, an upgraded version of Design 1 for dual polarization realised from two layer interdigital sheets. Design 3: Single Band Single Layer Dual Polarized (SB-SLDP) IDC HIS. Table 2.1 shows all three designs are planar and provide advantages above techniques implementing vias which complicates the design such as in [68, 71, 75]. Design 1 surpasses all miniaturisation techniques featuring optimum miniaturisation at periodicity 0.03λ with a generous fractional bandwidth of 20% as compared to interdigital HIS [84, 87, 86] and lumped component technique [82], as in Table 2.1. Designs 2 and 3 offer dual polarization, considerable advantage in fractional bandwidth, and compactness as compared to fractional tripoles [77]; for example, while multilayer technique [78] and convoluted structure [71] are electrically smaller, but with added complexity, as in Table 2.1. Moreover, SB-DLDP Design 2 is very much similar to single band 2-Layer IDC HIS reported in [61], which has been implemented for MRI applications; however, complete analytical design methodology with insights on interlayer coupling as well as upgrading the structure to a dual band system is what defines the thesis work originality. Also, SB-SLDP Design 3 is very much similar in structure to single band Mid-Patch IDC HIS [92], but proposed thesis work defines a robust analytical approach as the structure has also been upgraded into dual band.

2.4.2 Multiband compact high impedance surfaces

Interest is growing in multiband communication systems that utilize frequency bandwidth more efficiently, and thus, provide a future alternative to Ultra Wideband (UWB) technology. Requirements for systems with multi functionality renders the design of multiband HIS significant research attention. Different methods have been reported to realise high impedance surfaces featuring multiple resonance performance which fall into 3 main categories; Genetic Algorithms, combined multi-resonant elements and multilayer structures are some being inspired by counterpart frequency selective surfaces.

In [93–95], multiband HIS designs were proposed as originated from a uniplanar unit cell, introducing fractal elements to generate higher order resonances as combined with the Genetic Algorithm (GA) technique to determine optimum unit cell design parameters that meet requirements of resonance frequencies and bandwidth. On the other hand, multiband HIS designs were reported possible by considering stacked capacitive multilayer surfaces operated by altering periodicity and layer spacing to generate required resonance frequencies such as multiple capacitive FSS layers [96]. Also, in [97], double capacitive patch layers connected with multiple vias where reflection phase properties and dual band are mechanically tuned as the vias length and location are varied within the two layer structure instead of conventional unit cell parameters.

Another technique to realise multiband HIS is by implementing multi-resonant elements which traces back to work conducted on frequency selective surfaces such as single layer double square elements [98–100] and multi-ring elements [101] and these concepts have been applied by analogy to multiband HIS design. Examples include wearable textile double square dual band HIS presented for on body communications; planar in [102] and mushroom type in [103]. Moreover, multi-resonant structures based on perturbations were reported for multiband HIS inspired by design guidelines addressed for perturbed dipole FSS elements [104]. Therefore, perturbed dipoles and fractal tri-poles were demonstrated to realise multiband HIS with reflection properties governed by element dimensions [105–107]. In addition, combined resonant elements were reported for dual band HIS such as square ring with internal cross [108], double bow-tie geometry [109, 110] and Jerusalem cross [111]. Other structures were reported such as planar via-less wideband symmetrical multi-hexagonal multiband HIS [112] operating at periodicity in the order of 0.4λ, calculated with respect to an upper resonant frequency of 20GHz. Also, combined double square and double ring elements realising a dual band HIS were reported in [113, 63] for the structure arranged in a checkerboard surface suitable for broadening the bandwidth and designed for radar cross section reduction. Finally, in [115, 116], a dual band HIS was possible by introducing slots within a patch HIS element for reflection phase properties controlled by slot dimensions and location.

Therefore, compact but not miniaturised multiband high impedance surfaces implementing various methods have been observed through reviewing the literature. Some are summarized in Table 2.2 as compared against the thesis contribution in realising miniaturised dual band high impedance surfaces.

Considering dual band HIS discussed in the thesis, two miniaturisation approaches have been presented. First, the lumped component approach is implemented such that HIS unit cell comprises of two identical patch subunit cells concatenated and loaded with surface mount lumped capacitors of unequal values realising a dual band, as discussed in Chapter 3. Chapter 4 presents reduced mutual coupling dual band HIS based on gridded patch subunit cells concatenated and loaded with capacitors of unequal values. While Chapter 6 and

Chapter 7 present three miniaturised dual band HIS structures inspired by concepts discussed in Chapter 3, but implementing interdigital distributed capacitors as the miniaturisation method. Dual Band Single Layer Single Polarized (DB-SLSP) Design 1 is where two HIS subunit cells are concatenated and engineered with interdigital capacitors of different capacitance densities such that dual band is realised as operated for single polarization. Dual Band Dual Layer Dual Polarized (DB-DLDP) Design 2 is where DB-SLSP Design 1 is implemented into 90 degree rotated dual layers, therefore, a dual band HIS suitable for dual polarization. Dual Band Single Layer Dual Polarized (DB-SLDP) Design 3 is novel engineered concatenated subunit cells comprising of a centre patch element miniaturised using interdigital capacitors, printed as a planar single layer and operated as a dual band dual polarized HIS.

Table 2.2 Thesis Miniaturised Dual Band HIS Designs Compared to Literature

Reference	Technique	Substrate			Band 1		Band 2	
		ε_r	$\frac{H}{\lambda}$	$\frac{P}{\lambda}$	f_r (GHz)	%BW	f_r (GHz)	%BW
[102]	Concentric Square	1.38	0.04	0.73	2.45	8.2	5.5	7
[111]	Jerusalem Cross	1.05	0.06	0.65	2.43	8.2	5.72	12
[107]	Perturbed Dipoles	2.2	0.06	0.54	12.6	8.4	15.4	3.58
[106]	Perturbed Dipoles	4	0.05	0.48	8	7.6	14	3
[112]	Multi Hexagonal	3.38	0.05	0.41	15.3	11	20.65	3.9
[95]	Genetic Algorithm	2.98	0.38	0.2	8	67.2	23	18.8
[95]	Genetic Algorithm	13	0.02	0.19	1.58	4.43	1.96	2.2
[110]	Bowtie Patch	4.4	0.03	0.19	1.54	11	2.5	4
Chp. 3	2-Patch+Capacitors	4.3	0.01	0.03	0.43	2.4	0.9	0.6
Chp. 3	2-Patch+Capacitors	4.3	0.02	0.09	0.43	4.5	0.9	1.5
Chp. 4	2-Gridded Patch+ Capacitors	4.3	0.02	0.09	0.43	1.4	0.9	2.2
Chp. 6	Design 1 DBSLSP-IDC	4.3	0.046	0.15	0.9	13.4	1.8	2
Chp. 7	Design 1 DBSLSP-IDC	3.38	0.028	0.18	1.5	9.4	2.5	3
Chp. 7	Design 2 DBDLDP-IDC	3.38	0.028	0.18	1.5	8.5	2.5	2.5
Chp. 7	Design 3 DBSLDP-IDC	4.3	0.031	0.13	1	9.5	1.5	2

Table 2.2 summarizes all thesis proposed designs as compared against available literature where electrical thickness and periodicity are calculated with respect to highest band wavelength. It can be observed that optimum compactness of periodicity miniaturised to 0.03λ utilized in lumped component loading, as detailed in Chapter 3, and 0.09λ in gridded patch lumped component loaded HIS is detailed in Chapter 4, but at the expense of degraded fractional bandwidth which is contributed to equivalent series resistor associated with lumped components, substrate losses and close band separation. Whereas a wider fractional band-

width is observed in alternative elements such as Concentric Square [102], Jerusalem Cross [111], Perturbed Dipoles [107, 106] and Multi Hexagonal [112]; however, HIS periodicities are in the order of 0.7λ to 0.4λ and the extra bandwidth is aided by wider band separation in contrary to lumped component miniaturised designs proposed. On the other hand, miniaturised interdigital HIS dual band Designs 1, 2 and 3, presented in Chapter 6 and Chapter 7, offer improvement in fractional bandwidth, but miniaturisation of the unit cell is limited in the order of 0.18λ to 0.13λ where unit cell size is of significant importance to engineer interdigital elements that realise the required capacitance. Unit cell size and operational bandwidth observed in interdigital designs are very much comparable to available techniques such as Genetic Algorithm [95] and Bowtie Patch design [110] where trade-off's are recommended to be made between manufacturing constraints, bandwidth, size and complexity.

2.4.3 Inter-unit cell mutual coupling in dual band HIS

Miniaturised dual band HIS has been proposed in the thesis by concatenating two subunit cells comprised of planar capacitive patch elements where each is unequally loaded by a high capacitance density element utilizing available miniaturisation techniques either lumped component, Chapter 3, or distributed interdigital capacitance loading, Chapter 6. Therefore, each subunit cell is regarded as a resonator where inter element coupling is expected and possesses significant design limitation as dual band miniaturised HIS is concerned. Inter unit cell mutual coupling is a crucial subject matter that has been extensively discussed within the thesis and contributes to the supreme novelty of the conducted research study. According to the literature, methods to deal with inter unit cell mutual coupling in multiband HIS design is only limited to a couple of publications that deal with mutual coupling as with respect to frequency selective surface and metamaterial absorber designs. In [80], a two layer dual band frequency selective surface was proposed implementing lumped component loading within a ring slot resonator structure, being the top layer, where each adjacent unit cell was placed in a Faraday cage structure, made of closely spaced metallic vias surrounding each unit cell, in order to isolate adjacent unit cells operating at different frequencies. However, the level of band isolation was not clearly detailed and presence of vias always brings design complexity meaning planar HIS are preferable; such that this method has not been favourable to use. In [117], a single band metamaterial absorber based on a square ring FSS element was analysed and designed using an analytical circuit model approach. In order to determine circuit model components and resonance frequency, surface currents developed in each unit cell within the periodic structure were predicted and mutual coupling induced between adjacent unit cells was considered to calculate coupling capacitance based on coupled line theory [118]. Authors of this publication suggested that this method can be applied to other FSS geometries.

However, it was also suggested that prior knowledge of surface current direction of flow within the periodic structure is essential, and therefore, provides significant design constraints if considering complex unit cell geometries such as multi resonant elements.

Research study conducted within this thesis provides unprecedented original new techniques on dealing with inter unit cell mutual coupling. Chapter 4 presents the use of metallic strips incorporated within a lumped capacitor loaded patch HIS unit cell such that the inductive metallic lines act as guard conductors and provide isolation between adjacent subunit cells where inter unit cell mutual coupling is significantly reduced and each band is generated by corresponding to a capacitively loaded subunit cell. A dual band and triple band miniaturised HIS is demonstrated, while in Chapter 6, dual band miniaturised HIS using interdigital capacitors are analysed in terms of factors that influence mutual coupling between subunit cells. It has been found that inter unit cell mutual coupling is generated due to capacitive (electric) and inductive (magnetic) factors governed by unit cell geometry such as periodicity, interelement spacing, substrate permittivity and thickness demonstrated to have influence on reflection phase properties of the HIS. Therefore, in Chapter 7, a novel approach to predict expected percentage shift in resonance frequency from design requirement, due to inter unit cell mutual coupling, is proposed as based on multiple linear regression analysis. A mathematical model, as function of unit cell parameters contributing to inter unit cell mutual coupling, is developed such that a simple design procedure is achieved in designing dual band miniaturised HIS incorporating interdigital capacitors. The aim of this model is to provide a straightforward simplistic design approach where two single band miniaturised interdigital HIS structures are modelled at design frequencies that take inter unit cell mutual coupling into account, following design procedures detailed in Chapter 7. Furthermore, the developed multiple regression mathematical models are validated through three different original dual band HIS design prototypes also detailed in Chapter 7.

2.5 Measurement Techniques

This section details basic guidelines and concepts in antenna and HIS measurements as applicable to work conducted in subsequent technical chapters within the thesis.

2.5.1 Antenna return loss measurements

To assess the performance of an antenna , it is important to measure how well the device is matched to the source. A perfect match antenna will accept all the input power efficiently such that maximum power is delivered and nothing is reflected back to the generator. This is determined by considering measurements of input reflection coefficient at the antenna input impedance point. An ideal match is when linear magnitude of input reflection coefficient is zero ($(|\Gamma_{\text{in}}| = 0)$), but practically losses are inevitable where an upper limit of reflection coefficient log-magnitude up to ($|\Gamma_{\text{in}}| \leqslant -10$ dB) is acceptable. Antenna matching has different terminologies such as reflection/transmission characteristics, S-parameters ($S_{11}, S_{21}, S_{22}, S_{12}$) or Return Loss (RL), which are all interrelated. This thesis deals with validating antenna match as integrated over a HIS, therefore, input reflection coefficient magnitude ($|\Gamma_{\text{in}}| = 20\log(|S_{11}|)$) is of interest conducting One-port measurement using vector network analyzer.

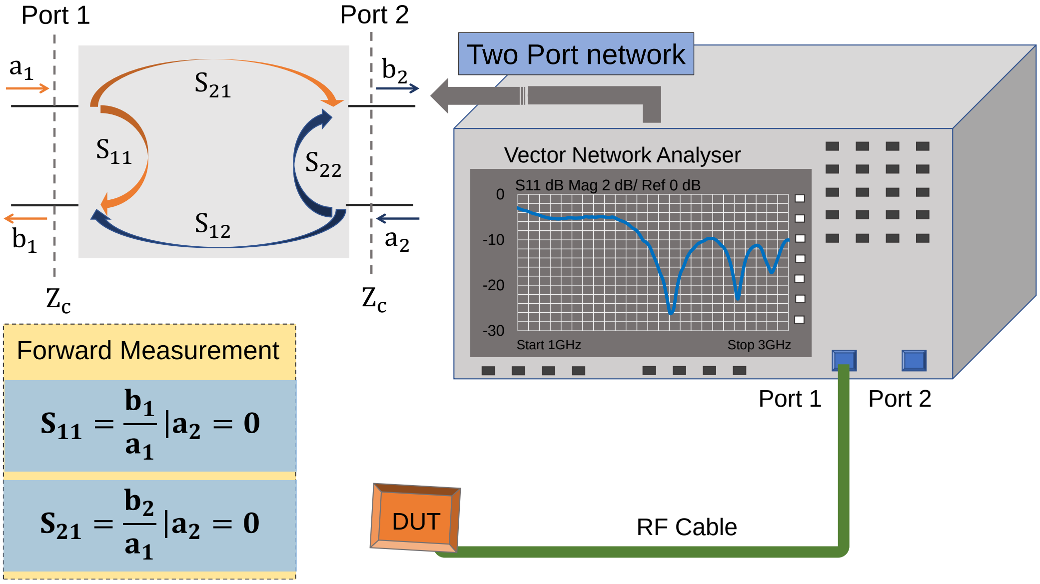

Fig. 2.6 Return loss 1-port measurement setup.

A Vector Network Analyzer (VNA) is an instrument capable of measuring the magnitude and phase of S-parameters to test RF and Microwave networks such as filters, amplifiers, antennas and couplers. One port or two port measurements are possible depending on the application. A schematic diagram of one-port measurement setup is presented in Fig. 2.6. Success of the measurement depends on maintaining accuracy level and minimizing system errors. Errors during measurement can be classified into two groups. The first source of errors can be attributed to measurement uncertainty such as noise in the device, uncertainty in the cables, repeatability effects, and thermal drift which are classified as “random measurement errors” [119]. In order to minimize the random measurement errors, the equipment must be handled with care as well as the proper choice of clean and undamaged cables. Other form of errors are called “systematic measurement errors” which are inevitable and occur because of imperfection of the device especially connections, system leakage or parasitic coupling as well as errors from cable characteristics, test fixtures and adapters. Systematic measurement errors are taken into account by calibrating the VNA before measurements [119]. The VNA, through calibration, calculates corresponding error terms based on calibration standards compatible with the instrument and applicable to the aimed measurement. During calibration, defined standards are of well known response such that these error terms can be calculated and, therefore, compensated when performing the measurement. An Open Short Match (OSM) calibration method is considered to VNA Port 1 before it is connected to Device Under Test (DUT) for the reflectivity measurements conducted throughout the thesis.

2.5.2 Antenna gain measurements

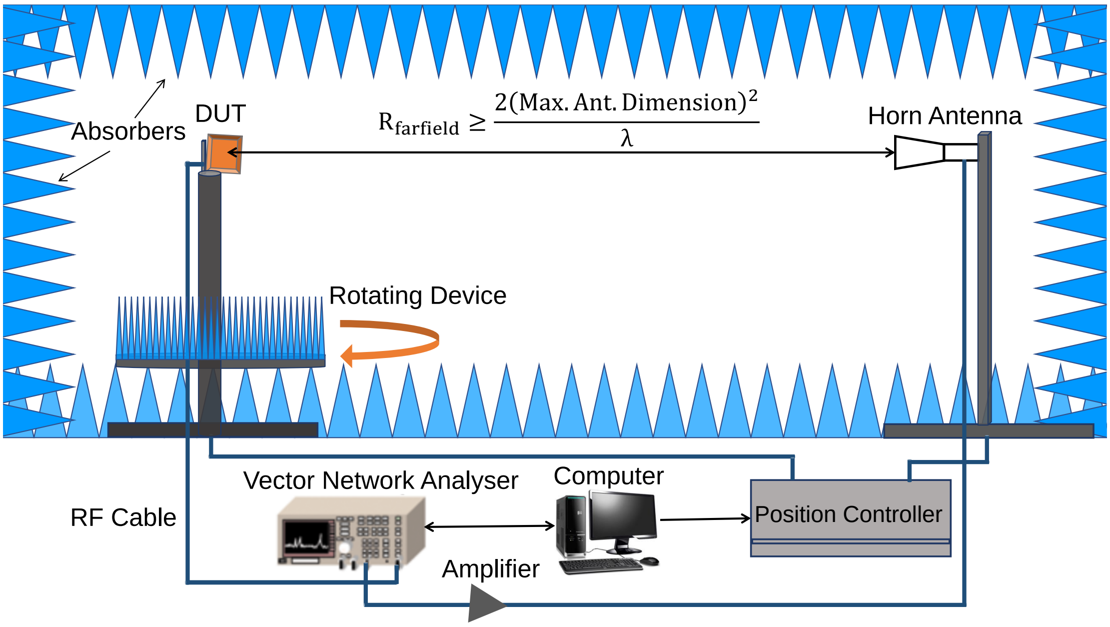

Fig. 2.7 Gain pattern measurement setup.

Another aspect of significant importance in characterizing antenna performance are measurements of antenna gain pattern. Antennas are not expected to encounter uniform radiation in all directions. Specifically, when HIS is implemented as a ground plane for a given antenna, optimum antenna/HIS performance is realised by achieving a good match and improved antenna gain in bore-sight directions and suppressed side-lobes. Measurements of antenna radiation pattern are typically carried out in an indoor antenna range called an Anechoic

Chamber offering controlled test conditions as compared to outdoor measurements. An Anechoic chamber is a large room lined with electromagnetic absorbing material having a pyramid shape structure with the aim of minimizing environmental effects while conducting radiation pattern measurements. Measurements of antenna gain pattern are conducted within an Anechoic chamber setup accompanied with test equipment as demonstrated in Fig. 2.7. The Anechoic chamber used is large enough to enable gain pattern measurements from 300 MHz to 18 GHz. A reference standard HF 906 horn antenna operating from 1GHz to 18GHz is used during the measurements. The Device Under Test (DUT), mounted above a rotating positioning system, is aligned with the reference horn antenna at a distance sufficient enough to allow far field radiation pattern measurements. A programmed network analyzer sources an RF transmit signal amplified where Co-poplar E and H plane gain measurements are conducted. The device under test gain patterns are normalized with respect to a reference antenna of known gain and received power.

2.5.3 NRL Arch reflectivity measurements

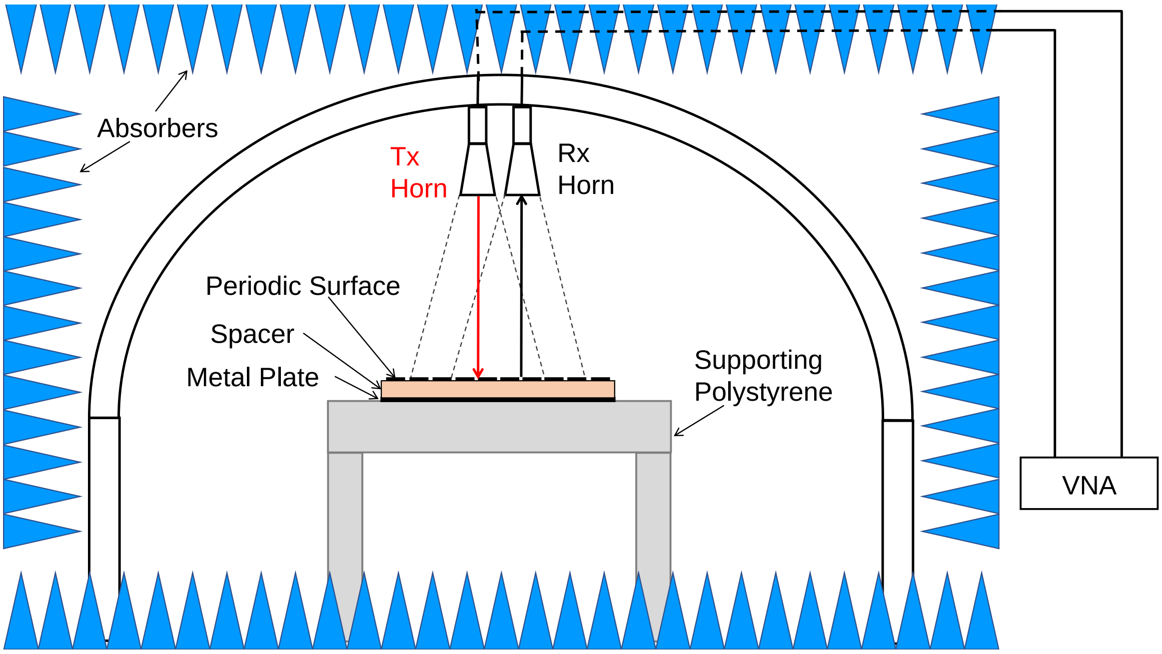

Fig. 2.8 NRL Arch reflectivity measurement setup at normal incidence.

Measurements of reflection coefficient in periodic structures is conducted using the well known NRL Arch, which was first developed for the Naval Research Laboratory (NRL) by the Massachusetts Institute of Technology in 1940s [120]. NRL Arch was mainly used in radar absorbers testing over a wide range of microwave frequencies. The setup for the measurement system is detailed in Fig. 2.8 where the Arch is secured to two horn antennas, one is a transmitter (Tx) and the other is a receiver (Rx). The presence of the Arch allows measurements of samples at difference angles of incidences, which are not of interest in this thesis and the current shown setup is for normal incidence mode where the two horn antennas can be placed as close as their width aperture permits, pointing towards the sample under test. The sample of interest is the High Impedance Surface (HIS), which comprises of periodic metallic surface, supporting dielectric material and a metal plate. Horn antennas are placed within the far field range with respect to sample under test. Therefore, the sample size matters in the measurements and must be at least one wavelength of the lowest operating frequency such that the half power beamwidth of horn antennas are not conflicted and are within the range where diffraction of surface waves from the edges of finite surfaces are picked by the horn antennas. The horn antennas used in the measurements are operated within a bandwidth of 2-18 GHz, therefore, samples are best designed within this frequency range such that mismatch errors are minimized. Measurements are conducted within an Anechoic chamber such that reflections, refractions and interference are minimized. The two horn antennas are controlled by a two port Vector Network Analyser (VNA). However, before any reflectivity measurement is conducted, the VNA must be calibrated. Calibration of the NRL Arch system is done by performing reflectivity measurements for a metal plate of the same size as the sample with both placed at the same height/thickness intended for the sample such that both are measured at the same level where a reference plane is established for consistency of measurements.

2.6 Conclusion

A full literature review on periodic electromagnetic structures has been provided such that different terminologies are distinguished and the concept of high impedance surfaces is highlighted. Thereafter, theory and principles of high impedance surfaces as regard to surface wave suppression and constructive in-phase reflection properties have been detailed. A comprehensive literature review on miniaturisation techniques, methods to realise multiband compact HIS structures and advances on managing inter unit cell coupling has been extensively discussed and compared against proposed research study within the thesis. Finally, antenna-HIS return loss and radiation pattern measurement setups as well as HIS reflectivity measurements using NRL arch have been explained as related to experimental work conducted within the thesis.

Chapter 3

Dual Band High Impedance Surface Miniaturised By Lumped Capacitors

3.1 Introduction

This chapter investigates miniaturised dual band High Impedance Surface (HIS) design by incorporating surface mount lumped capacitor loading. Design concepts and detailed parametric study regarding miniaturised dual HIS are presented. Limitations and constraints due to inter unit cell mutual coupling are also addressed.

3.2 Simple Patch Miniaturised HIS

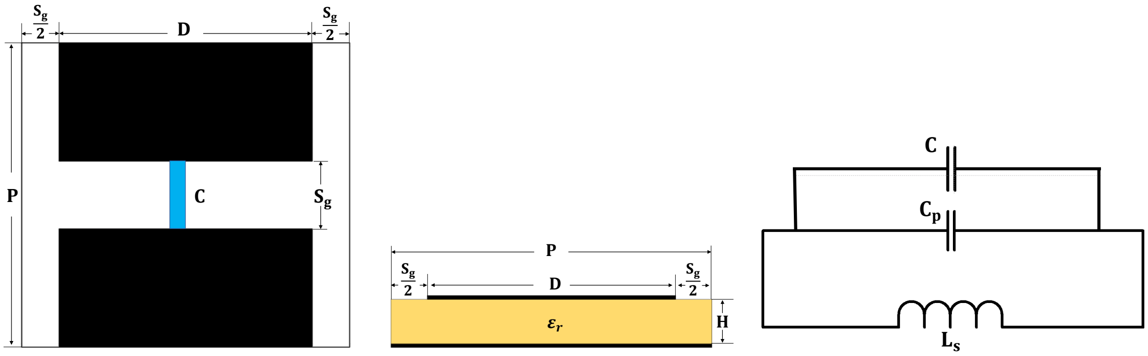

(a) Top View (b) Side View (c) Equivalent Circuit Model

Fig. 3.1 Capacitive Patch HIS loaded with lumped capacitor.

A simple single band planar capacitive patch High Impedance Surface (HIS) loaded with lumped capacitor is presented in Fig. 3.1. The HIS structure, excluding the surface mount capacitor (C), comprises of capacitive FSS-based layer which is supported on electrically thin substrate and backed by metal as shown in , Fig. 3.1a and Fig. 3.1b respectively. For electrically small unit cell, single band HIS structure equivalent circuit model, which is demonstrated in Fig. 3.1c, comprises of mutual capacitance ($\mathrm{C_p}$) in parallel with loaded capacitance (C) as well as substrate inductance $\mathrm{L_s}$ which is the equivalence of a shorted electrically small transmission line section.

Therefore, miniaturised simple patch resonant frequency is given by:

$$\mathrm{f_{r(patch)}} = \frac{1}{2\pi\sqrt{(\mathrm{C}+\mathrm{C_p})\mathrm{L_s}}} \tag{3.1}$$

Mutual capacitance ($\mathrm{C_p}$), developed between patch gap, is function of HIS unit cell periodicity (P), interelement spacing ($\mathrm{S_g}$), and dielectric permittivity (ε_r) [121] :

$$\mathrm{C_p} = \varepsilon_0 \varepsilon_{eff} \frac{2\mathrm{P}}{\pi} \log \frac{1}{\sin\left[\dfrac{\pi \mathrm{S_g}}{2\mathrm{P}}\right]} \tag{3.2}$$

where $\varepsilon_{eff} = \frac{\varepsilon_r + 1}{2}$ is the effective permittivity.

and substrate inductance ($\mathrm{L_s}$) for an electrically thin substrate of thickness (H) is given by:

$$\mathrm{L_s} = \mu_0 \mu_r \mathrm{H} \tag{3.3}$$

Therefore, if lumped capacitance does not exist, miniaturisation of capacitive patch HIS unit cell involves increasing substrate thickness and unit cell periodicity such that inductance ($\mathrm{L_s}$) and mutual capacitance ($\mathrm{C_p}$) increases for the resonance frequency reduces. However, this leads to a bulky HIS with electrically large unit cell which invalidate lumped circuit model approach and breaches grating lobe limit. By loading the patch unit cell element with lumped reactive capacitor (C), within gap ($\mathrm{S_g}$), it is possible to significantly increase the effective sheet capacitance of the structure and considerably reduce the resonance frequency while maintaining a very thin substrate. Therefore, the unit cell size can also be drastically reduced since the mutual capacitance is insignificant as compared to the loaded component where a unit cell size of 0.02λ was demonstrated in [82] for a single band HIS. This approach is implemented in realising dual band miniaturised HIS structure by concatenating two subunit cell HIS of this type as will be discussed next.

3.3 Lumped Component Loaded Dual Band HIS

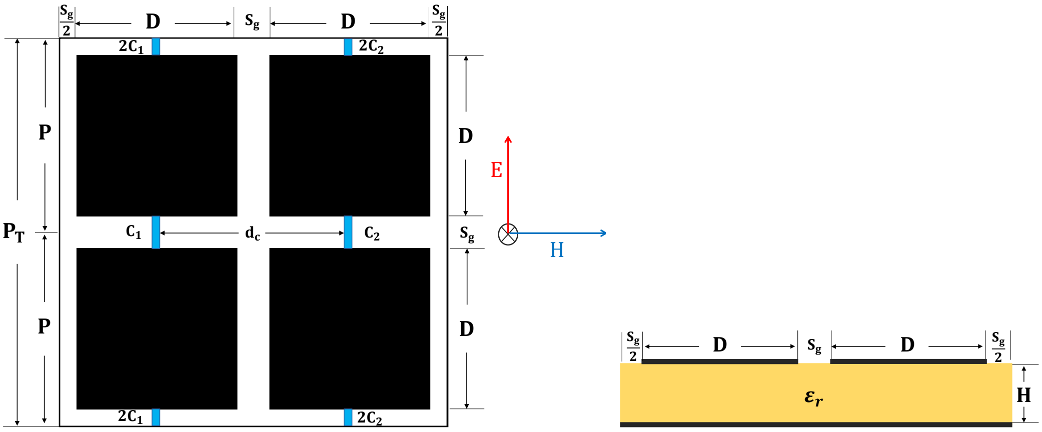

(a) Top View (b) Side View

Fig. 3.2 Dual band miniaturised HIS using lumped surface mount capacitors.

A miniaturised dual band High Impedance Surface (HIS) is presented in Fig. 3.2. The HIS unit cell, of total periodicity (P_T), constitute of two adjacent subunit cells each loaded by two different lumped capacitances C_1 and C_2 which are spaced by distance d_c, Fig. 3.2a. Setting $C_1 > C_2$; C_1 contributes to lower band resonance (Band 1) while upper band resonance (Band 2) is generated by subunit cell loaded with C_2.

Each band resonance is absolutely controlled by the value of associated lumped capacitor where the unit cell periodicity is expected to have least effect and can be chosen significantly electrically small such that an optimum miniaturised HIS unit cell is realised. However, this is only possible up to a certain extent where significant reduction of periodicity renders lumped components less effective, also, degrading the HIS fractional bandwidth. An example is presented for a case study where a miniaturised dual band HIS Reference Design is modelled to operate at 430 MHz and 900 MHz within a periodicity of 30 mm and substrate thickness 6.4 mm. A two step analysis is conducted in order to investigating the correlation between varying unit cell periodicity, substrate thickness and loaded capacitors. In the first case case, Case 1, only unit cell periodicity is reduced from 30 mm to 10 mm, also, C_1 and C_2 are adjusted such that the resonance frequencies does not change. In the second case, Case 2, both periodicity and substrate thickness are reduced to 10 mm and 3.2 mm respectively while C_1 and C_2 are also tuned such that resonance frequencies are maintained at 430 MHz and 900 MHz. Table 3.1 presents design parameter values considered for Reference Design, first case (Case 1) and second case (Case 2). The three designs are modelled on CST Microwave Studio and reflection phase properties, observed at normal incidence, are analysed.

Table 3.1 430-900 MHz Miniaturised HIS Optimized For Reduced Periodicity

HIS Unit cell Parameters	Reference Design	Case 1	Case 2
Substrate material	FR4	FR4	FR4
Substrate permittivity (ε_r)	4.3	4.3	4.3
Interelement spacing(S_g)	1 mm	1 mm	1 mm
Substrate thickness(H)	6.4 mm	6.4 mm	3.2 mm
Periodicity(P_T)	30 mm	10 mm	10 mm
Electrical periodicity w.r.t Band 2	0.09	0.03	0.03
Band 1 capacitance (C_1)	19 pF	19 pF	40 pF
Band 2 capacitance (C_2)	6.5 pF	12 pF	16 pF
Distance between lumped components(d_c)	15 mm	5 mm	5 mm
±90° Band 1 bandwidth	4.5%	5.5%	2.4%
±90° Band 2 bandwidth	1.5%	0.3%	0.6%

Fig. 3.3 presents Reference Design reflection phase plot which demonstrates that the miniaturised dual band HIS resonates at 430 MHz and 900 MHz as designed on a unit cell periodicity of 30 mm, substrate thickness of 6.4 mm, capacitances ($C_1 = 19$ pF) and ($C_2 = 6.5$ pF). For dual band HIS Case 2, unit cell periodicity is reduced from 30 mm to 10 mm while maintaining substrate thickness at 6.4 mm, an increase in both band resonance frequencies is expected. Therefore, capacitances C_1 and C_2 are increased in an attempt that dual band resonances of 430 MHz and 900 MHz are not changed. This is observed possible for the lower band but not for the upper band which undergoes significant reduction in fractional bandwidth degrading from 1.5% to 0.3% as HIS (Reference Design) reflection phase is compared to that of HIS (Case 1), Fig. 3.3. As the result of significant mutual coupling between the bands, it is not possible to tune the upper band resonance frequency to 900 MHz and the degraded 0.3% fractional bandwidth is of no particular use in communication systems which renders the design in effective.

Thereafter, in dual band HIS design Case 2, unit cell periodicity is reduced from 30 mm to 10 mm as well as substrate thickness is reduced from 6.4 mm to 3.2 mm. In order to account for the effect of periodicity and substrate thickness reduction, lumped components C_1 and C_2 are increased by around a factor of 2 such that dual band frequencies are maintained to 430 MHz and 900 MHz. Comparing reflection phase plots, Fig. 3.3, both dual band HIS Reference Design and HIS Case 2 operate at the same frequencies, however, at the expense of around 50% reduction in HIS ±90°bandwidth in both Band 1 and Band 2, which is expected due to the reduction in substrate thickness.

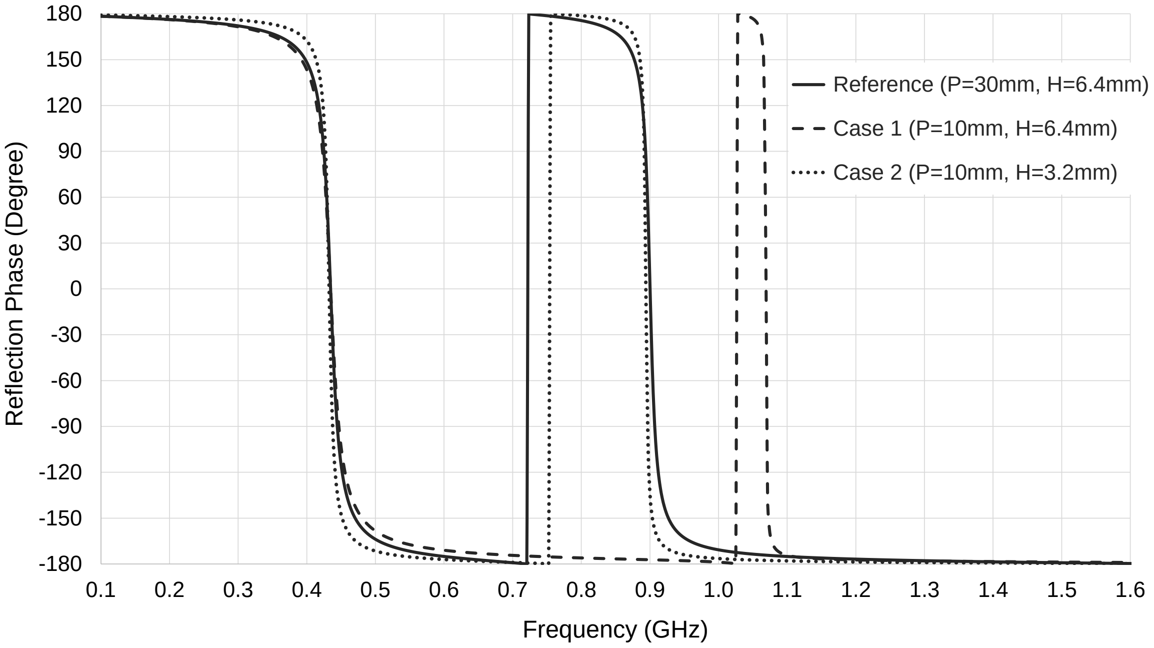

Fig. 3.3 Lumped capacitor loaded dual band miniaturised HIS simulated reflection phase. Design optimized for reduced periodicity. Unit cell parameters detailed in Table 3.1.

In conclusion, a dual band HIS design is possible at miniature electrical periodicity in the order of $\frac{\lambda}{70}$, for a 10 mm unit cell electrically calculated with respect to the lower band resonance frequency of 430 MHz. However, there is a limitation to the reduction of HIS unit cell periodicity such that variation of lumped capacitors are inefficient and the high band cannot be realised. Reducing the HIS unit cell periodicity as associated with reduced HIS substrate thickness make it possible to give more freedom when varying the lumped capacitors such that design frequencies are met. Nevertheless, this is at the expense of reduced operational bandwidth and the requirement of a very large lumped capacitors values, which will be no problem if practically possible. Next is parametric analysis of the dual band design of interest, Fig. 3.2, providing some design guidelines and highlighting mutual coupling.

3.4 Parametric Study Lumped Capacitors Dual Band HIS

In this section, parametric Study is considered to investigate the effect of varying dual band miniaturised HIS unit cell parameters while analysis on variation of resonance frequencies, operational bandwidth and percentage band separation in dual band are discussed. Parameters of interest are; substrate permittivity (ε_r), substrate thickness (H), lumped component separation distance (d_c), capacitors (C_1, C_2) and unit cell periodicity (P). A dual band HIS designed at 430 MHz and 900 MHz of unit cell parameters as in Table 3.2 is considered as the Reference design while varying each of design parameters individually.

Table 3.2 Dual Band Lumped Capacitor Loaded HIS - Reference Design

Unit Cell Parameters	Values
Substrate material	FR4
Substrate permittivity (ε_r)	4.3
Interelement spacing(S_g)	$P/30$
Substrate thickness(H)	6.4 mm
Periodicity(P)	30 mm
Electrical periodicity w.r.t Band 2	0.09
Band 1 design frequency	430 MHz
Band 2 design frequency	900 MHz
Band 1 capacitance (C_1)	19 pF
Band 2 capacitance (C_2)	6.5 pF
Distance between lumped components(d_c)	$0.5P_T$
±90° Band 1 bandwidth	4.5%
±90° Band 2 bandwidth	1.5%

3.4.1 Substrate permittivity (ε_r) effect

The effect of substrate permittivity is investigated for $(\varepsilon_r = 1, 4.3, 10)$. The HIS unit cell parameters and lumped capacitors are fixed as detailed in Table 3.2. Simulated reflection phase graphs, observed at normal incidence, are presented in Fig. 3.4. Variation of substrate permittivity will not have major effect on the dual band performance since the unit cell is dominated by the lumped capacitors and the results prove that. However, it can be observed that as the permittivity is increased $(\varepsilon_r = 1, 4.3, 10)$, the resonance frequency in both bands is reduced, but, Band 2 undergoing more significant reduction in the resonance frequency. This is due to the fact that mutual capacitance (C_p) is increased as permittivity increases, Eq. (3.2). In each subunit cell, the lumped capacitor is effectively in parallel with the mutual capacitance (C_p) which is generated between patch gap (S_g). For the lower band, increasing C_p will not have significant effect on Band 1 resonance frequency because $(C_1 \gg C_p)$. As for the upper band, when permittivity is increased mutual capacitance is comparable to lumped capacitance $(C_2 < C_1)$ and therefore have notable impact on Band 2 resonance frequency.

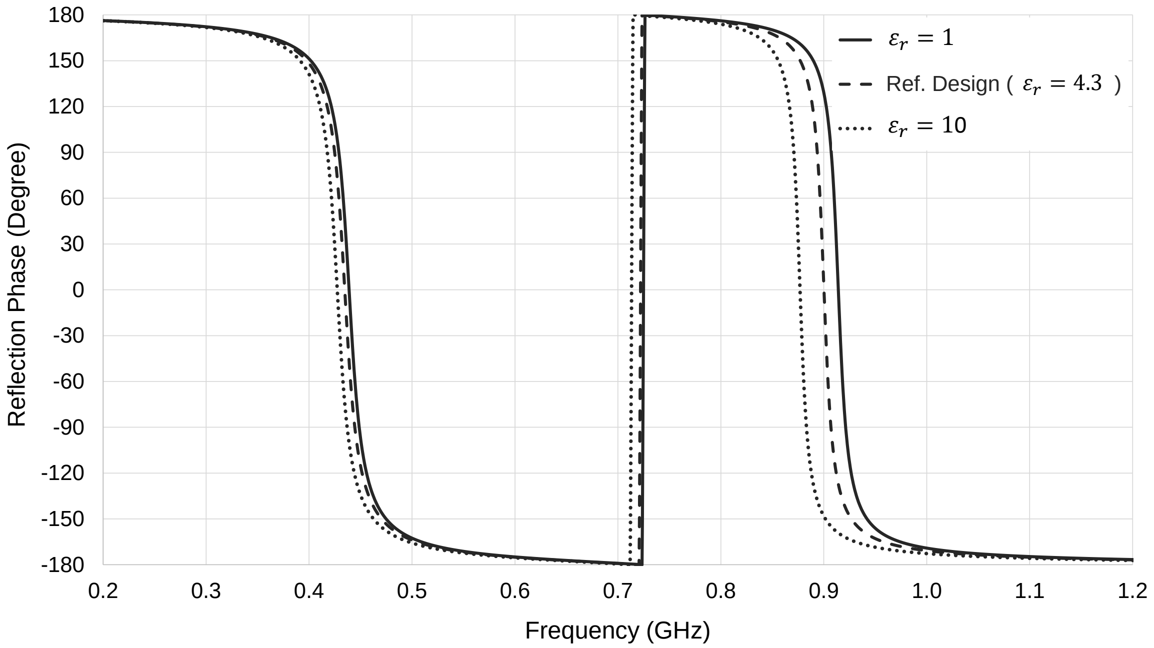

Fig. 3.4 Simulated reflection phase of lumped capacitor loaded dual band HIS. Parametric study on permittivity (ε_r). Unit cell parameters are fixed as of Ref. Design, Table 3.2.

3.4.2 Component separation distance $(\mathrm{d_c})$ effect

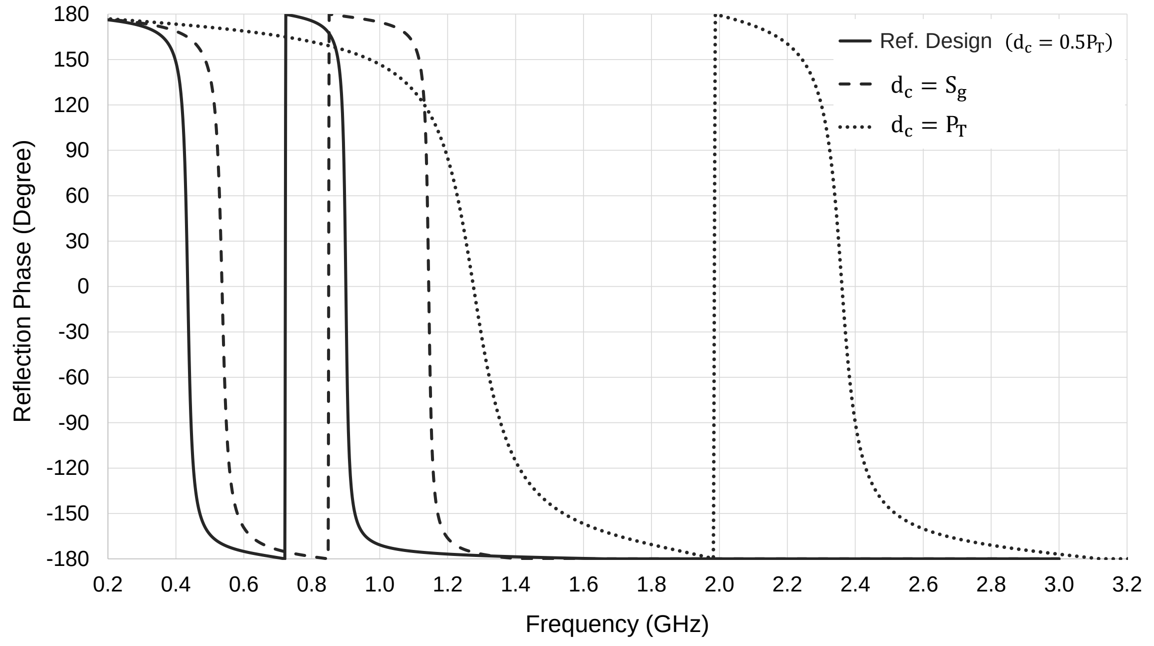

Fig. 3.5 Simulated reflection phase of lumped capacitor loaded dual band HIS. Parametric study on separation distance $(\mathrm{d_c})$. Unit cell parameters are fixed as of Ref. Design, Table 3.2.

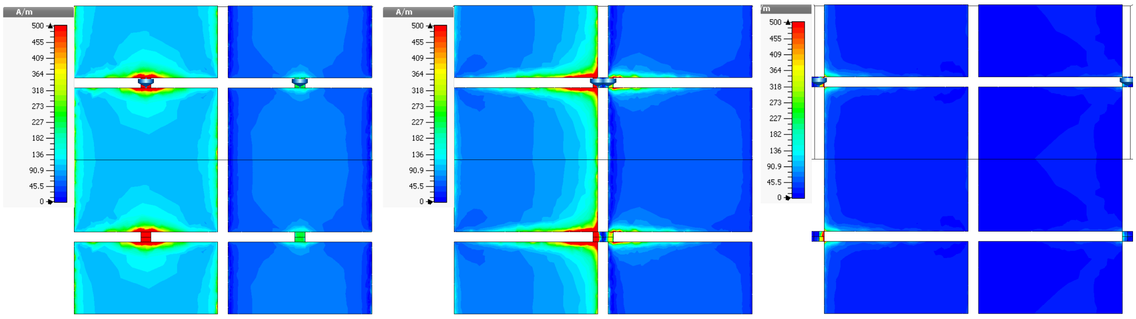

(a) $d_c = 0.5P_T$ (b) $d_c = S_g$ (c) $d_c = P$

Fig. 3.6 Lower band surface currents. Varying capacitors separation distance (d_c).

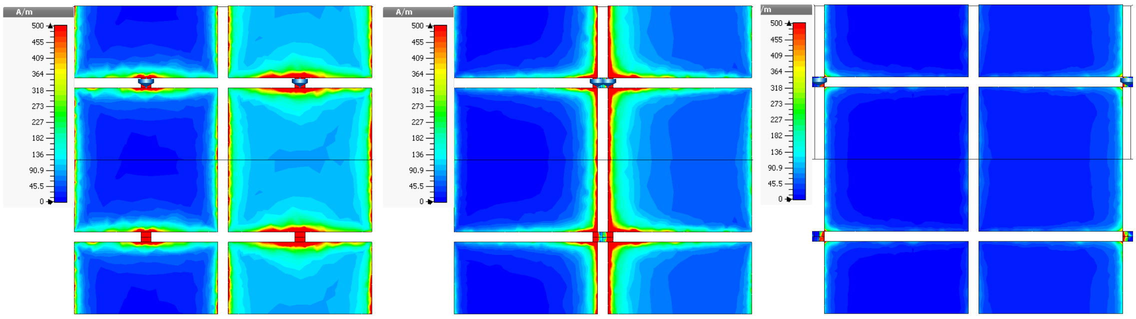

(a) $d_c = 0.5P_T$ (b) $d_c = S_g$ (c) $d_c = P$

Fig. 3.7 Upper band surface currents. Varying capacitors separation distance (d_c).

Miniaturisation of dual band HIS using lumped capacitors, Fig. 3.2a, is optimum when capacitors' separation distance is $(d_c = 0.5P)$. To demonstrate the concept, a parametric study varying $(d_c = 0.5P_T, S_g, P_T)$ is conducted where reflection phase and surface currents are observed and presented in Fig. 3.5, Fig. 3.6 and Fig. 3.7. When the capacitors are loaded within the center of the unit cell $(d_c = 0.5P_T)$, the HIS resonates at 430 MHz and 900 MHz, Fig. 3.5, and the surface currents are evenly distributed within each subunit cell where the capacitors significantly contribute to the dual band HIS resonance, as shown in Fig. 3.6a and Fig. 3.7a, for the lower and upper bands respectively. However, loading capacitors C_1 and C_2 closely spaced within the unit cell, at a distance equivalent to the interelement spacing $(d_c = S_g)$, has the effect to increase mutual interaction between the lumped capacitors and reduces the effectiveness of capacitive loading within each subunit cell; where the resonance frequency, in both bands, is increased to 540 MHz and 1140 MHz as shown in Fig. 3.5. Furthermore, when the components are spaced by $(d_c = S_g)$, surface currents observed in the lower band, Fig. 3.6b, and the upper band, Fig. 3.7b, demonstrate that the current distribution is concentrated within the intelement spacing and is unevenly distributed within the patch unit cell where the capacitors are; therefore, miniaturisation is less effective, which justifies the corresponding increase in each band resonance frequency. On the other hand, loading capacitors C_1 and C_2 at the edge of the unit cell, within a spacing $(d_c = P_T)$, has rendered miniaturisation the least effective. Observing reflection phase plots in both bands, resonance frequencies are increased to 1280 MHz and 2400 MHz as shown in Fig. 3.5. Moreover, surface currents which are observed in the lower band, Fig. 3.7b, and the upper band, Fig. 3.7c, demonstrate the effect of locating the capacitors within a distance $(d_c = P_T)$. It can be observed that, in both bands, each subunit cell conducts insignificant current amplitude where the surface currents are concentrated at the edges of the unit cell rendering the loaded capacitors the least effective, which also explains the corresponding significant increase in the lower band and upper band resonance frequencies as observed in reflection phase plot demonstrated in Fig. 3.5. This leads to the conclusion that for optimal miniaturisation of dual band HIS, lumped capacitors should be loaded within the centre patch of each subunit cell such that capacitors are symmetrical and well balanced within the periodic structure.

3.4.3 Band 1 capacitance (C_1) effect

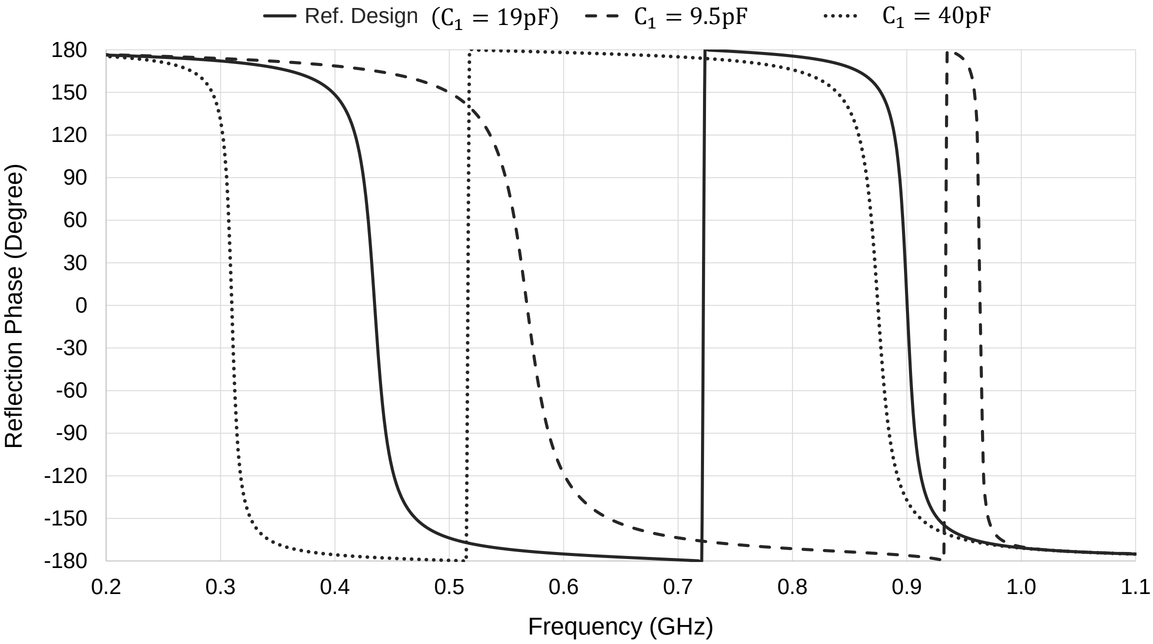

Fig. 3.8 Simulated reflection phase of lumped capacitor loaded dual band HIS. Parametric study on Band 1 capacitor (C_1). Unit cell parameters are fixed as of Ref. Design, Table 3.2.

The lower band (Band 1) is controlled by the value of capacitance (C_1) loaded within the subunit cell on the left, Fig. 3.2a, and it is assumed to possess no impact on the upper band

(Band 2). However, a parametric study was conducted on C_1, as it is reduced by a factor of 2 and increased by a factor of 2 with respect to reference design modelled to operate at 430 MHz and 900 MHz and whose dimensions are fixed as in Table 3.2, proves otherwise. Fig. 3.8 shows simulated reflection phase plots, observed at normal incidence, to demonstrate the effect of lower band capacitance (C_1) on both bands' resonance frequencies and fractional bandwidth. As C_1 is reduced from 19 pF to 9.5 pF, lower band resonance frequency increases by 30% while $\pm 90^\circ$ bandwidth is increased from 4.5% to 6.6%. On the other hand, as C_1 is increased from 19 pF to 40 pF, lower band resonance frequency drops by 30% associated by reduction in $\pm 90^\circ$ bandwidth from 4.5% to 3%. Moreover, varying lower band capacitance (C_1) has an undesired impact on the upper band resonance frequency which is most observed when C_1 reduces from 19 pF to 9.5 pF causing upper band resonance frequency to increase by 7% with respect to reference design, also associated with significant loss in $\pm 90^\circ$ bandwidth which is reduced from 1.5% to 0.4%. This is the optimum value C_1 can be reduced to while Band 2 still exists.

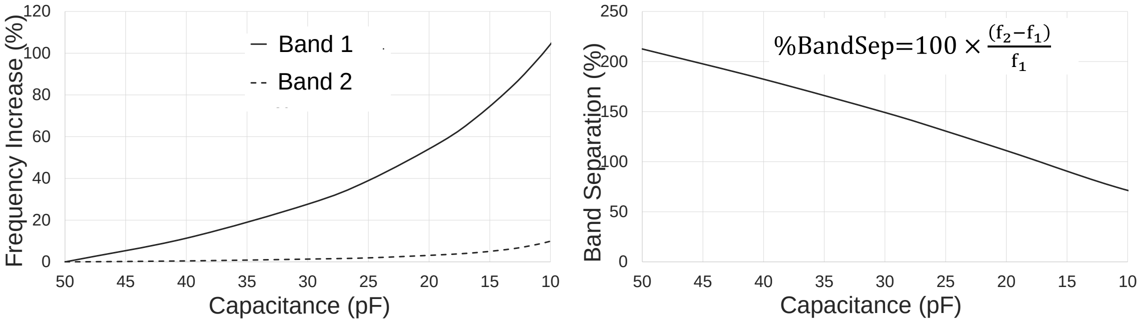

(a) Percentage Frequency Increase

(b) Band Separation

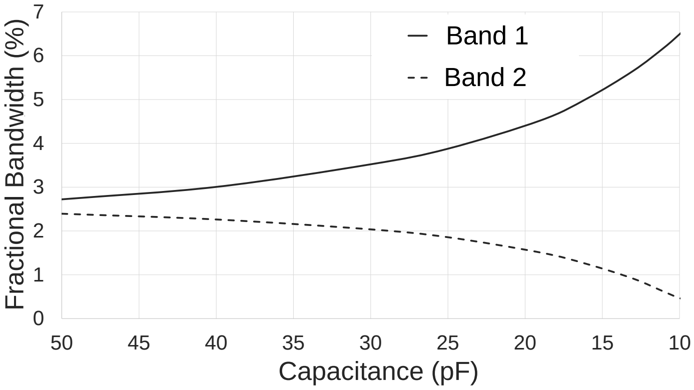

(c) Fractional Bandwidth

Fig. 3.9 Band 1 capacitance (C_1) effect on resonance frequency, band separation and fractional bandwidth. Miniaturised dual band HIS dimensions are fixed as in Table 3.2.

Dual band miniaturised HIS dimensions are fixed, as in Table 3.2, while the effect of Band 1 capacitance (C_1) is further investigated. Reducing C_1 from 50 pF to 10 pF, observations on Band 1 and Band 2 percentage resonance frequency change, percentage band separation and fractional bandwidth are made. Fig. 3.9a presents percentage increase in resonance frequency in both bands with respect to reference frequency when $(C_1 = 50\text{ pF})$. As expected, Band 1 resonance frequency is dominated by variations of C_1, increasing as C_1 reduces. However, impact of C_1 on Band 2, caused by inter unit cell mutual coupling, is significant for a frequency deviation of 10% as C_1 approaches C_2, narrowing the upper band fractional bandwidth to 0.5%. Corresponding variation in fractional bandwidths for both bands as C_1 increases are presented in Fig. 3.9c which demonstrates that Band 1 fractional ±90° bandwidth is enhanced by the reduction of C_1 while Band 2 fractional ±90° Bandwidth diminishes. As very much anticipated, band separation also reduces when C_1 reduces, as shown Fig. 3.9b.

3.4.4 Band 2 capacitance (C_2) effect

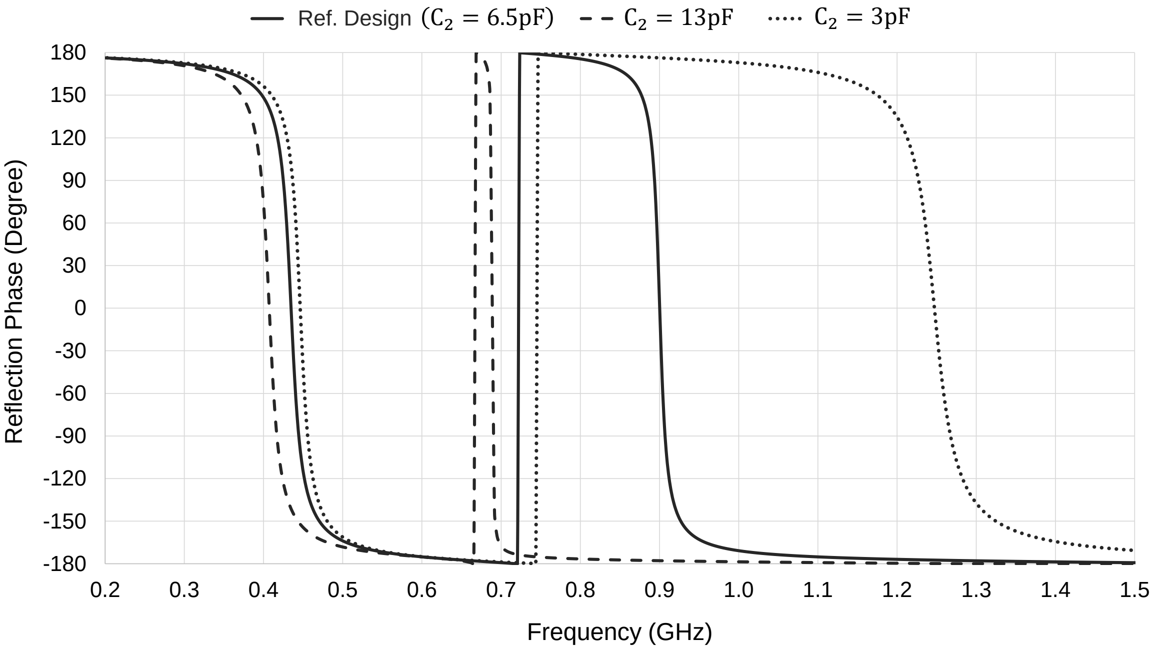

Fig. 3.10 Simulated reflection phase of lumped capacitor loaded dual band HIS. Parametric study on Band 2 capacitor (C_2). Unit cell parameters are fixed as of Ref. Design, Table 3.2.

Fig. 3.10 shows simulated reflection phase plot as upper band (Band 2); capacitance (C_2) is increased/decreased by a factor of 2, with respect to reference design $(C_2 = 6.5\text{pF})$ within fixed dual band HIS design unit cell parameters, as in Table 3.2. Upper band resonance frequency is reduced by 23% as C_2 increases from 6.5 pF to 13 pF as compared to 39% increase as C_2 reduces from 6.5 pF to 3 pF. Lower band coupling into upper band is evident as upper band fractional ±90° bandwidth significantly degrades to 0.5% when C_2 increases to 13 pF approaching $(C_1 = 19\text{pF})$. On the other hand lower band (Band 1) resonance frequency is also affected by variation of Band 2 capacitance (C_2) presenting a maximum reduction in resonance frequency of 6.4% for the case when C_2 is increased from 6.5 pF to 13 pF.

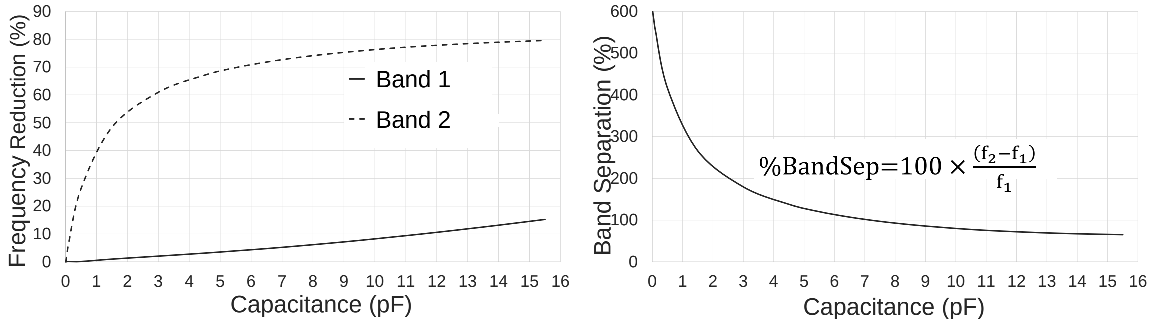

(a) Percentage Frequency Decrease

(b) Band Separation

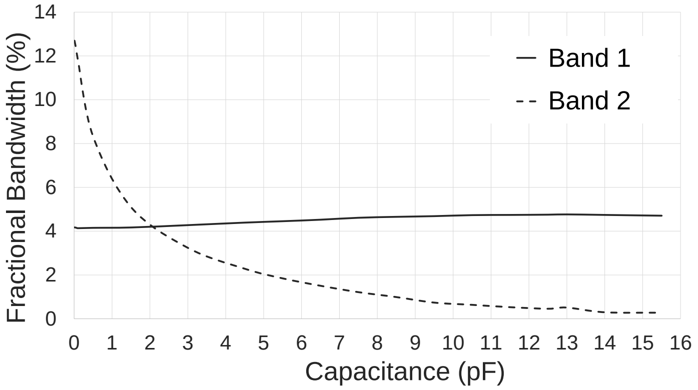

(c) Fractional Bandwidth

Fig. 3.11 Band 2 capacitance (C_2) effect on resonance frequency, band separation and fractional bandwidth. Miniaturised dual band HIS dimensions are fixed as in Table 3.2.

Further analysis is conducted on Band 2 capacitance as it is increased from $(C_2 = 0.01\text{pF})$ to $(C_2 = 15.5\text{pF})$, fixing Band 1 capacitance to $(C_1 = 19\text{pF})$ and dual band miniaturised HIS unit cell parameters as of reference design, as in Table 3.2. Percentage frequency reduction in Band 1 and Band 2 resonance frequencies, calculated with respect to that when $(C_2 = 0.01\text{pF})$, is plotted versus increasing Band 2 capacitance (C_2), Fig. 3.11a. When C_2 increases, Band 2 undergoes significant reduction in resonance frequency as well as Band 1 whose resonance frequency is reduced due to variation in C_2. A maximum of a 15% reduction in Band 1 frequency is observed at $(C_2 = 15.5\text{pF})$, after which Band 2 is not usable, as in Fig. 3.11a. Moreover, associated percentage band separation for this case study is presented in Fig. 3.11b and observed to reduce with increased C_2 where bands can get as close as 65% before Band 2 diminishes. The resulting effects, as a consequence of inter unit cell mutual coupling, produces a significant reduction in Band 2 operational bandwidth as C_2 increases while Band 1 bandwidth is almost constant which is demonstrated in Fig. 3.11c.

3.4.5 Periodicity (P_T) effect

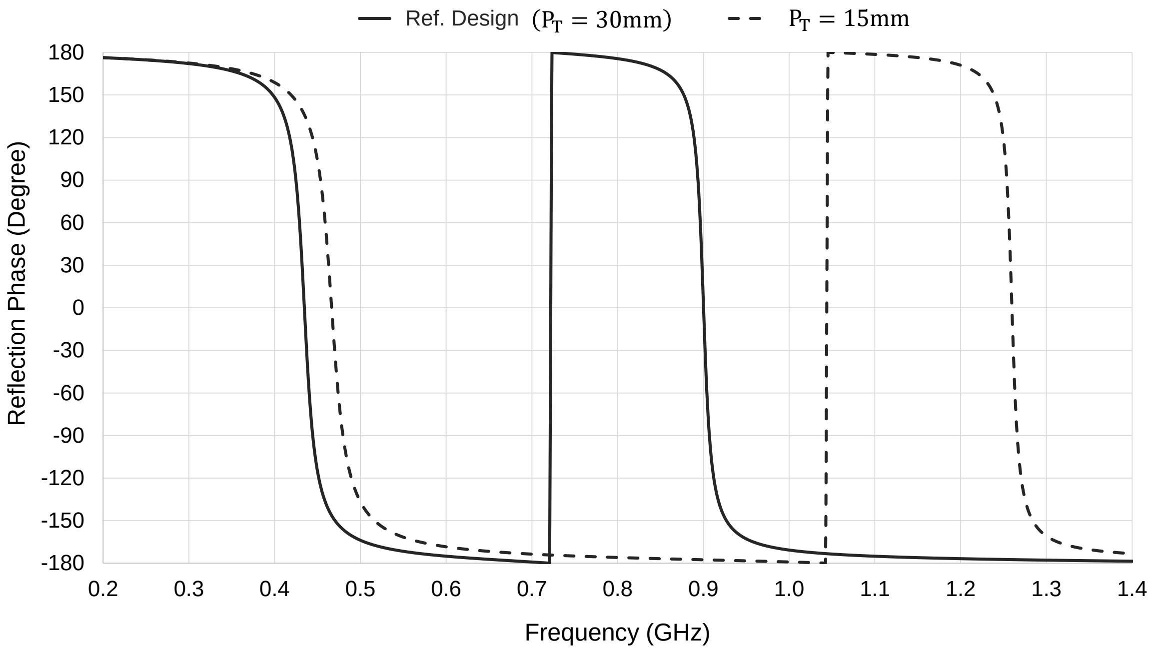

Fig. 3.12 Simulated reflection phase of lumped capacitor loaded dual band HIS. Parametric study on periodicity (P_T). Unit cell parameters are fixed as of Ref. Design, Table 3.2.

The effect of varying dual band miniaturised HIS unit cell total periodicity (P_T) also includes explicit analysis on the effect of interelement spacing $\left(\frac{S_g}{P_T} = \frac{1}{30}\right)$ and distance between lumped capacitors $(d_c = 0.5P_T)$. Design parameters and lumped capacitors values are fixed as in Table 3.2 while investigating the effect of unit cell periodicity P_T. Simulated reflection phase plots for dual band HIS modelled on CST Microwave Studio, normal incidence, as unit cell periodicity is reduced from 30 mm to 15 mm, are presented in Fig. 3.12. It can be observed that reducing electrical unit cell periodicity increases resonance frequency by 7% and 40% for lower band (Band 1) and upper band (Band 2) respectively, calculated with respect to reference design resonance frequency. Therefore, significant frequency shift in Band 2 is observed when the electrical periodicity is reduced by 50%, as in Fig. 3.12, where upper band is very much under the effect of inter element mutual coupling.

Furthermore analysis of electrical unit cell total periodicity $(\mathrm{P_T})$ effect is provided where $\mathrm{P_T}$ is reduced from 0.09λ to 0.006λ, calculated with respect to a reference design high band frequency of 900 MHz, while lumped capacitors $(\mathrm{C_1},\mathrm{C_2})$ and other unit cell parameters are maintained fixed as in Table 3.2. Percentage frequency increase, percentage band separation and fractional bandwidth are discussed.

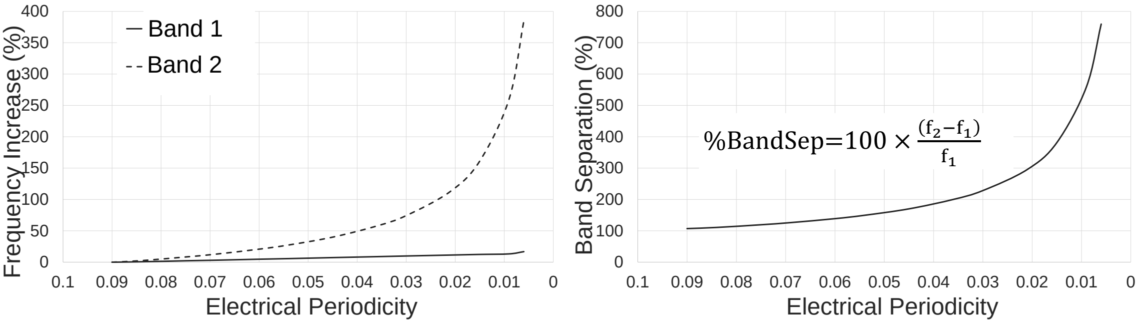

(a) Percentage Frequency Increase (b) Band Separation

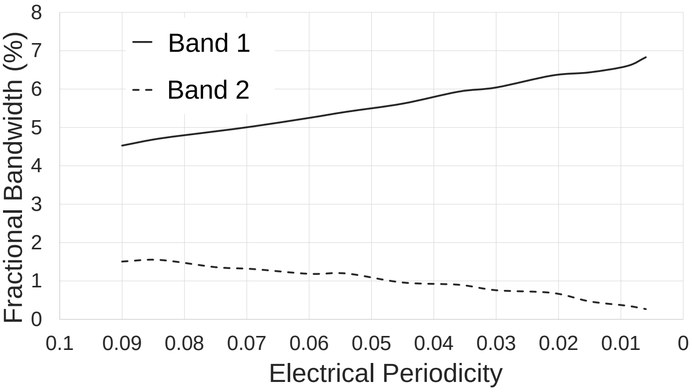

(c) Fractional Bandwidth

Fig. 3.13 Periodicity $(\mathrm{P_T})$ effect on resonance frequency, band separation and fractional bandwidth. Miniaturised dual band HIS dimensions are fixed as in Table 3.2.

Fig. 3.13a presents percentage frequency increase versus reduction in unit cell electrical periodicity considered with respect to resonance frequency when $\mathrm{P_T} = 0.09\lambda$. Band 1 percentage frequency increase is steady/linear at maximum 17% as periodicity reduces to 0.006λ. However, Band 2 percentage frequency increases non-linearly, recording a maximum of 385% as periodicity reduces to 0.006λ, and significant inter unit cell mutual coupling is encountered. Therefore, band separation is expected to increase as periodicity reduces where this is illustrated in percentage band separation plot versus electrical periodicity, as in Fig. 3.13b. Moreover, Fig. 3.13c, dual band HIS fractional $\pm 90^\circ$ bandwidth versus change in electrical periodicity provides significant insights on mutual coupling consequences on both bands. As periodicity reduces, lower band (Band 1) fractional bandwidth is improved since the upper band (Band 2) resonance frequency is shifted further apart, however, Band 2 bandwidth degrades significantly. Miniaturisation of dual band HIS using lumped capacitors can be made effective by the proper choice of unit cell size, which enhances bandwidth, while opting for significant reduction in periodicity increases mutual coupling between elements.

3.4.6 Substrate thickness (H) effect

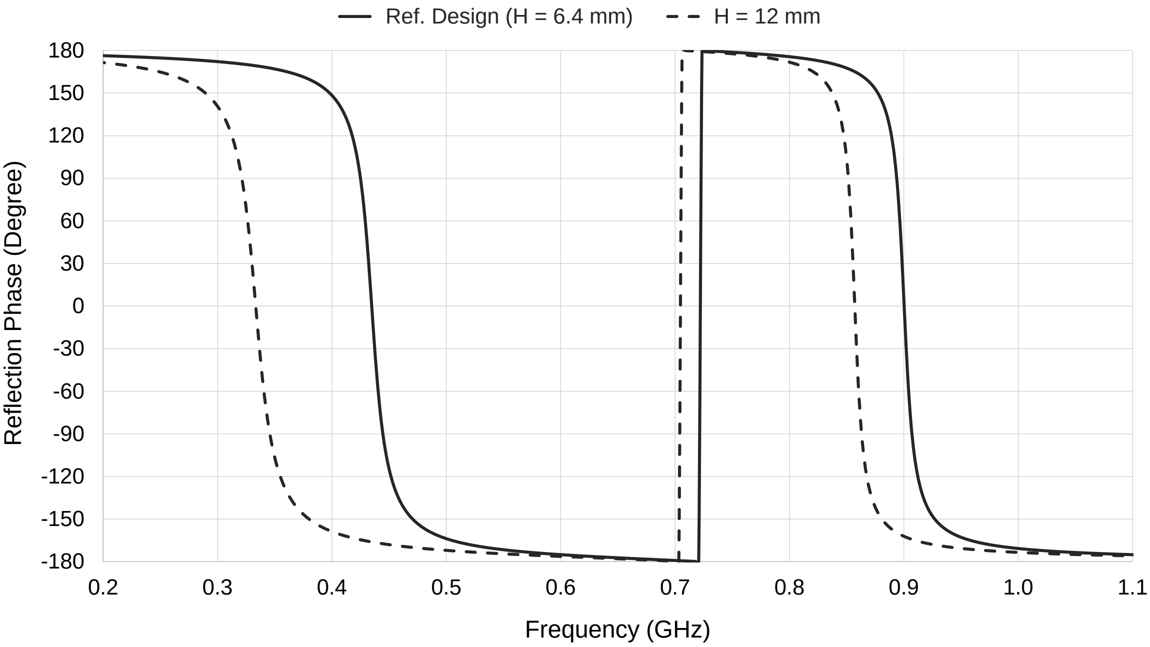

Fig. 3.14 Simulated reflection phase of lumped capacitor loaded dual band HIS. Parametric study on substrate thickness (H). Unit cell parameters are fixed as of Ref. Design, Table 3.2.

Miniaturised dual band HIS unit cell design parameters and value of capacitors are fixed as in Table 3.2, while the analysis of dielectric substrate thickness (H) effect on the resonance frequency is considered when H is increased from 6.4 mm to 12 mm. Reflection phase simulation plots, as in Fig. 3.14, lower band (Band 1) resonance frequency, which is reduced by 23% and fractional ±90° bandwidth increases from 4.5% to 7.5%, while upper band (Band 2) resonance frequency is reduced by 5% and fractional ±90° bandwidth reduces from 1.5% to 1.4%. Therefore, varying the substrate thickness has different effects on both Band 1 and Band 2.

Percentage frequency increase, percentage band separation and fractional bandwidth, in both bands, are discussed next. Substrate electrical thickness, calculated with respect to reference design upper band frequency, is increased from 0.005λ to 0.04λ. Percentage frequency reduction in Band 1 and Band 2, calculated with respect to resonance frequency when $(\mathrm{H} = 0.005\lambda)$, is plotted versus substrate electrical thickness, as in Fig. 3.15a. For the case when substrate thickness increases to 0.04λ, Band 1 resonance frequency reduces significantly by 50% while Band 2 resonance frequency reduces by 24%.

In Fig. 3.15b, percentage band separation plot versus electrical substrate thickness illustrates the percentage variation in resonance frequency in both bands where as electrical thickness increases, band separation increases. Moreover, plots of Band 1 and Band 2 fractional ±90° bandwidth versus electrical thickness are presented in Fig. 3.15c; Band 1 bandwidth increases as electrical substrate thickness increases compared to a steady slight reduction in Band 2 fractional bandwidth. This is believed to be due to significant mutual coupling among bands which is more prominent as substrate thickness increases.

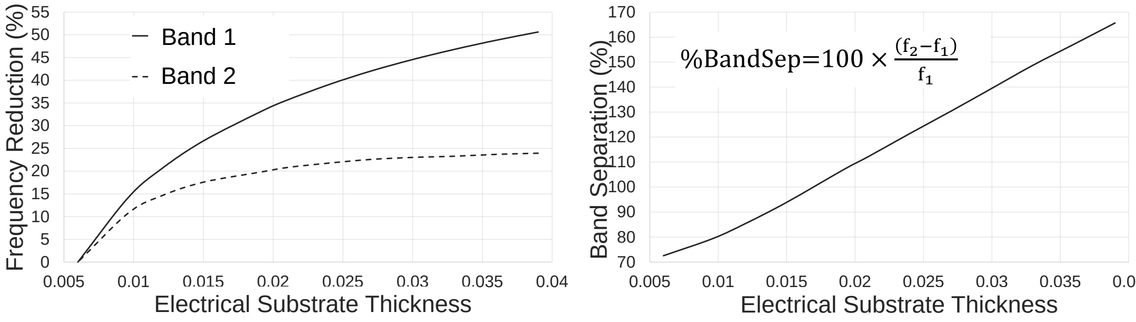

(a) Percentage Frequency Decrease

(b) Band Separation

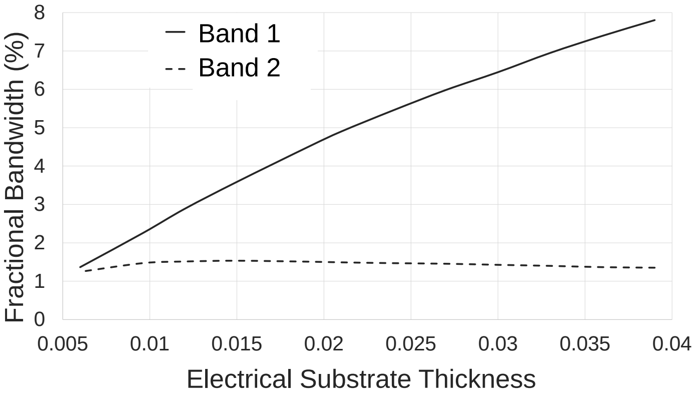

(c) Fractional Bandwidth

Fig. 3.15 Miniaturised dual HIS. Effect of substrate thickness (H) on resonance frequency, band separation and fractional bandwidth. Unit cell parameters are fixed as in Table 3.2.

3.4.7 Comments on inter unit cell mutual coupling

Miniaturised dual band HIS implementing lumped capacitors, of unequal values, in adjacent subunit cells is possible. Therefore, it is desired that dual band miniaturised HIS, unit cell structure, as in Fig. 3.2, be tuned by the sole variation of lumped capacitors. However, as of parametric study conducted, mutual coupling is significant between bands as it varies with lumped capacitors (C_1, C_2), substrate thickness and periodicity. Fig. 3.16 presents simulated surface current plots of miniaturised dual band HIS whose unit cell structure is shown in Fig. 3.2 and design parameters are detailed in Table 3.2. Strong mutual coupling between subunit cells is observed in the upper band, 900 MHz, as a high intensity of unwanted current amplitude is conducted in the subunit cell on the left which contributes to the lower band, as in Fig. 3.16b. While; Lower band, 430 MHz, mutual coupling from upper band into lower band subunit cell is of less intensity, as in Fig. 3.16a.

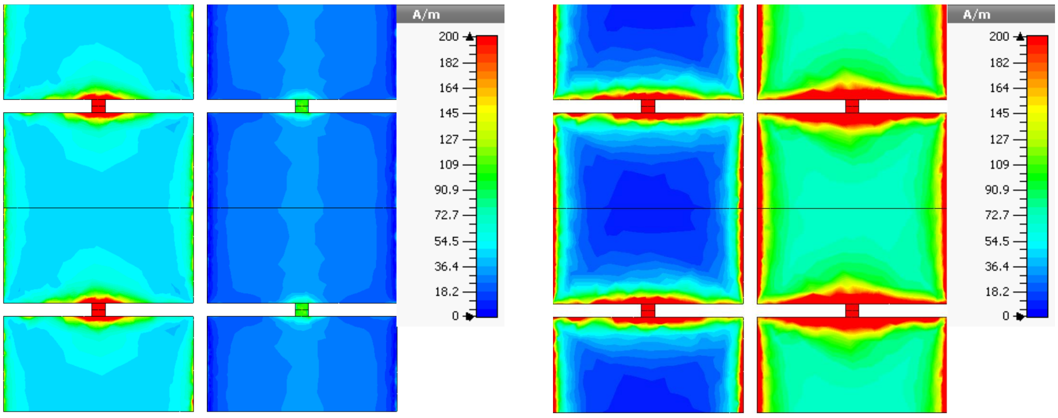

(a) 430 MHz Band (b) 900 MHz Band

Fig. 3.16 Surface current amplitude in miniaturised dual band HIS loaded with capacitors.

3.5 Conclusion

A miniaturised dual band HIS implementing lumped capacitor loading has been presented. Parametric analysis has been conducted to demonstrate the factors that affect dual band performance concentrating on resonance frequencies and fractional bandwidth. Mutual coupling was an issue in the design limiting its performance and degrading its operational bandwidth. The effect of varying the unit cell periodicity and substrate thickness had a significant effect on mutual coupling between bands, where coupling increases when substrate thickness is increased, associated with reduction in periodicity which limits miniaturisation capability. In the next chapter an improved design for miniaturised HIS using lumped capacitances will be presented with a novel approach to manage mutual coupling where dual band miniaturised high impedance surfaces are discussed.

Chapter 4

Dual Band Lumped Capacitor HIS Design Accounting For Mutual Coupling

4.1 Introduction

In Chapter 3, miniaturised dual band High Impedance Surface (HIS) using lumped capacitor loading were discussed. The main drawback was the existence of significant inter unit cell mutual coupling between both bands. In this chapter, a dual band HIS unit cell miniaturised using lumped capacitors is further discussed with proposed solution to encounter mutual coupling. Therefore, a novel technique where a miniaturised HIS gridded with guard conductors is presented and proven to minimize mutual coupling between each subunit cell, where each band is independently realised by the proper choice of loaded capacitor which is mechanically tuned. Parametric analysis is conducted for insights into the structure's mechanism and design methodology. Design equations as well as equivalent circuit modelling are proposed with special attention to the effect of unit cell periodicity , substrate thickness and guard conductor grids.

Furthermore, the novel dual band HIS design , which is miniaturised with lumped capacitors and gridded with guard conductors, is experimentally verified as related to antenna applications. The novel dual HIS is incorporated with an ultra wide band monopole antenna to replace conventional metal ground plane and realise a low profile platform tolerant antenna system, where design limitations are also discussed.

4.2 Methodology To Reduce Mutual Coupling

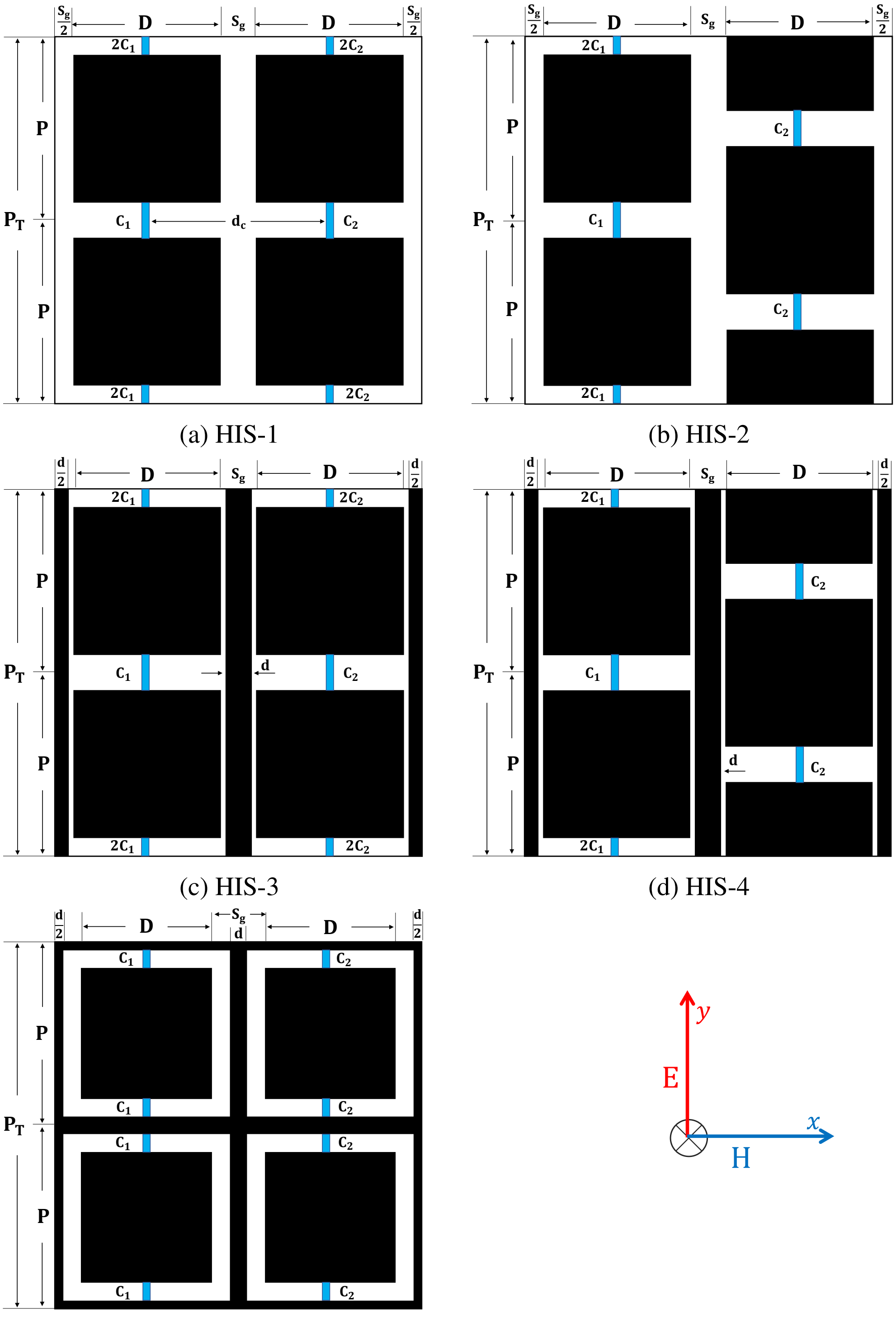

(a) HIS-1

(b) HIS-2

(c) HIS-3

(d) HIS-4

(e) HIS-5

Fig. 4.1 Lumped component loaded miniaturized dual band HIS designs 1 to 5 are compared.

In this section, a design methodology to reduce mutual coupling in dual band HIS loaded with lumped capacitors is discussed. Five High Impedance Surface (HIS) unit cell configurations are introduced; HIS 1, HIS 2, HIS 3, HIS 4 and HIS 5 as shown in Fig. 4.1. All designs are modelled on a single layer dielectric substrate of thickness (H) and then backed by metal.

Fig. 4.1a shows HIS 1: A dual band miniaturised design using lumped capacitor loading, Chapter 3. Main drawback of this design is mutual coupling between subunit cell elements.

Fig. 4.1b shows HIS 2: A dual band miniaturised HIS where the right subunit cell patches are displaced by quarter the periodicity with respect to left side subunit cell patches.

Fig. 4.1c shows HIS 3: A dual band miniaturised HIS where metal lines of thickness (d) are inserted within 75% of interelement spacing.

Fig. 4.1d shows HIS 4: A dual band miniaturised HIS where metal lines, thickness (d), are inserted within 75% of interelement spacing, also, right subunit cell patches are displaced by quarter the periodicity along y-direction, with respect to left subunit cell patches.

Fig. 4.1e shows HIS 5: A novel dual band miniaturised HIS where guard conductors metal mesh grid structure are incorporated along the patch subunit cells. This offers advantage to mechanically tune each band independently by varying the associated capacitance loaded within corresponding subunit cell.

4.2.1 Unit cell configuration effect on resonance frequency

Table 4.1 Dual Band Miniaturised Lumped Capacitor Loaded HIS 1

Unit Cell Parameters	Values
Substrate material	FR4
Substrate permittivity (ε_r)	4.3
Interelement spacing(S_g)	1 mm
Substrate thickness(H)	6.4 mm
Periodicity(P)	31 mm
Band 1 design frequency	430 MHz
Band 2 design frequency	900 MHz
Band 1 capacitance (C_1)	19.4 pF
Band 2 capacitance (C_2)	6.3 pF
Distance between lumped components(d_c)	0.5P

Dual band miniaturised HIS designs 1 to 5 are modelled on CST Microwave Studio and simulated at normal incidence where reflection phase properties are of interest with the aim to investigate the consequences resulting from modifying unit cell configuration on the resonance frequency. Unit cell periodicity, substrate thickness, permittivity, lumped capacitances C_1 and C_2 are all fixed as of reference design (HIS 1) , which is modelled at 430 MHz and 900 MHz and whose design parameters are shown in Table 4.1.

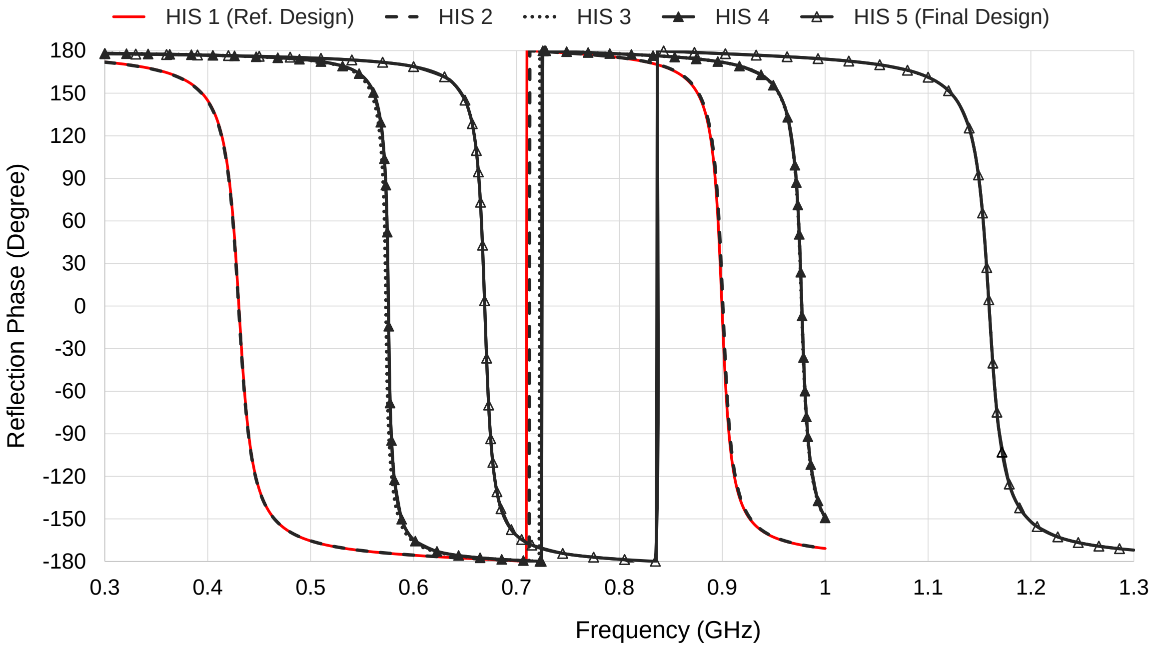

Fig. 4.2 Simulated reflection phase plots comparing HIS design configurations.

Reflection phase plots are shown in Fig. 4.2. As HIS 2 is compared to HIS 1, it can be observed that shifting the subunit cell patches by quarter the periodicity alters the distance between lumped components C_1 and C_2 but have no effect on the resonance frequency. While inserting a 0.75 mm metallic line, which is of inductive nature, has the effect of increasing the resonance frequency by 34% and 9% in Band 1 and Band 2 respectively as observed with respect to reference design HIS 1 As HIS 3 is compared to HIS 1. On the other hand, HIS 4 produced identical reflection phase response as HIS 3 since shifting subunit cell patches has been proven to have no effect on resonance frequency when HIS 2 and HIS 1 were compared. In the final design, HIS 5, each subunit cell is engineered with inductive metallic guard conductors and therefore is inductively loaded increasing Band 1 and Band 2 resonance frequencies by 56% and 29% respectively, as calculated with respect to reference design HIS 1.

4.2.2 Mutual coupling analysis comparing HIS 1, HIS 3 and HIS 5

In the previous section; five different dual band HIS configurations, miniaturised with lumped capacitors, are discussed and compared in respect to the effect of adding metallic tracks on the resonance frequency. However, prior analysis did not provide conclusive insights on mutual coupling. An upcoming study will investigate miniaturised dual band HIS configurations HIS 1, HIS 3, and HIS 5 as focused on highlighting each band's capacitor tuning capability. Also, minimum possible band separation is observed. It will be shown that the final design HIS 5, featuring guard conductors, has shielded each subunit cell from one another, therefore, offering significant reduction in mutual coupling and highly independent tuning capacity.

Each of HIS design configurations HIS 1, HIS 3, and HIS 5 is modelled on a 6.4 mm FR4 ($\varepsilon_r = 4.3, \tan\delta = 0.025$) substrate and a fixed unit cell periodicity of 31 mm, $0.09\lambda_{0.9\mathrm{GHz}}$. Loaded capacitors C_1 and C_2 are tuned such that all designs resonate at 430 MHz and 900 MHz. Unit cell design parameters are detailed in Table 4.2.

Table 4.2 Miniaturised HIS 1, HIS 3, and HIS 5 Designed to Operate at 430-900 MHz

HIS Unit Cell Parameters	HIS 1 (Ref. Design)	HIS 3	HIS 5 (Final Design)
Substrate material	FR4	FR4	FR4
Substrate permittivity (ε_r)	4.3	4.3	4.3
Substrate thickness (H)	6.4 mm	6.4 mm	6.4 mm
Periodicity(P)	31 mm	31 mm	31 mm
Interelement spacing($\mathrm{S_g}$)	1 mm	1 mm	3 mm
Band 1 capacitance (C_1)	19.4 p	35.5 p	48.2 pF
Band 2 capacitance (C_2)	6.3 pF	7.7 pF	10.6 pF
Capacitors distance ($\mathrm{d_c}$)	0.5P	0.5P	0.5P
Conductor width (d)	−−	0.75 mm	1 mm

First, the effect of reducing lower band capacitance (C_1) is investigated as it is varied in HIS configurations HIS 1, HIS 3 and HIS 5; observing resonance frequency displacement and band separation. Decreasing Band 1 capacitance is expected to increase the lower band (Band 1) resonance frequency and desired to have no effect on the upper band (Band 2). Simulated reflection phase plots for the case when C_1 is reduced up to the limit that the upper band ±90° bandwidth is maintained within 0.5% are presented in Fig. 4.3 for all three configurations. Percentage frequency change is calculated with respect to reference design modelled at 430 MHz and 900 MHz. Fig. 4.3, HIS 1, as C_1 is reduced from 19.4 pF to 11 pF, lower band resonance frequency is increased by 26% while an unwanted 5% increase in the upper band frequency is observed as a consequence to expected mutual coupling.

While in HIS 3, metal tracks are inserted within 75% of interelement spacing, as C_1 is reduced from 35.5 pF to 13 pF, Band 1 resonance frequency increases by 62% where Band 2 unwanted frequency increase is reduced to 1.5%, as in Fig. 4.3. Therefore, as HIS 1 and HIS 3 are compared, adding metallic tracks has produced a shielding effect between lower and upper band subunit cells where the two bands can get as close as 220 MHz implementing HIS 3 design as compared to a band separation of 401 MHz in HIS 1 design. However, significant control on inter unit cell mutual coupling is observed as the unit cell is gridded with metallic tracts in prototype HIS 5, as in Fig. 4.1e, whereas lower band capacitance (C_1) is reduced from 48.2 pF to 14.6 pF, Band 1 resonance frequency increases by 76% while Band 2 experienced a 2% unwanted increase in resonance frequency, but, band separation is minimized to 163 MHz. Maximized reduction in mutual coupling is achieved in HIS 5 configuration where metallic grids provide significant shielding between each band and Band 1 is tuned with more freedom.

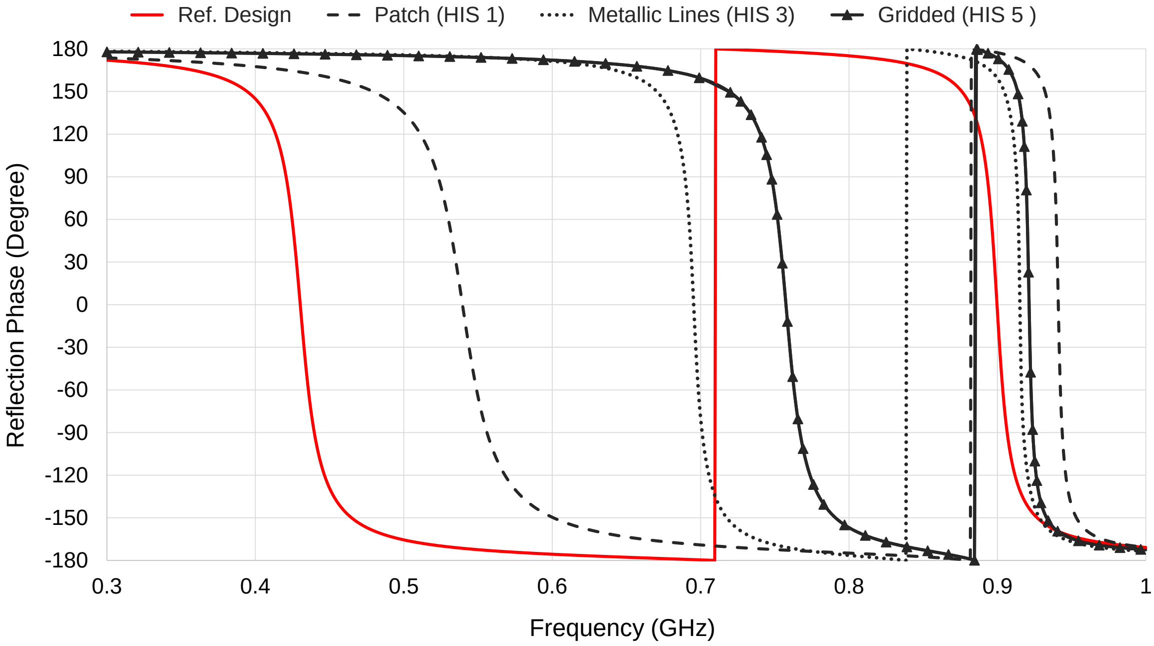

Fig. 4.3 Simulated reflection phase. Lower band capacitance (C_1) is reduced in HIS configurations HIS 1, HIS 3, HIS 5; all are initially designed at 430 MHz and 900 MHz.

Second, the effect of increasing upper band capacitance (C_2) is discussed when varied in miniaturised dual band HIS configurations HIS 1, HIS 3 and HIS 5, as in Fig. 4.1. The upper band is controlled by C_2. If mutual coupling is not significant, increasing upper band capacitance (C_2) is expected to decrease Band 2 resonance frequency and desired to have no effect on Band 1. Simulated reflection phase plots are presented in Fig. 4.4 for the case when C_2 is increased up to the limit that upper band ±90° bandwidth is maintained within

0.5%, in all HIS configurations of interest. Percentage frequency change is calculated with respect to reference design modelled at 430 MHz and 900 MHz. HIS 1 reflection phase plot, shown in Fig. 4.4, demonstrates that when C_2 increases from 6.3 pF to 10.4 pF, Band 2 resonance frequency reduces by 17.5% while an unwanted 4% frequency reduction in Band 1 occurs, which is due to mutual coupling. In HIS 3 design, where metal tracks are inserted within 75% of interelement spacing, C_2 is increased from 7.7 pF to 14 pF reducing resonance frequency by 24% and 0.9% as observed in Band 2 and Band 1 respectively, as also shown in Fig. 4.4. Optimum variation of C_2 renders a minimum band separation of 326 MHz and 262 MHz, when comparing dual band HIS configurations HIS 1 and HIS 3 respectively. Therefore, metallic lines have reduced frequency shift in Band 1 but the bands cannot get any closer than 262 MHz. Nevertheless, implementing unit cell gridded with metallic tracts as in HIS 5, which unit cell structure is shown in Fig. 4.1e, has better control on tuning the bands as well as closer bands separation being possible. Therefore, HIS 5 reflection phase plot, shown in Fig. 4.4, demonstrates that as C_2 increases from 10.6 pF to 29 pF, Band 2 resonance frequency reduces by 37% while Band 1 resonance frequency reduces by 0.9% and the bands can get as close as 139 MHz. Therefore, as the effect of C_2 is studied, mutual coupling is significantly reduced as guard conductors are included in the design while the effect of Band 1 on Band 2 subunit cells is rendered insignificant as the gridded structure shields one subunit cell from another.

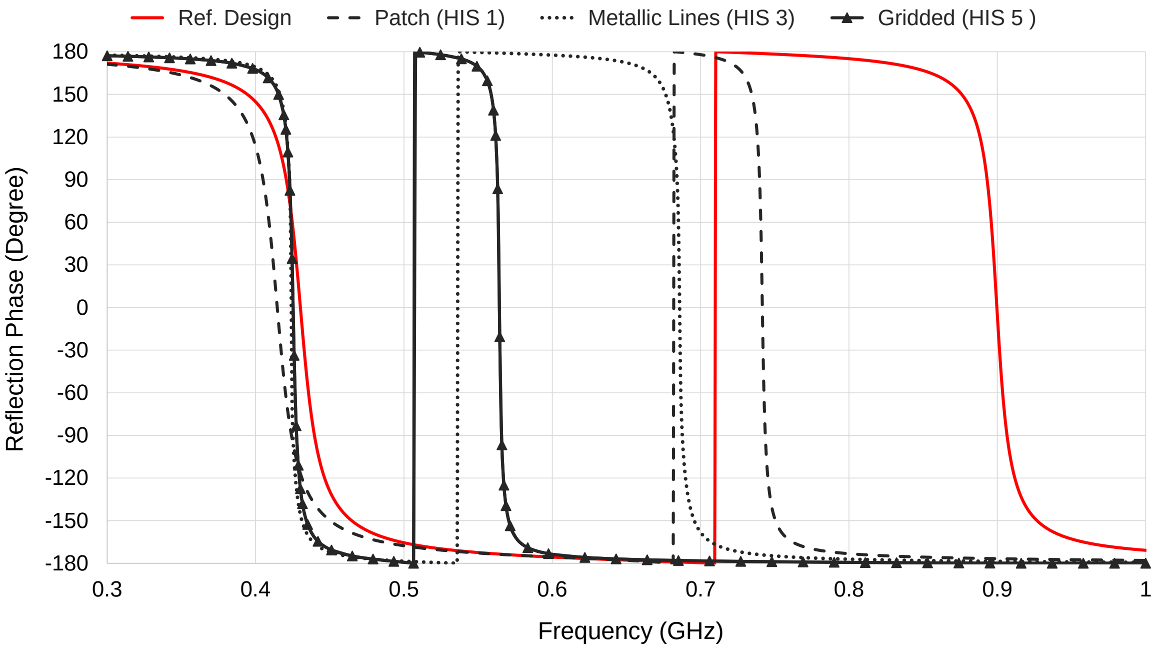

Fig. 4.4 Simulated reflection phase. Upper band capacitance (C_2) is increased in HIS configurations HIS 1, HIS 3, HIS 5; all are initially designed at 430 MHz and 900 MHz.

Table 4.3 and Table 4.4 summarize the minimum band separation that can be achieved in each of HIS configurations HIS 1, HIS 3 and HIS 5 as with respect to when lumped components C_1 and C_2 are varied alternatively while unit cell dimensions are fixed, as in Table 4.2. In both cases, when either C_1 or C_2 are varied, HIS 5 design which feature guard conductors as implemented within the metallic patches provide the best control on mutual coupling where it is observed to realize optimum band separation for maximum corresponding variation in either capacitors. Therefore, the two subunit cells are isolated from one another due to the existence of the gridded inductive lines which provide more flexibility to optimize each band resonance frequency independently.

Table 4.3 Band Separation Achieved When Band 1 Lumped Capacitor C_1 Is Reduced Comparing HIS Configurations HIS 1, HIS 3 And HIS 5

Design Prototype	Reduction In C_1	Band Separation
Capacitive patch (HIS 1)	19.4 pF to 11 pF	326 MHz
Capacitive patch with metallic tracks (HIS 3)	35.5 pF to 13 pF	262 MHz
Gridded capacitive patch (HIS 5)	48.2 pF to 14.6 pF	139 MHz

Table 4.4 Band Separation Achieved When Band 1 Lumped Capacitor C_2 Is Reduced Comparing HIS Configurations HIS 1, HIS 3 And HIS 5

Design Prototype	Increase In C_2	Band Separation
Capacitive patch (HIS 1)	6.3 pF to 10.4 pF	401 MHz
Capacitive patch with metallic tracks (HIS 3)	7.7 pF to 14 pF	220 MHz
Gridded capacitive patch (HIS 5)	10.6 pF to 29 pF	163 MHz

4.2.3 Surface current plots comparing HIS 1 and HIS 5

Simulated surface current plots comparing dual band miniaturised patch, HIS 1, and gridded miniaturised patch, HIS 5, are considered when monitored at a lower band frequency of 430 MHz and upper band frequency of 900 MHz. The left subunit cell corresponds to the lower band while subunit cells on the right corresponds to the upper band.

Simulated surface currents in HIS 1 and HIS 5 are compared in Fig. 4.5, which are observed at the lower band of 430 MHz. It can be seen that the gridded capacitive design, HIS 5, provides significant shielding between each band where current amplitude is concentrated within the left side subunit cell loaded with C_1 generating the lower band, as in Fig. 4.5b.

On the other hand, capacitive patch HIS 1 surface current amplitude was observed to be conducted in both subunit cells which are mutually coupled, as shown in Fig. 4.5a.

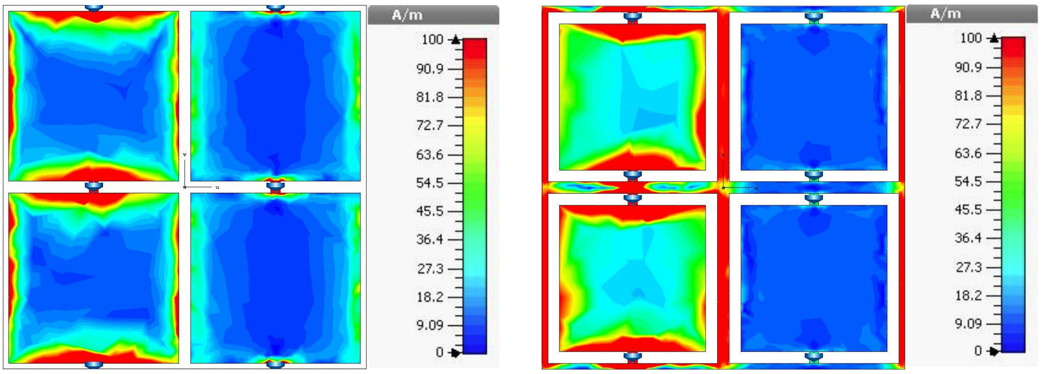

(a) Capacitive Patch (HIS 1) (b) Gridded Capacitive Patch (HIS 5)

Fig. 4.5 Simulated surface current amplitude for HIS 1 and HIS 5, observed at 430 MHz.

Similarly, as in Fig. 4.6, simulated surface currents observed at the upper band frequency of 900 MHz signifies the improvement made by implementing HIS 5 design. Gridded capacitive patch HIS 5 offers practical control on mutual coupling where the subunit cell on the right, loaded with C_2, is only active as the upper band is concerned, as in Fig. 4.6b. However, when only patch elements are implemented (HIS 1), as in Fig. 4.6a, both subunit cells are strongly coupled and conduct significant currents which jointly contribute to the upper band resonance.

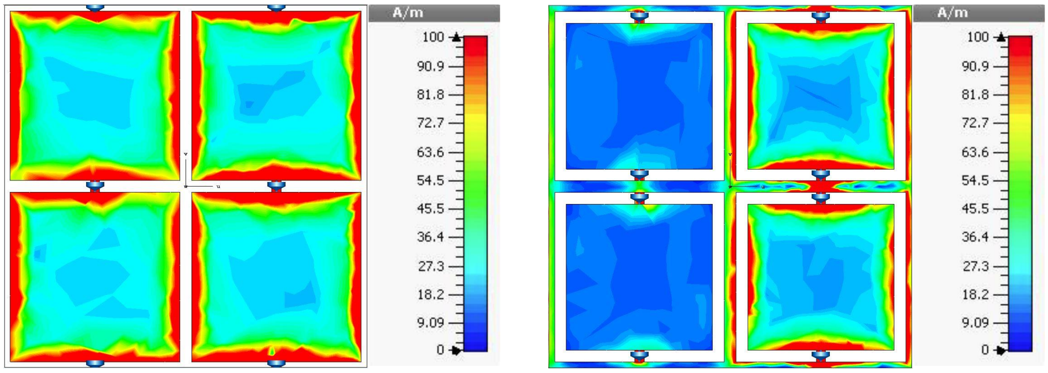

(a) Capacitive Patch (HIS 1) (b) Gridded Capacitive Patch (HIS 5)

Fig. 4.6 Simulated surface current amplitude for HIS 1 and HIS 5, observed at 900 MHz.

4.3 Gridded Miniaturised Dual Band HIS Analysis

Fig. 4.7 presents top and side view of the dual band capacitive High Impedance Surface (HIS) which is gridded with guard conductors and miniaturised using lumped capacitor loading. In this section, parametric analysis on the effect of guard conductors will only be conducted since the effect of other unit cell parameters such as periodicity, substrate thickness, permittivity and lumped components follow the same analogy as discussed in Chapter 3 for a miniaturised dual band HIS.

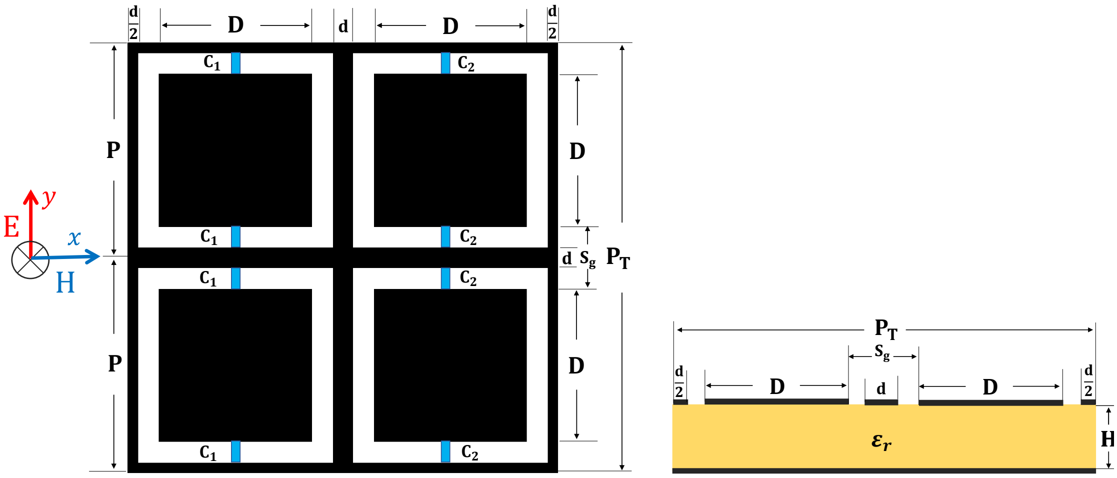

(a) Top View (b) Side View

Fig. 4.7 Gridded dual band miniaturised HIS capacitive patch loaded with lumped capacitors.

4.3.1 Guard conductor width (d) effect on resonance frequency

Table 4.5 430-900 MHz Original Design Miniaturised Gridded Capacitive Patch HIS

HIS Unit Cell Parameters	Original Design ($d = 1$ mm)
Substrate material	FR4
Substrate permittivity (ε_r)	4.3
Substrate thickness (H)	6.4 mm
Periodicity(P)	31 mm
Interelement spacing(S_g)	3 mm
Band 1 capacitance (C_1)	19.4 p
Band 2 capacitance (C_2)	6.3 pF
Capacitors distance (d_c)	0.5P

As discussed so far, adding guard conductors has reduced dual band mutual coupling. However, conductors are of inductive nature and they are expected to influence the resonance frequency. Capacitors and unit cell parameters are all fixed as reference HIS design detailed in Table 4.5, where the effect of guard conductor width (d) is investigated as varied at 1 mm, 2 mm, and 0.5 mm. Observing reflection phase properties for the miniaturised gridded HIS is modelled on CST Microwave Studio and simulated at normal incidence for the three cases of guard conductor width which are compared in Fig. 4.8. As conductor width is increased, its inductive effect is reduced increasing the resonance frequency by 9.5% and 9% in Band 1 and Band 2 respectively when the case of (d = 2 mm) and (d = 1 mm) are compared. While, reducing guard conductor width increases its inductive effect, therefore, reducing the resonance frequency by 4% and 2% in Band 1 and Band 2 respectively when the case of (d = 0.5 mm) and (d = 1 mm) are compared, Fig. 4.8. However, as conductor width is reduced, reduction in the resonance frequency is not significant which suggests that the increased inductive effect has counterpart influence where the gridded structure can be ineffective, also, indicates that the gridded structure possess parallel loading to each subunit cell.

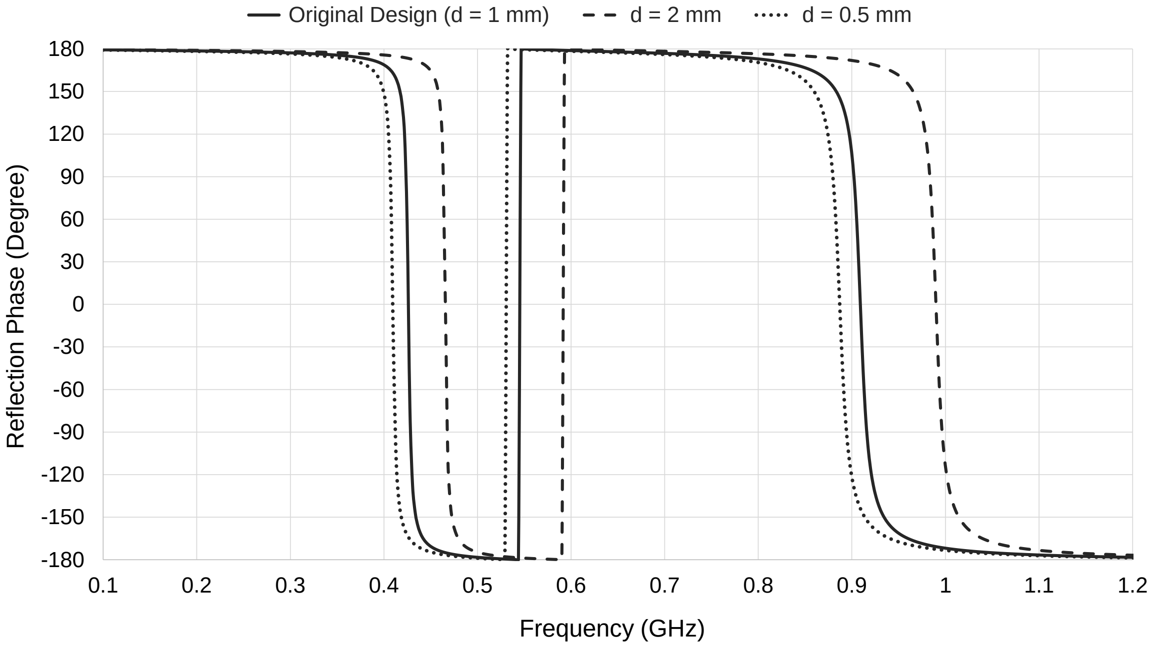

Fig. 4.8 Simulated reflection phase. Conductor width (d) varied in lumped capacitor loaded gridded dual band HIS. Unit cell parameters and capacitors are fixed as in Table 4.5.

4.3.2 Guard conductor width (d) effect on mutual coupling

Further analysis on the conductor width effect is performed as dual band gridded capacitive lumped capacitor loaded miniaturised HIS are designed to operate at 430 MHz and 900 MHz by only tuning conductor width (d) and lumped capacitors C_1 and C_2 with consistency in all other unit cell parameters as shown in Table 4.6.

In Fig. 4.7a, capacitance (C_1) control Band 1 (subunit cell on the left) and capacitance (C_2) generates Band 2 (subunit cell on the right). The level of inter element mutual coupling control is investigated as lumped capacitors C_1 and C_2 vary consecutively in HIS designs when ($d = 0.5$ mm, 2 mm) is up to the limit so that the upper band ±90° fractional bandwidth does not fall below 0.5%. This is in order to investigate the tuning capability in the presence of a thin and thick conductor where insights on recommended conductor width are given such that the gridded structure provides complete isolation between subunit cells. Analysis will include simulated reflection phase plots as well as surface current plots.

Table 4.6 430-900 MHz Miniaturised Gridded HIS Designed At Different Conductor Width

HIS Unit Cell Parameters	($d = 0.5$ mm)	($d = 2$ mm)
Substrate material	FR4	FR4
Substrate permittivity (ε_r)	4.3	4.3
Substrate thickness (H)	6.4 mm	6.4 mm
Periodicity(P)	31 mm	31 mm
Electrical periodicity w.r.t Band 2	0.09	0.09
Interelement spacing(S_g)	3 mm	3 mm
Band 1 capacitance (C_1)	43.5 p	57 p
Band 2 capacitance (C_2)	10.2 pF	13 pF
Capacitors distance (d_c)	0.5P	0.5P

The lower band capacitance (C_1) is varied while other design parameters are fixed as in Table 4.6. The effect of decreasing C_1, as with respect to 430-900 MHz reference design, is considered in simulated reflection phase plots, as in Fig. 4.9. For the case ($d = 0.5$ mm), C_1 is reduced from 43.5 pF to 13 pF, therefore, Band 1 resonance frequency increases by 75% in addition to an undesired increase of 3.5% in Band 2 resonance frequency, which renders a minimum band separation of 168 MHz. On the other hand, for the case ($d = 2$ mm), C_1 was reduced from 57 pF to 16 pF, therefore, Band 1 resonance frequency was increased by 82% associated with an undesired increase of 1.4% in Band 2 resonance frequency and contributed to a minimum band separation of 129 MHz. Therefore, implementing a wider conductor has reduced the unwanted frequency shift in the upper band and allowed closer bands to be possible, effectively reducing the influence of lower band subunit cell capacitance on the upper band.

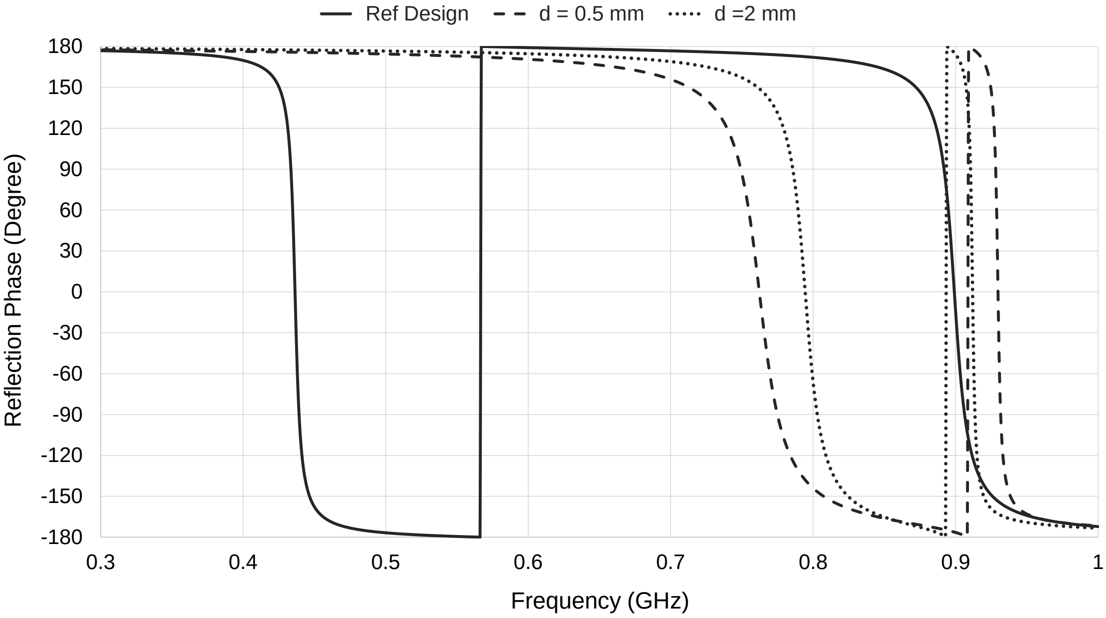

Fig. 4.9 Simulated reflection phase. Lower band capacitance (C_1) is reduced in lumped capacitor loaded gridded dual band HIS while setting conductor width to 0.5 mm and 2 mm.

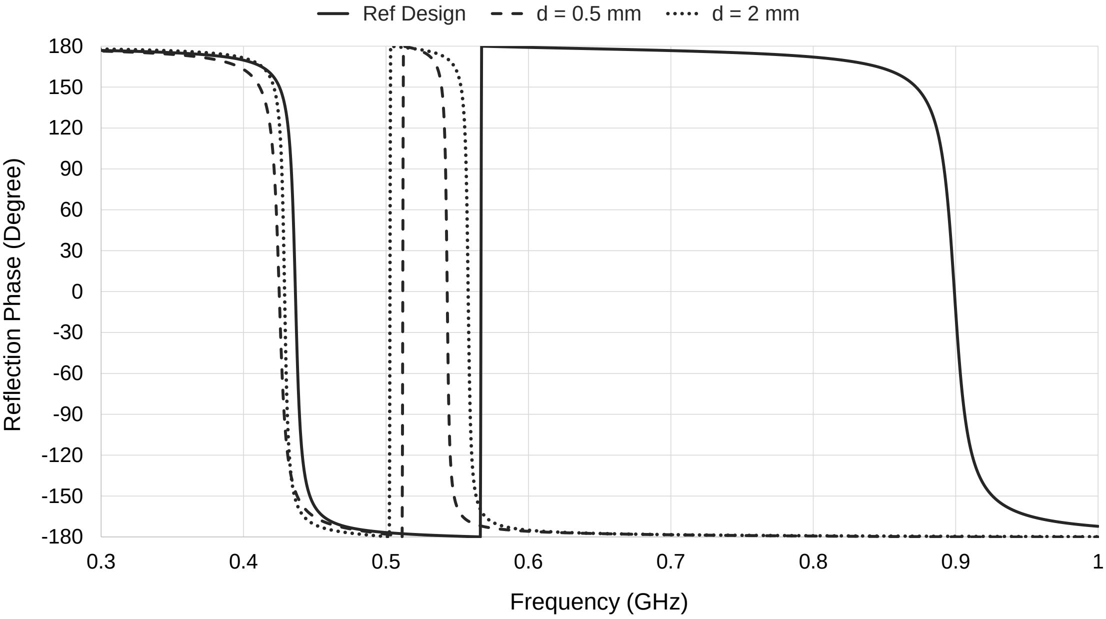

Fig. 4.10 Simulated reflection phase. Upper band capacitance (C_2) is increased in lumped capacitor loaded gridded dual band HIS while setting conductor width to 0.5 mm and 2 mm.

Similarly, miniaturised dual band gridded HIS design parameters are fixed as in Table 4.6. Upper band capacitance (C_2) effect is considered as it is reduced in two conductor width cases ($d = 0.5$ mm, 2 mm) observing simulated reflection phase properties, Fig. 4.10. When ($d = 0.5$ mm), as C_2 increases from 10.2 pF to 30 pF, Band 2 resonance frequency reduces by 39.5% associated with undesired reduction of 2.5% in Band 1 frequency, therefore, a band separation of 118 MHz. For ($d = 2$ mm), as C_2 increases from 13 pF to 35 pF, Band 2 resonance frequency reduces by 38% in addition to an undesired frequency reduction of 1.5% in Band 1, rendering a band separation of 129 MHz. Therefore, even though bands are brought closer when ($d = 0.5$ mm), the improvement in band isolation is prominent when a thicker conductor width is implemented since it reduces the unwanted frequency shift in the lower band.

On a final note, simulated surface current amplitude plots observed in gridded miniaturised HIS, designed to operate at 430 MHz and 900 MHz, are considered for two conductor width cases ($d = 0.5$ mm) and ($d = 2$ mm), design parameters as in Table 4.6. For both 430 MHz and 900 MHz bands, surface current plots presented in Fig. 4.11 and Fig. 4.12 clearly demonstrate that thicker conductor width ($d = 2$ mm) provides superior and effective subunit cell isolation which retrospectively reduces mutual coupling between bands as the current intensifies within the subunit cell corresponding to resonance frequency of interest.

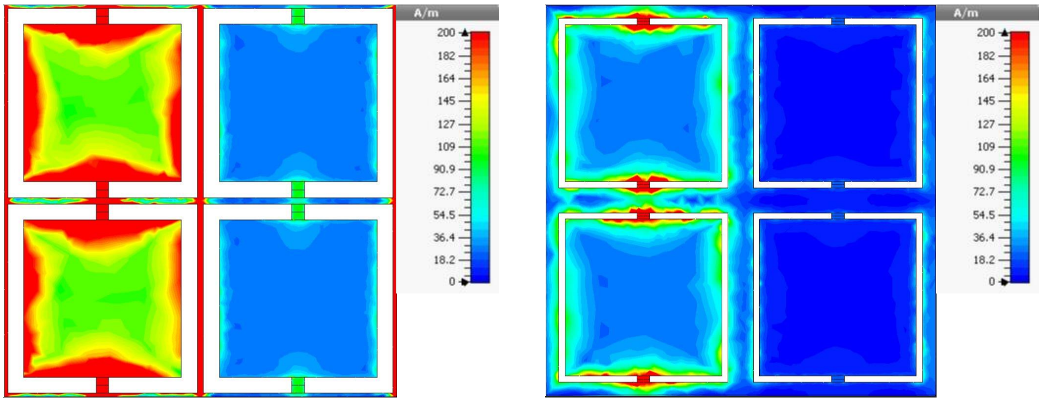

(a) $d = 0.5$ mm (b) $d = 2$ mm

Fig. 4.11 Surface current amplitude observed at 430 MHz. Conductor width (d) effect in miniaturised dual band gridded capacitive patch HIS. Unit cell design parameters, Table 4.6.

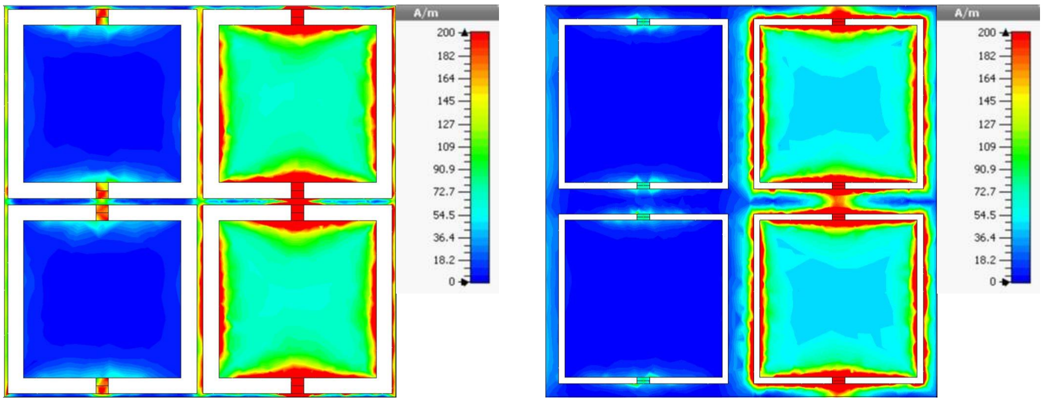

(a) d = 0.5 mm (b) d = 2 mm

Fig. 4.12 Surface current amplitude observed at 900 MHz. Conductor width (d) effect in miniaturised dual band gridded capacitive patch HIS. Unit cell design parameters, Table 4.6.

4.4 Gridded Miniaturised Dual Band HIS ECM

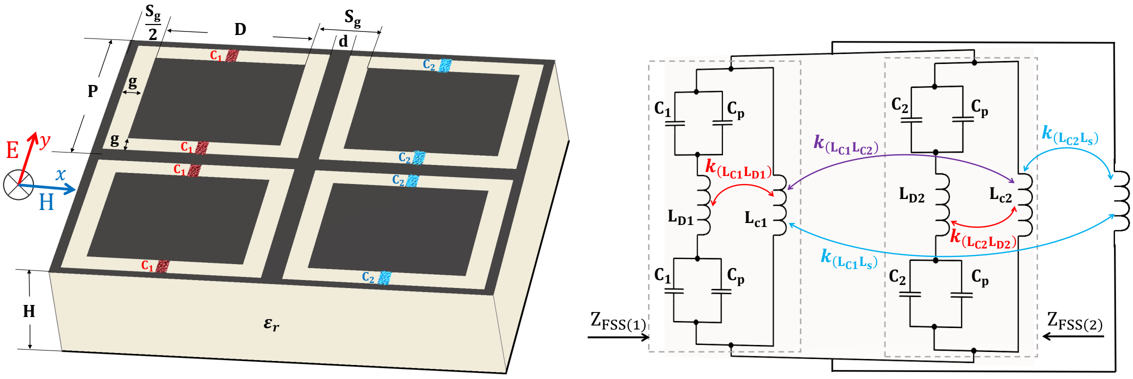

(a) Unit Cell 3D View (b) Equivalent Circuit Model

Fig. 4.13 Dual band gridded lumped capacitor loaded high impedance surface.

In this section physical insights on gridded capacitive patch HIS miniaturised using lumped component loading is discussed proposing empirical Equivalent Circuit Model (ECM) to explain structure's mechanism. Fig. 4.13a shows a 3D view of miniaturised dual band HIS that constitutes of FSS based top metallic surface, supported by a substrate thickness (H) and backed by metal, while the top metallic surface comprises of square patch adjacent subunit cells gridded with metallic conductors and loaded with lumped capacitances of unequal values ($C_1 > C_2$). Design novelty is presented by the ability to suppress inter element mutual coupling by implementing grid structure whose width plays a significant role to control mutual coupling.

The equivalent circuit model for electrically small gridded dual band HIS is proposed in Fig. 4.13b as an analogy to the gridded capacitive frequency selective surface reported in [100]. The mechanism of the equivalent circuit model is explained below:

- Within subunit cell periodicity (P), two adjacent gridded square subunit cells are treated as two individual resonators, each operating at different frequencies.
- For (subunit cell)$_\mathrm{i}$; Patch impedance is the series combination of lumped capacitance ($\mathrm{C_i}$), patch mutual capacitance ($\mathrm{C_p}$) generated within subunit cell gap (g) , and patch inductance ($\mathrm{L_{Di}}$). While a square conductor surrounding each subunit cell of centre patch width (D) has an inductive effect and is represented by inductance ($\mathrm{L_{Ci}}$) in parallel with patch impedance.

  where index $(\mathrm{i} = 1,2)$ refers to subunit cell corresponding to Band 1 and Band 2 respectively.
- Therefore, the two subunit cells are mutually coupled, also forming a parallel combination with substrate inductance ($\mathrm{L_s}$).

Moreover, inductors described in the empirical ECM, as in Fig. 4.13b, are magnetically coupled. Patch inductance is expected to be relatively small,therefore, coupling between ($\mathrm{L_{D1}}$, $\mathrm{L_{D2}}$), ($\mathrm{L_{D1}}$, $\mathrm{L_s}$) and ($\mathrm{L_{D2}}$, $\mathrm{L_s}$) are neglected for a simplified model. Coupling factors of interest are:

- $k_{(\mathrm{L_{Ci}L_{Di}})}$ is the coupling factor between grid conductor inductance ($\mathrm{L_{Ci}}$) and patch inductance ($\mathrm{L_{Di}}$) in each subunit cell $(\mathrm{i} = 1,2)$
- $k_{(\mathrm{L_{C1}L_{C2}})}$ is the coupling factor between grid conductor inductance ($\mathrm{L_{C1}}$) and ($\mathrm{L_{C2}}$) in (subunit cell)$_1$ and (subunit cell)$_2$ respectively.
- $k_{(\mathrm{L_{Ci}L_s})}$ is the coupling factor between grid conductor inductance ($\mathrm{L_{Ci}}$) and substrate inductance ($\mathrm{L_s}$) in each subunit cell $(\mathrm{i} = 1,2)$.

Next, the equivalent circuit model lumped elements are explained below:

$\mathrm{C_p}$ is the subunit cell mutual capacitance generated within gap (g) and defined as [100, 121]:

$$\mathrm{C_p} = \varepsilon_0 \varepsilon_{eff} \frac{2\mathrm{P}}{\pi} \log \frac{1}{\sin\left[\frac{\pi \mathrm{g}}{2\mathrm{P}}\right]} \tag{4.1}$$

where $\varepsilon_{eff} = \dfrac{\varepsilon_r + 1}{2}$ is the effective permittivity. P is the subunit cell periodicity.

$\mathrm{L_C}$ is the subunit cell inductance due to the gridded structure of the conductor width (d), defined as [100]:

$$\mathrm{L_C} = \mu_0 \frac{\mathrm{P}}{2\pi} \log \frac{1}{\sin\left[\frac{\pi}{2}\frac{\mathrm{d}}{\mathrm{P}}\right]} \tag{4.2}$$

where P is the subunit cell periodicity. Subunit cells are identical, therefore, Band 1 and Band 2 inductances in the equivalent circuit model are identical $(\mathrm{L_{C1}} = \mathrm{L_{C2}} = \mathrm{L_C})$

$\mathrm{L_D}$ is the inductance of the inner patch within the subunit cell, which also includes the effect of outside grid inductance on the centre patch within the subunit cell, defined as [122]:

$$\mathrm{L_D} = \mu_0 \frac{\mathrm{D}}{2\pi} \log \frac{1}{\sin\left[\frac{\pi}{2}\frac{\mathrm{D}}{\mathrm{P}}\right]} + \frac{\mathrm{g}}{\mathrm{D}+\mathrm{d}}\,\mathrm{L_C} \tag{4.3}$$

where P and D are the subunit cell periodicity and patch width respectively. Also, subunit cells are identical, therefore, Band 1 and Band 2 inner patch inductances in the equivalent circuit model are identical $(\mathrm{L_{D1}} = \mathrm{L_{D2}} = \mathrm{L_D})$.

$\mathrm{L_s}$ is the inductance of shorted electrically thin substrate, of thickness (H), defined as:

$$\mathrm{L_s} = \mu_0 \mu_r \mathrm{H} \tag{4.4}$$

Next, the circuit model is verified as resonance frequency and is compared against unit cell simulations for the dual band miniaturised gridded capacitive HIS modelled on CST Microwave Studio, and observed at normal incidence. The influence of conductor width (d), substrate thickness (H) and subunit cell periodicity (P) are discussed when each are individually analysed fixing all other unit cell parameters where the structure's mechanism is verified.

4.4.1 Conductor width $(\mathbf{d})$ effect

It has been shown by simulations that reducing grid conductor width reduces the resonance frequency and a thin conductor grid has least control on mutual coupling between bands as it enhances interaction among subunit cells. Conductor width effect is discussed to compare ECM approach to CST simulations. The grid width is reduced from $(\mathrm{d} = 2.5\ \mathrm{mm})$ to $(\mathrm{d} = 0.01\ \mathrm{mm})$ as lumped capacitances $(\mathrm{C_1}, \mathrm{C_2})$, subunit cell periodicity, substrate thickness, and interelement spacing are fixed.

Coupling factors are optimized in the ECM such that the magnetic coupling between grid inductances and substrate inductance are properly modelled in association with conductor effect. Table 4.7 shows that as conductor width reduces, inductances L_{C1}, L_{C2}, L_{D1} and L_{D2} are increased which illustrates the increase in associated coupling factors. Therefore, Thin grids are ineffective and enhance the undesired mutual coupling between subunit cells.

Table 4.7 Conductor Width (**d**) Effect – Circuit Model Elements. Gridded Miniaturised Dual Band HIS - Unit Cell: FR4 ($\varepsilon_r = 4.3, \tan\delta = 0.025$) **H** = 6.4 mm P = 15 mm $\mathbf{S_g}$ = 3 mm $\mathbf{C}_1$ = 48 pF $\mathbf{C}_2$ = 10.5 pF

d (mm)	L_s (nH)	L_C (nH)	L_D (nH)	$k_{(L_{C1}L_{C2})}$	$k_{(L_{C1}L_{D1})}$	$k_{(L_{C2}L_{D2})}$	$k_{(L_{C1}L_s)}$	$k_{(L_{C2}L_s)}$
2.5	8	4.3	0.2	0.2	0.01	0.01	0.4	0.4
1.5	8	6	0.46	0.29	0.06	0.06	0.47	0.47
1	8	7.1	0.7	0.32	0.11	0.11	0.48	0.48
0.5	8	9.3	1	0.51	0.12	0.12	0.5	0.5
0.01	8	21.4	2.7	0.608	0.38	0.275	0.575	0.575

Furthermore, expected analytical resonance frequency is in strong agreement with suggested resonance from full wave simulations as demonstrated in Table 4.8. Subsequent reduction in both bands resonance frequency is anticipated since grid inductances, L_C and L_D, in both subunit cells are increased as conductor width reduces.

Table 4.8 Conductor Width (**d**) Effect – Resonance Frequency. Gridded Miniaturised Dual Band HIS - Unit Cell: FR4 ($\varepsilon_r = 4.3, \tan\delta = 0.025$) **H** = 6.4 mm P = 15 mm $\mathbf{S_g}$ = 3 mm $\mathbf{C}_1$ = 48 pF $\mathbf{C}_2$ = 10.5 pF

					Simulated		Circuit Model	
d (mm)	g (mm)	C_p (pF)	L_C (nH)	L_D (nH)	f_1 (MHz)	f_2 (MHz)	f_1 (MHz)	f_2 (MHz)
2.5	0.25	0.85	4.3	0.22	511	1072	511	1074
1.5	0.75	0.6	6	0.46	445	949	447	949
1	1	0.53	7.1	0.7	426	909	425	908
0.5	1.25	0.48	9.3	1	409	887	404	887
0.01	1.495	0.44	21.4	2.7	392	864	395	864

4.4.2 Substrate thickness (H) effect

HIS electrically thin substrate is of an inductive nature, therefore, its effect is discussed as ECM is concerned. Lumped capacitors, unit cell parameters and conductor width are fixed as substrate thickness is reduced from (H = 12 mm) to (H = 3 mm). Table 4.9 shows that within a fixed conductor width, reducing substrate thickness only reduces substrate inductance (L_s) and coupling factor ($k_{(L_{C1}L_s)}, k_{(L_{C2}L_s)}$) is increased. Therefore, as substrate thickness decreases, the grid lines are strongly coupled to the HIS ground plane, which results in reducing mutual coupling between the HIS subunit cells. Moreover, in Table 4.10, simulated and analytical resonance frequency values are with good agreement where as substrate inductance reduces dual band resonance frequencies increase.

Table 4.9 Substrate Thickness (**H**) Effect – Circuit Model Elements. Gridded Miniaturised Dual Band HIS - Unit Cell: FR4 ($\varepsilon_r = 4.3, \tan\delta = 0.025$) P = 15 mm **S$_g$** = 3 mm **d** = 1 mm **g** = 1 mm **C$_1$** = 48 pF **C$_2$** = 10.5 pF **C$_p$** = 0.53 pF

H (mm)	L_s (nH)	L_C (nH)	L_D (nH)	$k_{(L_{C1}L_{C2})}$	$k_{(L_{C_1}L_{D_1})}$	$k_{(L_{C2}L_{D2})}$	$k_{(L_{C1}L_s)}$	$k_{(L_{C2}L_s)}$
12	15	7.1	0.7	0.4	-0.03	0.11	0.36	0.36
6.4	8	7.1	0.7	0.4	-0.03	0.11	0.48	0.48
3	4	7.1	0.7	0.4	-0.03	0.11	0.62	0.62

Table 4.10 Substrate Thickness (**H**) Effect – Resonance Frequency. Gridded Miniaturised Dual Band HIS - Unit Cell: FR4 ($\varepsilon_r = 4.3, \tan\delta = 0.025$) P = 15 mm **S$_g$** = 3 mm **d** = 1 mm **g** = 1 mm **L$_D$** = 0.7 nH **L$_C$** = 7.1 nH **C$_p$** = 0.53 pF **C$_1$** = 48 pF **C$_2$** = 10.5 pF

H (mm)		Simulated		Circuit Model	
	L_s (nH)	f_1 (MHz)	f_2 (MHz)	f_1 (MHz)	f_2 (MHz)
12	15	401	868	400	874
6.4	8	426	909	425	909
3	4	484	1022	487	1023

4.4.3 Periodicity (P) effect

Variation of subunit cell periodicity (P) is considered in this section for a fixed substrate thickness and lumped capacitor values. Subunit cell periodicity is reduced from (P = 30 mm) to (P = 7.5 mm). Therefore, interelement spacing (S_g), grid conductors (d) and patch gap (g) are eventually reduced since they are in direct relation to periodicity:
$(S_g = \frac{P}{5})$, $(d = \frac{S_g}{3})$, and $(g = \frac{S_g - d}{2})$.

Reduction in periodicity has consequently reduced mutual capacitance (C_p), grid inductances ($L_{C1} = L_{C2} = L_C$) and patch inductances ($L_{D1} = L_{D2} = L_D$), as in Table 4.11, where both bands simulated and analytical circuit model strongly agree with the expected increase in resonance frequencies. Also, the presence of grid conductors along the capacitive patch elements has rendered variation in both bands resonance frequencies consistent with respect to variation in unit cell periodicity.

Table 4.11 Periodicity (**P**) Effect – Resonance Frequency. Gridded Miniaturised Dual Band HIS - Unit Cell: FR4 ($\varepsilon_r = 4.3, \tan\delta = 0.025$) **H** = 6.4 mm **C**$_1$ = 48 pF **C**$_2$ = 10.5 pF

						Simulated		Circuit Model	
P (mm)	d (mm)	g (mm)	C_p (pF)	L_C (nH)	L_D (nH)	f_1 (MHz)	f_2 (MHz)	f_1 (MHz)	f_2 (MHz)
30	2	2	1	13.7	1.3	323	685	333	685
15	1	1	0.53	7.1	0.7	426	910	425	909
7.5	0.5	0.5	0.26	3.5	0.32	592	1307	591	1309

On the other hand, and as dual band mutual coupling is concerned, reduction in subunit cell periodicity increases dual band mutual coupling. As periodicity reduces, consequently the grid conductor width is reduced which weakens the desired isolation between adjacent subunit cells. Also, gaps between the centre patch and surrounding conductor reduces which increases mutual coupling between each subunit cell grid inductance and centre patch inductance, therefore, weakening the coupling between gridded capacitive HIS surface and ground plane. This is demonstrated through interpolated coupling coefficients in ECM, Table 4.12.

Table 4.12 Periodicity (**P**) Effect – Circuit Model Elements. Gridded Miniaturised Dual Band HIS - Unit Cell: FR4 ($\varepsilon_r = 4.3, \tan\delta = 0.025$) **H** = 6.4 mm **C**$_1$ = 48 pF **C**$_2$ = 10.5 pF

P (mm)	L_s (nH)	L_C (nH)	L_D (nH)	$k_{(L_{C1}L_{C2})}$	$k_{(L_{C1}L_{D1})}$	$k_{(L_{C2}L_{D2})}$	$k_{(L_{C1}L_s)}$	$k_{(L_{C2}L_s)}$
30	8	13.7	1.3	0.35	-0.2	-0.2	0.67	0.67
15	8	7.1	0.7	0.4	-0.03	-0.03	0.4	0.4
7.5	8	3.5	0.32	0.42	+0.01	+0.01	0.15	0.19

4.5 Gridded Miniaturised HIS Experimental Study

Miniaturised gridded dual band HIS of unit cell configuration as in Fig. 4.7, is modelled to operate at 875 MHz and 1120 MHz within a unit cell periodicity of 31 mm ($0.09\lambda_{875\text{MHz}}$) and supported on a 6.4 mm FR4 substrate ($\varepsilon_r = 4.3, \tan\delta = 0.025$). Adjacent alternate subunit cells (P = 15.5 mm) are loaded with two different capacitors(C_1 = 11 pF and C_2 = 7 pF) and fitted within a gap (g = 1 mm). Subunit cells are gridded with guard conductors of width (d = 1 mm). Fig. 4.14b presents simulated reflection coefficient, observed at normal incidence, for the miniaturised dual band gridded HIS modelled on CST Microwave Studio.

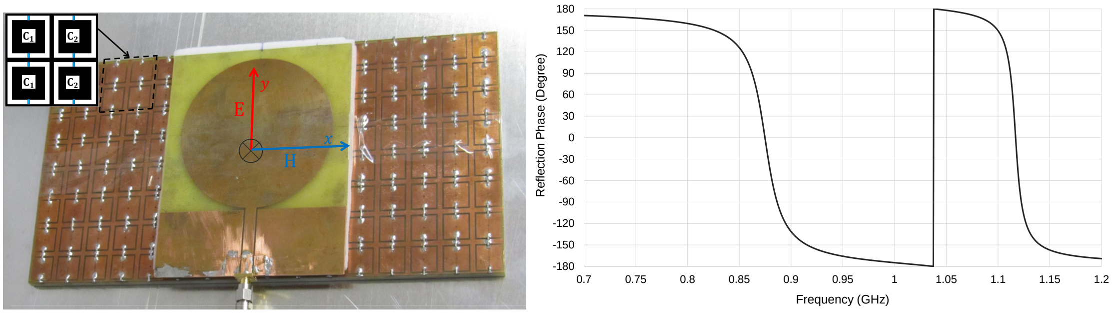

(a) Manufactured Antenna/HIS System (b) Unit Cell Reflection Phase

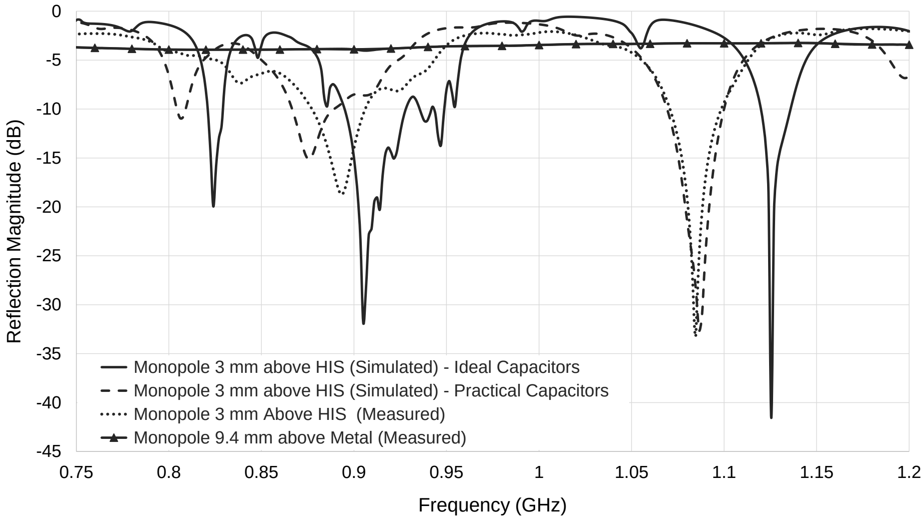

(c) Input Reflection Coefficient Magnitude

Fig. 4.14 UWB monopole antenna 0.01λ above miniaturised gridded capacitive patch lumped capacitor loaded dual band high impedance surface.

An Ultra Wideband (UWB) monopole antenna, printed on a 1.6 mm FR4 substrate ($\varepsilon_r = 4.3, \tan\delta = 0.025$), operating from 900 MHz is integrated 3 mm above the manufactured dual band miniaturised HIS, comprising of an array of 4 by 8 unit cells as shown in Fig. 4.14a. Moreover, Fig. 4.14c shows simulated and measured reflection magnitude of UWB monopole antenna integrated at $0.01\lambda_{1.12\mathrm{GHz}}$ above a miniaturised dual band gridded HIS structure and compared to the monopole placed at an equivalent height of $0.035\lambda_{1.12\mathrm{GHz}}$ above a metal surface. Considering antenna/HIS input match simulations for when the lumped capacitors are initially modelled as ideal components, it can be observed that there is significant disagreement between the simulated and measured antenna match reflection magnitude plots and resonance frequencies evident in both bands, as in Fig. 4.14c. Nevertheless, surface mount capacitors are associated with an Equivalent Series Resistor (ESR) and an Equivalent Series Inductor (ESL). Therefore, practical capacitors are included in the prediction model where a simulated and measured antenna-HIS system matching and resonance frequencies are of a better agreement as they are compared in Fig. 4.14c. For the low band, simulated ($|S_{11}| = -15$dB) is observed at 876 MHz as compared to measured ($|S_{11}| = -18.7$ dB), which is at 893 MHz associated with -10 dB bandwidth of 4%. Therefore, simulated and measured lower band resonance frequencies are offset by 17 MHz, which is not significant considering practical capacitor tolerance, measurement errors and numerical modelling inaccuracies. While for the upper band, reflection coefficient magnitude of simulation and measurement are in excellent agreement where an input match of -33 dB is observed at 1085 MHz and a -10 dB bandwidth of 2.5%.

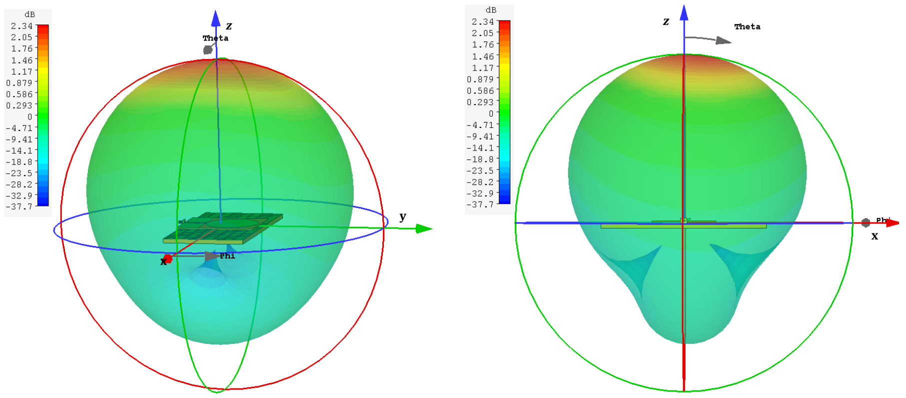

(a) E-Plane 3D View (b) H-Plane 3D View

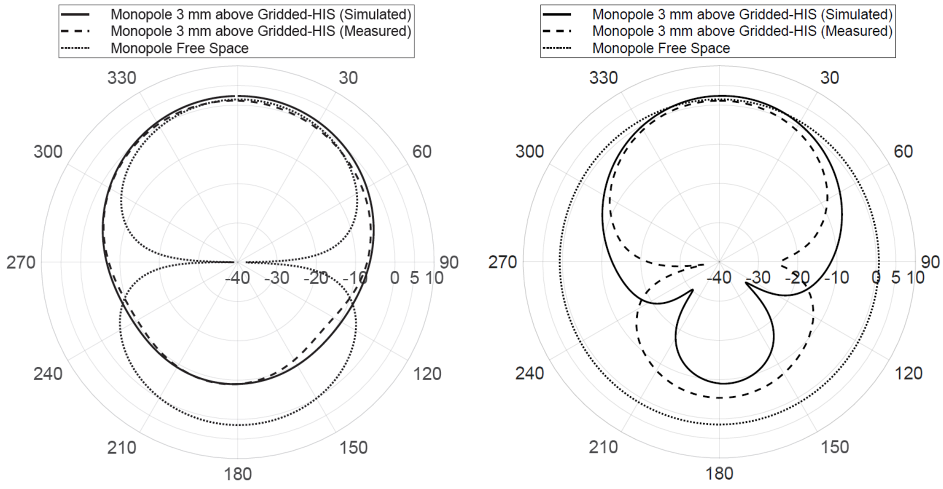

(c) E-Plane Polar Plots (d) H-Plane Polar Plots

Fig. 4.15 Lower Band, 880 MHz, simulated and measured gain pattern for low profile UWB monopole antenna 0.01λ above dual band lumped capacitor loaded gridded HIS.

Furthermore, Monopole $0.01\lambda_{1.12\text{GHz}}$ E and H plane gain pattern are considered for measurements conducted in an anechoic chamber and gain normalized with respect to a reference linearly polarized high gain horn antenna (HF 906) operating from 1 GHz to 18 GHz, compared to CST Microwave Studio simulations and also, collectively compared to radiation gain pattern of UWB monopole in free space. Resonance frequencies of 880 MHz and 1080 MHz are considered where antenna matching is below -10 dB in both measurements and simulations.

Regarding the lower band, 880 MHz, E and H plane polar plots gain pattern, are presented in Fig. 4.15c and Fig. 4.15d. A forward gain of 2.34 dBi and 1.12 dBi in simulations and measurements are observed respectively showing insignificant improvement while backward radiation is suppressed by 11dB. Nevertheless, the HIS provides improved antenna total efficiency of 33.5% as compared to a total efficiency of 7.5% when the antenna is placed at the same proximity to a metal surface; based on simulated results.

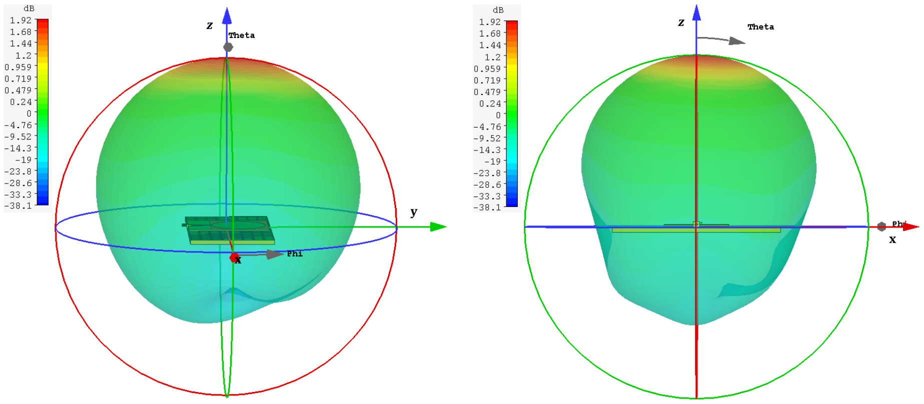

(a) E-Plane 3D View

(b) H-Plane 3D View

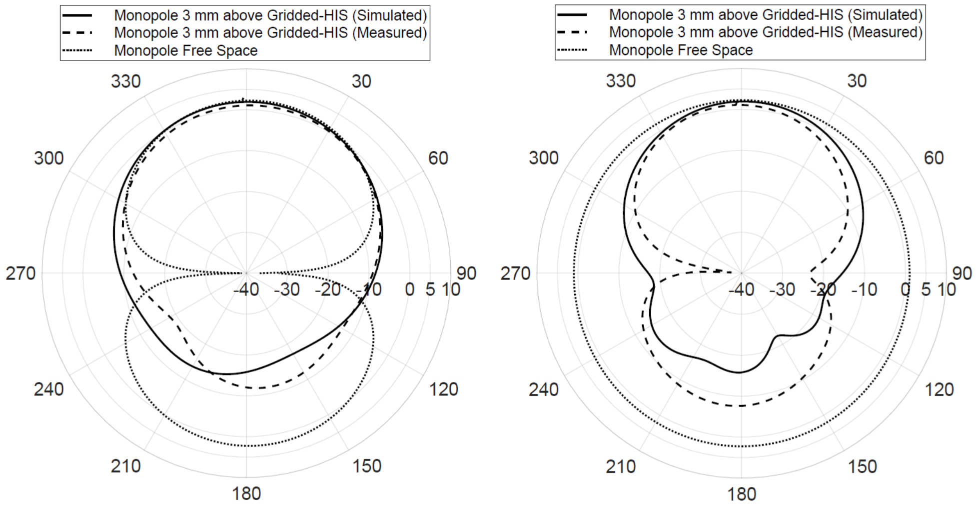

(c) E-Plane Polar Plots

(d) H-Plane Polar Plots

Fig. 4.16 Upper Band, 1080 MHz, simulated and measured gain pattern for low profile UWB monopole antenna 0.01λ above dual band lumped capacitor loaded gridded HIS.

As for the upper band, 1080 MHz, E and H plane simulated and measured gain patterns are in good agreement and detailed in Fig. 4.16c and Fig. 4.16d where measured boresight antenna gain is improved by 1.1 dB, as compared to the antenna in free space. Simulated total efficiency of 28% is realised for the antenna above HIS as compared to 15% total efficiency for the antenna placed above a metal surface.

Therefore, in both bands, substantial degradation in the antenna performance occur even though antenna matching is significantly improved by incorporating the gridded miniaturised dual band HIS. This is attributed to several factors that increased system losses such as the use of lossy FR4 substrate as well as ESR and ESL associated with lumped capacitors which have consequently reduced HIS effectiveness where a limited fractional bandwidth of 3% and 1% is noted in the lower and upper bands respectively.

4.6 Conclusion

Miniaturised HIS implementing lumped component loading has been proved effective to considerably reduce unit cell size where dual band performance was hindered by mutual coupling between adjacent subunit cells. This chapter has presented the design methodology of a novel miniaturised HIS that effectively reduced inter unit cell mutual coupling. The design featured an inductive grid structure to isolate adjacent subunit cells where each is individually tuned to the required band as controlled by the loaded capacitor value. The HIS mechanism has been explained in greater depth through a parametric analysis and empirical equivalent circuit model highlighting the effect of a guard conductor grid on the structure's performance. A Dual band unit miniaturised high impedance surface was proposed. Furthermore, dual band gridded miniaturised HIS was experimentally verified for a low profile UWB monopole antenna to be realised. Design limitations have been discussed, especially the significance of lumped capacitor resistive losses to degrade antenna performance. The next chapter will discuss miniaturisation of HIS using interdigital capacitors as an alternative approach to overcome lumped components losses.

Chapter 5

Single Band Interdigital High Impedance Surface Design Methodology

5.1 Introduction

Miniaturising High Impedance Surface (HIS) using lumped components has been discussed in Chapter 3 and Chapter 4. This technique offered great advantage to reduce the unit cell size significantly. However, capacitor's equivalent series resistance and inductance degrades the HIS performance. This chapter provides detailed design concepts to miniaturised single band HIS using Interdigital Capacitors (IDCs) as discussed analytically based on an equivalent circuit model approach. Three different single band interdigital HIS designs are presented. Interdigital HIS Design 1 features a Single Band Single Layer Single Polarized (SB-SLSP) interdigital HIS; the basic structure which design concepts apply to all what follows. In Design 1, SB-SLSP IDC HIS, analytical parametric study is conducted for gained insights on interdigital capacitor design, also experimentally verified as integrated with a planar antenna to realise a low profile antenna-HIS system. Next, interdigital HIS Design 2 is considered, which features a Single Band Dual Layer Dual Polarized (SB-DLDP) interdigital HIS as implemented using two layer interdigital capacitive surfaces. Finally, novel interdigital HIS Design 3 is discussed where a Single Band Single Layer Dual Polarized (SB-SLDP) interdigital HIS is presented, discussed analytically and verified experimentally as fabricated and integrated with a planar monopole antenna. The main focus of this thesis is dual band HIS design. However, this chapter is of significant importance as interdigital HIS is concerned. It provides all important design guidelines for three interdigital HIS prototypes discussed, where dual band HIS design is based on the integration of two single band interdigital HIS as will be discussed in Chapter 6 and Chapter 7.

5.2 Single Band Interdigital HIS Design 1 Fundamentals

5.2.1 Unit cell structure

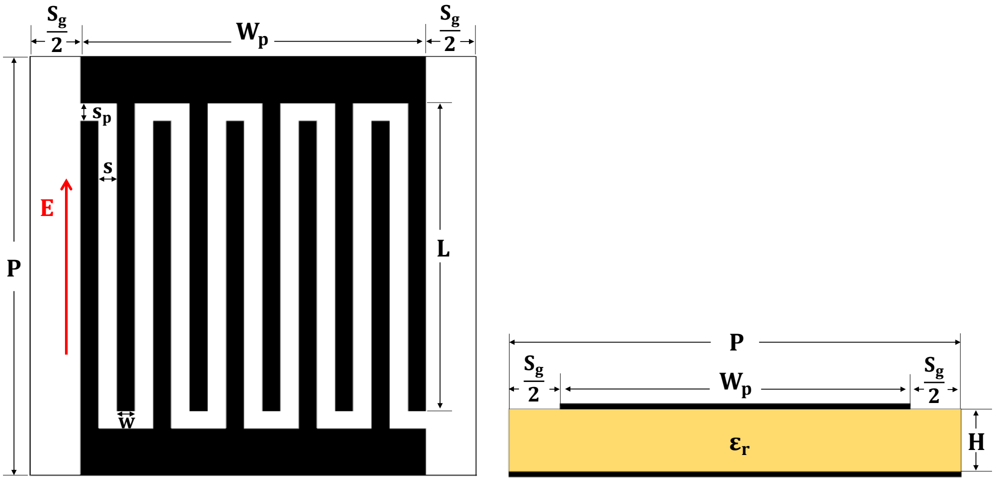

(a) Top View (b) Side View

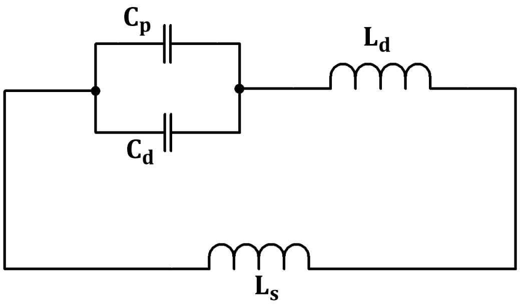

(c) Equivalent Circuit Model

Fig. 5.1 Single Band Single Layer Single Polarized Interdigital HIS.

Single Band Single Layer Single Polarized (SB-SLSP) interdigital HIS Design 1 parameters:

P	Unit cell IDC HIS periodicity
W_p	Unit cell IDC HIS patch width
S_g	Unit cell IDC HIS interelement spacing
H	Unit cell IDC HIS substrate thickness
L	Unit cell IDC HIS digits length
w	Unit cell IDC HIS digits width
s	Unit cell IDC HIS digits side/lateral gap
s_p	Unit cell IDC HIS end digits top/bottom gap

The structure comprises of Interdigital Capacitor (IDC) engineered within patch type unit cell, as shown in Fig. 5.1a, printed on a dielectric material and backed by metal, as in Fig. 5.1b. The HIS is polarization dependent where its effective sheet capacitance is maximized as the HIS is excited by vertically polarized electric field (E), as in Fig. 5.1a. The Equivalent Circuit Model (ECM) of the structure is detailed in Fig. 5.1c.

The resonance frequency is given by:

$$f_{r_{(SB\text{-}SLSP)}} = \frac{1}{2\pi\sqrt{(C_d + C_p)(L_d + L_s)}} \tag{5.1}$$

where

C_d and L_d are the interdigital capacitance and inductance respectively.

L_s is the dielectric substrate inductance which is linearly proportional to the HIS electrically thin dielectric substrate of thickness (H):

$$L_s = \mu_0 \mu_r H \tag{5.2}$$

and

C_p is the mutual capacitance generated within unit cell periodicity (P) and gap $(L + s_p)$ [123, 121]:

$$C_p = \varepsilon_0 \varepsilon_{eff} \frac{2P}{\pi} \log \frac{1}{\sin\left[\frac{\pi}{2}\frac{(L + s_p)}{P}\right]} \tag{5.3}$$

A square unit cell interdigital area is maintained where unit cell parameters are related as:

$$P = L + S_g + s_p = W_p + S_g \tag{5.4}$$

Also, Interdigital Capacitor (IDC) patch width (W_p) is function of periodic interdigital digits width (w), side gap (s) and number of digits (N_d), which is given by:

$$W_p = (w + s)N_d - s \tag{5.5}$$

IDC digits width (w) to IDC digits side gap (s) ratio is:

$$X_{ws} = \frac{w}{s} \tag{5.6}$$

Miniaturisation of interdigital HIS is governed by the design of interdigital capacitance (C_d) and inductance (L_d) which depends on the unit cell structure which will be detailed next.

5.2.2 Interdigital capacitance $(\mathrm{C_d})$

Conventional patch HIS unit cell loaded with interdigital elements presented in Fig. 5.1a. For maximum capacitive effect, interdigital digits length is maximized for optimum HIS miniaturisation. Therefore, a square interdigital area is considered setting $(\mathrm{L}+\mathrm{s_p}) \simeq \mathrm{P}$. Interdigital capacitance $(\mathrm{C_d})$, above a ground plane, is given by [124]:

$$\mathrm{C_d} = 2\varepsilon_0\varepsilon_{eff}\frac{\mathrm{K(k)}}{\mathrm{K'(k)}}(\mathrm{N_d}-1)\mathrm{L} \tag{5.7}$$

where $\varepsilon_{eff} = \dfrac{\varepsilon_r+1}{2}$ is the effective permittivity.
L and $\mathrm{N_d}$ are the interdigital digits length and number respectively.
and, $\dfrac{\mathrm{K(k)}}{\mathrm{K'(k)}}$ is the complete elliptical integral of first kind [124]:

$$\frac{\mathrm{K(k)}}{\mathrm{K'(k)}} = \begin{cases} \dfrac{1}{\pi}\ln\left(2\dfrac{1+\sqrt{\mathrm{k}}}{1-\sqrt{\mathrm{k}}}\right), & 0.707 \le \mathrm{k} \le 1 \\[2ex] \dfrac{\pi}{\ln\left(2\dfrac{1+\sqrt{\mathrm{k'}}}{1-\sqrt{\mathrm{k'}}}\right)}, & 1 \le \mathrm{k} \le 0.707 \end{cases} \tag{5.8}$$

k and $\mathrm{k'}$ are constants function of IDC digits width (w) and IDC side gap (s) [124]:

$$\mathrm{k} = \tan^2\left(\frac{\pi}{4}\frac{\mathrm{a}}{\mathrm{b}}\right) \quad \text{and} \quad \mathrm{k'} = \sqrt{1-\mathrm{k}^2} \tag{5.9}$$

where $\mathrm{a} = \dfrac{\mathrm{w}}{2}$ and $\mathrm{b} = \dfrac{(\mathrm{w}+\mathrm{s})}{2}$
Also, k is defined in terms of interdigital digits width to gap ratio $(\mathrm{X_{ws}} = \dfrac{\mathrm{w}}{\mathrm{s}})$:

$$\mathrm{k} = \tan^2\left(\frac{\pi}{4}\frac{\mathrm{X_{ws}}}{\mathrm{X_{ws}}+1}\right) \tag{5.10}$$

Next, design curves, interpolated from interdigital capacitance equation, are presented to provide intuition on understanding the significance of proper choice of interdigital design parameters such that capacitance is maximized and optimum miniaturisation is achieved. Interdigital capacitance is function of unit cell parameters such as substrate permittivity (ε_r), digits gap (s), digits width to gap ratio $(\mathrm{X_{ws}} = \dfrac{\mathrm{w}}{\mathrm{s}})$ and number of digits $(\mathrm{N_d})$.
First, interdigital capacitance per surface area $(\mathrm{W_p} \times \mathrm{L})$, in $\mathrm{pF/mm^2}$, is plotted versus interdigital digits width to gap ratio $(\mathrm{X_{ws}})$ for a fixed interdigital gap $(\mathrm{s} = 0.1\ \mathrm{mm})$ where

substrate permittivity is varied for ($\varepsilon_r = 1, 3, 5$ and 4), as shown in Fig. 5.2. For a given X_{ws}, interdigital capacitance density is increased as substrate effective permittivity increases according to the family of curves plotted. Also, maximum capacitance density is observed for digits width to gap ratio ($X_{ws} = 0.5$) irrespective of the choice of effective permittivity, as shown in Fig. 5.2.

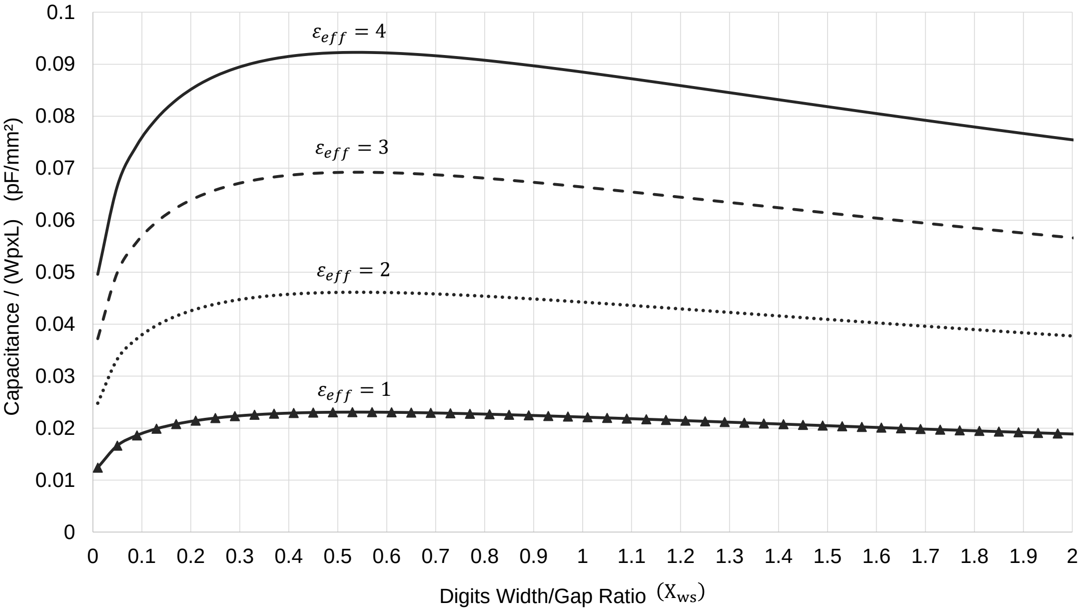

Fig. 5.2 Interdigital capacitance density versus digits width to gap ratio (X_{ws}) as effective permittivity varies ($\varepsilon_{reff} = 1, 2, 3, 4$). Interdigital digits gap (s = 0.1 mm).

Then, interdigital capacitance density in pF/mm^2, as per interdigital area ($W_p \times L$) and independent of effective permittivity (ε_{reff}), is plotted versus interdigital digits width to gap ratio ranging from ($0.01 \leq X_{ws} \leq 5$) where a family of curves for digits gap (s) varying from 0.01 mm to 0.5 mm is considered, as shown in Fig. 5.3. Therefore, optimum choice of digits gap, digits width and effective surface area is discussed such that capacitance is maximized within a miniaturised HIS unit cell. For a given digits width to gap ratio (X_{ws}), interdigital capacitance per unit area is increased as digits gap (s) is reduced where digits are strongly coupled. Hence, implementing interdigital elements which are closely spaced generates more capacitance within a reduced surface area. However, for a fixed digits gap (s), capacitance density is maximum when digits width (w) is half the digits gap (s), ($X_{ws} = 0.5$). Therefore, capacitance density degrades significantly as coupling between interdigital digits is reduced where digits width to gap ratio diverts from the optimum value of ($X_{ws} = 0.5$) and proper design choice is required.

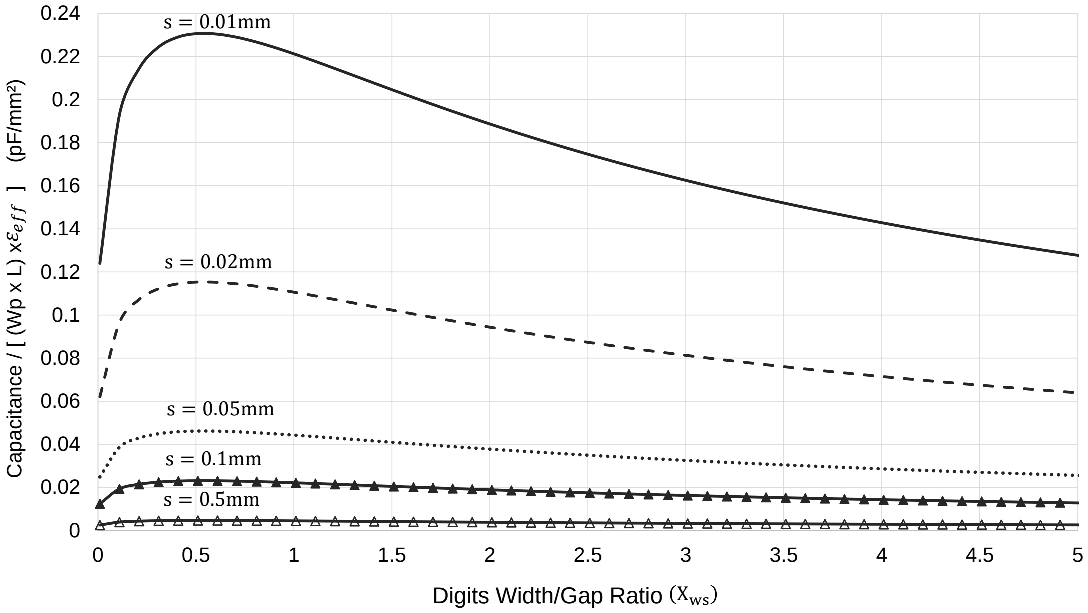

Fig. 5.3 Interdigital capacitance density per effective permittivity versus digits width to gap ratio (X_{ws}). Interdigital digits gap varies $(s(mm) = 0.01, 0.02, 0.05, 0.1, 0.5)$.

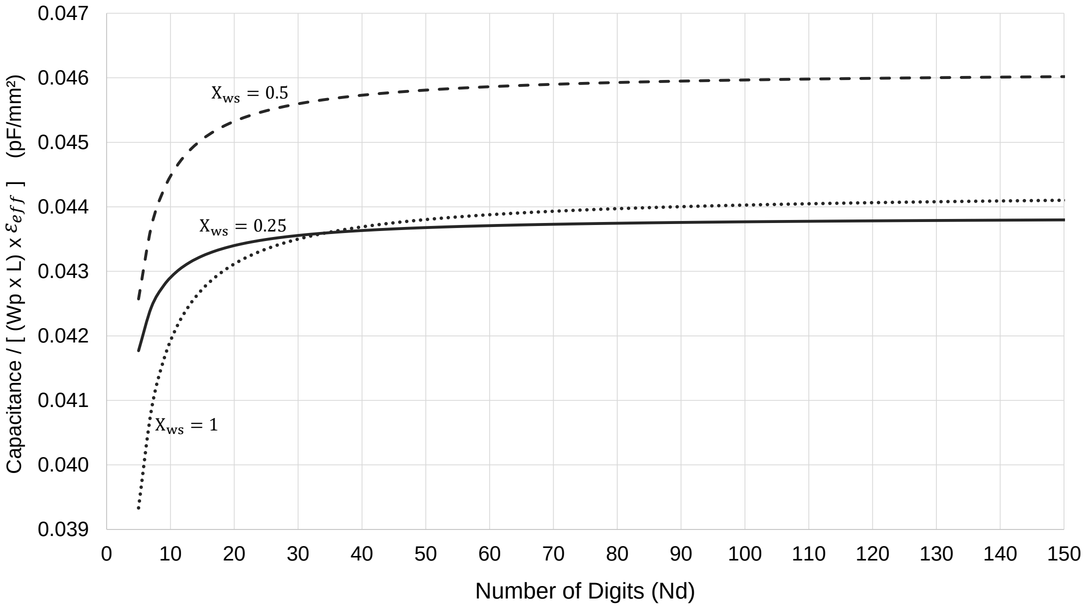

Fig. 5.4 Interdigital capacitance density versus number of digits (N_d). Digits width to gap ratio varied $(X_{ws} = 0.25, 0.5, 1)$ at a fixed interdigital digits gap of $(s = 0.1\text{ mm})$.

Finally, capacitance density per unit cross sectional area $(W_p \times L)$ and independent of effective permittivity (ε_{reff}) are plotted versus the interdigital number of digits (N_d), as shown in Fig. 5.4. The interdigital digits gap is fixed at $(s = 0.1\text{ mm})$ while a family of curves as interdigital digits width to gap ratio is varied for $(\mathrm{X_{ws}} = 0.25, 0.5, 1)$ is plotted. The digits width to gap ratio $(\mathrm{X_{ws}} = 0.5)$ is considered as an example and demonstrates that capacitance density rapidly increases as the number of digits $(\mathrm{N_d})$ increases, but then reaches a steady state when $(\mathrm{N_d} > 100)$ where any further increase of digits number is ineffective. A similar concept applies for cases where $(\mathrm{X_{ws}} = 0.25, 1)$ is observed. Therefore, aiming to increase interdigital capacitance by opting to only increase the number of digits $(\mathrm{N_d})$ is proven ineffective and would require a larger surface area to realise high capacitance values. Furthermore, interdigital digits coupling is maximized to generate optimum capacitance within a unit area when interdigital digits width to gap ratio is $(\mathrm{X_{ws}} = 0.5)$. For example, to achieve a unit capacitance density of 0.043 $(\mathrm{pF/mm^2})$, $(\mathrm{N_d} = 7, 11, 19)$ for $(\mathrm{X_{ws}} = 0.5, 0.25, 1)$ respectively reflects on miniaturisation power.

5.2.3 Interdigital inductance - approximation 1

Interdigital structure featuring high capacitance density with closely spaced intact digits can be approximated in analogy of periodic metallic dipoles [123, 121]:

$$\mathrm{L_{d(aprox1)}} = \mu_0 \frac{\mathrm{P}}{2\pi} \log \frac{1}{\sin\left[\frac{\pi}{2}\frac{\mathrm{W_p}}{\mathrm{P}}\right]} \tag{5.11}$$

Approximated interdigital inductance $(\mathrm{L_{d(aprox1)}})$, detailed in Eq. (5.11), is beneficial as a quick approximation of inductance to estimate the interdigital capacitance design parameters (digits gap (s), width (w), and number $(\mathrm{N_d})$) that are expected to generate the required capacitance in conjunction with design requirements such as frequency, periodicity, substrate permittivity and thickness. However, this method posses inaccuracies since interdigital inductance is under estimated. Nevertheless, interdigital inductance is practically not negligible. Next, proposed two methods to model interdigital inductance for better accuracy.

5.2.4 Interdigital inductance - approximation 2

For digits gap to substrate thickness $\left(\frac{\mathrm{s}}{\mathrm{H}} \ll 1\right)$, Interdigital inductance $(\mathrm{L_{d(aprox2)}})$ can be approximated as the inductance generated in a microstrip line section of width $(\mathrm{W_p})$ and length (L) [124, 125] . Therefore, $\mathrm{L_{d(aprox2)}}$, in nH, is:

$$\mathrm{L_{d(aprox2)}} = 0.2\mathrm{L}\left[\ln\left(\frac{\mathrm{L}}{\mathrm{W_p}+\mathrm{t}}\right) + 1.193 + \frac{\mathrm{W_p}+\mathrm{t}}{3\mathrm{L}}\right] \cdot \mathrm{K_d} \tag{5.12}$$

where L is the interdigital digits length. W_p is the interdigital plate width. t is the copper thickness. All dimensions are in mm.

K_d is the correction term when $\left(\frac{W_p}{H} > 0.05\right)$ such that the effect of HIS ground plane and substrate thickness (H) is taken into account [124]:

$$K_d = 0.57 - 0.145 \ln \frac{W_p}{H} \tag{5.13}$$

5.2.5 Interdigital inductance - approximation 3

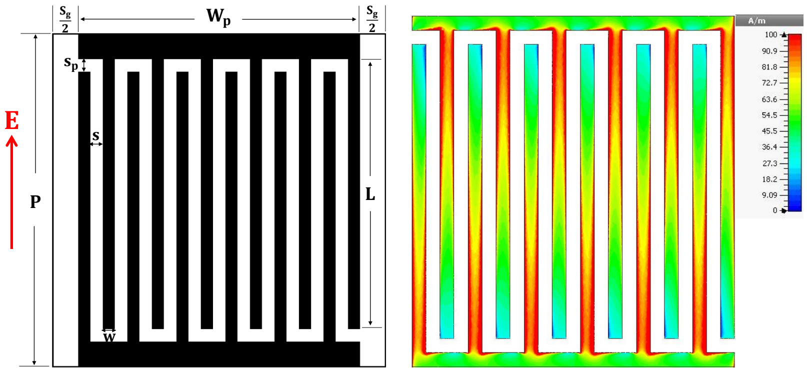

(a) Top View (b) Surface Current (900 MHz)

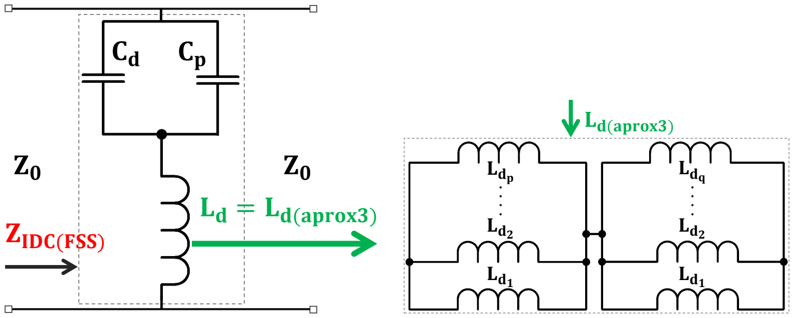

(c) Interdigital Capacitive Surface ECM (d) Interdigital Self Inductance ECM

Fig. 5.5 Single band interdigital capacitive surface detailed self inductance structure.

Proposed original method to determine the equivalent interdigital inductance as function of elementary inductances of individual digits. Top view of the interdigital capacitive surface unit cell structure and corresponding equivalent circuit model are presented in Fig. 5.5a and Fig. 5.5c respectively. An interdigital HIS optimized for 900 MHz as modelled on 7.6 mm FR4 ($\varepsilon_r = 4.3, \tan\delta = 0.025$) substrate is considered. Fig. 5.5b shows surface current distribution as observed in the top and lower digits, of length (L) and width (w), and which are supported by metallic strip of width (W_p). The top plate connecting digits

of number (p), generates an equivalent inductance as the result of elementary digits strip inductances connected in parallel. Where similar concept applies to the lower digits, of number (q), connected to the lower plate. The total equivalent inductance, of total digits number ($N_d = p + q$), is the series equivalence of top and lower interdigital plate inductances according to the expanded interdigital self inductance ECM, shown in Fig.5.5d.
The elementary digit self inductance (L_{di}), in nH, is [126, 127, 124, 125]:

$$L_{di} = 0.2L\left[\ln\left(\frac{L}{w+t}\right) + 1.193 + \frac{w+t}{3L}\right]K_d \tag{5.14}$$

where L is the digits length. w is the digits width. t is the copper thickness. All dimensions are in mm. K_d is defined in Eq. (5.13) as the correction factor when $\left(\frac{W_p}{H} > 0.05\right)$.
Therefore, the equivalent interdigital inductance, $L_{d(aprox3)}$, is :

$$L_{d(aprox3)} = \frac{L_{di}}{p} + \frac{L_{di}}{q} \tag{5.15}$$

where p and q are the top and bottom periodic digits number respectively, defined as:

$$p, q = \begin{cases} \frac{N_d}{2}, \frac{N_d}{2} & N_d \text{ even number} \\ \\ \frac{(N_d - 1)}{2}, \frac{(N_d - 1)}{2} + 1 & N_d \text{ odd number} \end{cases} \tag{5.16}$$

5.3 Single Band Interdigital HIS Design 1 Parametric Study

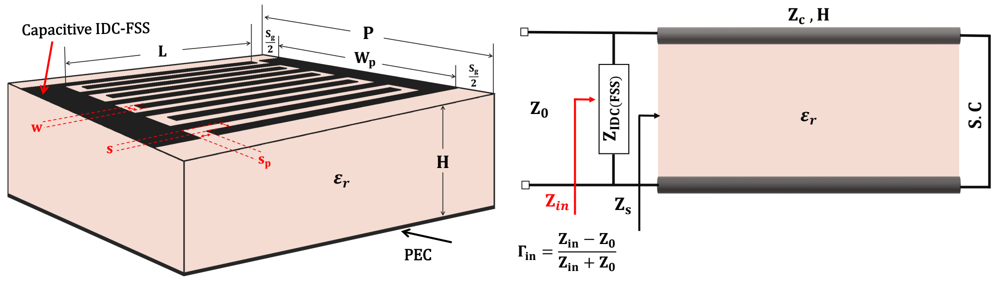

(a) 3D View (b) Transmission Line Model

Fig. 5.6 Miniaturised Single Band Single Layer Single Polarized (SB-SLSP) interdigital HIS.

The fundamental design equations of single band IDC HIS Design 1, shown in Fig. 5.6a, has been discussed in the previous section. Nevertheless, IDC HIS electromagnetic properties depend on the physical dimensions of the structure where the equivalent circuit model elements are interrelated. Parametric analysis on unit cell periodicity (P), substrate thickness (H), substrate relative permittivity (ε_r), digits number ($\mathrm{N_d}$), digits length (L), digits gap (s), digits width (w), and digits width to gap ratio ($\mathrm{X_{ws}} = \frac{\mathrm{w}}{\mathrm{s}}$) is conducted to investigate the effects on resonance frequency and operational bandwidth. Interdigital HIS is regarded as an FSS-based capacitive layer, supported by dielectric material and backed by metal. Fig. 5.6b shows transmission line model of interdigital HIS impedance ($\mathrm{Z_{IDC(FSS)}}$) loaded at the input of a shorted transmission line section of length (H). The input reflection coefficient (Γ_{in}) is:

$$\Gamma_{\mathrm{in}} = \frac{\mathrm{Z_{in}} - \mathrm{Z_0}}{\mathrm{Z_{in}} + \mathrm{Z_0}} \tag{5.17}$$

$\mathrm{Z_0} = 120\pi$ is the free space impedance. $\mathrm{Z_{in}}$ is interdigital HIS input impedance, defined as:

$$\mathrm{Z_{in}} = \frac{\mathrm{Z_s}\,\mathrm{Z_{IDC(FSS)}}}{\mathrm{Z_s} + \mathrm{Z_{IDC(FSS)}}} \tag{5.18}$$

$\mathrm{Z_{IDC(FSS)}}$ is the Interdigital FSS-based capacitive surface impedance:

$$\mathrm{Z_{IDC(FSS)}} = j\omega\mathrm{L_d} + \frac{1}{j\omega(\mathrm{C_d} + \mathrm{C_p})} \tag{5.19}$$

where ω is the angular frequency. $\mathrm{L_d}$ and $\mathrm{C_d}$ are the interdigital inductance and capacitance respectively. $\mathrm{C_p}$ is the mutual patch capacitance.

$\mathrm{Z_s}$ is the input impedance of a shorted electrically small transmission line section, which has a characteristic impedance ($\mathrm{Z_c}$) and a phase constant ($\beta = \frac{2\pi}{\lambda_g}$), defined as [128]:

$$\mathrm{Z_s} = j\mathrm{Z_c}\tan(\beta\mathrm{H}) \tag{5.20}$$

In Table 5.1, design parameters of an interdigital HIS, designed at 960 MHz, is detailed and taken as a reference for the analytical parametric study, which is conducted next.

Table 5.1 Reference Design 960 MHz SB-SLSP Interdigital HIS Design 1

Unit Cell Parameters	Values
FR4 Substrate permittivity (ε_r)	4.3
Substrate thickness(H)	6.4 mm
Periodicity(P)	12.5 mm
Interelement spacing($\mathrm{S_g}$)	1 mm
Number of digits $\mathrm{N_d}$	12
Digits side gap/width (s = w)	0.5 mm
Digits length (L)	11 mm

5.3.1 Substrate thickness (H) effect

Miniaturised interdigital HIS reference design parameters are fixed as given in Table 5.1 while substrate thickness (H) is reduced from 6.4 mm to 3.2 mm and 1.6 mm. Table 5.2 presents circuit model design components resulting when substrate thickness (H) is reduced, therefore, reducing substrate inductance (L_s) and interdigital inductance (L_d). As H reduces to 0.5H and 0.25H, the resonance frequency increases by 35% and 81% respectively, associated with a reduction in ±90° bandwidth to 6.7% and 4% respectively. Fig. 5.7 shows the corresponding analytical reflection phase plot to demonstrate the substrate thickness effect, which when increased the resonance frequency increases and the fractional bandwidth reduces.

Table 5.2 Interdigital HIS Substrate Thickness Effect - Unit Cell: FR4 ($\varepsilon_r = 4.3, \tan\delta = 0.025$) $\mathbf{P} = 12.5$ mm $\mathbf{S_g} = 1$ mm $\mathbf{W_p} = 11.5$ mm $\mathbf{L} = 11$ mm $\mathbf{N_d} = 12$ $\mathbf{s} = \mathbf{w} = 0.5$ mm

IDC HIS Circuit Parameters	Reference Design (H)	50% H	25% H
Substrate thickness (H)	6.4 mm	3.2 mm	1.6 mm
Substrate inductance (L_s)	8 nH	4 nH	2 nH
Interdigital inductance (L_d)	1.6 nH	1.3 nH	0.94 nH
Interdigital capacitance (C_d)	2.8 pF	2.8 pF	2.8 pF
Mutual Patch capacitance (C_p)	1.5e-3 pF	1.5e-3 pF	1.5e-3 pF
Resonance frequency (f_r)	960 MHz	1290 MHz	1730 MHz
% Increase in f_r	–	35%	81%
±90° Bandwidth	11%	6.7%	4%

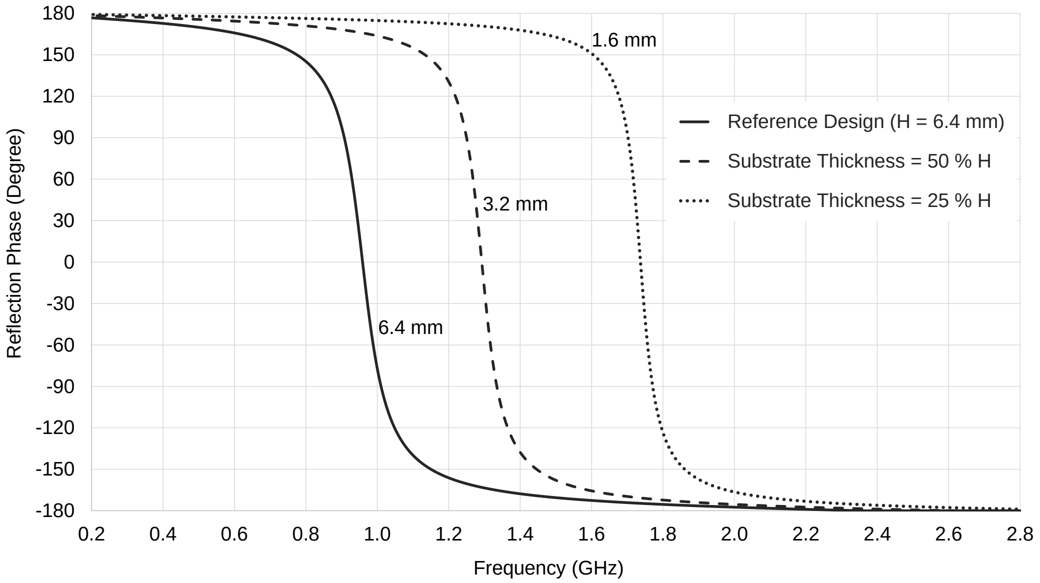

Fig. 5.7 Interdigital HIS substrate thickness (H) effect.

5.3.2 Unit cell periodicity (P) effect

Reference design parameters are fixed as given in Table 5.1 while only increasing unit cell periodicity (P) by consecutive factors of 2. Table 5.3 presents the circuit model analytical values where only mutual capacitance (C_p) is increased reducing the resonance frequency. Analytical reflection phase plot, Fig. 5.8 shows that resonance frequency reduces by 3% and 11% when the periodicity increases from 12.5 mm to 25 mm and 50 mm respectively. Increasing the periodicity reduces the HIS fractional bandwidth and is of least significance as miniaturisation is concerned.

Table 5.3 Interdigital HIS Periodicity Effect - Unit Cell: FR4 ($\varepsilon_r = 4.3, \tan\delta = 0.025$) $\mathbf{H} = 6.4$ mm $\mathbf{S_g} = 1$ mm $\mathbf{W_p} = 11.5$ mm $\mathbf{L} = 11$ mm $\mathbf{N_d} = 12$ $\mathbf{s} = \mathbf{w} = 0.5$ mm

IDC HIS Circuit Parameters	Reference Design (P)	2P	4P
Unit cell periodicity (P)	12.5 mm	25 mm	50 mm
Mutual Patch capacitance (C_p)	1.5e-3 pF	0.15 pF	0.78 pF
Interdigital inductance (L_d)	1.6 nH	1.6 nH	1.6 nH
Interdigital capacitance (C_d)	2.8 pF	2.8 pF	2.8 pF
Substrate inductance (L_s)	8 nH	8 nH	8 nH
Resonance frequency f_r	960 MHz	935 MHz	850 MHz
% Reduction in f_r	–	3%	11%
±90° Bandwidth	11%	10.5%	9.5%

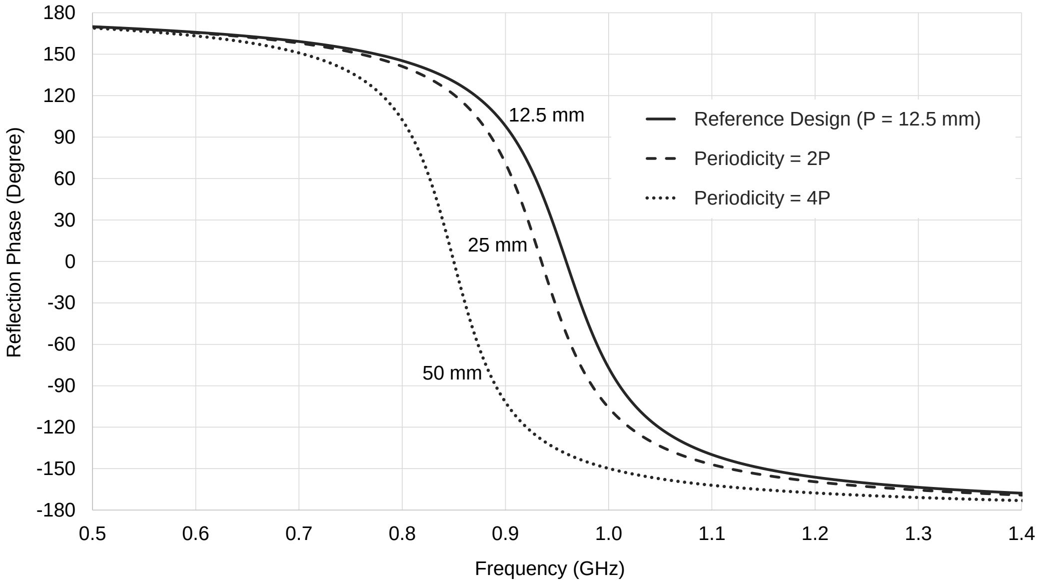

Fig. 5.8 Interdigital HIS periodicity (P) effect.

5.3.3 Substrate permittivity (ε_r) effect

Reference design parameters are fixed as given in Table 5.1 while the substrate permittivity (ε_r) is varied. As shown in Table 5.4, interdigital capacitance $(\mathrm{C_d})$ and mutual capacitance $(\mathrm{C_p})$ increases as the permittivity is increased by multiples of 2, from $(\varepsilon_r = 1)$, however, the resonance frequency reduces. Analytical reflection phase plot, shown in Fig 5.9, demonstrates consecutive reduction in the resonance frequency by 300 MHz, as permittivity increases retrospectively $(\varepsilon_r = 1, 2, 4.3, 8)$. Therefore,an average reduction of 22%, which is associated with a degradation in the HIS ±90° bandwidth.

Table 5.4 Interdigital HIS Substrate Relative Permittivity Effect - Unit Cell: $\mathbf{P} = 12.5$ mm $\mathbf{H} = 6.4$ mm $\mathbf{S_g} = 1$ mm $\mathbf{W_p} = 11.5$ mm $\mathbf{L} = 11$ mm $\mathbf{N_d} = 12$ $\mathbf{s} = \mathbf{w} = 0.5$ mm

IDC HIS Circuit Parameters	$\frac{\varepsilon_r}{4}$	$\frac{\varepsilon_r}{2}$	Ref. Design ε_r	$2\varepsilon_r$
Substrate permittivity (ε_r)	1	2	4.3	8
Interdigital capacitance $(\mathrm{C_d})$	1 pF	1.6 pF	2.8 pF	4.8 pF
Mutual Patch capacitance $(\mathrm{C_p})$	0.6e-3 pF	0.8e-3 pF	1.5e-3 pF	2.5e-3 pF
Interdigital inductance $(\mathrm{L_d})$	1.6 nH	1.6 nH	1.6 nH	1.6 nH
Substrate inductance $(\mathrm{L_s})$	8 nH	8 nH	8 nH	8 nH
Resonance frequency $(\mathrm{f_r})$	1570 MHz	1275 MHz	960 MHz	735 MHz
Consecutive % Reduction in $\mathrm{f_r}$	0%	18.5%	24%	23%
±90° Bandwidth	17.8%	14.4%	11%	8.5%

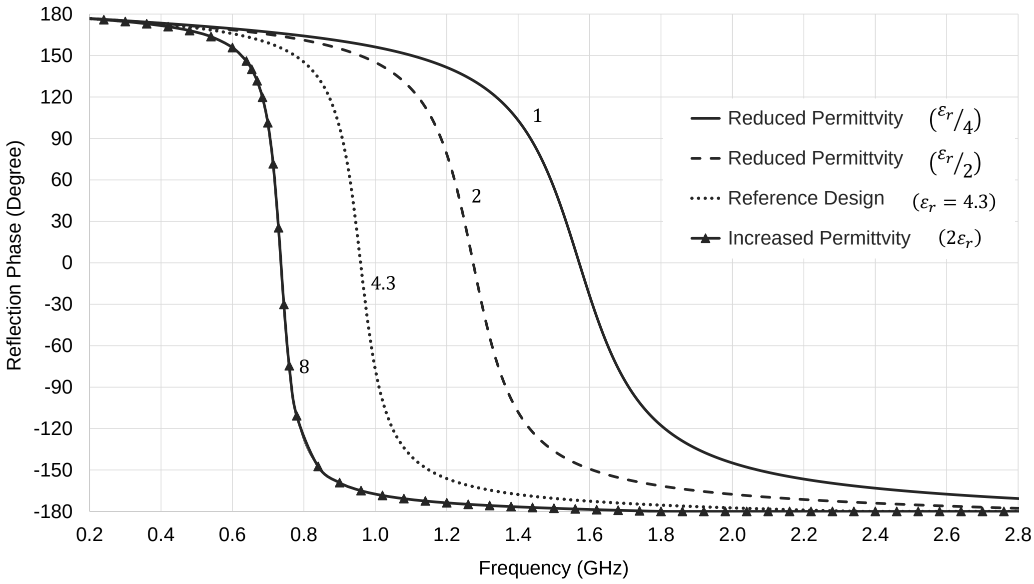

Fig. 5.9 Interdigital HIS substrate relative permittivity (ε_r) effect.

5.3.4 Interdigital number of digits $(\mathrm{N_d})$ effect

Interdigital number of digits $(\mathrm{N_d})$ is reduced by consecutive factors of 2, while IDC HIS unit cell parameters are fixed as given in Table 5.1. Reducing $\mathrm{N_d}$ reduces interdigital capacitance $(\mathrm{C_d})$, in addition to reducing interdigital patch plate of width $(\mathrm{W_p})$, which increases interdigital inductance $(\mathrm{L_d})$. Therefore, the resonance frequency increases as circuit model analysis suggests, Table 5.5. Analytical reflection phase, shown in Fig. 5.10, demonstrates that when $\mathrm{N_d}$ reduces from 12 to 6 and 3 the resonance frequency increases by 40% and 105% respectively, and the HIS fractional bandwidth improves.

Table 5.5 Interdigital HIS Number of Digits Effect - Unit Cell: FR4 $(\varepsilon_r = 4.3, \tan\delta = 0.025)$ $\mathbf{P} = 12.5$ mm $\mathbf{H} = 6.4$ mm $\mathbf{S_g} = 1$ mm $\mathbf{L} = 11$ mm $\mathbf{s} = \mathbf{w} = 0.5$ mm

IDC HIS Circuit Parameters	Reference Design $(\mathrm{N_d})$	$\frac{\mathrm{N_d}}{2}$	$\frac{\mathrm{N_d}}{4}$
Interdigital digits number $(\mathrm{N_d})$	12	6	3
Interdigital capacitance $(\mathrm{C_d})$	2.8 pF	1.3 pF	0.5 pF
Interdigital inductance $(\mathrm{L_d})$	1.6 nH	2.7 nH	4.3 nH
Mutual Patch capacitance $(\mathrm{C_p})$	1.5e-3 pF	1.5e-3 pF	1.5e-3 pF
Substrate inductance $(\mathrm{L_s})$	8 nH	8 nH	8 nH
Resonance frequency $(\mathrm{f_r})$	960 MHz	1350 MHz	1980 MHz
% Increase in $\mathrm{f_r}$	–	40%	105%
±90° Bandwidth	11%	13.6%	17.3%

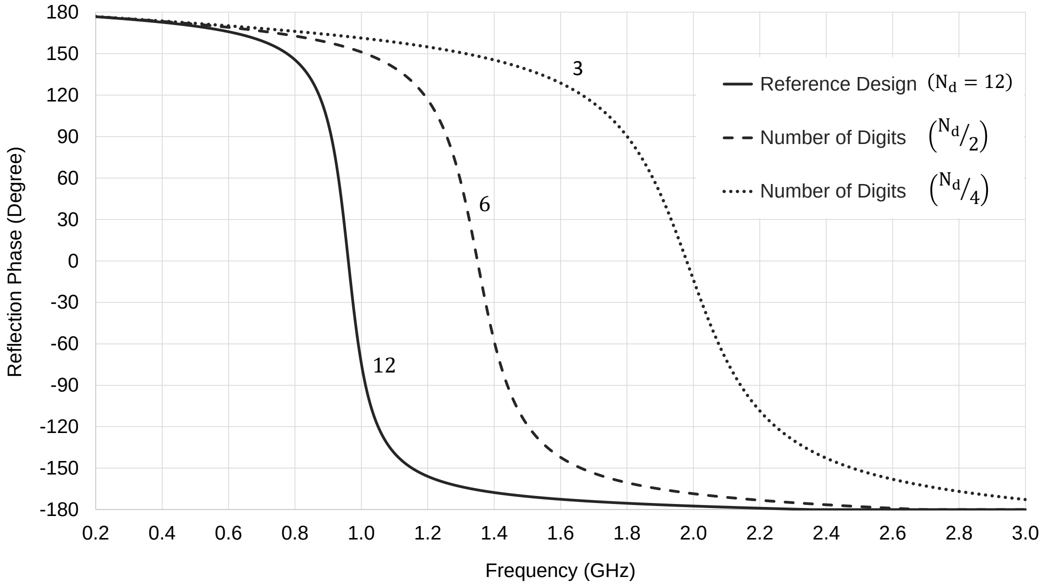

Fig. 5.10 Interdigital HIS number of digits $(\mathrm{N_d})$ effect.

5.3.5 Interdigital digits length (L) effect

Interdigital parameters fixed as reference design parameters as given in Table 5.1, while interdigital digits length (L) is reduced by consecutive factors of 2. Analytical circuit model parameter values, shown in Table 5.6, demonstrates that mutual capacitance (C_p), interdigital capacitance (C_d) and inductance (L_d) reduces due to the reduction in L, which increases the resonance frequency. Analytical reflection phase, shown in Fig. 5.11, demonstrates that the resonance frequency increases by 45% and 90% when the digits length (L) is reduced from 11 mm to 5.5 mm and 2.75 mm respectively, where the HIS ±90° bandwidth increases.

Table 5.6 Interdigital HIS Digits Length Effect-Unit Cell: FR4 ($\varepsilon_r = 4.3, \tan\delta = 0.025$) $\mathbf{P} =$ 12.5 mm $\mathbf{H} = 6.4$ mm $\mathbf{S_g} = 1$ mm $\mathbf{W_p} = 11.5$ mm $\mathbf{N_d} = 12$ $\mathbf{s} = \mathbf{w} = 0.5$ mm

IDC HIS Circuit Parameters	Reference Design (L)	$\frac{L}{2}$	$\frac{L}{4}$
Interdigital digits length (L)	11 mm	5.5 mm	2.75 mm
Interdigital capacitance (C_d)	2.8 pF	1.4 pF	0.7 pF
Interdigital inductance (L_d)	1.6 nH	0.6 nH	0.3 nH
Mutual Patch capacitance (C_p)	1.5e-3 pF	0.07 pF	0.17 pF
Substrate inductance (L_s)	8 nH	8 nH	8 nH
Resonance frequency (f_r)	960 MHz	1390 MHz	1830 MHz
% Increase in f_r	–	45%	90%
±90° Bandwidth	11%	17.5%	24%

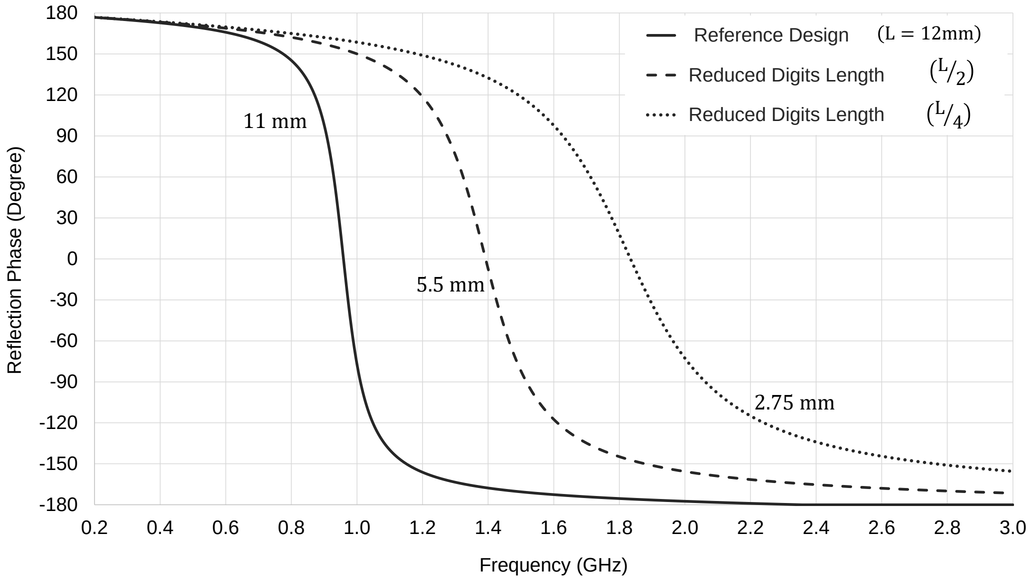

Fig. 5.11 Interdigital HIS digits length (L) effect.

5.3.6 Interdigital digits gap/width $(\mathrm{s} = \mathrm{w})$ effect

Interdigital digits gap (s) and width (w) are reduced but kept equal $(\mathrm{X_{ws}} = \frac{\mathrm{w}}{\mathrm{s}} = 1)$, where the HIS parameters are fixed as given in Table 5.1. According to analytical circuit model parameter, interdigital inductance $(\mathrm{L_d})$ and mutual capacitance $(\mathrm{C_p})$ increases which reduces resonance the frequency, as shown in Table 5.7. However, the frequency reduction is insignificant citing 5% and 10% when $(\mathrm{s} = \mathrm{w})$ reduces from 0.5 mm to 0.25 mm and 0.125 mm respectively as demonstrated in reflection phase plot, shown in Fig 5.12. This is due to no variation in the interdigital capacitance since $(\mathrm{s} = \mathrm{w})$.

Table 5.7 Interdigital HIS Digits Gap and Width Effect at $(\mathrm{X_{ws}} = 1)$ - Unit Cell: FR4 $(\varepsilon_r = 4.3, \tan\delta = 0.025)$ $\mathbf{P} = 12.5$ mm $\mathbf{H} = 6.4$ mm $\mathbf{S_g} = 1$ mm $\mathbf{N}_\mathrm{d} = 12$ $\mathbf{L} = 11$ mm

IDC HIS Circuit Parameters	Ref. Design $(\mathrm{s} = \mathrm{w})$	$\frac{\mathrm{s}}{2} = \frac{\mathrm{w}}{2}$	$\frac{\mathrm{s}}{4} = \frac{\mathrm{w}}{4}$
Interdigital digits gap/width $(\mathrm{s} = \mathrm{w})$	0.5 mm	0.25 mm	0.125 mm
Interdigital digits plate width $(\mathrm{W_p})$	11.5 mm	5.75 mm	2.875 mm
Interdigital inductance $(\mathrm{L_d})$	1.6 nH	2.6 nH	4 nH
Mutual Patch capacitance $(\mathrm{C_p})$	1.5e-3 pF	2.3e-3 pF	2.8e-3 pF
Interdigital capacitance $(\mathrm{C_d})$	2.8 pF	2.8 pF	2.8 pF
Substrate inductance $(\mathrm{L_s})$	8 nH	8 nH	8 nH
Resonance frequency $(\mathrm{f_r})$	960 MHz	915 MHz	860 MHz
% Reduction in $\mathrm{f_r}$	–	5%	10%
±90° Bandwidth	11%	9.5%	8%

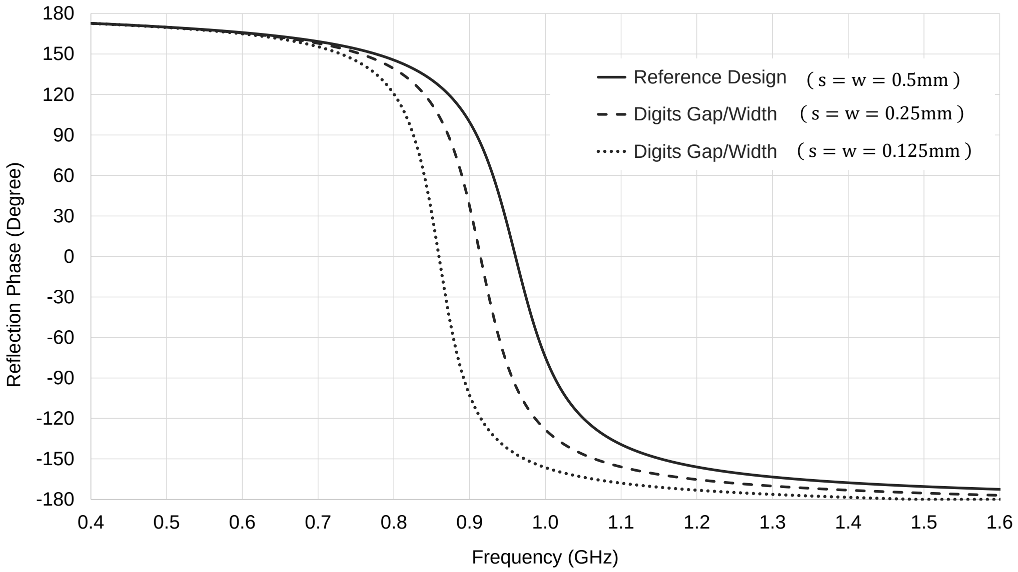

Fig. 5.12 Interdigital HIS digits gap (s) and width (w) effect where $(\mathrm{s} = \mathrm{w})$.

5.3.7 Interdigital digits gap (s) effect

Reference HIS design parameters are fixed as given in Table 5.1, while the gap between interdigital digits (s) is reduced by consecutive factors of 2. According to analytical circuit model, reducing digits gap increases interdigital capacitance (C_d), interdigital inductance (L_d) and mutual capacitance (C_p), therefore, reducing the resonance frequency by an average of 12%, as shown in Table 5.8. In addition, analytical reflection phase, shown in Fig. 5.13, demonstrates the effect of reducing the interdigital digits gap from 0.5 mm to 0.25 mm and 0.125 mm, where the HIS resonance frequency and fractional bandwidth reduces.

Table 5.8 Interdigital HIS Digits Gap Effect - Unit Cell: FR4 ($\varepsilon_r = 4.3, \tan\delta = 0.025$) $\mathbf{P} = 12.5$ mm $\mathbf{H} = 6.4$ mm $\mathbf{S_g} = 1$ mm $\mathbf{N}_d = 12$ $\mathbf{L} = 11$ mm $\mathbf{w} = 0.5$ mm

IDC HIS Circuit Parameters	Reference Design (s)	$\frac{s}{2}$	$\frac{s}{4}$
Interdigital digits gap (s)	0.5 mm	0.25 mm	0.125 mm
Interdigital digits plate width (W_p)	11.5 mm	8.75 mm	7.375 mm
Interdigital capacitance (C_d)	2.8 pF	3.6 pF	4.6 pF
Interdigital inductance (L_d)	1.6 nH	1.95 nH	2.2 nH
Mutual Patch capacitance (C_p)	1.5e-3 pF	2.3e-3 pF	2.8e-3 pF
Substrate inductance (L_s)	8 nH	8 nH	8 nH
Resonance frequency (f_r)	960 MHz	835 MHz	735 MHz
% Reduction in f_r	–	12%	23%
±90° Bandwidth	11%	9%	7.5%

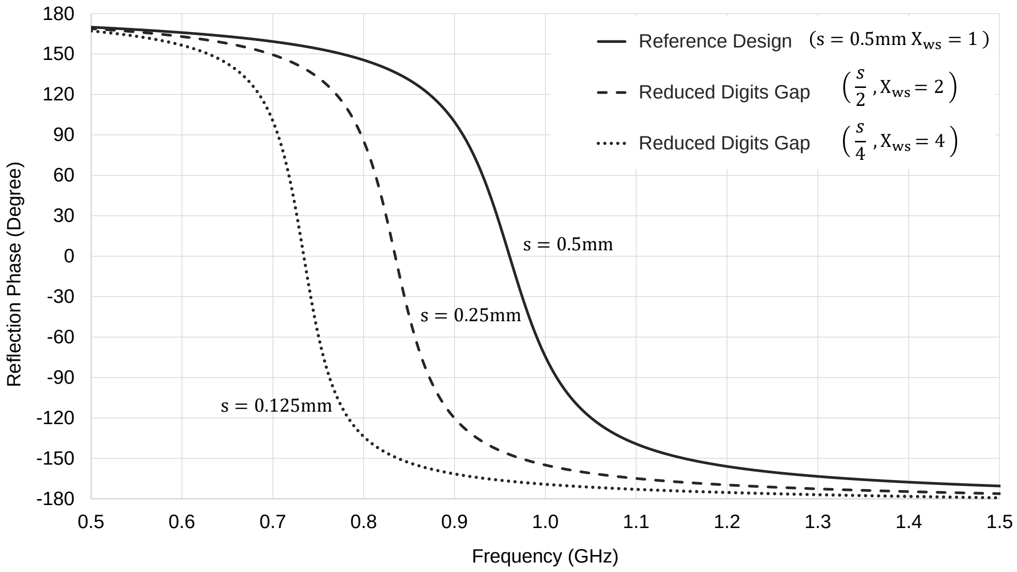

Fig. 5.13 Interdigital HIS digits gap (s) and digits width to gap ratio (X_{ws}) effect.

5.3.8 Interdigital digits width (w) effect

Interdigital digits width (w) is varied while fixing all HIS design parameters as given in Table 5.1. Reducing the digits width (w) has opposite effect as when digits gap (s) is reduced. According to analytical circuit model, reducing digits width by a factor of 2, reduces interdigital capacitance (C_d) and increases interdigital inductance (L_d), which results in increasing the resonance frequency and fractional bandwidth by an average of 11% and 0.5% respectively, as demonstrated in Table 5.1 and analytical reflection phase plot, Fig. 5.14.

Table 5.9 Interdigital HIS Digits Width Effect - Unit Cell: FR4 ($\varepsilon_r = 4.3, \tan\delta = 0.025$) $\mathbf{P} = 12.5$ mm $\mathbf{H} = 6.4$ mm $\mathbf{S_g} = 1$ mm $\mathbf{N}_\mathrm{d} = 12$ $\mathbf{L} = 11$ mm $\mathbf{s} = 0.5$ mm

IDC HIS Circuit Parameters	Reference Design (w)	$\frac{w}{2}$	$\frac{w}{4}$
Interdigital digits width (w)	0.5 mm	0.25 mm	0.125 mm
Interdigital digits plate width ($W_\mathbf{p}$)	11.5 mm	8.5 mm	7 mm
Interdigital capacitance (C_d)	2.8 pF	2.2 pF	1.75 pF
Interdigital inductance (L_d)	1.6 nH	2 nH	2.3 nH
Mutual Patch capacitance (C_p)	1.5e-3 pF	1.5e-3 pF	1.5e-3 pF
Substrate inductance (L_s)	8 nH	8 nH	8 nH
Resonance frequency (f_r)	960 MHz	1065 MHz	1170 MHz
% Increase in f_r	–	11%	22%
±90° Bandwidth	11%	11.5%	12.3%

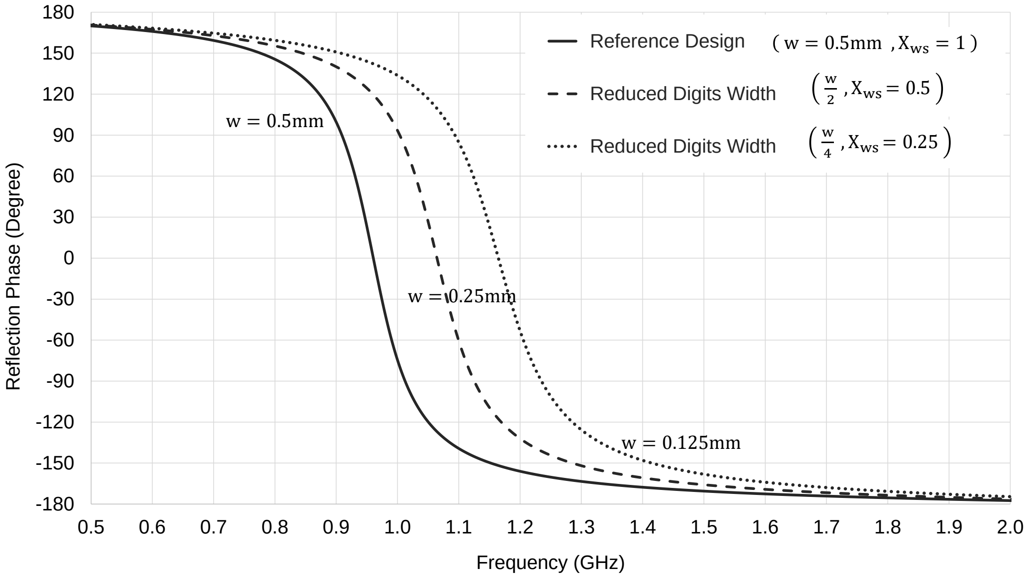

Fig. 5.14 Interdigital HIS digits gap (w) and digits width to gap ratio (X_{ws}) effect.

5.4 Single Band Interdigital HIS Design 1 Verification

In this section, effective implementation of interdigital capacitors within an optimum unit cell size is discussed. Moreover, Single Band Single Layer Single Polarized (SB-SLSP) interdigital HIS Design 1 is compared against its counterpart technique where surface mount capacitors are used. Thereafter, HIS Design 1 is fabricated and integrated with a monopole antenna where a low profile antenna system is realised.

5.4.1 Optimizing interdigital HIS for effective miniaturisation

Where HIS miniaturisation using Interdigital Capacitors (IDC) is possible, it is important that a miniature unit cell size and substrate thickness is maintained such that a compact light weight HIS is realised, therefore, a high IDC density within a given surface area is required. Nevertheless, according to the previously conducted parametric study, maximizing interdigital capacitor density strongly depends on unit cell size and is possible by maximizing the number of digits $(\mathrm{N_d})$, minimizing digits gap (s), setting digits width to gap ratio to $(\mathrm{X_{ws}} = 0.5)$, and engineering the interdigital elements within the entire unit cell surface area.

Table 5.10 Interdigital Single Band HIS Design 1 Unit Cell and ECM Parameters. Modelled on 6.4 mm FR4 $(\varepsilon_r = 4.3, \tan\delta = 0.025)$. 1550 MHz Optimized For Reduced Periodicity.

SB-SLSP IDC HIS Parameters	Original	Optimized
Periodicity (P)	12 mm	6 mm
Electrical periodicity (P/λ)	0.06	0.03
Number of digits $(\mathrm{N_d})$	10	10
Digits side gap $(\mathrm{s} = \mathrm{w})$	0.5 mm	0.28 mm
Digits length (L)	4.8 mm	5 mm
Interdigital capacitance $(\mathrm{C_d})$	1.1 pF	1.1 pF
Interdigital inductance $(\mathrm{L_d})$	0.7 nH	1 nH
Mutual capacitance $(\mathrm{C_p})$	80e-3 pF	1.4e-3 pF
Substrate inductance $(\mathrm{L_d})$	8 nH	8 nH

Two interdigital SB-SLSP HIS structures are compared. Both are designed to operate at 1550 MHz and modelled on 6.4 mm (0.03λ) FR4 substrate $(\varepsilon_r = 4.3, \tan\delta = 0.025)$. Interelement spacing to periodicity ratio is fixed at 1/12 for consistency. The original design, Fig. 5.15a, features a 0.06λ unit cell where interdigital elements are structured within a rectangular surface area. With an optimized design, as in Fig. 5.15b, the unit cell is reduced by 50% to 0.03λ and interdigital elements are engineered within the whole unit cell square surface area. Original and optimized interdigital HIS design unit cell and analytical circuit model parameters are given in Table 5.10. Both designs generate the same interdigital capacitance (C_d) of 1.1 pF. However, optimized interdigital HIS unit cell digits width and gap are reduced as compared to the original design. The number of digits (N_d), is expected to increase as unit cell size reduces, but not for this particular case as the calculation suggested. Reduced size design has a larger interdigital inductance (L_d) and reduced mutual capacitance (C_p), as detailed in Table 5.10. The reflection phase plot for original and optimized interdigital HIS structures, as modelled on CST Microwave Studio and simulated at normal incidence, demonstrates both designs to resonate at 1550 MHz featuring a ±90° bandwidth of 20%, as in Fig. 5.15c. Effective miniaturisation is achieved by implementing optimized SB-SLSP IDC HIS of periodicity 0.03λ, but, possess manufacturing limitations to accurately fabricate a digit track width of 0.28 mm, therefore, a trade off between manufacturing possibilities and modelling is required.

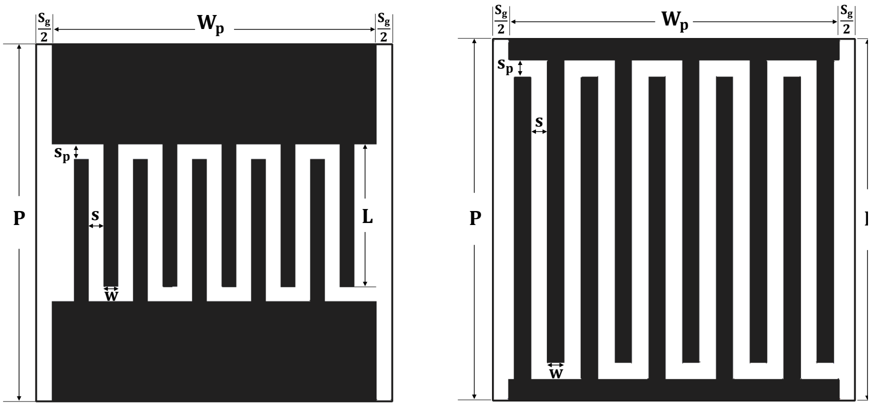

(a) 0.06λ Unit Cell (b) 0.03λ Unit Cell

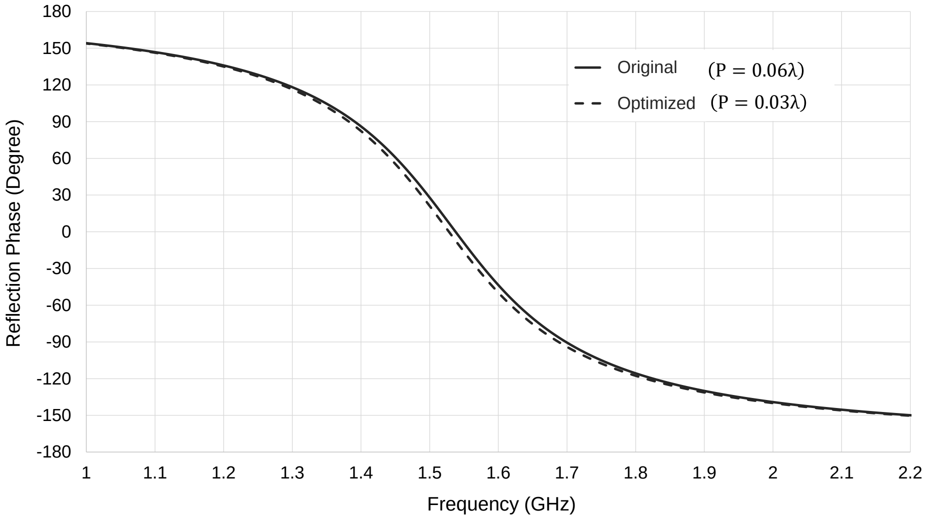

(c) Reflection Phase

Fig. 5.15 Single band interdigital HIS Design 1. Optimized for reduced periodicity.

5.4.2 Experimental verification

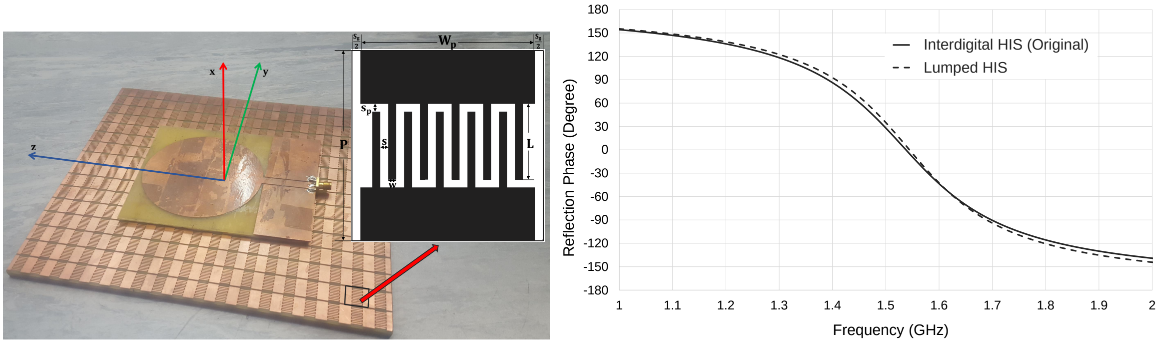

(a) Manufactured Antenna/HIS System (b) Unit Cell Reflection Phase

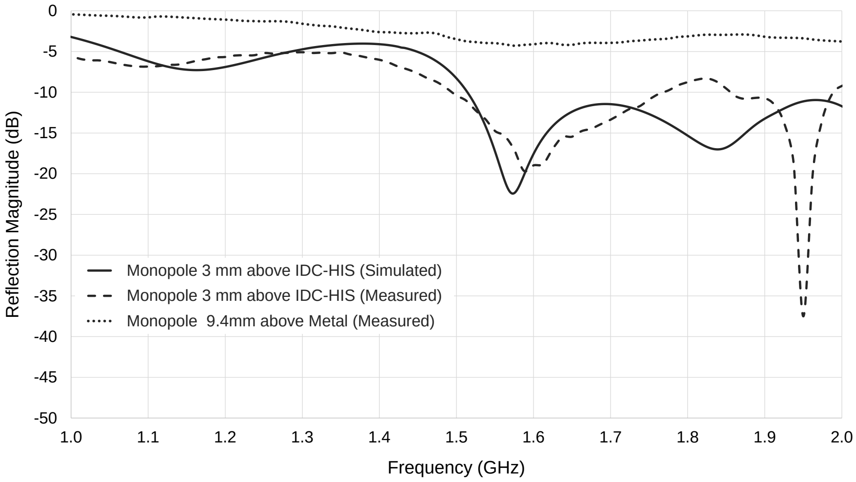

(c) Input Reflection Coefficient Magnitude

Fig. 5.16 Low profile UWB monopole antenna 3 mm above miniaturised interdigital HIS.

Interdigital HIS design in Fig. 5.15b was hindered by manufacturing constraints, therefore, the design in Fig. 5.15a is manufactured and considered in the next analysis.

Interdigital HIS (Original design), in Fig. 5.15a, designed to operate at 1550 MHz, is compared against the case where lumped components replace Interdigital Capacitor (IDC) in the form of an equivalent series impedance comprising of capacitor $(\mathrm{C_d} = 1\ \mathrm{pF})$ and inductance $(\mathrm{L_d} = 0.7\ \mathrm{nH})$, therefore, counterpart miniaturisation technique is assessed. At normal incidence, IDC and lumped component HIS simulated reflection phase plots strongly agree, as shown in Fig. 5.16b.

SB-SLSP interdigital HIS Design 1, Fig. 5.15a, is then manufactured into a 216 mm × 192 mm periodic array as printed on 6.4 mm FR4 substrate $(\varepsilon_r = 4.3, \tan\delta = 0.025)$ and backed by metal. The surface is integrated with a linearly polarized Ultra Wide Band (UWB) monopole antenna operating from 900 MHz. A monopole antenna, of electrical dimensions $0.06\lambda_{1.55\mathrm{GHz}} \times 0.05\lambda_{1.55\mathrm{GHz}}$, is printed on 1.6 mm FR4 substrate $(\varepsilon_r = 4.3, \tan\delta = 0.025)$ and centred 3mm above IDC HIS $(x = y = z = 0)$ featuring a total electrical height of $0.05\lambda_{1.55\mathrm{GHz}}$, as in Fig. 5.16a. Simulated and measured magnitude of reflection coefficients are presented in Fig. 5.16c as compared against when the antenna is placed $0.05\lambda_{1.55\mathrm{GHz}}$ above a metal surface. The antenna is well matched to the surface for $(|\mathrm{S}_{11}| = -17\mathrm{dB})$ and $(|\mathrm{S}_{11}| = -15\mathrm{dB})$ in simulation and measurement respectively, observed at 1550 MHz. While, measured $|\mathrm{S}_{11}|$ degrades to -4dB for antenna $0.05\lambda_{1.55\mathrm{GHz}}$ above a metal surface, therefore, a low profile antenna system is realised as interdigital HIS is implemented.

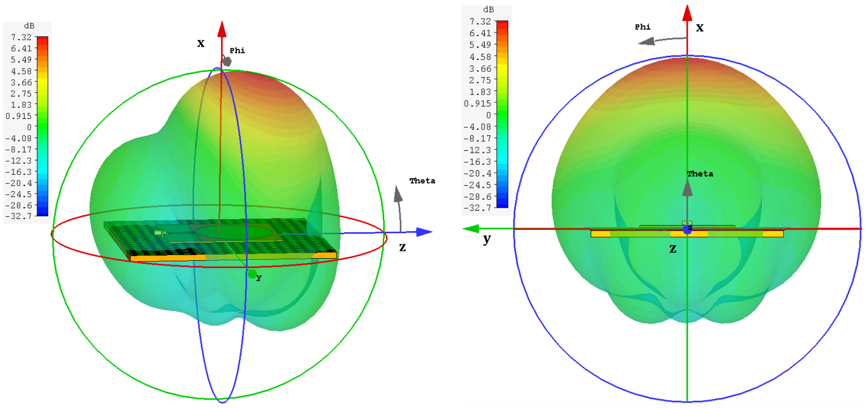

(a) E Plane 3D View (b) H Plane 3D View

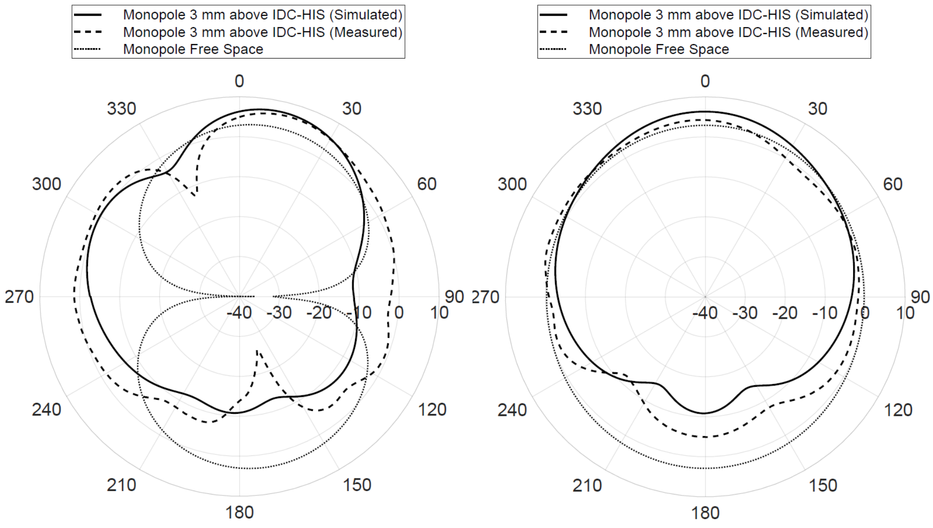

(c) E Plane Polar Plots (d) H Plane Polar Plots

Fig. 5.17 Monopole SB-SLSP IDC HIS system 1550 MHz E H plane radiation pattern.

Measurement of radiation patterns for UWB monopole mounted 0.015λ above interdigital HIS is conducted in an anechoic chamber. Fig. 5.17 shows measured E and H plane radiation gain patterns, which are observed at 1550 MHz, normalized with respect to a reference linearly polarized high gain horn antenna (HF 906) operating from 1 GHz to 18 GHz and compared to corresponding simulated radiation pattern for the antenna-HIS system modelled in CST Microwave Studio, also, collectively compared to radiation gain pattern of UWB monopole in free space. In Fig. 5.17c, the E plane's, maximum gain is at 15 degrees tilted angle and is 7.3 dBi and 6.7 dBi for simulation and measurements respectively and signifies an improvement of around 4 dB with respect to the monopole gain in free space where backward radiation is suppressed by 12.5 dB. Also, the E plane radiation gain patterns, observed at 0°, as shown in Fig. 5.17c, is 6.3 dBi and 4.9 dBi for simulation and measurements respectively and reasonably agree with H plane simulated and measured gain, observed at 0°, as shown in Fig. 5.17d. Simulated total efficiency for antenna 0.015λ above IDC HIS was 68%.

5.5 Single Band Interdigital HIS Design 2 – Dual Layer Dual Polarized

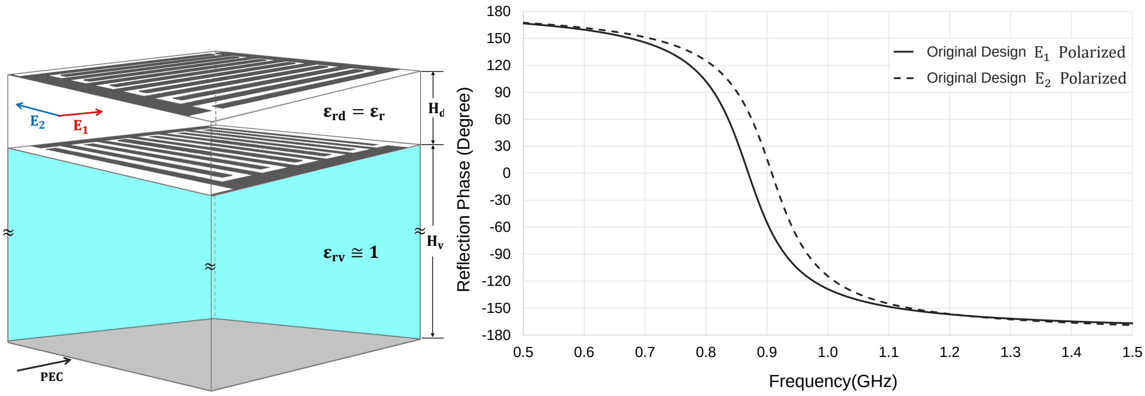

(a) 3D Model

(b) Original Design Reflection Phase

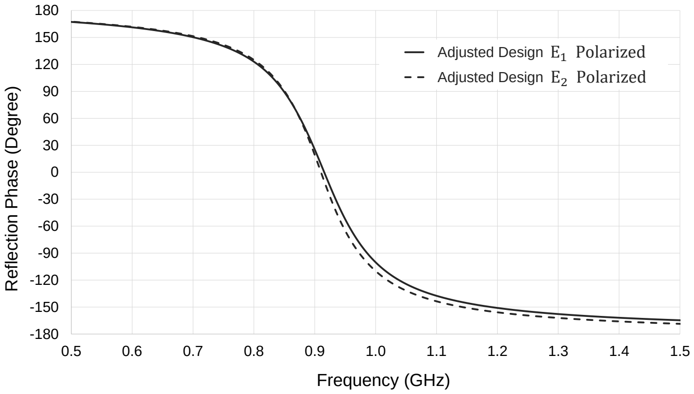

(c) Adjusted Design Reflection Phase

Fig. 5.18 Single Band Dual Layer Dual Polarized (SB-DLDP) interdigital HIS Design 2.

Fig. 5.18a presents a lightweight miniaturised Single Band Dual Layer Dual Polarized (SB-DLDP) HIS Design 2. The structure is composed of two identical interdigital capacitive layers, orthogonally rotated by 90° with respect to each other, printed on both sides of a thin dielectric material of thickness (H_d), supported by rohacell material of thickness (H_v) and backed by metal. At normal incidence, the top interdigital layer is driven by E_1 polarized wave while the lower interdigital layer is operated by E_2 polarization, as shown in Fig. 5.18a. Both interdigital surfaces are identical to SB-SLSP HIS Design 1 and designed according to the methodology detailed in Section 5.2. Nevertheless, top dual layer interdigital capacitive surface has been reported in [89] for a miniaturised FSS. However, the work presented in the thesis addresses a new methodology to design the surface proposing accurate modelling of interdigital inductance as well as discussing mutual coupling between closely spaced interdigital layers from the HIS prospective where the circuit model and methodology are detailed in Appendix B and validated in this section. Moreover, an upgraded dual band design is presented in Chapter 7.

Table 5.11 Single Band Dual Layer Dual Polarized (SB-DLDP) Interdigital HIS Design 2 – 900 MHz Prototype Optimized at 0.8 mm FR4, 6.8 mm Rohacell, P = 12.5 mm, $S_g = 1$ mm

IDC HIS Parameters	Original	New Re-designed
Design frequency (f_r)	900 MHz	930 MHz
Interdigital capacitance (C_d)	2.84 pF	2.58 pF
Number of digits (N_d)	12	11
Digits gap/width ($s = w$)	0.5 mm	0.55 mm
Digits length (L)	11 mm	11 mm

In this section, the mechanism of the Single band interdigital HIS Design 2 is discussed. HIS Design 2, as in Fig. 5.18a, is modelled on 7.6 mm FR4 ($\varepsilon_r = 4.3, \tan\delta = 0.025$) to resonate at 900 MHz. Integrating two interdigital capacitive layers spaced by ($H_d = 0.8$ mm) results in interlayer coupling and causes a reduction in resonance frequency. This is evident in the simulated reflection phase plot for both E_1 and E_2 polarizations, which are compared in Fig. 5.18b. For E_1 polarization top surface resonance frequency is reduced to 870 MHz, while for lower surface E_2 polarization resonance frequency is maintained at 900 MHz since lower layer effective substrate thickness is reduced to 6.8 mm, which indirectly produces a reversed effect to interlayer coupling. Therefore, according to the methodology discussed in Appendix B, interlayer coupling is taken into consideration when the surface is re-designed at 930 MHz, taking the expected percentage frequency shift into account, which requires interdigital capacitance to reduce from 2.84 pF to 2.58 pF. Minor adjustment in the structure digit number and dimensions are implemented where original and re-designed parameters are compared in Table 5.11. The simulated reflection phase plot for the re-designed SB-DLDP interdigital HIS Design 2 operating at 900 MHz is presented in Fig. 5.18c where both E_1 and E_2 polarizations demonstrate strong agreement in resonance frequency featuring a fractional bandwidth of 15% as designed within a unit cell periodicity of 0.0375λ.

5.6 Single Band Interdigital HIS Design 3 – Single Layer Dual Polarized

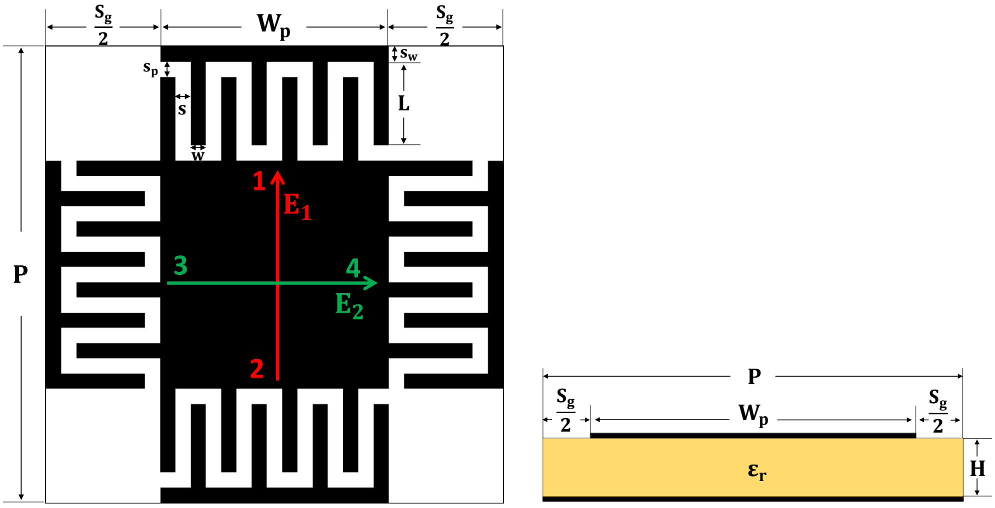

(a) Top View

(b) Side View

Fig. 5.19 Single Band Single Layer Dual Polarized (SB-SLDP) interdigital HIS Design 3.

A Single Band Single Sayer Dual Polarized (SB-SLDP) interdigital HIS Design 3 is presented in Fig. 5.19. A design methodology to model this structure for optimum miniaturisation will be discussed using an equivalent circuit model provided that the interdigital HIS is electrically small. A similar structure has been reported in [92], but current work presents a novel design methodology and optimized circuit model. SB-SLDP interdigital HIS is experimentally verified as manufactured and incorporated with a monopole antenna to realise a low profile platform tolerant antenna system. Furthermore, Chapter 7 details a novel Dual Band Single Layer Dual Polarized (DB-SLDP) interdigital HIS as based on the current model.

5.6.1 Unit cell design methodology

Fig. 5.19 shows Single Band Single Layer Dual Polarized (SB-SLDP) interdigital HIS whose interdigital capacitive surface is printed on a single layer substrate backed by metal. The

HIS unit cell is miniaturised by incorporating identical interdigital capacitors within four sub-unit cell regions where interdigital capacitance concepts of section 5.2 apply. Top and bottom sub-unit cells 1 and 2 contribute to E_1 polarized wave resonance, while left and right sub-unit cells 3 and 4 are excited by E_2 polarization.
Unit cell periodicity (P) in terms of IDC plate width (W_p) and interelement spacing (S_g) is:

$$P = W_p + S_g \tag{5.21}$$

To realise dual polarization, the unit cell of Fig. 5.19a is square. Also, the centre patch square with area $(W_p \times W_p)$. For maximized capacitance, unit cell parameters are associated as:

$$W_p = S_g \tag{5.22}$$

$$L + s_w + s_p = \frac{W_p}{2} = \frac{S_g}{2} \tag{5.23}$$

5.6.2 Equivalent circuit model

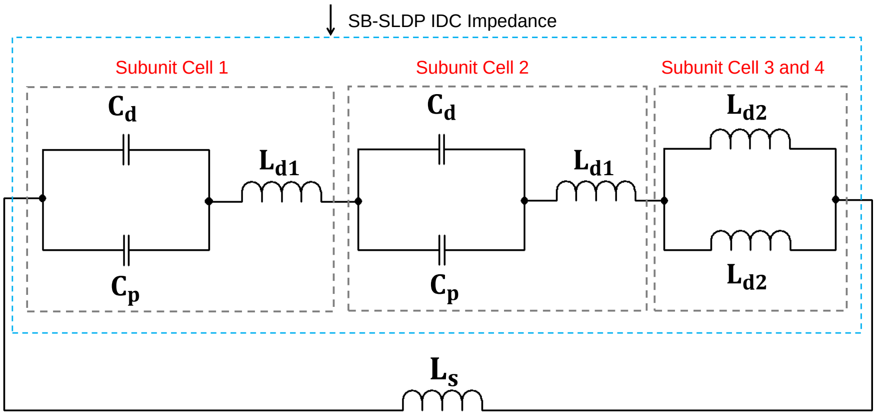

Fig. 5.20 ECM Single Band Single Layer Dual Polarized (SB-SLDP) Interdigital HIS.

Equivalent Circuit Model (ECM) for SB-SLDP interdigital HIS Design 3 is detailed in Fig. 5.20. E_1 polarization is considered in the analysis for convenience where identical concepts apply for E_2 polarization. The detail of the ECM is as follows: Identical interdigital subunit cells 1 and 2 are loaded with interdigital capacitance (C_d) in parallel with mutual capacitance (C_p), then, in series with associated interdigital inductance (L_{d1}). Subunit cells 3 and 4 generate identical parasitic inductances (L_{d2}) connected in parallel.

Therefore, the SB-SLDP interdigital HIS Design 3 capacitive impedance is given by :

$$Z_{(\text{SB-SLDP})} = j\omega\left(2L_{d1} + \frac{L_{d2}}{2}\right) + \frac{2}{j\omega(C_d + C_p)} \tag{5.24}$$

where ω is the angular frequency.
SB-SLDP interdigital HIS Design 3 resonance frequency is given by:

$$f_{r_{(\text{SB-SLDP})}} = \frac{1}{2\pi\sqrt{0.5(C_d + C_p)(2L_{d1} + 0.5L_{d2} + L_s)}} \tag{5.25}$$

where $L_s = \mu_0 H$ is the inductance of interdigital HIS substrate of thickness (H).
C_p is the mutual capacitance within subunit cell gap $(L + s_p)$ and is given by Eq. (5.3).
C_d is the interdigital capacitance in each subunit cell (Section 5.2.2).
L_{d1} is the interdigital inductance generated in subunit cell 1 and 2 (Section 5.6.3).
L_{d2} is the interdigital inductance generated in subunit cell 3 and 4 (Section 5.6.4).

5.6.3 Interdigital inductance (L_{d1}) design equations

For E_1 polarized unit cell, interdigital inductance (L_{d1}) is developed in each of subunit cell 1 and 2, Fig. 5.19a. It is the equivalent self inductance of a strip line section of length $(L + s_w + s_p)$ and width (W_p) where interdigital digits number (N_d) is large and the digit gap is much smaller than substrate thickness $\left(\frac{s}{H} \ll 1\right)$. L_{d1}, in nH, is [124, 125]:

$$L_{d1} = 0.2(L + s_w + s_p)\left[\ln\left(\frac{L + s_w + s_p}{W_p + t}\right) + 1.193 + \frac{W_p + t}{3(L + s_w + s_p)}\right] K_{d1} \tag{5.26}$$

where W_p is the interdigital plate width. s_w is plate depth. L is digits length. s_p is digits top/bottom gap. t is copper thickness. All dimensions are in mm.
K_{d1} is the correction factor considering HIS substrate thickness (H) effect for $\left(\frac{W_p}{H} > 0.05\right)$, [124] :

$$K_{d1} = 0.57 - 0.145 \ln \frac{W_p}{H} \tag{5.27}$$

Where effectively miniaturised dual polarized interdigital HIS is required, $L + s_w + s_p = \frac{W_p}{2}$. Copper thickness (t) is neglected. Inductance (L_{d1}), in Eq. (5.26), in nH, is simplified as:

$$L_{d1} = 0.2\left(\frac{W_p}{2}\right)\left[\ln\left(\frac{1}{2}\right) + 1.193 + \frac{2}{3}\right] K_{d1} \backsimeq 0.12 W_p K_{d1} \tag{5.28}$$

5.6.4 Interdigital inductance ($\mathrm{L_{d2}}$) design equations

For an $\mathrm{E_1}$ polarized unit cell, the inductance developed in subunit cells 3 and 4 is considered while neglecting the large inductance generated within the strip line connecting the subunit cells. Therefore, identical interdigital inductance ($\mathrm{L_{d2}}$) is developed in subunit cells 3 and 4 where the digits gap is much smaller than the substrate thickness $\left(\frac{\mathrm{s}}{\mathrm{H}} \ll 1\right)$. Interdigital self inductance ($\mathrm{L_{d2}}$), in nH, developed within a strip line of length ($\mathrm{W_p}$) and width ($\mathrm{L+s_w+s_p}$) is [124, 125]:

$$\mathrm{L_{d2}} = 0.2\mathrm{W_p}\left[\ln\left(\frac{\mathrm{W_p}}{(\mathrm{L+s_w+s_p})+\mathrm{t}}\right) + 1.193 + \frac{(\mathrm{L+s_w+s_p})+\mathrm{t}}{3\mathrm{W_p}}\right]\mathrm{K_{d2}} \tag{5.29}$$

where $\mathrm{W_p}$ is the interdigital plate width. $\mathrm{s_w}$ is the plate depth. L is the digits length. $\mathrm{s_p}$ is the digits top/bottom gap. t is the copper thickness. All dimensions are in mm.
$\mathrm{K_{d2}}$ is the factor considering substrate thickness (H) effect when $\left(\frac{\mathrm{L+s_w+s_p}}{\mathrm{H}} > 0.05\right)$ [124]:

$$\mathrm{K_{d2}} = 0.57 - 0.145\ln\frac{\mathrm{L+s_w+s_p}}{\mathrm{H}} = 0.57 - 0.145\ln\frac{\mathrm{W_p}}{2\mathrm{H}} \tag{5.30}$$

Since the unit cell is square, where $\mathrm{L+s_w+s_p} = \frac{\mathrm{W_p}}{2}$, and neglecting copper thickness (t); therefore, interdigital inductance ($\mathrm{L_{d2}}$), in nH, simplifies to:

$$\mathrm{L_{d2}} \backsimeq 0.41\mathrm{W_p}\mathrm{K_{d2}} \tag{5.31}$$

5.6.5 Experimental verification

Single Band Single Layer Dual Polarized (SB-SLDP) interdigital HIS Design 3, as in Fig. 5.19b, is modelled on 6.4 mm FR4 ($\varepsilon_r = 4.3, \tan\delta = 0.025$) to operate at 1500 MHz within a periodicity 0.13λ. Unit cell and circuit model design parameters are detailed in Table 5.12, while Fig. 5.21b gives full wave normal incidence simulated reflection phase plots of SB-SLDP IDC HIS Design 3, which is modelled on CST Microwave Studio; therefore, demonstrating a resonance at 1500 MHz and corresponding $\pm 90^\circ$ operational bandwidth of 15% in both $\mathrm{E_1}$ and $\mathrm{E_2}$ polarizations which strongly agree with the analytical reflection phase plot deduced from the proposed ECM. The HIS was fabricated into an array of 9 by 7 unit cells comprising a board of dimensions 234 mm by 182 mm and printed on a single layer 6.4 mm FR4 substrate. The interdigital HIS is incorporated within 3 mm as a ground plane for an UWB monopole antenna, as demonstrated in Fig. 5.21a.

Table 5.12 SB-SLDP Interdigital HIS Design 3 Operated at 1500 MHz – Unit Cell and Circuit Parameters as Modelled on 6.4 mm FR4 ($\varepsilon_r = 4.3, \tan\delta = 0.025$)

SB-SLDP HIS Parameters	Values
Periodicity(P)	26 mm
Interelement Spacing(S_g)	13.6 mm
Number of digits N_d	12
Digits gap/width ($s = w$)	0.5 mm
Digits length (L)	5.8 mm
Interdigital capacitance (C_d)	1.5 pF
Patch Capacitance (C_p)	0.4 nH
Interdigital inductance (L_{d1})	0.8 nH
Interdigital inductance (L_{d2})	3 nH
Dielectric Substrate inductance (L_s)	8 nH

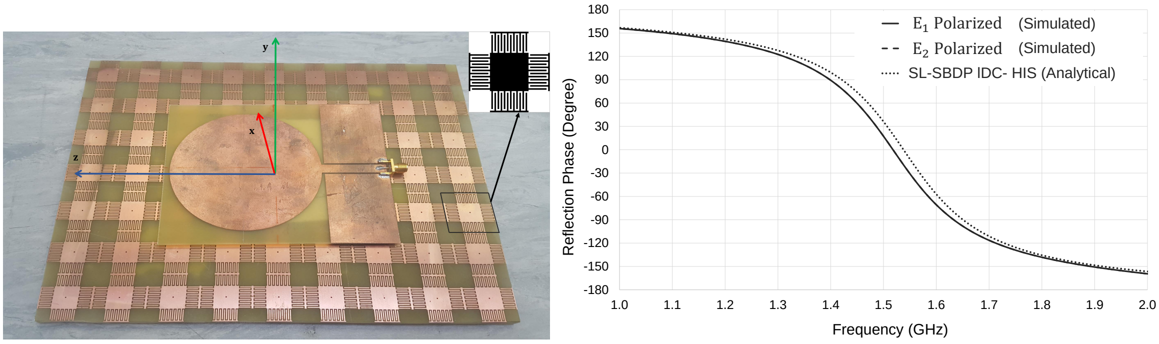

(a) Manufactured Antenna/HIS System (b) Unit Cell Reflection Phase

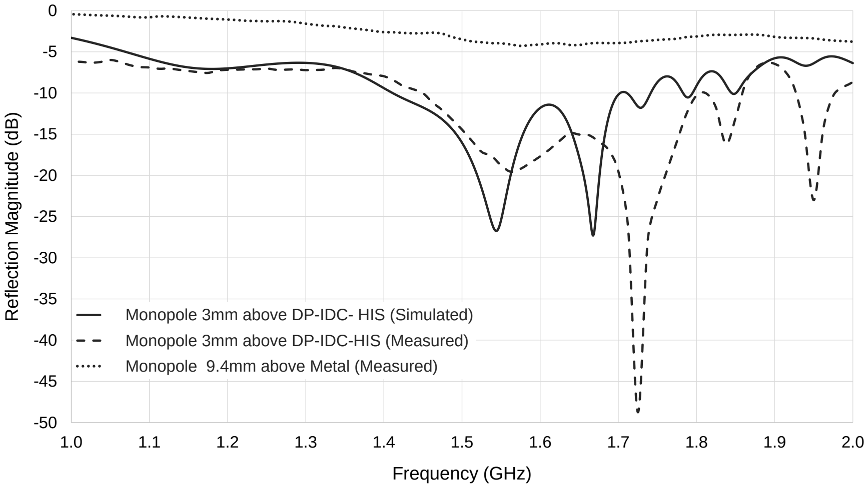

(c) Input Reflection Coefficient Magnitude

Fig. 5.21 Low profile UWB monopole antenna 3 mm above miniaturised SB-SLDP IDC HIS

The UWB antenna operates from 900 MHz, measures 96 mm by 120 mm and printed on 1.6 mm FR4 substrate ($\varepsilon_r = 4.3, \tan\delta = 0.025$). Simulated and measured monopole - HIS system reflection magnitude as compared to monopole $0.047\lambda_{1.5\text{GHz}}$ above metal surface is presented in Fig. 5.21c. Observed, at 1500 MHz, the measured antenna input matching significantly improves from ($|S_{11}| = -3.5$ dB), for antenna above metal, to ($|S_{11}| = -17$ dB) when HIS is incorporated, therefore, a low profile antenna - HIS system is possible. Discrepancies between simulations and measurements are expected, but as in Fig. 5.21c they possess reasonable agreement, both encountering a frequency shift. Simulated monopole - HIS is best matched at 1540 MHz ($|S_{11}| = -28$ dB) as compared to 1560 MHz ($|S_{11}| = -20$ dB) in measurements.

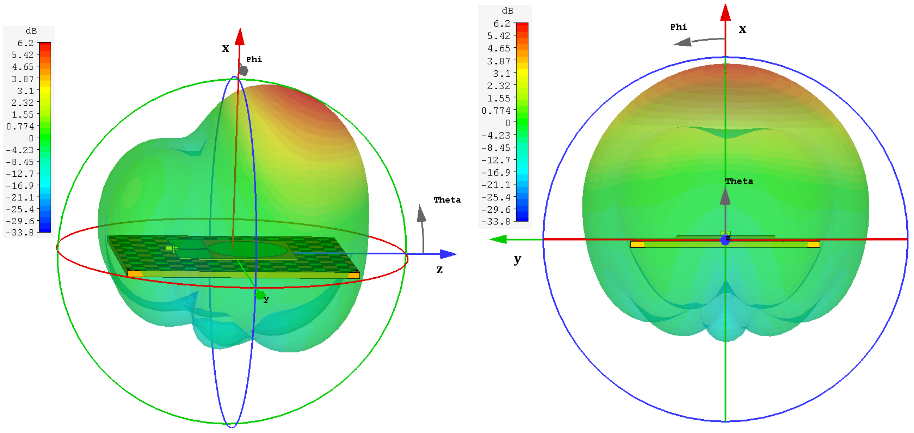

(a) E-Plane 3D View (b) H-Plane 3D View

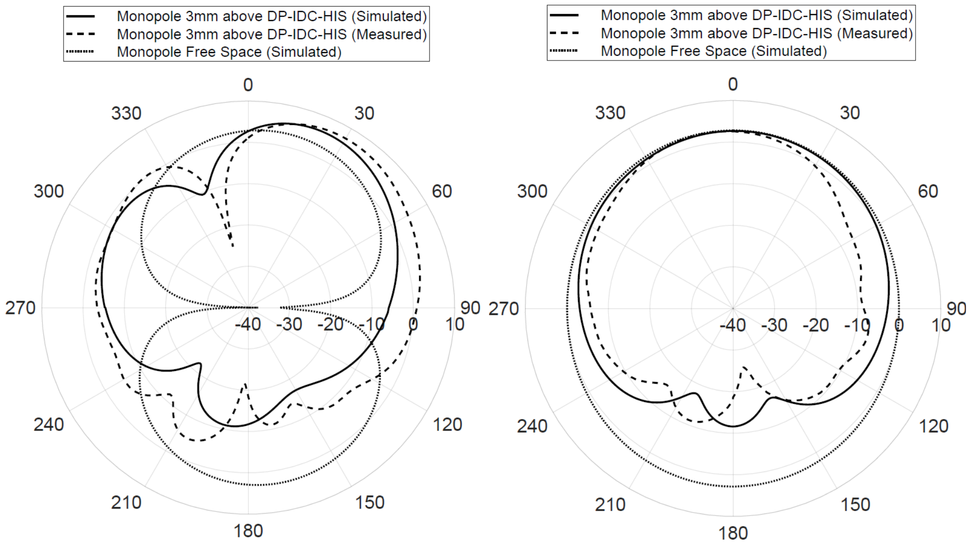

(c) E-Plane Polar Plots (d) H-Plane Polar Plots

Fig. 5.22 Monopole – SB-SLDP IDC HIS system 1500 MHz E H plane radiation pattern.

The E and H plane gain patterns, in Fig. 5.22, were observed at 1500 MHz for UWB monopole integrated at 0.015λ above SB-SLDP interdigital HIS Design 3 as measured in an anechoic chamber, normalized with respect to a reference linearly polarized high gain horn antenna (HF 906) operating from 1 GHz to 18 GHz. The patterns were compared against simulated gain for the system modelled on CST Microwave Studio and also compared to monopole gain in free space. 3D simulated E-plane gain pattern (Theta cut) is presented in Fig. 5.22a, while E plane gain polar plots are presented in Fig. 5.22c. A maximum gain of 7 dBi at around 30 degrees from boresight is observed in both simulation and measurement, an improvement of around 4 dB with respect to the monopole gain in free space. E plane backward radiation is reduced by around 14 dB with respect to antenna in free space. H plane 3D simulated gain pattern (Phi cut) is presented in Fig. 5.22b. Since the gain pattern of the antenna is squinted, information on maximum gain from H plane is not detected. However, simulated and measured H plane gain polar plots, Fig. 5.22d, show reasonable agreement. Also, Boresight 0 degree gain for E and H planes agree at around 3 dBi. H plane backward radiation is suppressed by 14 dB as compared with respect to the antenna in free space. Simulated antenna/HIS system radiation and total efficiencies were 68% and 66.75% respectively.

5.7 Conclusion

Miniaturisation of High Impedance Surface (HIS) using Interdigital Capacitors (IDCs) has been discussed in this chapter. Interdigital capacitors are effectively meandered digits, closely spaced and generating high capacitive density as an electric field illuminates the digits along their longest electrical path. By concept, IDC should be engineered within a capacitive patch HIS element occupying the full unit cell area such that the HIS surface is dominated by the choice of interdigital capacitance. Interdigital HIS can be modelled using numerical software requiring several iterative simulations such that unit cell dimensions are optimized for the HIS to operate at a given design frequency. This is very inefficient to apply. Therefore, this Chapter, has provided essential design guidelines, as related to modelling techniques, where IDCs have been implemented effectively using an equivalent circuit model approach and design equations have been proposed such that interdigital HIS was realised using simplified methods which minimized simulation iterations. Even though this Chapter focused on single band interdigital HIS design, it is of significant importance since the design methodologies discussed do apply to miniaturised dual band interdigital HIS design which is detailed in subsequent chapters. Nevertheless, where this chapter is concerned, three different interdigital HIS designs were proposed.

Design1: miniaturised Single Band Single Layer Single Polarized (SB-SLSP) interdigital HIS has been discussed first. It is the basic interdigital HIS prototype and the simplest form of HIS miniaturisation using IDC, but polarization dependent. A miniaturised interdigital HIS unit cell of 0.03λ has been proposed implementing interdigital capacitors. Moreover, an equivalent circuit model has been presented to describe the structure's mechanism and design equations on modelling interdigital capacitance as well as series inductance. A novel approach to model interdigital inductance based on unit cell current decomposition has been detailed in Section 5.2.5 and provided high accuracy in modelling the interdigital HIS unit cell. The work has been consolidated with a complete analytical parametric study on a full range of parameters such as dielectric permittivity and thickness, periodicity, interdigital digits number, digits gap and digits width. Interdigital SB-SLSP HIS has been validated experimentally as the surface was fabricated and integrated with a planar linearly polarized monopole antenna such that a low profile antenna - HIS system is realised.

Design 2: Single Band Dual Layer Dual Polarized (SB-DLDP) interdigital HIS has been discussed next. The miniaturised HIS is dual polarized comprising of two identical interdigital capacitive surface layers, closely spaced but orthogonal to each other where each was modelled according to the methodology discussed in interdigital IDC HIS Design 1. The structure is light weight and composed of two different material composites, a thin dielectric separating the two interdigital capacitive layers and a rohacell material supporting the dual band capacitive layers, then a HIS ground plane. Design methodology has been discussed with insights on interlayer coupling providing an effective solution to take this design constraint into account. A case study has been considered and validated numerically for a miniaturised SB-DLDP interdigital HIS optimized to resonate at 900 MHz, unit cell periodicity of 0.0375λ.

Design 3: Single Band Single Layer Dual Polarized (SB-SLDP) interdigital HIS has been discussed last. An equivalent circuit model has been proposed to accurately model the interdigital HIS effectively where corresponding design equations were presented. The surface has been experimentally validated as integrated with a planar monopole antenna, where an efficient low profile antenna - HIS system has been realised, while a miniaturised HIS unit cell of 0.0375λ has been considered. The novelty of this structure has been highlighted, which has a great potential to upgrade into a dual band HIS, implemented in a highly effective manner and discussed in Chapter 7.

The next Chapter will focus on dual band miniaturised interdigital HIS design with an introduction to dual band mutual coupling.

Chapter 6

Dual Band Interdigital High Impedance Surface - Accounting For Mutual Coupling

6.1 Introduction

Miniaturised dual band high impedance surfaces are of great advantage for the integration in dual band systems which are highly desirable to meet requirements of multifunctional bandwidth efficient devices. The miniaturisation of HIS by integrating a simple patch structure with interdigital capacitor has been discussed in Chapter 5 where techniques and concepts for three different single band HIS prototypes have been extensively discussed. This chapter implements the design methodology of Single Band Single Layer Single Polarized (SB-SLSP) interdigital HIS Design 1, detailed in Chapter 5, to realise a dual band HIS where all design equations and circuit modelling apply. Consequently, the objectives of dual band HIS design are addressed where a comprehensive investigation on inter unit cell mutual coupling in a dual band system is carried out. Dual band mutual coupling is analysed experimentally and numerically through full wave simulations on CST Microwave Studio observed at normal incidence. Therefore, factors that influence inter unit cell mutual coupling are investigated through a complete parametric analysis. Moreover, the system mechanism is illustrated followed by a methodology to realise a simplified design process for a miniaturised dual band interdigital HIS while taking mutual coupling into consideration.

6.2 Interdigital Dual Band HIS Design Methodology

6.2.1 Unit cell structure

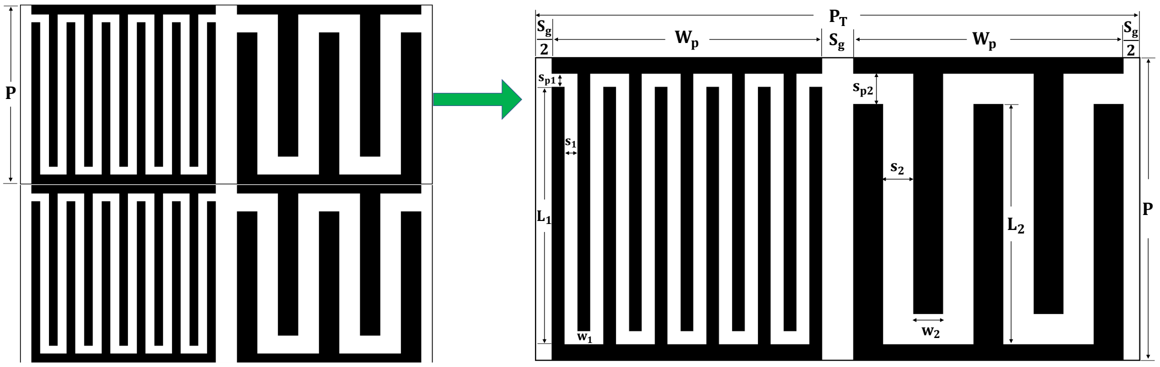

(a) Top View (b) Detailed Top View

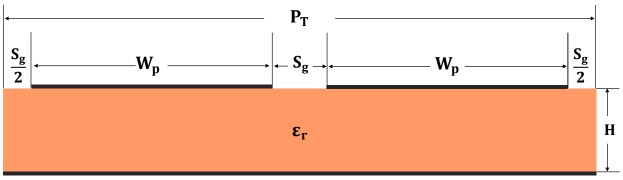

(c) Side View

Fig. 6.1 Miniaturised Dual Band Single Layer Single Polarized (DB-SLSP) interdigital HIS.

Miniaturised Dual Band Single Layer Single Polarized (DB-SLSP) interdigital HIS, which is polarization dependent, is presented in Fig. 6.1. The design comprises of an FSS-based capacitive layer supported by a dielectric material and backed by metal, as shown in Fig. 6.1c. The top metallic capacitive structure constitutes of two concatenated subunit cells of identical size. Each subunit cell is engineered with interdigital capacitance of different capacitance density, therefore, a two band system is possible. As in Fig. 6.1b, the subunit cell on the left, of higher interdigital capacitance density, corresponds to the lower band and subunit cell on the right, engineered with less dense interdigital elements, which generates the upper band. Both bands are set to occupy total unit cell periodicity (P_T). Nevertheless, time consuming simulations are to be avoided. Therefore, design of a dual band interdigital HIS is based on optimizing each band individually. Following equivalent circuit model design guidelines detailed in Chapter 5, each subunit cell interdigital structure is optimized to operate at the required design frequency within subunit cell periodicity (P) and substrate thickness (H). Thereafter, both subunit cells are integrated into one HIS structure and a dual band is possible.

6.2.2 Periodicity limitation

To avoid grating lobe, for any angle of incidence, the total periodicity $(\mathrm{P_T})$ of dual band unit cell should be less than half the highest band frequency wavelength [33].

$$\mathrm{P_T} \leqslant \frac{\lambda_\mathrm{N}}{2} \tag{6.1}$$

where λ_N is the wavelength at upper band frequency of number N.

Miniaturisation of HIS using IDC has the potential to realise multiband band system. Nevertheless, each band is initially designed independently and the total unit cell periodicity $(\mathrm{P_T})$ is divided equally with respect to band number (N).

Therefore, the individual band subunit cell periodicity (P) grating lobe limit as function of the highest band operating wavelength (λ_N) is:

$$\mathrm{P} \leqslant \frac{\lambda_\mathrm{N}}{2\mathrm{N}} \tag{6.2}$$

Number of band $(\mathrm{N} = 2)$ as this chapter is concerned.

6.2.3 Substrate thickness limitation

For the accuracy of ECM approach, also, light weight HIS is desired. The electrical substrate thickness, normalized to the upper band operating wavelength (λ_N), is limited to:

$$\frac{\mathrm{H}}{\lambda_\mathrm{N}} \leqslant 0.04 \tag{6.3}$$

6.2.4 Dual band HIS design procedure summarized

In [129] the author of this thesis has reported a dual band interdigital high impedance surface of unit cell configuration as in Fig. 6.1. The structure was designed at 480 MHz and 930 MHz featuring a unit cell miniaturised at $0.125\lambda_{930\ \mathrm{MHz}}$. The design was based on repetitive simulations of both bands' subunit cell such that the interdigital HIS resonates at the desired frequencies. At this stage mutual coupling between bands was acknowledged but not managed where the two band subunit cells are modified by multiple simulations indirectly taking coupling into account. Flow chart presented in Fig. 6.2 summarizes the design steps involved. Nevertheless, this procedure is impractical and inefficient to model dual band interdigital HIS with no insights about the amount of mutual coupling involved. In Section 6.3, inter unit cell mutual coupling in a practical design case study is discussed.

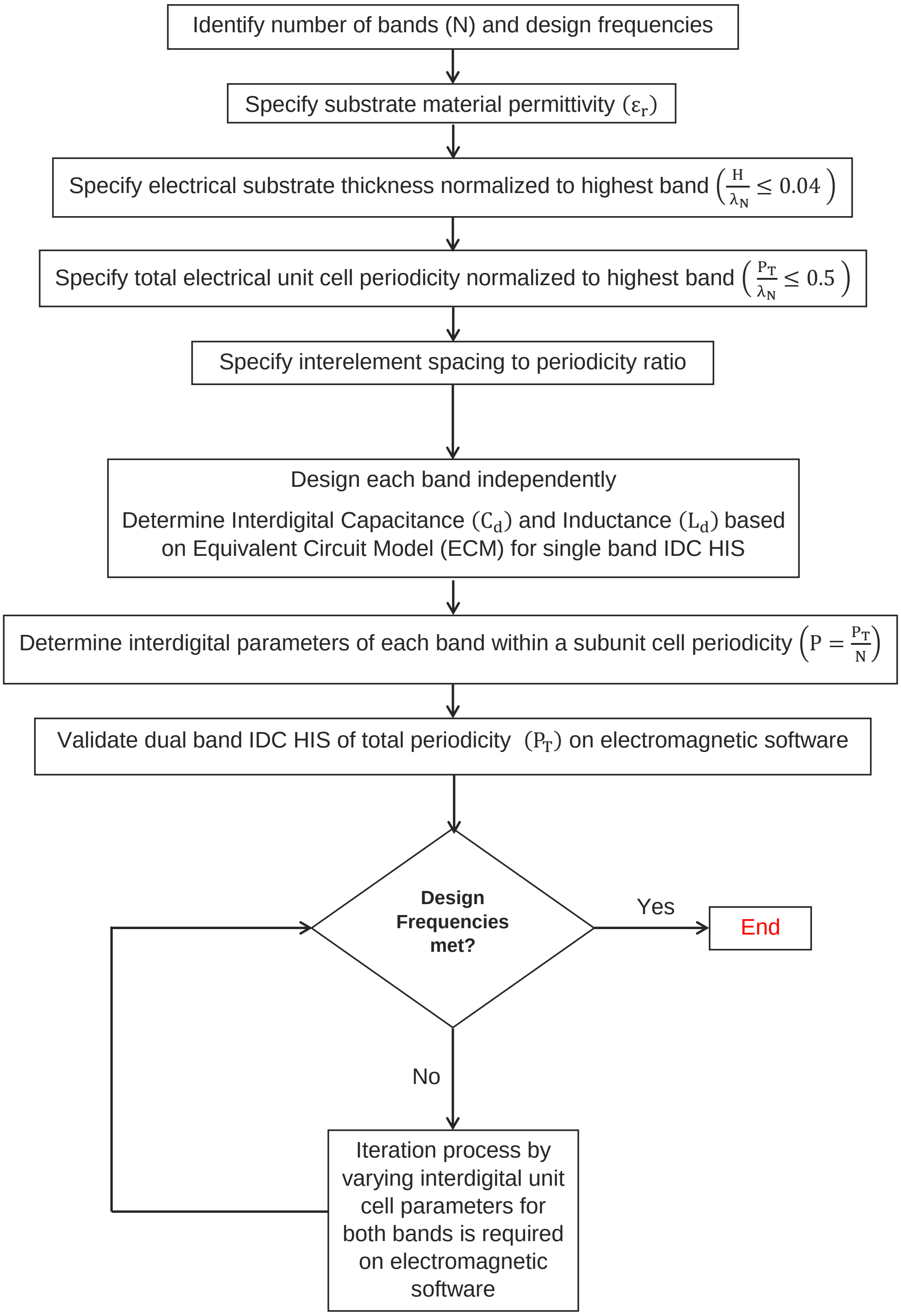

Fig. 6.2 Design procedure for dual band interdigital HIS conducted through iteration.

6.3 Introduction to Dual Band Mutual Coupling

In this section a dual band miniaturised interdigital High Impedance Surface (HIS) design is presented, where the design limitations due to mutual coupling is addressed. Design frequencies of 900 MHz and 1800 MHz are considered for the HIS is initially modelled as a single band and thereafter integrated into a dual band system.

6.3.1 Single band to dual band interdigital HIS

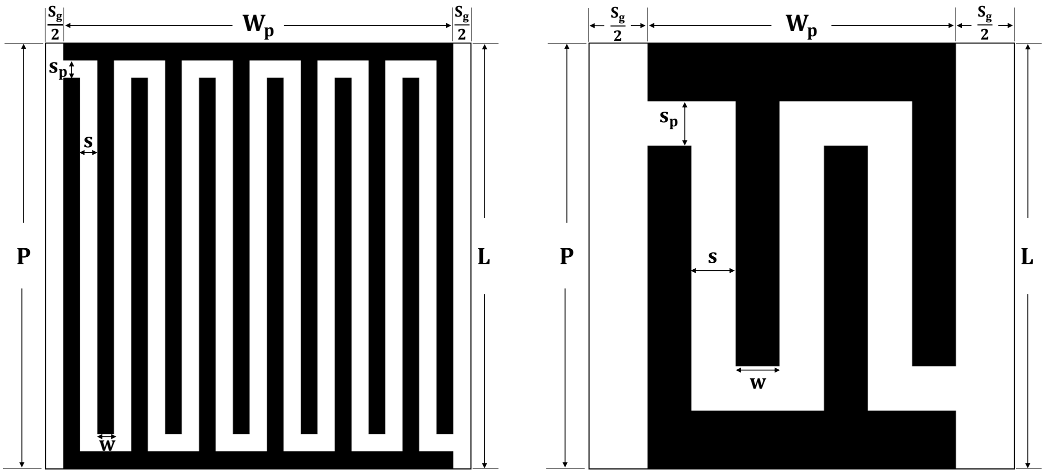

(a) 900 MHz band

(b) 1800 MHz band

Fig. 6.3 Dual band interdigital high impedance surface subunit cells detailed top view.

Table 6.1 Dual Band Interdigital HIS Subunit Cell Design Parameters

IDC HIS Parameters	900 MHz (Bands 1)	1800 MHz (Bands 2)
Substrate material	FR4	FR4
Substrate thickness $(\mathrm{H_d})$	1.6 mm	1.6 mm
Rohacell thickness $(\mathrm{H_v})$	6 mm	6 mm
Subunit cell periodicity (P)	12.5 mm	12.5 mm
Electrical periodicity (P/λ)	0.0375	0.06
Number of digits $(\mathrm{N_d})$	12	4
Digits side gap (s)	0.5 mm	1.3 mm
Digits width (w)	0.5 mm	1.3 mm
Digits top/bottom gap $(\mathrm{s_p})$	0.5 mm	1.3 mm
Digits length (L)	11 mm	7.8 mm
Interdigital capacitance $(\mathrm{C_d})$	2.84 pF	0.77 pF
Interdigital capacitance $(\mathrm{L_d})$	1.6 nH	1 nH

The dual band interdigital HIS subunit cells top view model of 900 MHz (Band 1) and 1800 MHz (Band 2) are presented in Fig. 6.3a and Fig. 6.3b respectively. Initially, individual bands, are optimized as a single band interdigital HIS of prototype SB-SLSP HIS Design 1 as of methodology discussed in Chapter 5. Analytical subunit cell design parameters are determined and detailed in Table 6.1. Thereafter, reflection phase characteristics, for each band, is considered as observed at normal incidence. Both bands, 900 MHz and 1800 MHz, are modelled on FR4 dielectric material ($\varepsilon_r = 4.3, \tan\delta = 0.025$), subunit cell periodicity 12.5 mm and HIS total substrate thickness 7.6 mm. Each of the 900 MHz and 1800 MHz interdigital capacitive layer is manufactured into an array of 24 by 23 unit cells printed on a 300 mm × 300 mm 1.6 mm FR4 substrate. A miniaturised lightweight interdigital HIS is realised for each band manufactured board is supported by a 6 mm Rohacell material and then backed by a metal sheet, Fig. 6.4, as an initial design step.

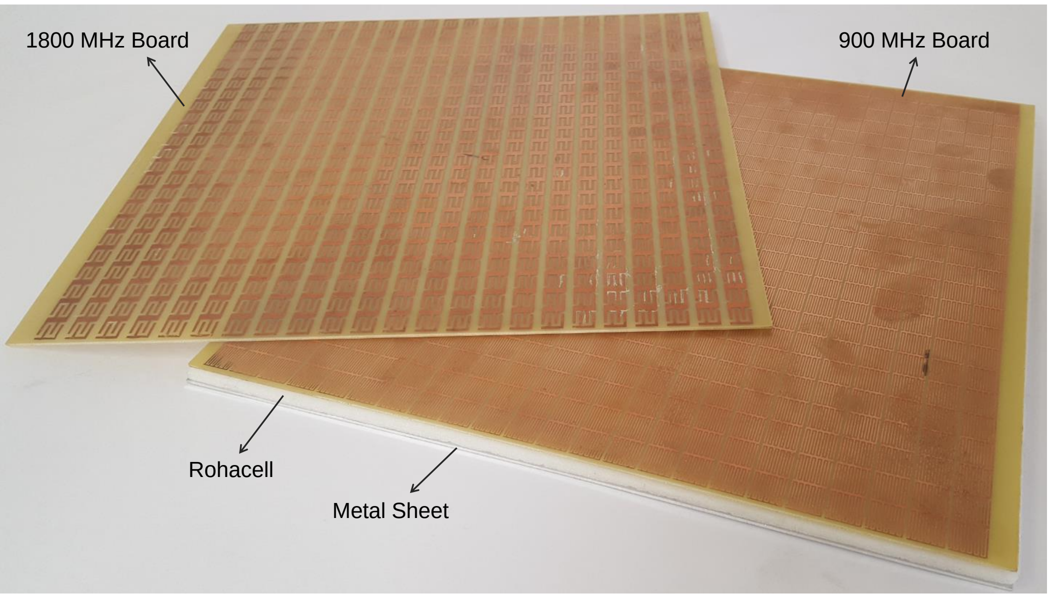

Fig. 6.4 900 MHz and 1800 MHz single band 300 mm × 300 mm IDC HIS fabricated on 1.6 mm FR4 ($\varepsilon_r = 4.3, \tan\delta = 0.025$), supported by 6 mm Rohacell and backed by a metal.

Reflectivity measurements, at normal incidence , of manufactured 900 MHz and 1800 MHz sub-band boards, Fig. 6.4, were conducted in an anechoic chamber using NRL Arch setup as in Fig 6.5. NRL Arch reflectivity measurement is a technique first developed in a Naval Research Laboratory to measure reflectivity of microwave absorbing surfaces. Information on this technique can be found in Chapter 2. In the measurement setup, Fig. 6.5, two horn antennas operating within a bandwidth of 2-18 GHz were used. The choice of manufactured board size of 300 mm × 300 mm was restricted by manufacturing constraints. Nevertheless, knowing that the NRL Arch horn antennas are of a very narrow beamwidth, the interdigital

HIS sample electrical size of $0.9\lambda_{0.9\text{GHz}} \times 0.9\lambda_{0.9\text{GHz}}$ is acceptable. Reflectivity measurements are calibrated with respect to a metal plate of the same dimensions as fabricated interdigital 900 MHz and 1800 MHz HIS boards for a reliable measurements. The two single band high impedance surface 900 MHz and 1800 MHz designs are also separately modelled on CST Microwave Studio to compare with measurements.

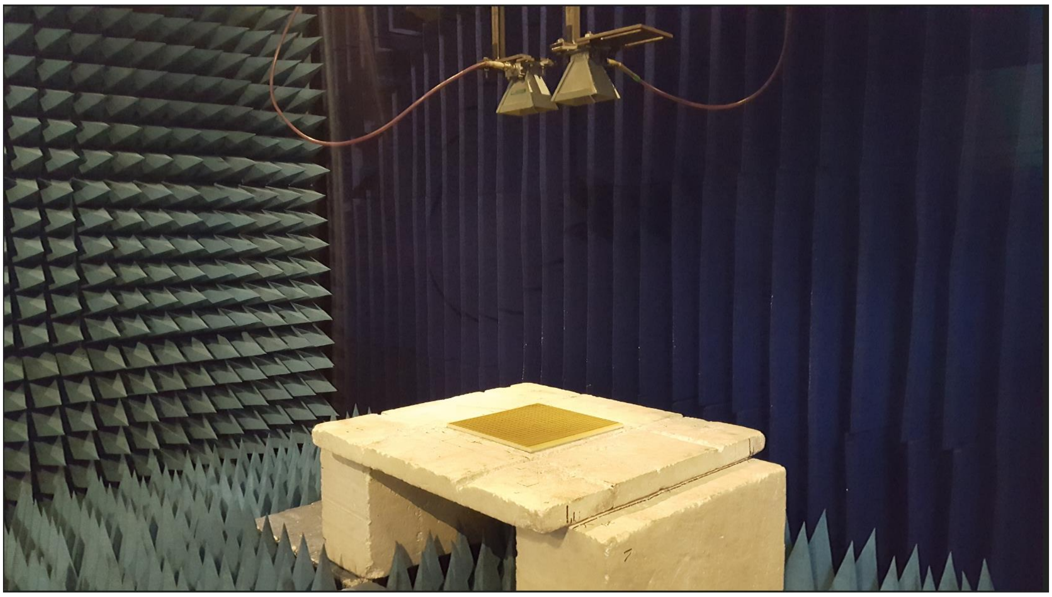

Fig. 6.5 Reflectivity measurement setup using NRL Arch.

Simulated and measured reflection phase plots for periodic interdigital HIS for 900 MHz and 1800 MHz single band interdigital HIS designs are presented in Fig. 6.6 and Fig. 6.7 respectively; showing good agreement and proving the circuit model optimization methodology extensively discussed in Chapter 5. Although discrepancies between simulations and measurements are anticipated due to software numerical computational errors as well as measurements/environmental errors such as calibration, alignment mismatch, scattering from board and interaction with chamber. However, for the 900 MHz band, Fig. 6.6, variance in resonance frequency between measurements and simulation are prominent due to mismatch error which exists as the design is outside the NRL Arch horn antennas operating bandwidth ranging from 2-18 GHz and board size was desired to be larger. On the other hand, for the 1800 MHz band, mismatch errors are less significant and the board electrical size is a satisfactory $1.8\lambda_{1.8\text{GHz}} \times 1.8\lambda_{1.8\text{GHz}}$ where simulated and measured reflection phase is of a better agreement, as shown in Fig. 6.7.

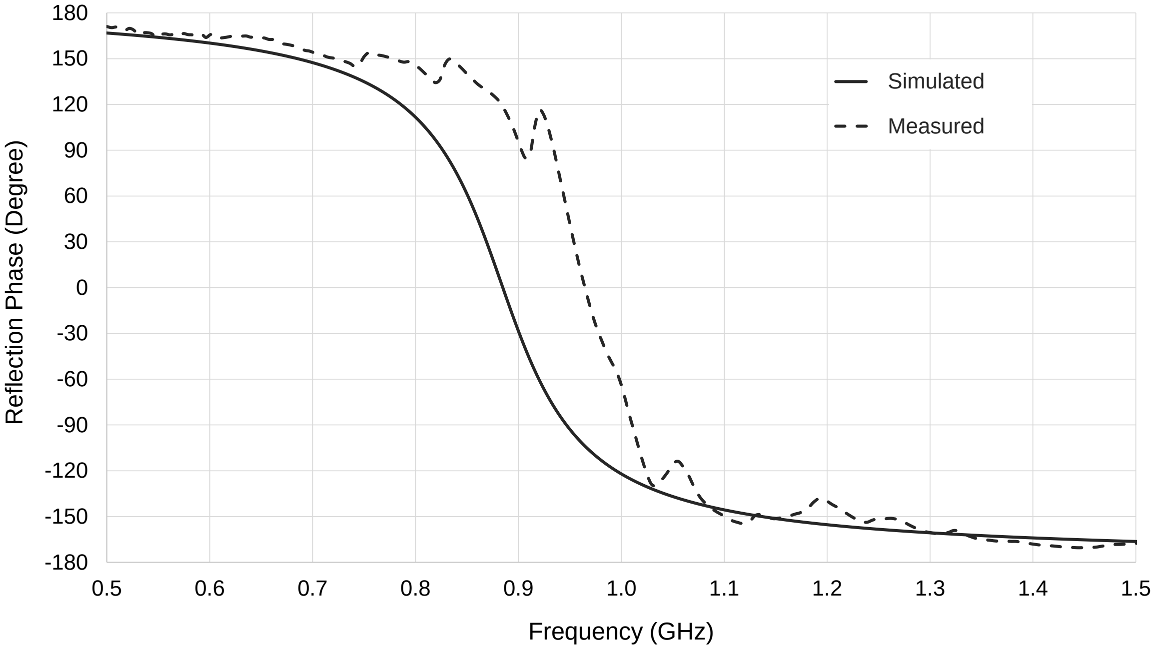

Fig. 6.6 Single band 900 MHz IDC HIS simulated and measured reflection phase.

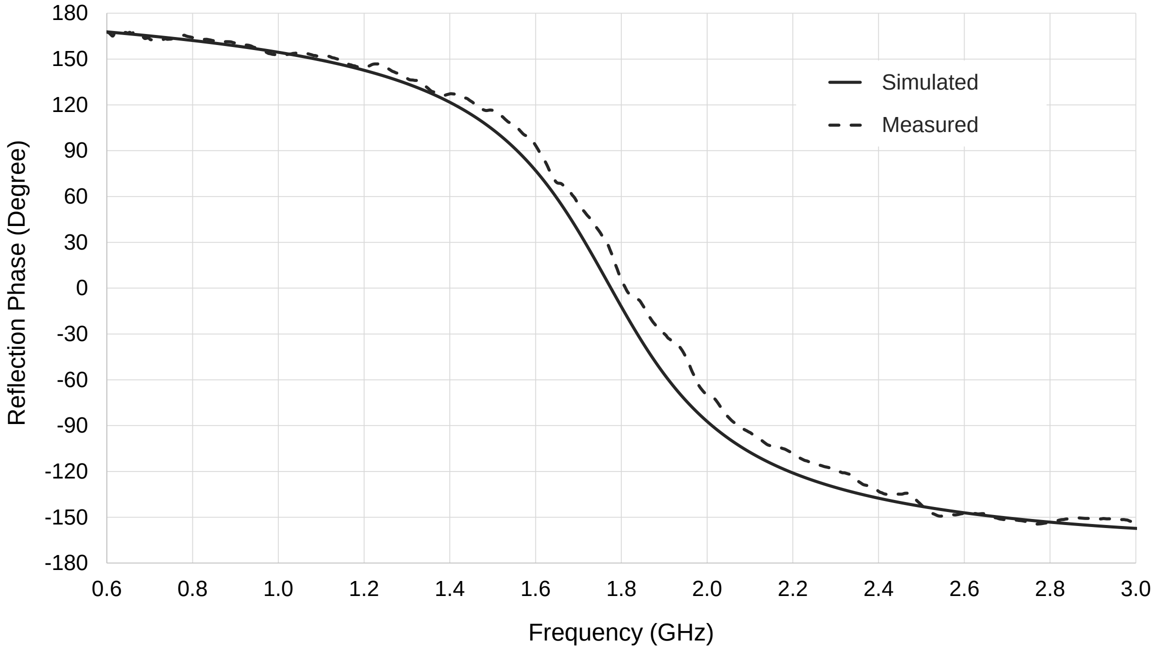

Fig. 6.7 Single band 1800 MHz IDC HIS simulated and measured reflection phase.

The dual band miniaturised interdigital HIS, operating at 900 MHz and 1800 MHz, is realised as two subunit cells, initially optimized as individual single band structures, and are concatenated forming a HIS of total periodicity $0.15\lambda_{1.8\text{GHz}}$. Combined interdigital

HIS is fabricated on a 12 by 11 periodic array of periodicity 25 mm, printed on 1.6 mm FR4 substrate ($\varepsilon_r = 4.3, \tan\delta = 0.025$). Subsequently, the dual band interdigital capacitive surface 300 mm × 300 mm PCB is supported by a 6 mm Rohacell material and backed by metal, as shown in Fig. 6.8.

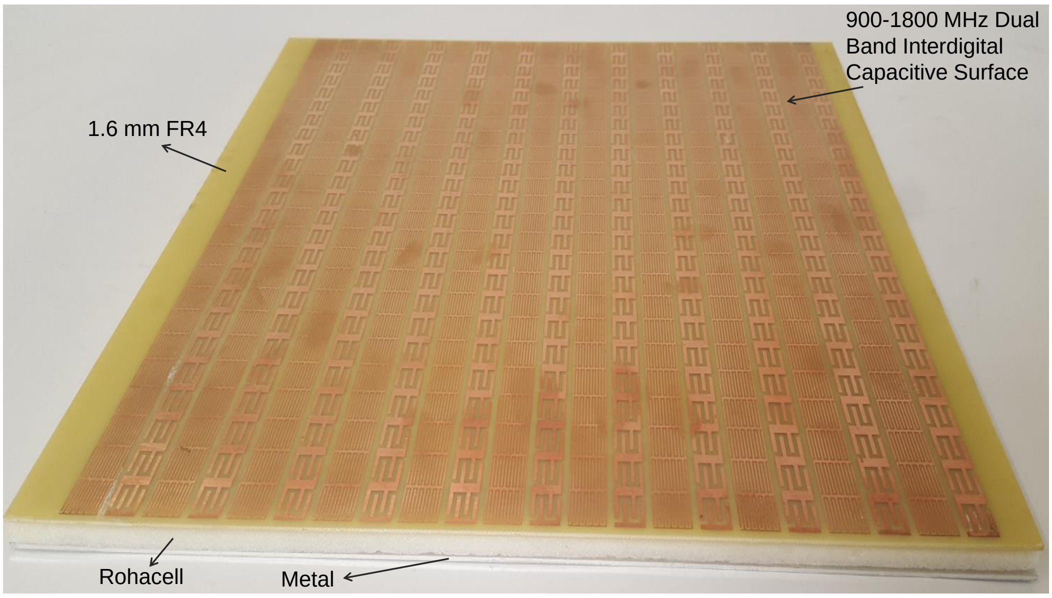

Fig. 6.8 900 - 1800 MHz dual band 300 mm × 300 mm IDC HIS fabricated on 1.6 mm FR4 substrate ($\varepsilon_r = 4.3, \tan\delta = 0.025$), supported by 6 mm Rohacell and backed by a metal plate.

Reflectivity measurements of dual band interdigital high impedance surface are performed using NRL Arch system in the same fashion described earlier, as single band high impedance structures designed at 900 MHz and 1800 MHz were discussed earlier. A miniaturised dual band interdigital high impedance surface is also modelled on CST Microwave Studio for normal incidence to compare with reflectivity measurements. Simulated and measured reflection phase plots of 900 MHz and 1800 MHz miniaturised interdigital dual band high impedance surface are presented in Fig. 6.9 where resonance frequencies show good agreement. However, in both bands, resonance frequencies are shifted from design requirements of 900 MHz and 1800 MHz. As observed in Fig. 6.9, Band 1 resonance frequency is increased by 19% and 26% in simulation and measurement respectively. While Band 2 resonance frequency is increased by 71% and 65% as observed in simulation and measurement respectively. Frequency shift in both Band 1 and Band 2 are attributed to inter unit cell mutual coupling. Nevertheless, the effect of mutual coupling is more prominent in the upper band which encountered significant degradation in fractional bandwidth.

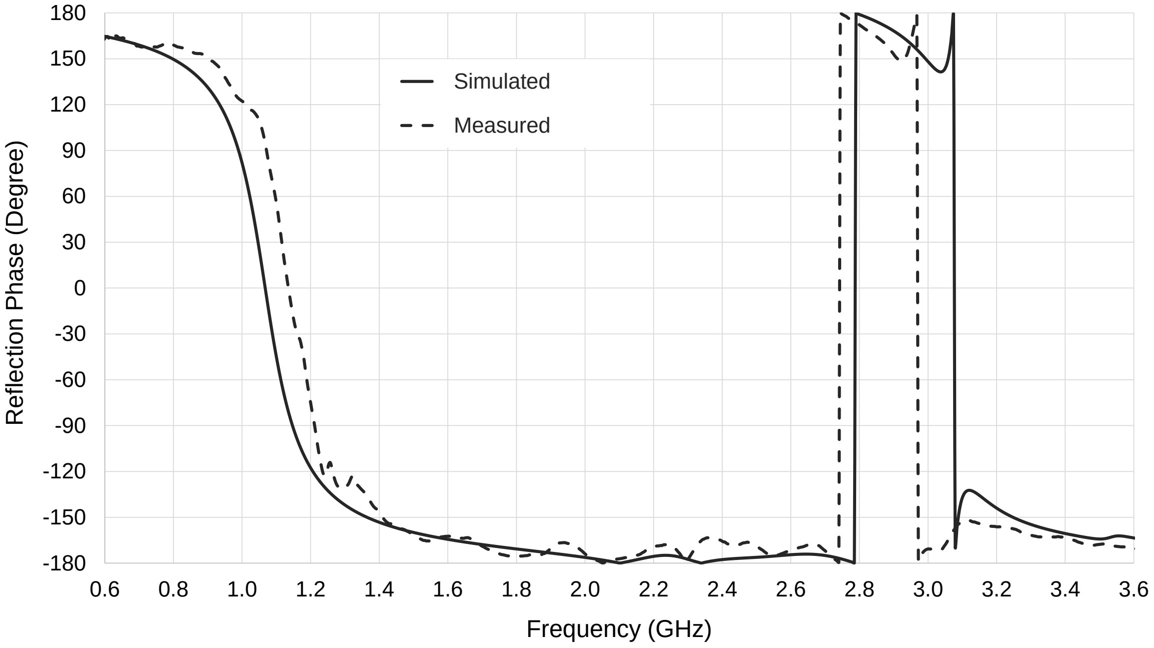

Fig. 6.9 Miniaturised 900-1800 MHz dual band interdigital HIS reflection phase.

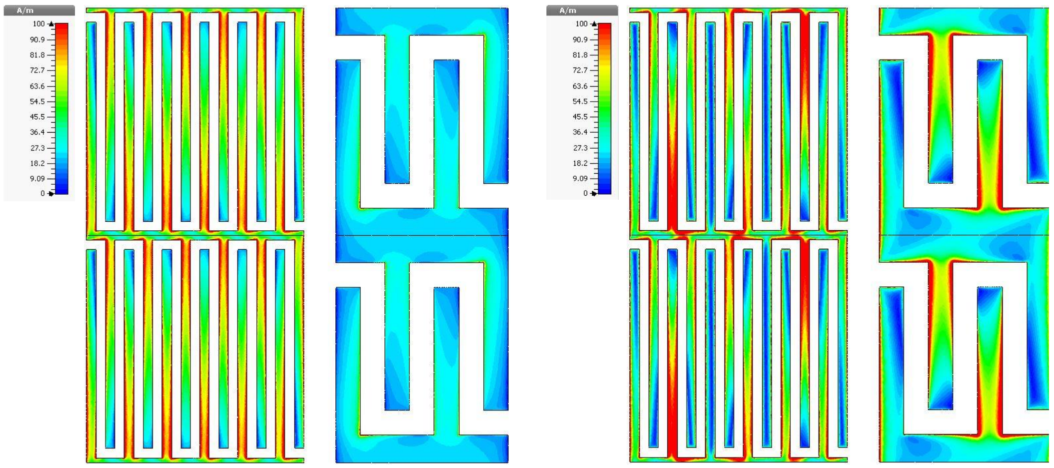

(a) 900 MHz Band

(b) 1800 MHz Band

Fig. 6.10 Simulated surface current amplitude in miniaturised dual band interdigital HIS.

Mutual coupling between subunit cells can be further explained from simulated surface currents observed at the same intensity level for a miniaturised interdigital dual band high impedance structure monitored at 900 MHz and 1800 MHz which are presented in Fig. 6.10. For the first band, 900 MHz, current amplitude is of maximum intensity within the subunit cell on the left, which contributes to the lower band resonance with little impact from the subunit cell on the left designed for the upper band resonance, Fig. 6.10a, which justifies the smaller 26% percentage shift in Band 1 resonance frequency, observed in measured reflection phase plots. On the other hand, observing surface current amplitude monitored at the second band, 1800 MHz, it can be observed that a significant current is conducted in both subunit cells; not only the right interdigital subunit cell, which generates the upper band, but also the left lower band subunit cell which possess significant loading into the upper band, as observed in Fig. 6.10b. The lower band subunit cell loading effect on the upper band is more significant and interpreted as reducing the capacitive effect for the upper band, therefore, explaining the 65% percentage increase in upper band frequency with respect to the design requirement of 1800 MHz, observed in measurements. Therefore, both bands are affected by inter unit cell mutual coupling, but more significant as the upper band is concerned.

Furthermore, the smith chart of simulated input impedance for 900 MHz and 1800 MHz miniaturised dual band interdigital HIS as well as the single bands designed individually is presented in Fig. 6.11, therefore, demonstrating the effect of mutual coupling in dual band interdigital HIS design. Single band interdigital HIS designs demonstrate a high impedance at 900 MHz (Band 1) and 1800 MHz (Band 2). However, as dual band interdigital HIS is concerned, mutual coupling had significant impact altering the surface characteristics; a high impedance at lower band whose resonance frequency is shifted to 1100 MHz and a lossy impedance observed in the upper band whose frequency is shifted to 3100 MHz.

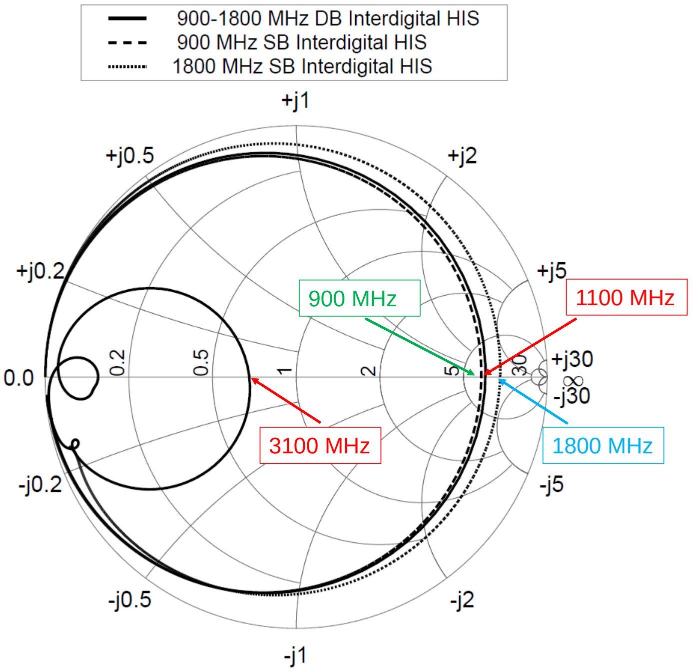

Fig. 6.11 Simulated input impedance smith chart of miniaturised 900-1800 MHz interdigital dual band HIS as compared to 900 MHz and 1800 MHz single band interdigital HIS.

6.3.2 Reverse engineered dual band interdigital HIS

As of previous analysis, to realise miniaturised dual band interdigital HIS from two individually designed bands, interaction between subunit cells must be taken into account, which are subject to mutual coupling. A method to redesign each band by calculating the estimated percentage frequency shift due to mutual coupling is proposed. The percentage frequency shift is defined as:

$$\%\mathrm{FreqShift} = \frac{\mathrm{f_{coupling}} - \mathrm{f_{dsn}}}{\mathrm{f_{dsn}}} \times 100 \tag{6.4}$$

where $\mathrm{f_{dsn}}$ is the required design frequency and $\mathrm{f_{coupling}}$ is the frequency resulting from coupling effect.

Therefore, to reverse engineer the dual band structure, new design frequencies for each band are calculated from perception of (%FreqShift) due to mutual coupling; defined as:

$$\mathrm{f_{new}} \frac{\mathrm{f_{dsn}}}{1 + \frac{\%\mathrm{FreqShift}}{100}} \tag{6.5}$$

Table 6.2 Revered Engineer Dual Band Interdigital HIS Subunit Cell Design Parameters

IDC HIS Parameters	900 MHz Band	1800 MHz Band
Required design frequency ($\mathrm{f_{new}}$)	790 MHz	1060 MHz
Substrate material	FR4	FR4
Substrate thickness ($\mathrm{H_d}$)	1.6 mm	1.6 mm
Rohacell thickness ($\mathrm{H_v}$)	6 mm	6 mm
Subunit cell periodicity (P)	12.5 mm	12.5 mm
Number of digits ($\mathrm{N_d}$)	16	8
Digits side gap (s)	0.34 mm	0.7 mm
Digits width (w)	0.34 mm	0.7 mm
Digits top/bottom gap ($\mathrm{s_p}$)	0.34 mm	0.7 mm
Digits length (L)	11 mm	7.8 mm
Interdigital capacitance ($\mathrm{C_d}$)	4 pF	2.3 pF

This technique is validated considering the previous case studied for 900 MHz and 1800 MHz dual band interdigital HIS. Knowing the expected frequency increase in each band is influenced by mutual coupling, each band is re-designed to operate at adjusted new resonance frequencies of 790 MHz and 1060 MHz corresponding to Band 1 and Band 2 respectively while unit cell periodicity, substrate material and substrate thickness are constantly maintained. Practically this means that each subunit cell capacitance density must be increased to accommodate the required reduction in resonance frequencies. Therefore, increasing interdigital capacitance density to 4 pF and 2.3 pF for lower and upper band subunit cells respectively, which is expected to compensate for each subunit cell loading effect on one another as a result of mutual coupling. Design of each band is conducted according to the methodology discussed in Chapter 5 and dual band interdigital HIS new design parameters are detailed in Table 6.2. Comparing design parameters of the redesigned dual band interdigital HIS in Table 6.2 with that of Table 6.1, since unit cell size is maintained constant increasing interdigital capacitance density in both subunit cells, are associated with the increased number of digits and reduction in track width and gaps as expected.

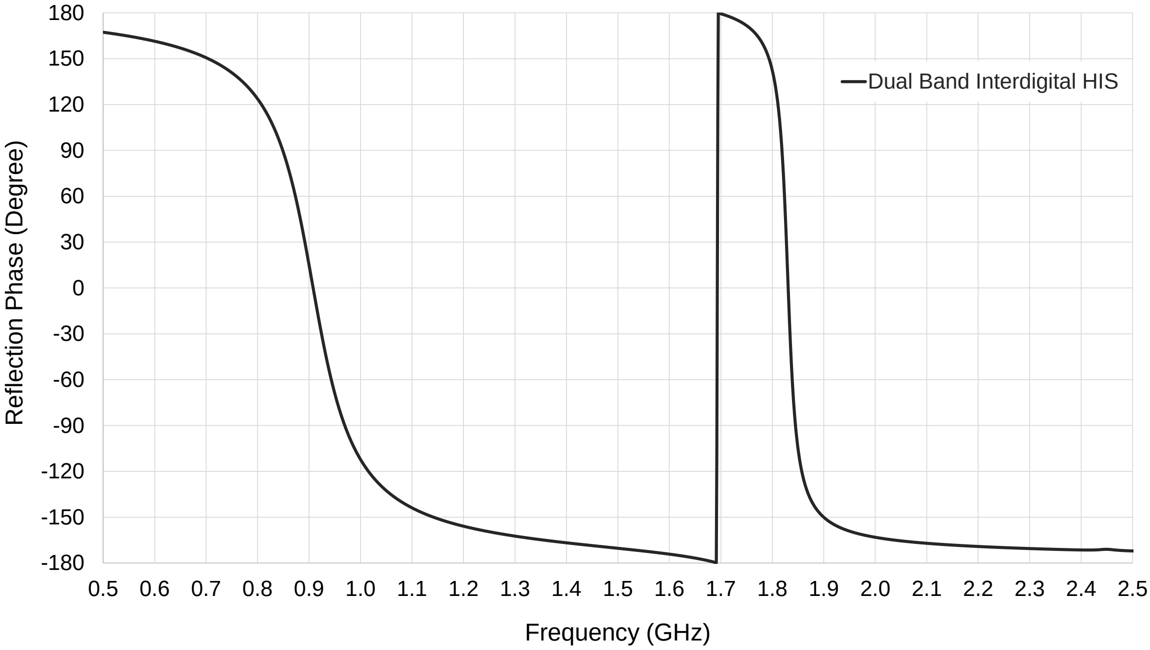

Fig. 6.12 Reversed engineered miniaturised 900-1800 MHz dual band interdigital HIS simulated reflection phase plot. Design parameters, Table 6.2

A miniaturised interdigital dual band HIS, of total periodicity $0.14\lambda_{1.8\mathrm{GHz}}$, designed on 1.6 mm FR4 substrate, supported by a 6 mm Rohacel material and backed by metal is modelled on CST Microwave Studio and reflection phase properties are observed at normal incidence. Fig. 6.12 shows a simulated reflection phase plot, which demonstrates that dual band interdigital HIS operates at 900 MHz and 1800 MHz within a fractional bandwidth of 13.5% and 1.4% respectively. Therefore, the reverse engineering design methodology has successfully accounted for inter unit cell mutual coupling.

Moreover, simulated surface currents are presented in Fig. 6.13. Where the lower band of 900 MHz is concerned, simulated surface current plots are shown in Fig. 6.13a, and it can be observed that the highest current density is concentrated within the subunit cell on the left, where the upper band is mutually coupled into the lower band, where surface currents are also conducted on the subunit cell to the right and is expected to contribute to the upper band resonance. However, the significance of inter-unit cell mutual coupling is demonstrated in the simulated surface current plots, observed at the upper band frequency of 1800 MHz. As shown in Fig. 6.13b, simulated surface current, observed at 1800 MHz, has significant current density conducted in both subunit cells, where the lower band subunit cell on the left contributes to the upper band resonance. Therefore, encountering mutual coupling between a two band high impedance surface is possible by taking the expected frequency displacement into account, which results in considering both subunit cells of the dual band interdigital HIS as contributing to each band resonance. Consequently, the capacitance density in both subunit cells is required to increase, where simulated surface current plots for original and reversed engineered HIS demonstrates the difference as compared in Fig. 6.12 and Fig. 6.10.

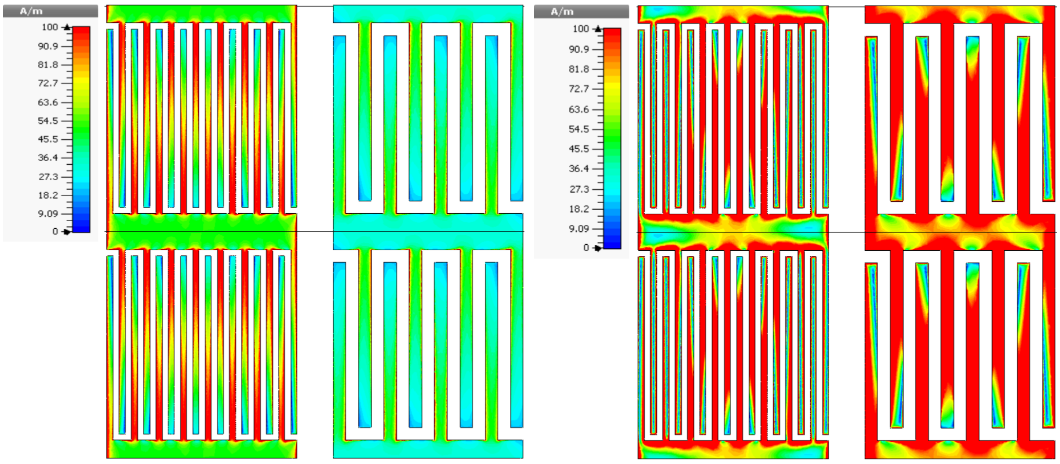

(a) 900 MHz Band

(b) 1800 MHz Band

Fig. 6.13 Simulated surface current amplitude in reversed engineered miniaturised dual band interdigital HIS.

Furthermore, the input impedance chart of simulated dual band interdigital HIS demonstrates a high impedance as observed for both 900 MHz and 1800 MHz frequency bands, as shown in Fig. 6.14. This emphasised that by taking mutual coupling into account, both bands develop a high impedance and the losses in fractional bandwidth are also encountered as compared in Fig. 6.14 and Fig. 6.11.

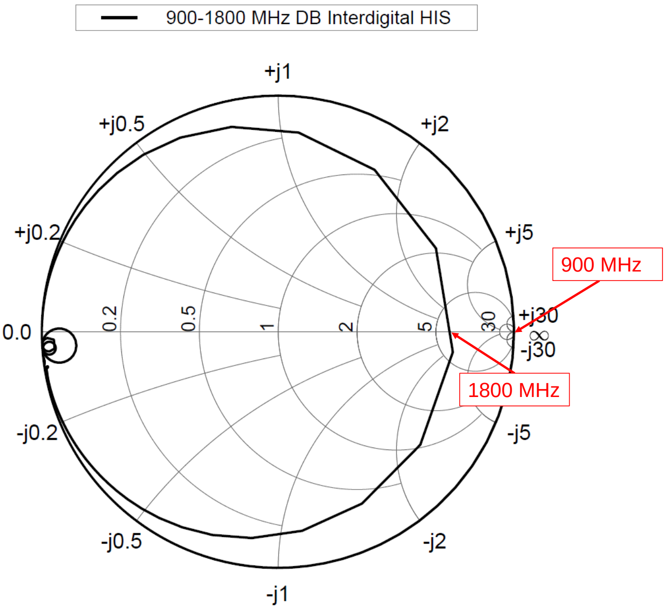

Fig. 6.14 Reversed engineered miniaturised 900-1800 MHz dual band interdigital HIS simulated input impedance smith chart.

6.3.3 Summary of design

A flow chart is presented in Fig. 6.15 to describe dual band interdigital high impedance surface design methodology starting from single band designs, calculating coupling illustrated by percentage frequency shift in each band (%FreqShift) and then taking coupling effect into account. As described in Fig. 6.15, starting from a single band HIS structure, which is modelled within a subunit cell periodicity (P), each band is designed individually then integrated into a dual band of total periodicity (P_T). An initial numerical simulation is required at this stage such that the percentage frequency shift in each band due to mutual coupling is calculated. Thereafter, single band subunit cells are reverse engineered and designed at the new altered resonance frequencies that include coupling effect and where the dual band is tested again. This works perfectly fine with no problems if mutual coupling is a standard known value. However, this process is very much structure specific; the design is not generic since mutual coupling level is expected to change with unit cell physical dimensions, frequency of operation and band separation. Therefore, the next analysis presents a parametric study of factors that contribute to dual band mutual coupling in full details addressing the necessity for a generalised design methodology.

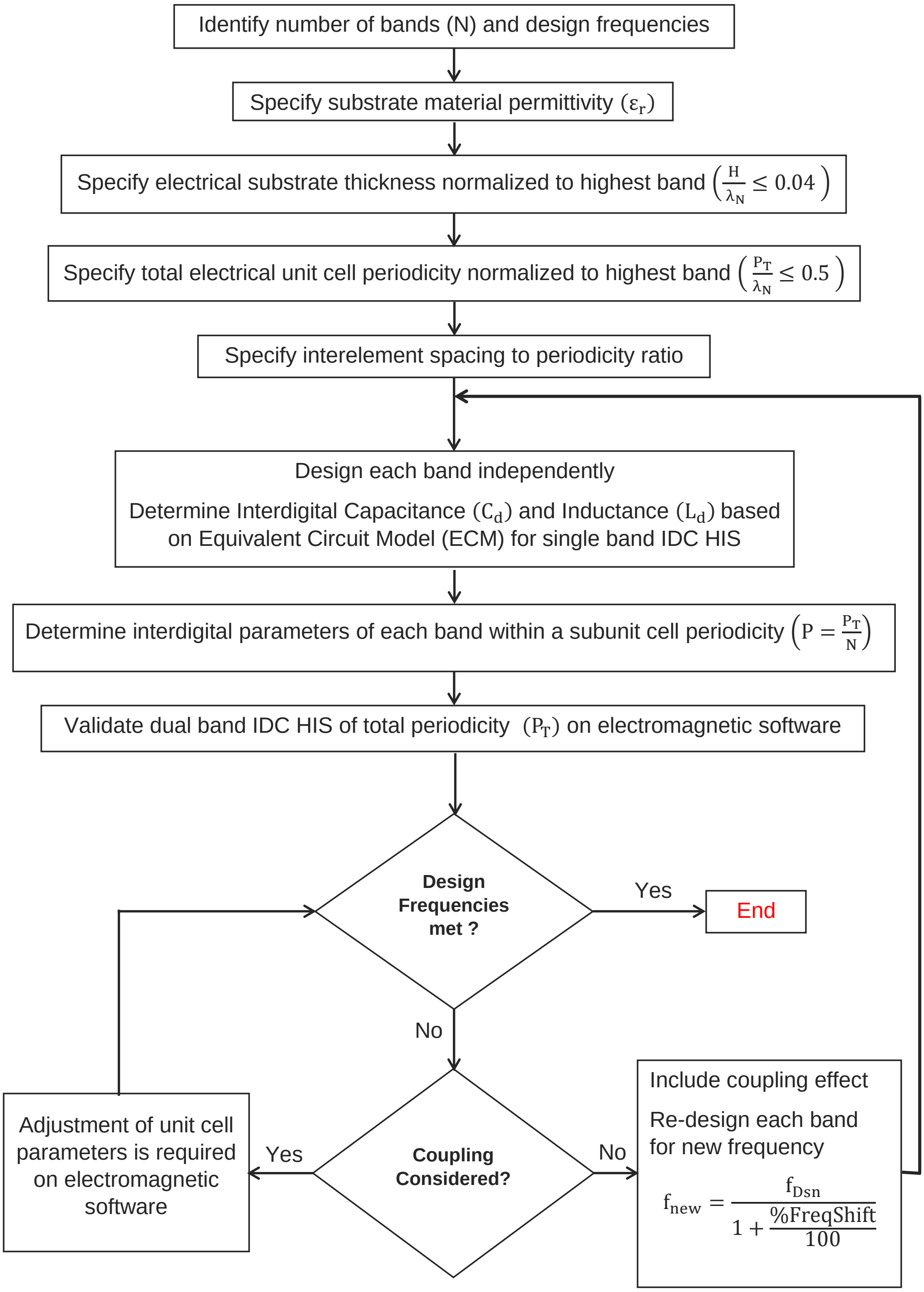

Fig. 6.15 Design procedure for miniaturised dual band interdigital HIS. Structure is revered engineered though numerically estimating frequency displacement due to mutual coupling.

6.4 Dual Band Interdigital HIS Mutual Coupling Analysis

Mutual coupling in dual band interdigital High Impedance Surface (HIS) has been discussed through a case study highlighting its significance as a major design constraint. A technique has been suggested to take mutual coupling effect into consideration by tailoring individual subunit cell design to accommodate the expected frequency displacement incurred in each band. However, the case study was very much structure specific. For the proposed technique to be applied, a generalised methodology should be deduced where all factors that influence inter unit cell mutual coupling are taken into consideration. In this section, an equivalent circuit model is first proposed describing the dual band interdigital HIS mechanism, therefore, leading to insights on expected factors contributing to inter unit cell mutual coupling. Thereafter, a complete parametric study investigating dual band interdigital HIS unit cell parameters that influence each band's resonance frequency and contribute to mutual coupling is conducted, therefore, setting the foundation for a generalised method, detailed in Chapter 7.

6.4.1 Equivalent circuit model

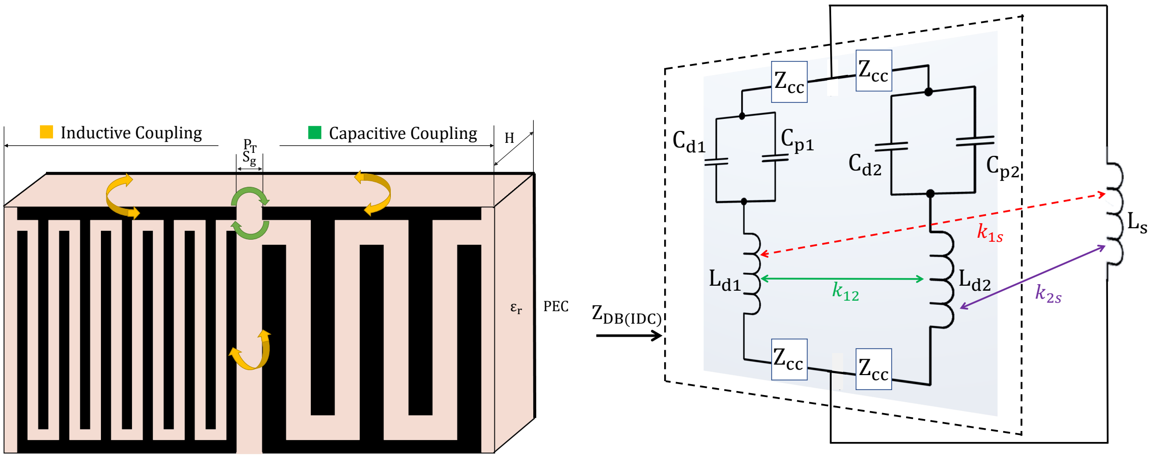

(a) 3D Model (b) Equivalent Circuit Model (ECM)

Fig. 6.16 Miniaturised dual band interdigital high impedance surface model.

A dual band interdigital 3D model layout is presented in Fig. 6.16a. Coupling between the two band system is thought to be generated by both capacitive and inductive effects, therefore, each subunit cell possesses impedance loading one on another. Capacitive coupling is generated due to interelement spacing and subunit cell impedance loading effects where the current is conducted from one subunit cell to another. The presence of substrate backed by a ground plane also elaborates inductive coupling as it interacts with the interdigital surface.

An empirical equivalent circuit model of dual band interdigital HIS is proposed in Fig. 6.16b. Each subunit cell is modelled according to an equivalent circuit model of single band interdigital HIS, discussed in Chapter 5. Therefore, comprising of interdigital capacitance $(\mathrm{C_{di}})$ in parallel with mutual patch capacitance $(\mathrm{C_{pi}})$ then in series with interdigital inductance $(\mathrm{L_{di}})$ where $(\mathrm{i} = 1,2)$ is referred to Band 1 and Band 2 respectively. A two band system is considered as two mutually coupled interdigital HIS resonators.

Capacitive coupling between both bands is represented by impedance $(\mathrm{Z_{cc}})$ comprising of series capacitance $(\mathrm{C_{cc}})$ and a small predicted inductance $(\mathrm{L_{cc}})$. Impedance $(\mathrm{Z_{cc}})$ is:

$$\mathrm{Z_{cc}} = j\omega \mathrm{L_{cc}} + \frac{1}{j\omega \mathrm{C_{cc}}} \tag{6.6}$$

On the other hand, inductive coupling is mainly generated as interdigital subunit cell inductances $(\mathrm{L_{d1}})$ and $(\mathrm{L_{d2}})$ and substrate inductance $(\mathrm{L_s})$ are mutually coupled and is illustrated by introducing coupling factors (k_{12}), $(k_{1\mathrm{s}})$, and $(k_{2\mathrm{s}})$ representing coupling between inductances $(\mathrm{L_{d1}},\mathrm{L_{d2}})$, $(\mathrm{L_{d1}},\mathrm{L_s})$, and $(\mathrm{L_{d2}},\mathrm{L_s})$ respectively.

The equivalent circuit model proposed provides a useful method to understand the mechanism of miniaturised dual band interdigital HIS, but the structure's complexity makes it very difficult to determine generalised quantitative values for $(\mathrm{Z_{cc}})$, and coupling factors (k_{12}), $(k_{1\mathrm{s}})$, and $(k_{2\mathrm{s}})$. For example, in the previous case study of 900 MHz and 1800 MHz dual band interdigital HIS, which is designed from two individual single band subunit cells, as detailed in Section 6.3.1, circuit elements that contribute to reflection phase characteristics as in Fig. 6.9 are: $(\mathrm{L_{cc}} = 0.4\,\mathrm{nH}, \mathrm{C_{cc}} = 9\,\mathrm{pF})$, $(\mathrm{L_{d1}} = 1.6\,\mathrm{nH}, \mathrm{C_{d1}} = 2.84\,\mathrm{pF})$, $(\mathrm{L_{d2}} = 1\,\mathrm{nH}, \mathrm{C_{d2}} = 0.77\,\mathrm{pF})$ and coupling factors $(k_{12} = -0.7, k_{1\mathrm{s}} = -0.3, k_{2\mathrm{s}} = -0.4)$.

Nevertheless, circuit elements such as interdigital capacitance, interdigital inductance, mutual capacitance and substrate inductance are explicit functions of unit cell parameters such as substrate permittivity, substrate thickness, unit cell periodicity, interelement spacing and band separation. Therefore, the next analysis is directed to a numerical parametric study conducted using CST Microwave Studio to investigate the effect of interdigital dual band HIS unit cell parameters and factors which are related to induce mutual coupling. The main focus will be on analysing resonance frequency percentage displacement with respect to each band design frequency as a function of parameters involved using the term %FreqShift, and percentage frequency shift, which is defined in Eq. (6.4).

6.4.2 Substrate permittivity effect

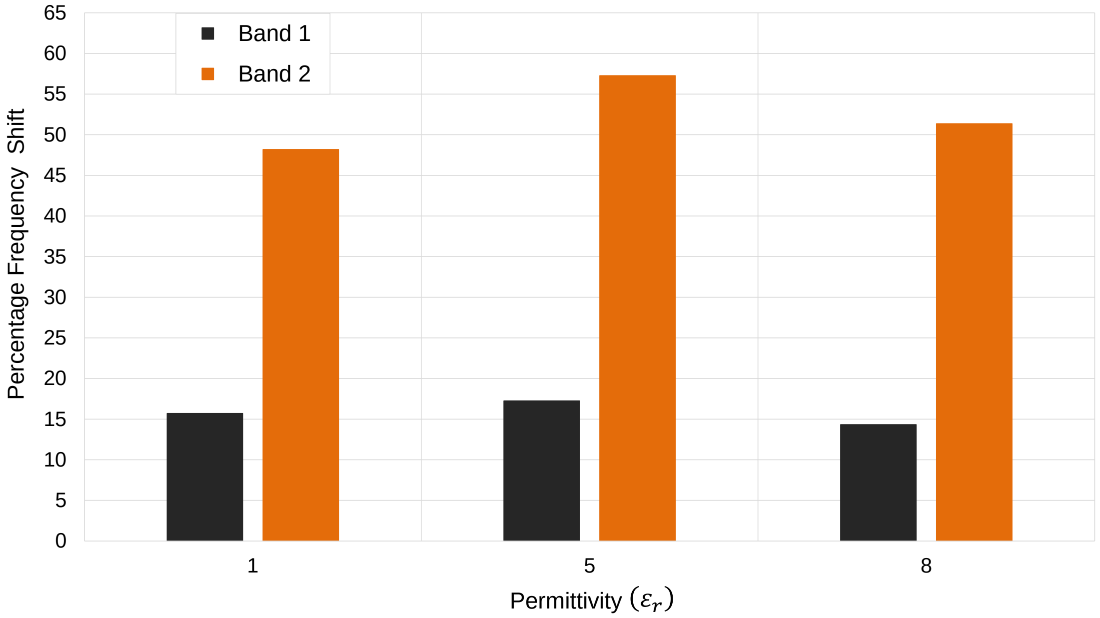

Fig. 6.17 dual band interdigital HIS percentage frequency shift versus substrate permittivity. $\varepsilon_r = 1,\ 5,$ and 8 is considered in dual bands separated by 100%. Substrate thickness $0.02\lambda_{\mathrm{N}}$. Unit cell periodicity $0.08\lambda_{\mathrm{N}}$. Interelement spacing to periodicity ratio 0.05.

While high impedance surfaces are printed on supporting substrates for mechanical reasons, the presence of substrate influence resonance frequency. Dual band design parameters are fixed as each dual is individually designed for Band 1 frequency (f_1) and Band 2 frequency $(\mathrm{f}_2 = 2\mathrm{f}_1)$ which corresponds to percentage band separation $(\%\mathrm{BandSep} = 100\%)$. Total unit cell electrical periodicity $(\mathrm{P_T})$ and substrate thickness (H), as normalized to high band frequency (f_2), are maintained constant at $0.08\lambda_{\mathrm{N}}$ and $0.02\lambda_{\mathrm{N}}$ respectively. Also interelement spacing to periodicity ratio is fixed at $(\frac{\mathrm{S_g}}{\mathrm{P_T}} = 0.05)$. Fig. 6.17 presents bar chart analysis investigating the effect of dual band interdigital HIS substrate relative permittivity (ε_r) versus percentage frequency shift, in each band, offset from design requirements because of dual band mutual coupling. Values of permittivity $(\varepsilon_r = 1,\ 5,\ \text{and}\ 8)$ are considered. While coupling has a more prominent effect on Band 2 shifting its resonance frequency by an average of 55% in all permittivity cases $(\varepsilon_r = 1,\ 5,\ \text{and}\ 8)$ as compared to an average frequency shift of 15% in Band 1 frequency. Therefore, percentage frequency shift in both bands, due to mutual coupling, is almost constant and not affected by the change in HIS substrate permittivity (ε_r), as shown in Fig. 6.17.

Moreover, substrate permittivity parametric analysis indirectly indicates the significance of varying interdigital capacitance geometrical parameters in each band subunit cell. In Chapter 5, interdigital capacitance ($\mathrm{C_d}$) is the function of interdigital number of digits ($\mathrm{N_d}$), digits length (L), digits gap (s), digits width (s) and permittivity (ε_r). As in the previous analysis, reduction in substrate permittivity (ε_r), within a fixed unit cell interdigital area and constant $\mathrm{C_d}$, requires increasing the number of digits ($\mathrm{N_d}$) as well as reducing the digits gap(s) and digits width (w). Therefore, by altering substrate permittivity (ε_r), interdigital capacitance density in each band subunit cell has explicitly changed, but will have no impact on dual band mutual coupling according to analysis in Fig. 6.17.

6.4.3 Substrate electrical thickness effect

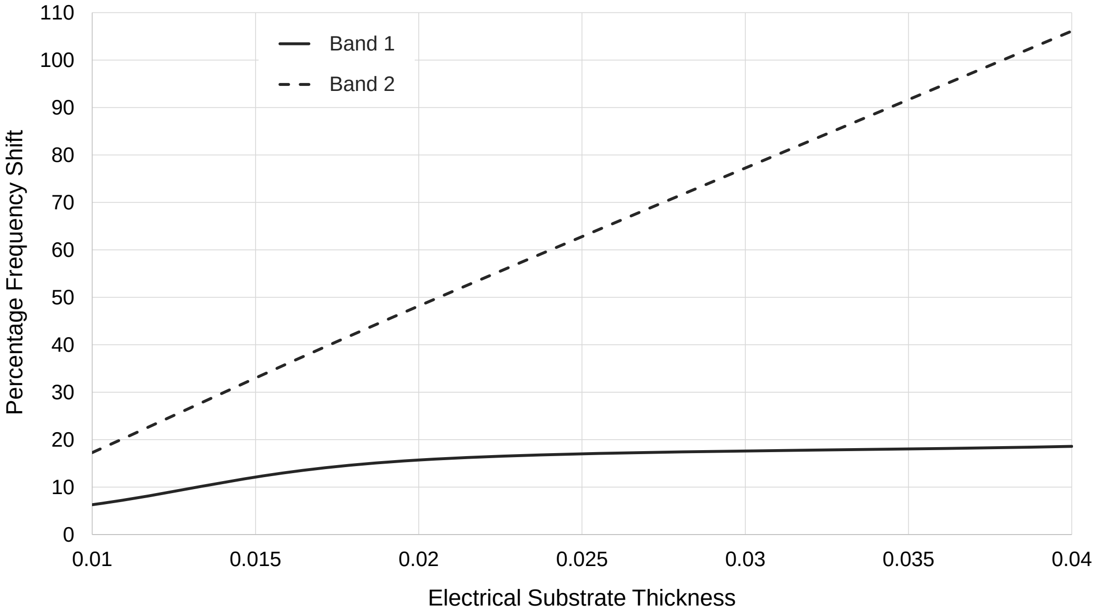

Fig. 6.18 Dual band interdigital HIS percentage frequency shift versus substrate electrical thickness. Percentage band separation 100%. Permittivity ($\varepsilon_r = 1$). Unit cell periodicity $0.08\lambda_{\mathrm{N}}$. Interelement spacing to periodicity ratio 0.05.

The effect of increasing HIS substrate thickness on each band frequency is considered. This has been investigated by varying the substrate thickness while fixing design frequencies, percentage band separation (%BandSep = 100%), substrate permittivity ($\varepsilon_r = 1$), electrical unit cell periodicity ($\mathrm{P_T} = 0.08\lambda_{\mathrm{N}}$) and interelement spacing to periodicity ratio ($\frac{\mathrm{S_g}}{\mathrm{P_T}} = 0.05$). Electrical substrate thickness, as normalized to high band wavelength, is increased from $0.01\lambda_{\mathrm{N}}$ to $0.04\lambda_{\mathrm{N}}$. Each band is individually designed then combined into a dual band HIS where percentage frequency displacement due to inter unit cell mutual coupling is calculated. Dual band interdigital HIS percentage frequency shift versus variation in HIS electrical substrate thickness is presented in Fig. 6.18. In both Band 1 and Band 2, percentage frequency shift increases linearly as the substrate thickness increases. Therefore, the HIS substrate backed by a metal plate is of an inductive nature and contributes to an inductive mutual coupling effect within the system, which is more significant in the upper band.

6.4.4 Unit cell electrical periodicity effect

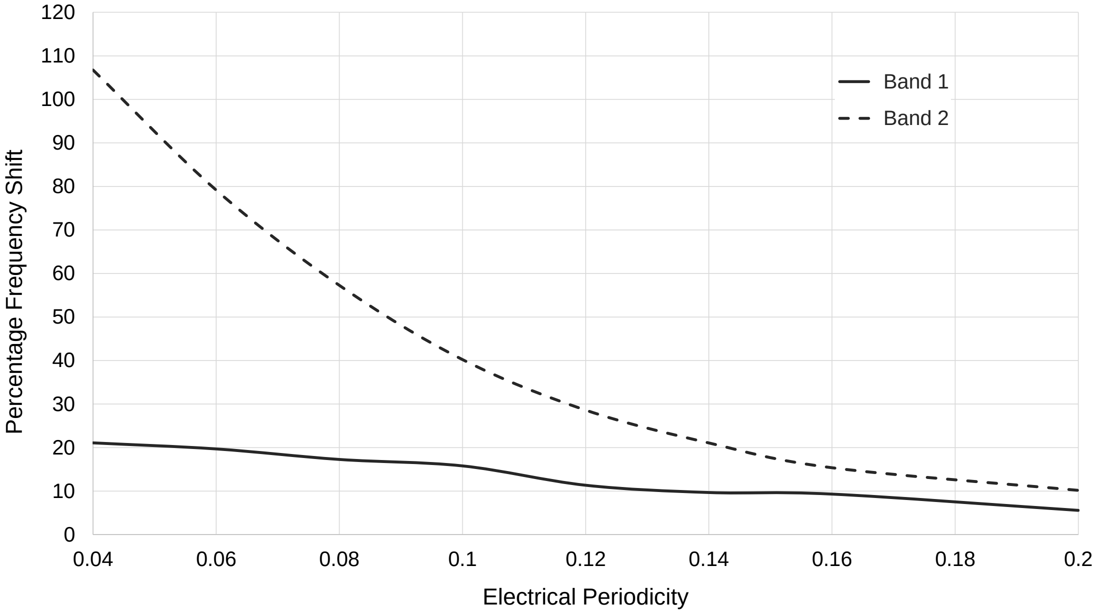

Fig. 6.19 Dual band interdigital HIS percentage frequency shift versus electrical periodicity. Percentage band separation 100%. Permittivity $(\varepsilon_r = 5)$. Interelement spacing to periodicity ratio 0.05. Electrical substrate thickness $0.02\lambda_{\mathrm{N}}$.

Parametric analysis on the influence of increasing HIS unit cell periodicity on Band 1 and Band 2 resonance frequency is discussed. Fixing unit cell parameters such as interelement spacing to periodicity ratio $(\frac{\mathrm{S_g}}{\mathrm{P_T}} = 0.05)$, substrate electrical thickness $(\mathrm{H} = 0.02\lambda_{\mathrm{N}})$ and permittivity $(\varepsilon_r = 5)$ while dual bands, separated by 100%, are designed at frequencies $(\mathrm{f_1} = 2\mathrm{f_1})$. HIS unit cell electrical periodicity is increased from $0.04\lambda_{\mathrm{N}}$ to $0.2\lambda_{\mathrm{N}}$ while percentage frequency shift in each of Band 1 and Band 2 is observed. Fig. 6.19 shows that at very small periodicities mutual coupling is at its utmost intensity such that design resonance frequencies are significantly offset from design requirements; however, mutual coupling reduces as periodicity increases. Moreover, since interelement spacing to periodicity ratio is maintained constant, reducing the periodicity effectively reduces the spacing between subunit cells and enhances coupling. Undesired capacitive coupling is induced by variations of top HIS capacitive layer governed by periodicity effect where energy is transferred from Band 1 to Band 2 and vice versa, but of prominent impact on upper band (Band 2).

6.4.5 Unit cell interelement spacing effect

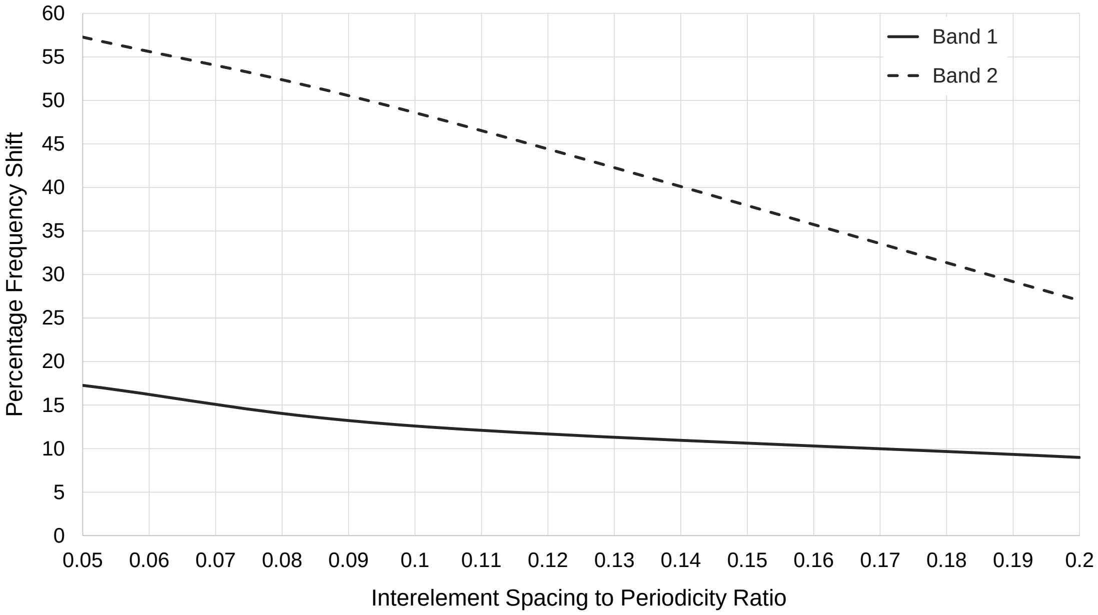

Fig. 6.20 Dual band interdigital HIS percentage frequency shift versus interelement spacing to periodicity ratio. Percentage band separation 100%. Permittivity $(\varepsilon_r = 5)$. Electrical periodicity $0.08\lambda_\mathrm{N}$. Electrical substrate thickness $0.02\lambda_\mathrm{N}$.

For a fixed electrical substrate thickness $(\mathrm{H} = 0.02\lambda_\mathrm{N})$ and permittivity $(\varepsilon_r = 5)$ dual band interdigital HIS is optimized at frequencies $(\mathrm{f}_1 = 2\mathrm{f}_1)$ maintaining a percentage separation of 100%. The effect of varying interelement spacing within a fixed dual band interdigital HIS unit cell with a total electrical periodicity of $(\mathrm{P_T} = 0.08\lambda_\mathrm{N})$ is considered. Interelement spacing to periodicity ratio is, therefore, increased from 0.05 to 0.2 while percentage frequency shift with respect to design requirements is observed; therefore, analysing its effect on inter unit cell mutual coupling. Fig. 6.20 demonstrates a direct linear relationship between interelement spacing variation and percentage frequency shift in both Band 1 and Band 2. Resonance frequency shift reduces as interelement spacing is increased. This is expected since the physical spacing between dual band interdigital subunit cells has increased and eventually reduces capacitive coupling while closely spaced subunit cells are significantly coupled. Nevertheless, the ratio of interelement spacing to unit cell periodicity should not exceed 0.2 to maintain a periodic structure. Therefore, opting to reduce mutual coupling by large subunit cell spacing is not recommended.

6.4.6 Band separation effect

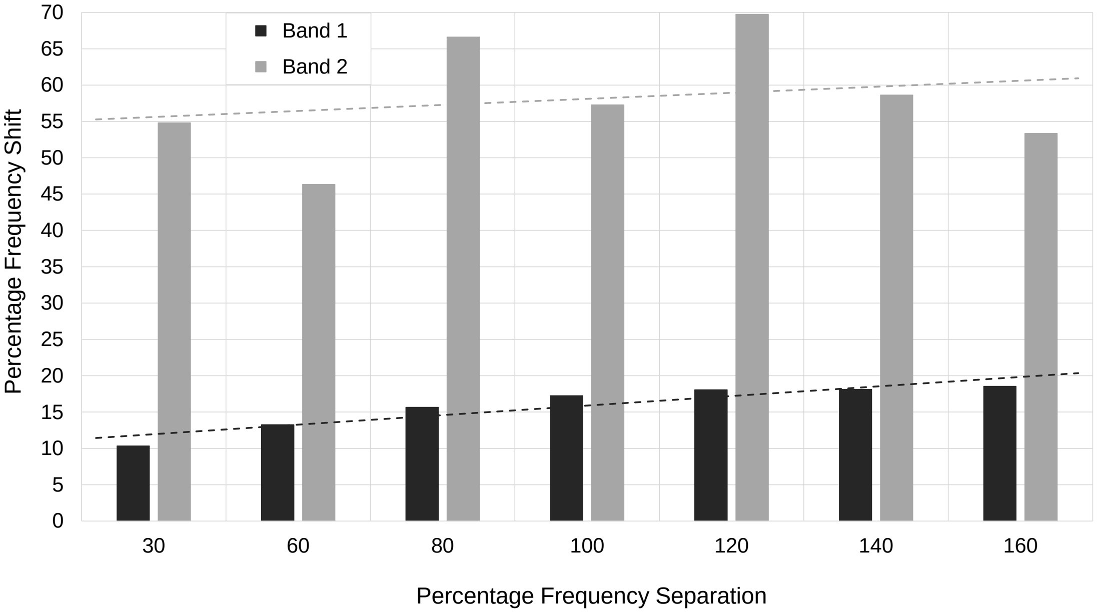

Fig. 6.21 Dual band interdigital HIS percentage frequency shift versus percentage band separation. Substrate permittivity ($\varepsilon_r = 5$). Electrical substrate thickness $0.02\lambda_{\mathrm{N}}$. Electrical periodicity $0.08\lambda_{\mathrm{N}}$. Interelement spacing to periodicity ratio 0.05.

Percentage band separation ($\%\mathrm{BandSep}$) refers to the percentage within which interdigital HIS Band 2 frequency is separated with respect to Band 1 frequency, defined as:

$$\%\mathrm{BandSep} = \frac{\mathrm{f}_2 - \mathrm{f}_1}{\mathrm{f}_1} \times 100 \tag{6.7}$$

where f_1 and f_2 are Band 1 and Band 2 resonance frequencies.

To investigate the influence of varying percentage band separation ($\%\mathrm{BandSep}$) on mutual coupling, as related to miniaturised interdigital dual band HIS and which is correlated to percentage shift in each band resonance frequency, two bands are designed individually for a fixed electrical substrate thickness ($\mathrm{H} = 0.02\lambda_{\mathrm{N}}$) and electrical periodicity ($\mathrm{P_T} = 0.08\lambda_{\mathrm{N}}$), as normalized to high band wavelength. Also, substrate permittivity ($\varepsilon_r = 5$) and interelement spacing to periodicity ratio ($\frac{\mathrm{S_g}}{\mathrm{P_T}} = 0.05$) are maintained constant. First, lower band design frequency is sustained at (f_1) while the upper band resonance frequency is varied such that percentage band separation (%BandSep) is varied accordingly. The effect of increasing percentage band separation from 30% to 160% on percentage frequency shift, as observed in Band 1 and Band 2, is presented in Fig. 6.21. Both bands resonance frequencies are shifted and offset from design requirements due to mutual coupling. However, percentage band shift in each band appears to be fluctuating with no clear pattern while the trend appears to be linear.

There is no concise judgement to be made in this parametric study due to the non systematic pattern in the predicted percentage frequency shift. Even though electrical substrate thickness and periodicity are constantly maintained, practically the physical dimensions of dual band interdigital HIS substrate thickness and unit cell periodicity are reduced since the upper band wavelength decreases when frequency (f_2) increases while constantly maintaining the lower band frequency (f_1). Therefore, the effects of reduced physical periodicity and substrate thickness are combined to increase and reduce the %FreqShift respectively.

In addition, increasing band separation has indirectly increased interdigital capacitance densities in both Band 1 and Band 2 as associated with reduced physical periodicity and substrate thickness, which in-turn required that the interdigital number of digits needs to increase and digits gap/width to decrease in order to accommodate that change. Variation of interdigital structure could possess some impact even though it is understood to be negligible.

Finally, percentage frequency shift in both bands, due to coupling, is quite relative and can be tolerated where the fluctuations are of minimal effect. This case study is not required to be investigated any further due to many parameters involved especially as the effect of periodicity and substrate thickness are solely addressed in previous sections. Where the current parametric analysis is concerned, it can be concluded that percentage band separation has some influence on percentage frequency shift in both bands and follows a linear trend. In the next chapter, a conclusive analytical model is established where the effect of percentage band separation is included in order to rule out its influence on mutual coupling and compensates for any errors introduced by simulations, computations and circuit model approximations.

6.5 Conclusion

This chapter has provided design guidelines for a miniaturised dual band interdigital high impedance surface. The design prototype is constituted of two individually designed single band interdigital HIS subunit cells integrated into one structure, which is polarization dependent, modelled as a single metallic interdigital layer, supported by a dielectric material and backed by a metal layer. The design methodology was based on concepts detailed in Chapter 5, which has been demonstrated as a robust method to optimize interdigital capacitance elements for the required capacitance and resonance frequency to be realised. Nevertheless, concatenating two single band interdigital HIS subunit cells into one structure was hindered by mutual coupling which has been observed to limit the dual band performance and degrade its functionality by shifting the resonance frequency from design requirements and reducing fractional bandwidth, as observed in both lower and upper bands. Mutual coupling has been discussed and deduced to be of inductive and capacitive origins where an empirical equivalent circuit model to describe the miniaturised dual band interdigital HIS mechanism has also been proposed.

Moreover, a parametric study to investigate main factors that affect dual band interdigital HIS inter unit cell coupling has been conducted. Mutual coupling significantly affects both band resonance frequencies and causes undesired displacement from design requirements. It has therefore been interpreted as the term "Percentage Frequency Shift" $(\%\text{FreqShift})$. The cause of this frequency shift was due to impedance loading from each band subunit cell into another as they have been integrated into one structure where they are mutually coupled. Based on an equivalent circuit model each band impedance is eventually a function of unit cell parameters. Therefore, main dual band interdigital unit cell parameters that contribute to mutual coupling have been observed to be periodicity, substrate thickness and interelement spacing. Also, substrate permittivity and band separation have been addressed and demonstrated to influence mutual coupling to some extent. The parametric analysis conducted within this chapter is of significant magnitude to generate a general model that predicts the mutual coupling level in a dual band interdigital HIS for any arbitrary unit cell dimensions. Therefore, in the next chapter, a novel design methodology to develop a model that predicts percentage frequency shift in each band as a function of all unit cell parameters involved where a generalised solution function of 5 parameters will be provided. Consequently a simple method to design miniaturised dual band interdigital HIS is achievable.

Chapter 7

Dual band Interdigital High Impedance Surface - Mutual Coupling Model

7.1 Introduction

Chapter 6 provided detailed conceptions to simplified design methodology that realises miniaturised dual band High Impedance Surface (HIS) incorporating interdigital capacitors where, individually designed single band interdigital HIS unit cells are then concatenated to realise a dual band structure. Nevertheless, simplicity of this approach is hindered by inter unit cell mutual coupling, which is highly anticipated and is believed to be of an inductive and capacitive nature as triggered by a variation of unit cell geometrical parameters whose effect is also profoundly discussed in Chapter 6. It has been found that inter unit cell mutual coupling is intensified by three main factors: increased substrate thickness, reduced periodicity and reduced interelement spacing, in addition to variation in substrate permittivity as well as band separation. Mutual coupling generates undesired frequency shift in both bands. To overcome this problem, while maintaining the simplified design method, Chapter 6 also proposed a design approach to include mutual coupling effect by prior knowledge of percentage expected frequency displacement in each band. But mutual coupling is influenced by 5-dimensional elements and for this method to be efficient it must be generalised and not structure specific. Therefore, a model is required to be able to predict the mutual coupling level in advance. In this chapter, a novel technique to predict the mutual coupling level is proposed. A mathematical model, based on multiple linear regression analysis, is introduced to estimate percentage frequency shift in each band as a function of all unit cell parameters which have impact on inter unit cell mutual coupling. A simple linear mathematical model is initially determined followed by an enhanced non-linear mathematical model proved of higher accuracy. Multiple linear regression models are verified in three different miniaturised dual band interdigital HIS designs. Design 1: Dual Band Single Layer Single Polarized (DB-SLSP) interdigital HIS. Design 2: Dual Band Dual Layer Dual Polarized (DB-DLDP) interdigital HIS. Design 3: Dual Band Single Layer Dual Polarized (DB-SLDP) interdigital HIS.

7.2 Dual Band Interdigital HIS Generalised Mutual Coupling Model

In this section, a method to manage inter unit cell mutual coupling in dual band interdigital HIS is proposed, where a mathematical model to effectively predict the expected percentage frequency shift in Band 1 and Band 2 is formulated. Therefore, mutual coupling is taken into account while implementing a simplified design methodology that realises a dual band interdigital HIS from two single band structures, individually modelled. Initially, the research question is stated highlighting the main problem and factors involved. Then, a quick introduction to regression analysis is given to introduce the reader to terms used thereafter.

7.2.1 Stating research question

Miniaturised dual band interdigital capacitor HIS is realised by concatenating two individually designed single band subunit cells as discussed in Chapter 6, as shown in Fig. 6.16a. Methodology of design was based on neglecting any interaction between subunit cells while applying an analytical circuit model approach, detailed in Chapter 5, which on its own involves many parameters optimized to achieve unit cell reflection characteristics that meet the required design resonance frequency. As expected, when two single band interdigital HIS subunit cells are integrated into one structure electromagnetic interaction of unwanted magnetic and electric interference occurs. This is denoted as "Mutual Coupling" between two subunit cells which causes an undesired frequency shift and degradation of bandwidth in both frequency bands. The previous parametric study, detailed in Chapter 6, emphasised factors that contribute to dual band interdigital HIS inter unit cell mutual coupling governed by the physical parameters of dual HIS structure, stated in order of significance: Unit cell periodicity $(\mathrm{P_T})$, interelement spacing $(\mathrm{S_g})$, substrate thickness (H), substrate permittivity (ε_r) and percentage band separation $(\%\mathrm{BandSep})$. Therefore, a 5-dimensional problem. An example of dual band interdigital HIS for a band separation of 100%, designed on a substrate permittivity $(\varepsilon_r = 1)$ and interelement spacing to periodicity ratio $(\frac{\mathrm{S_g}}{\mathrm{P_T}} = 0.05)$ is discussed for the sake argument and analysed in 3-dimensional perspective as the result of varying electrical substrate thickness as well as electrical unit cell periodicity, both normalized to high band wavelength.

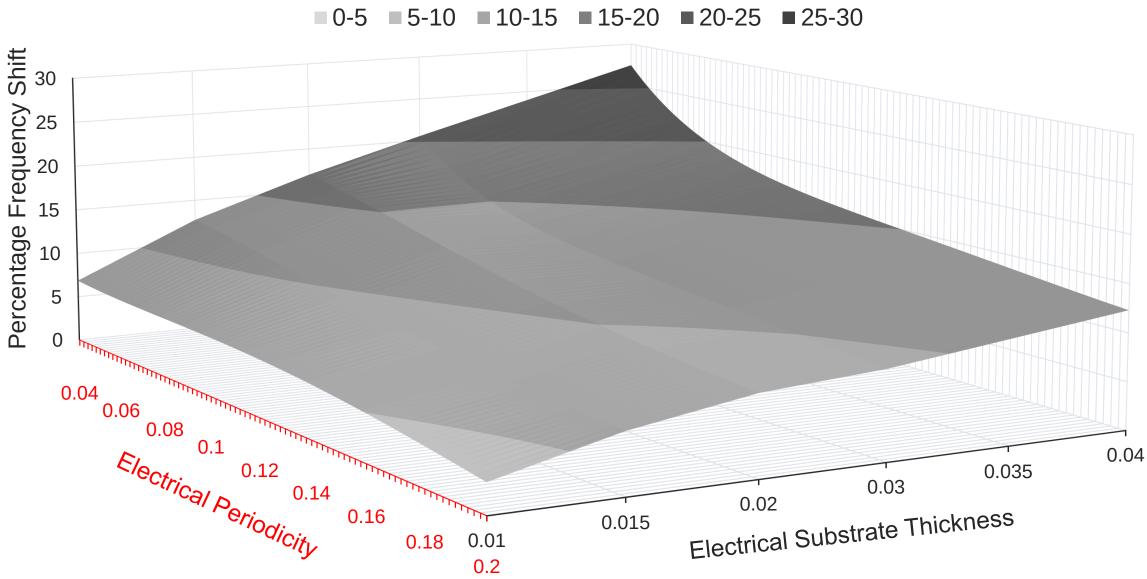

Fig. 7.1 Dual band IDC HIS lower band (Band 1) percentage frequency shift versus electrical substrate thickness and periodicity. Fixed, $\frac{\mathrm{S_g}}{\mathrm{P_T}} = 0.05$, %BandSep = 100% and $\varepsilon_r = 1$.

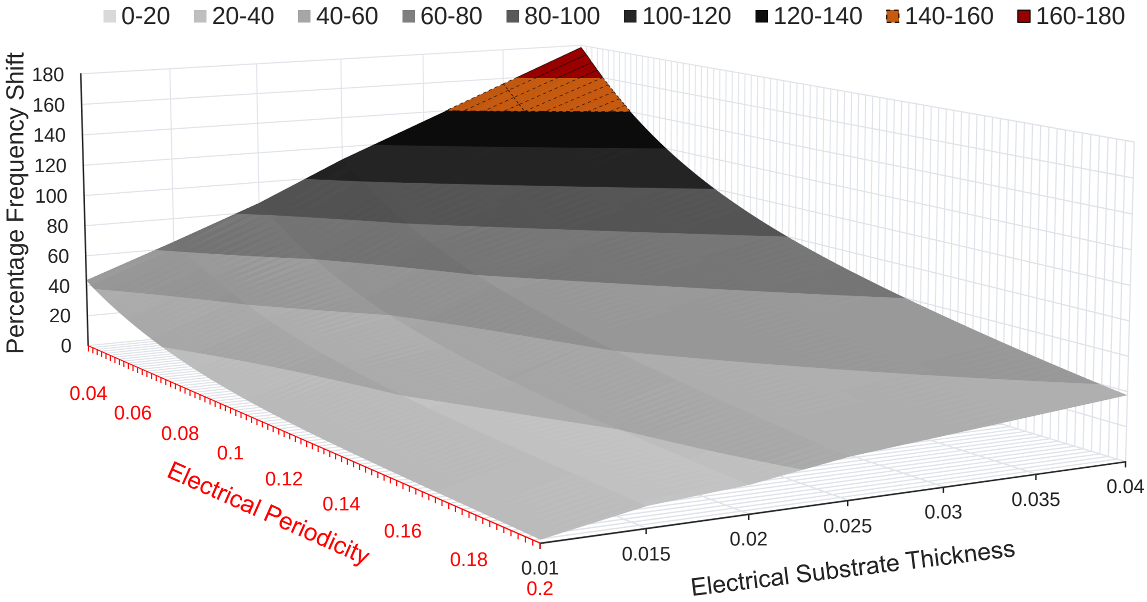

Fig. 7.2 Dual band IDC HIS lower band (Band 2) percentage frequency shift versus electrical substrate thickness and periodicity. Fixed, $\frac{\mathrm{S_g}}{\mathrm{P_T}} = 0.05$, %BandSep = 100% and $\varepsilon_r = 1$.

Fig. 7.1 and Fig. 7.2 present percentage frequency shift, in Band 1 and Band 2 respectively versus variation in both periodicity and substrate thickness. In both bands, coupling is at its maximum when electrical periodicity is minimum, $0.04\lambda_N$, and electrical substrate thickness is maximum, $0.04\lambda_N$, where frequency of both bands suffer from a maximum displacement with respect to design requirements. While least mutual coupling is where % frequency shift in both bands is minimum is when electrical periodicity is maximum, $0.2\lambda_N$, and electrical substrate thickness is minimum, $0.01\lambda_N$. The 3D modelling of percentage frequency shift for both bands in Fig. 7.1 and Fig. 7.2 demonstrates an obvious linear trend which the percentage frequency shift follows as the result of varying P_T and H even though Band 2 frequency shift diverts a little bit from linearity as coupling intensity increases. However, the above analysis is very much design specific and percentage frequency shift in each band is not generalised according to these terms. There are many different possibilities of %BandSep, ε_r, $\frac{S_g}{P_T}$, P_T, and H. Mutual coupling analysis would be insignificant and least beneficial at this stage if it was very particular to a given frequency band , unit cell parameters or design specific.
Therefore, research questions as related to dual band interdigital HIS design, knowing there is mutual coupling interference, are formulated:

- Is it possible to design a dual band interdigital HIS from two single band structures?
- Is it possible to define factors that contribute most to dual band mutual coupling?
- Can coupling be mapped to these factors and mathematically modelled in the simplest form possible?
- Is it possible to determine the relationship between these factors and their influence on dual band resonance frequencies where mutual coupling is involved?
- Is it possible to predict the percentage each band frequency is shifted due to mutual coupling for an arbitrary two band system, unit cell parameters and design requirement?

The answer is "YES" to all of the above !
Percentage frequency shift in each band has a linear relationship with 5-dimensional variables which is difficult to visualize all at once. Therefore, percentage frequency shift in each band is modelled as a linear function of unit cell electrical periodicity ($\frac{P_T}{\lambda_N}$), substrate electrical thickness ($\frac{H}{\lambda_N}$), interelement spacing to periodicity ratio ($\frac{S_g}{P_T}$), %BandSep, and ε_r where multiple linear regression is the best suited method. The mutual coupling level illustrated by the quantitative term percentage frequency shift "output" is mapped in a mathematical equation function of multiple "continuous variables" which are factors involved and discussed next.

7.2.2 What is regression analysis ?

Appendix C provides detailed insights on linear regression in terms of assumptions, mathematical terms involved and how this technique is applied. While, in the current chapter, general definitions and a quick summary of terms involved will be summarized as directly related to the mutual coupling model predicted for the purpose of designing a miniaturised dual band interdigital high impedance surface.

Regression analysis is a class of multi-variable techniques which can be utilized to analyse the effect of input(s) on a given output. It is, therefore, a statistical method which allows mathematical realisation in relating an outcome variable (output/dependant variable) to a set of predictor(s) (input/independent variable(s)). Regression can be linear, non-linear or logistic . Depending on the type of data analysed and how the output is related to input variables the correct regression model is implemented.

7.2.3 Multiple linear regression equation and assumptions

As previously discussed, two single band interdigital HIS are initially individually designed then concatenated as one unit cell HIS structure to generate a dual band system. Mutual coupling is inevitable, shifting the resonance frequencies in both bands and degrading the fractional bandwidth. If coupling is to be modelled, then percentage frequency shift must be determined. Therefore, the research question to be answered by multiple linear regression model is, Can percentage frequency shift in each band, of a dual band interdigital HIS system, be mathematically modelled as a function of independent continuous parameters that contribute to dual band mutual coupling ?
Multiple linear regression general expression is given by:

$$\mathrm{Y} = \mathrm{B}_0 + \mathrm{B}_1\mathrm{X}_1 + \mathrm{B}_2\mathrm{X}_2 + \mathrm{b}_3\mathrm{X}_3 + \mathrm{B}_4\mathrm{X}_4 + \mathrm{B}_5\mathrm{X}_5 + \in \tag{7.1}$$

where:
Y is the Dependant Variable (DV) is the output as a function of multiple inputs.
X_n is the Independent Variable (IV) of number (n), which is the input that contributes to output (Y).
B_0 is the intercept. B_n is the regression coefficient, which is the associated slope of independent variable (X_n) that indicates a direct linear change in (Y) for every unit change in X_n.
$\in$ is the error term.

Therefore, dual band interdigital HIS percentage frequency shift (%FreqShift), in each of Band 1 and Band 2, is recorded experimentally for very large combinations of independent variables investigated one at a time and conducted using full wave simulations on CST Microwave Studio, which are then arranged into a matrix format. Multiple linear regression fits dependant variable (Y) to a linear model function of 5 independent variables $(\mathrm{X}_1, \mathrm{X}_2, \mathrm{X}_3, \mathrm{X}_4, \mathrm{X}_5)$ based on least square method, Appendix C. IBM SPSS Statistics is used to conduct multiple linear regression on a large number of observations made.

Where the current analysis is concerned, Y is the percentage frequency shift (%FreqShift), in either Band 1 or Band 2 which are investigated individually. The main aim is to determine coefficients $(\mathrm{B}_0, \mathrm{B}_1, \mathrm{B}_2, \mathrm{B}_3, \mathrm{B}_4, \mathrm{B}_5)$ which reliably predict the output (Y) into a linear model with minimum errors. Accordingly, input Independent Variables (IV) defined in order of expected importance, are:
$\mathrm{X}_1 = \frac{\mathrm{H}}{\lambda_\mathrm{N}}$: Dual band interdigital HIS substrate electrical thickness as normalized to highest band wavelength, evaluated within the limits :

$$0.005 \leq \frac{\mathrm{H}}{\lambda_\mathrm{N}} \leq 0.04 \tag{7.2}$$

$\mathrm{X}_2 = \frac{\mathrm{P_T}}{\lambda_\mathrm{N}}$: Dual band interdigital HIS total electrical periodicity as normalized to highest band wavelength, analysed within the limits:

$$0.02 \leq \frac{\mathrm{P_T}}{\lambda_\mathrm{N}} \leq 0.25 \tag{7.3}$$

$\mathrm{X}_3 = \frac{\mathrm{S_g}}{\mathrm{P_T}}$: Dual band interdigital HIS interelement spacing $(\mathrm{S_g})$ to total unit cell periodicity $(\mathrm{P_T})$ ratio, examined within the limits:

$$0.05 \leq \frac{\mathrm{S_g}}{\mathrm{P_T}} \leq 0.2 \tag{7.4}$$

$\mathrm{X}_4 = \varepsilon_r$: Dual band interdigital HIS substrate permittivity, varied in the range:

$$1 \leq \varepsilon_r \leq 10 \tag{7.5}$$

$\mathrm{X}_5 = \%\mathrm{BandSep}$: Dual band interdigital HIS percentage band separation, Eq. (6.7), investigated within the range:

$$30\% \leq \%\mathrm{BandSep} \leq 200\% \tag{7.6}$$

Assumptions considered in multiple linear regression [130, 131] are satisfied in the current analysis and stated below:

- Independent variable(s) (predictors) are not correlated and non-singular.
- Independent variable(s) are a continuous set of data.
- Dependent variable (output) is highly correlated with each of the independent variables.
- Dependant variable is linearly related with independent variable(s) to a reasonable extent.
- Sample size is enough to model the output in best fit possible. It has been reported in [131] that sample size (m) as a function of the number of independent variables (n) must satisfy the relationship; $\mathrm{m} > 104 + \mathrm{n}$.
- Outliers are minimized and does not interfere with the fitted model.
- Residuals, defined as the difference between observed and predicted outcome , are normally distributed. Therefore , residuals are expected to follow a linear trend in a probability plot of predicted versus observed outputs.

7.2.4 Assessing the quality of linear regression model

SPSS Statistics Tables: Three main tables, output by SPSS, are important to statistically determine the effectiveness of the predicted model. Terms used are briefly explained and defined as they form the basis of results in the sections to follow as the mutual coupling model is formulated. More details can be found in Appendix C.

- "Model Summary" Table: contains information to evaluate the model's overall effectiveness as related to all independent variables. Correlation coefficient $(-1 \leqslant \mathbf{R} \leqslant 1)$ is a measure of the strength of relationship between the dependent variable (output) and independent variables (inputs). High **R**, negative/positive, which means that the output and inputs are statistically dependent and highly associated which is desired . A very small **R** indicates that the output is not related to the input. But key information in this table is $(0 \leqslant \textbf{R Square} \leqslant 1)$ which statistically measures how well the linear model explains the output as well as the strength of the linear relationship. It also measures the percentage of variation in output that is well explained by the inputs. **R Square** equation is detailed in Appendix C where $\mathbf{R} = \sqrt{\textbf{R Square}}$.

While regression computes coefficients that maximizes **R Square** with no information on the power of independent variables (predictors), **Adjusted R Square** is the unbiased estimator of **R Square** that examines independent variables usefulness in predicting the model coefficients for best fit and should be close to **R Square** for a well fitted model with properly chosen predictors. The standard error of estimates is included and it measures the accuracy of the predicted model. Minimum error is required which means a small standard error deviation.

- " Analysis Of Variance " (ANOVA) Table: A good straight line fit is evaluated for the model as a whole in the ANOVA table. ANOVA compares the variability between observed data, regression model and errors in fit of the model (residuals) as a function of the inputs (independent variables). The output of regression model detailed in the ANOVA table examines the variability within a regression model. However, not every term in the ANOVA table will be discussed where this chapter is concerned since they are related to one another, details are in Appendix C. Nevertheless, the focus will be on **p value** which should be less than 0.05 for a statistically significant result, where the null hypothesis tested by regression analysis can be ignored. Null hypothesis is the assumption that independent variables coefficients are zero and, therefore, do not contribute to the output where the regression model is inadequate. If **p value** < 0.05, all independent variables are of significant importance.

- "Coefficients" Table: This is where important information on the regression model is provided by SPSS output, which summarizes the results of multiple regression analysis and has all the information to evaluate the predicted coefficients of independent variables that constitute the regression model.

  Unstandardized Coefficients are regression coefficients that are multiplied by independent variables and used in the regression model. Standard error associated with each of the coefficients should be minimum. **p value** < 0.05 is required in each independent variable such that it is of statistically significant importance and contributes to predicting the regression model; where the corresponding null hypothesis is "Not True". Furthermore, it gives confidence in the choice of variables being decisive predictors. IBM SPSS Statistics converts the **Unstandardized Coefficients** to **Standardized Coefficients** such that regression coefficients have the same scale for a fair comparison. Absolute values are considered to compare which of the independent variables are of more ruling importance and explains the output best.

  In addition, the **95% Confidence Interval** of **Unstandardized Coefficients** is analysed and it is expected of a narrow width, for better accuracy, and not to include a zero. The 95% Confidence Interval is the interval within which the Unstandardized Coefficients are statistically valid, such that the regression model perfectly fits within a probability of 0.95 and **p value** < 0.05 is true.

Finally, a test of multicollinearity between independent variables is presented in the term **Tolerance**. If multicollinearity is suggested in any of the independent variables, it should be excluded from analysis. For (**Tolerance** < 0.1), independent variables are highly correlated which invalidates regression model coefficients.

SPSS Statistics Plots: Normality of residuals is also checked through a Normal Probability Plot (P-P) which indicates linearity of the model and validity of p values. Also it detects any outliers which would require to be accounted for to improve the model fit.

7.3 Linear Regression In Dual Band Interdigital HIS

Having examined the factors that contribute to mutual coupling in the design of miniaturised dual band interdigital HIS through parametric analysis and where, mutual coupling is illustrated by a shift in resonance frequency of each band,five main factors summarized: unit cell periodicity, interelement spacing, substrate thickness, permittivity and band separation are observed. The outcome of 4716 observations is made as continuous data collected using CST full wave simulations and interpolations techniques is statistically examined on IBM SPSS Statistics software to propose a linear model that predicts percentage frequency shift in each band as function of factors mentioned. This section will detail proposed mathematical models for Band 1 and Band 2 where multiple linear regression is applied as well as all tests hypotheses that validate the significance and reliability of design equations.

7.3.1 Band 1 linear multiple regression model

Multiple linear regression was applied to estimate the Percentage Frequency Shift in Band 1 (%FreqShift-Band1). A linear model is established from input parameters that contribute to dual band interdigital HIS inter unit cell mutual coupling.

Independent variables of interest are: substrate electrical thickness $(\frac{\mathrm{H}}{\lambda_{\mathrm{N}}})$, unit cell electrical periodicity $(\frac{\mathrm{P_T}}{\lambda_{\mathrm{N}}})$, interelement spacing to periodicity ratio $(\frac{\mathrm{S_g}}{\mathrm{P_T}})$, substrate permittivity (ε_r) and percentage band separation (%BandSep).

The outcome linear relationship is:

$$\%\text{FreqShift-Band1} = 8.92 + 284.14\frac{\text{H}}{\lambda_{\text{N}}} - 38.95\frac{\text{P}_{\text{T}}}{\lambda_{\text{N}}} - 17.62\frac{\text{S}_{\text{g}}}{\text{P}_{\text{T}}} - 0.33\varepsilon_r + 0.02\ \%\text{BandSep} \tag{7.7}$$

where λ_{N} is the upper band wavelength. Table 7.3 detail IV unstandardized coefficients.

Table 7.1 Band 1 Linear Multiple Regression - Model Summary

Model	R	R Square	Adjusted R Square	Std. Error of the Estimate
%FreqShift-Band 1	0.875	0.765	0.765	2.32

Table 7.1 presents the %FreqShift-Band1 model summary. **R Square** is 0.765, therefore, 76.5% of the variation of %FreqShift-Band1 can be explained by the proposed linear model using determined coefficients that are associated with inspected independent variable, Eq. (7.7), where ($\mathbf{R} = 0.875$) suggests high collinearity between %FreqShift-Band1 and all independent variables input to the system. Moreover, Table 7.2 ANOVA, **p value** < 0.001, suggests that %FreqShift-Band1 is well predicted by the proposed linear model including the corresponding variables of interest which all are statistically significant.

Table 7.2 Band 1 Linear Regression Model - ANOVA

Model		Sum of Squares	df	Mean Square	F	p value
%FreqShift-Band1	Regression	82454.186	5	16490.84	3063.15	< 0.001
	Residual	25351.496	4709	5.383626		
	Total	107805.682	4714			

The significant of the regression model output is next discussed by analysing the terms of the coefficients table, detailed in Table 7.3, where it can be observed that each of the independent variables possess no multicollinearity among each other since (**Tolerance** > 0.1) is in all of the variables included in the regression model. Also, all independent variable (**p value** < 0.001) suggest that there is a significant relationship between each of independent variables and outcome %FreqShift-Band1 and all included variables contribute to the better estimate of %FreqShift-Band1. Unstandardized coefficients are used to determine the required linear equation where the 95% Confidence Interval of each of the independent variables is detailed in Table 7.3. Standardized coefficients suggest that the electrical substrate thickness and electrical unit cell periodicity have the most significant importance in the model fit, which is proved in the parametric study in earlier sections. The model also suggests that increasing substrate thickness and %BandSep is expected to increase coupling which reflects on the increased %FreqShift-Band1. On the other hand, increasing electrical periodicity, interelement spacing and permittivity has the reverse effect. The model interprets well the physical concepts of dual band interdigital HIS coupling already understood from parametric analysis.

Table 7.3 Band 1 Linear Regression Model - Coefficients

	Unstandardized Coefficient		Standardized Coefficient		95% Confidence Interval of B		Collinearity Statistics
Model	B	Std. Error	Beta	p value	Lower Bound	Upper Bound	Tolerance
Intercept	8.92	0.184		< 0.001	8.55	9.28	
$\frac{H}{\lambda_N}$	284.14	3.726	0.621	< 0.001	276.83	291.44	0.752
$\frac{P_T}{\lambda_N}$	-38.95	0.672	-0.426	< 0.001	-40.27	-37.64	0.923
$\frac{S_g}{P_T}$	-17.62	0.577	-0.223	< 0.001	-18.75	-16.49	0.937
ε_r	-0.33	0.015	-0.179	< 0.001	-0.36	-0.31	0.777
%BandSep	0.02	0.001	0.177	< 0.001	0.018	0.022	0.983

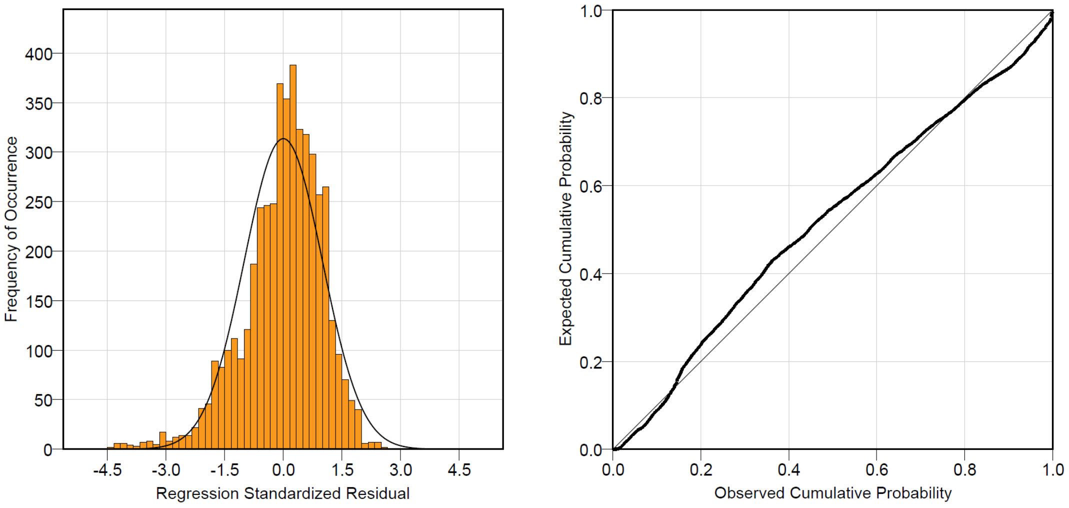

(a) Histogram (b) Normal P-P Plot

Fig. 7.3 Band 1 linear regression model standardized residuals normality diagnostics.

Investigations of normality, linearity, outliers and independence of residuals are analysed graphically. The histogram plot, Fig. 7.3a, presents standardized residuals as with respect to a number of observations which shows a reasonable normality with data skewed to the right, but the overall model is acceptable. Observed standardized residuals normality also reflects on the test for linearity of residuals illustrated by Normal P-P plot, Fig. 7.3b, which compares observed expected cumulative distribution function of standardized residuals, in Band 1 model, verses theoretical cumulative distribution function of a normal distribution. Standardized residuals are reasonably linearly distributed. The overall multiple linear regression model %FreqShift-Band1, as a function of physical parameters affecting mutual coupling in dual band interdigital HIS system, proves effective where 76.5% success is expected. The current model is further investigated for improved accuracy where data transformation is applied but still implementing multiple linear regression, which is discussed in Section 7.4.1.

7.3.2 Band 2 linear multiple regression model

Similarly, multiple linear regression is conducted to predict Percentage Frequency Shift in Band 2 (%FreqShift-Band2) based on 5 variables: substrate electrical thickness $(\frac{\mathrm{H}}{\lambda_\mathrm{N}})$, unit cell electrical periodicity $(\frac{\mathrm{P_T}}{\lambda_\mathrm{N}})$, interelement spacing to periodicity ratio $(\frac{\mathrm{S_g}}{\mathrm{P_T}})$, substrate permittivity (ε_r) and percentage band separation $(\%\mathrm{BandSep})$ to predict coupling within dual band HIS.

The outcome linear mathematical relationship is:

$$\%\text{FreqShift-Band2} = 64.33 + 2289\frac{\mathrm{H}}{\lambda_\mathrm{N}} - 482.54\frac{\mathrm{P_T}}{\lambda_\mathrm{N}} - 147.7\frac{\mathrm{S_g}}{\mathrm{P_T}} - 0.3\varepsilon_r + 0.03\%\text{BandSep} \tag{7.8}$$

where λ_N is the upper band wavelength. Table 7.6 detail IV unstandardized coefficients.

Table 7.4 Band 2 Linear Multiple Regression - Model Summary

Model	R	R Square	Adjusted R Square	Std. Error of the Estimate
%FreqShift-Band2	0.899	0.808	0.808	17.84

Table 7.5 Band 2 Linear Regression Model - ANOVA

Model		Sum of Squares	df	Mean Square	F	p-value
%FreqShift-Band2	Regression	6310205.9	5	1262041.2	3964.9	< 0.001
	Residual	1499204.3	4710	318.3		
	Total	7809410.2	4715			

A mathematically statistically significant model is determined where %FreqShift-Band2 can be estimated within 81% success due to high (**R Square** = 0.808), as detailed in Table 7.4. Also, model summary in Table 7.4. **Adjusted R Square** = 0.808, proves the analysis reliable where the model estimates is carried out effectively and strong correlation exists, **R** = 0.899. Furthermore, Table 7.5 ANOVA, suggests that the model overall has a high relationship with inputs which are statistically significant, **p value** < 0.001.

When analysing regression coefficients, in Table 7.6, it can be seen that the unstandardized coefficients (**B**) are of interest and they represent the rate of change of %FreqShift-Band2 as a function of the Independent Variables (IVs) included in the regression analysis. All independent variables are statistically significant and not correlated with one another for (**p value** < 0.001) and (**Tolerance** > 0.1) respectively. The 95% confidence coefficient interval is presented for each of independent variables included in the regression model for freedom of use where the regression model is still valid. As physically expected, coupling increases as periodicity is reduced and substrate thickness is increased where Band 2 will undergo a significant shift in resonance frequency. The regression model perfectly explains this situation, plus, included insights on other included parameters such as interelement spacing, substrate permittivity and %bandSep where it can be seen that %FreqShift-Band2 is reduced if these are increased, as detailed in Table 7.6. Standardized coefficients, as included in the regression outcome for a fair comparison of variables, suggests that the substrate thickness has a dominant effect on %FreqShift-Band2 followed by periodicity, interelement spacing, %bandSep and permittivity.

Table 7.6 Band 2 Linear Regression Model - Coefficients

Model	Unstandardized Coefficient		Standardized Coefficient	p value	95% Confidence Interval of B		Collinearity Statistics
	B	Std. Error	Beta		Lower Bound	Upper Bound	Tolerance
Intercept	64.33	1.41		< 0.001	61.55	67.1	
$\frac{H}{\lambda_N}$	2289.1	28.64	0.59	< 0.001	2232.93	2345.22	0.752
$\frac{P_T}{\lambda_N}$	-482.54	5.17	-0.62	< 0.001	-492.68	-472.41	0.923
$\frac{S_g}{P_T}$	-147.7	4.44	-0.22	< 0.001	-156.39	-139	0.937
ε_r	-0.299	0.115	-0.019	< 0.001	-0.53	-0.074	0.777
%BandSep	-0.027	0.006	-0.028	< 0.001	-0.04	-0.015	0.983

Finally, statistical plots for residuals were observed, as the result of applying multiple linear regression to predict Band 2 percentage frequency shift, are presented in Fig. 7.4. Residuals have a good normal distribution with a little skewness to the right due to some cases diverting from normality as seen in the histogram plot, as shown in Fig. 7.4a. The histogram plot also reflects on the Normal P-P plot for residuals in the regression model, which is not perfectly linear. This does not invalidate the assumption, but rather suggests room for improvement by studying the data further to improve the upper band model fit which is discussed in applying transformation techniques as will be discussed in section 7.4.2.

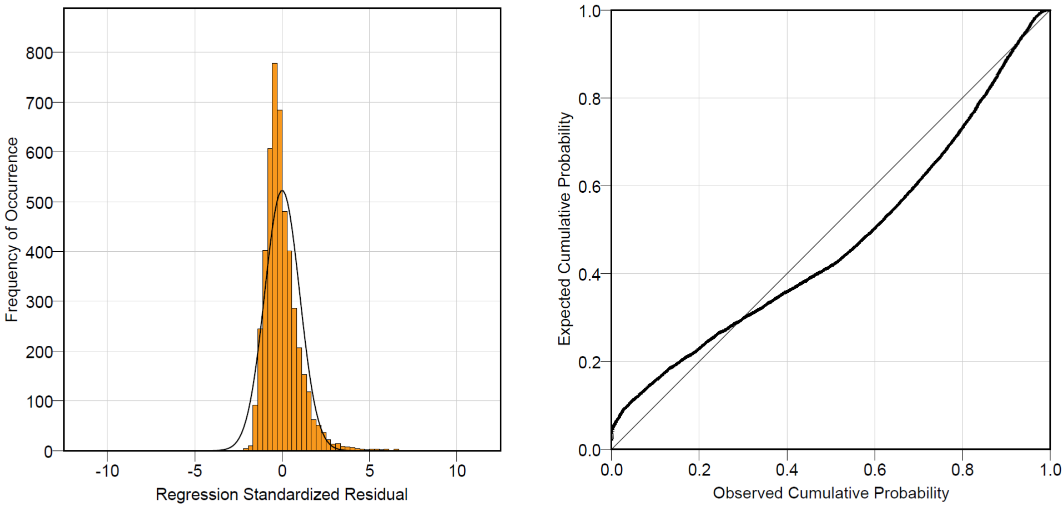

(a) Histogram

(b) Normal P-P Plot

Fig. 7.4 Band 2 linear regression model standardized residuals normality diagnostics.

7.4 Transformed Regression In Dual Band Interdigital HIS

Multiple linear regression is discussed in the previous section, where models for Band 1 and Band 2 (%FreqShift) that interprets coupling effects physically occurring in a dual band interdigital HIS are established. %FreqShift is, therefore, linearly related to each of the input variables whose associated coefficients are determined by regression analysis provided with good accuracy for each model. However, skewness in residual distributions of each band's model suggested the possibility of a non-linear relationship which requires improvement for better accuracy. This has been taken into consideration in this section by applying transformation techniques to the data such that improved linearity and model fit is achieved while the multiple linear regression technique is subsequently implemented.

7.4.1 Band 1 linear-log transformed regression model

An improved model to estimate %FreqShift-Band1 is presented in order to reduce skewness, improve normality and linearity of observed residuals as well as improve overall model fit as compared to the previously discussed linear-linear model, section 7.3.1. For these purposes, natural log transformation to independent variables electrical substrate thickness (X_1) and %bandSep (X_5) are applied. Linear-log multiple linear regression model general expression:

$$\mathrm{Y} = \mathrm{B}_0 + \mathrm{B}_1 \ln \mathrm{X}_1 + \mathrm{B}_2\mathrm{X}_2 + \mathrm{b}_3\mathrm{X}_3 + \mathrm{B}_4\mathrm{X}_4 + \mathrm{B}_5 \ln \mathrm{X}_5 + \in \tag{7.9}$$

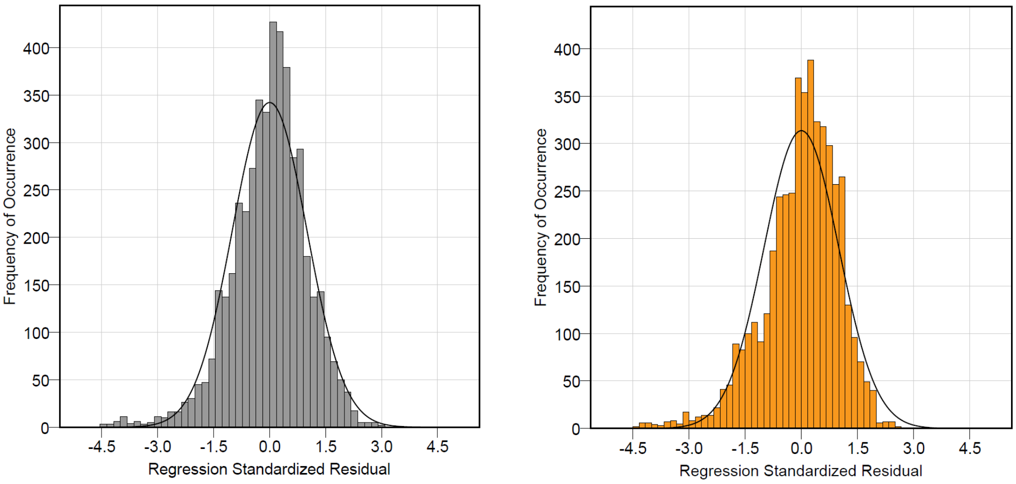

(a) linear-log Histogram (b) linear-linear Histogram

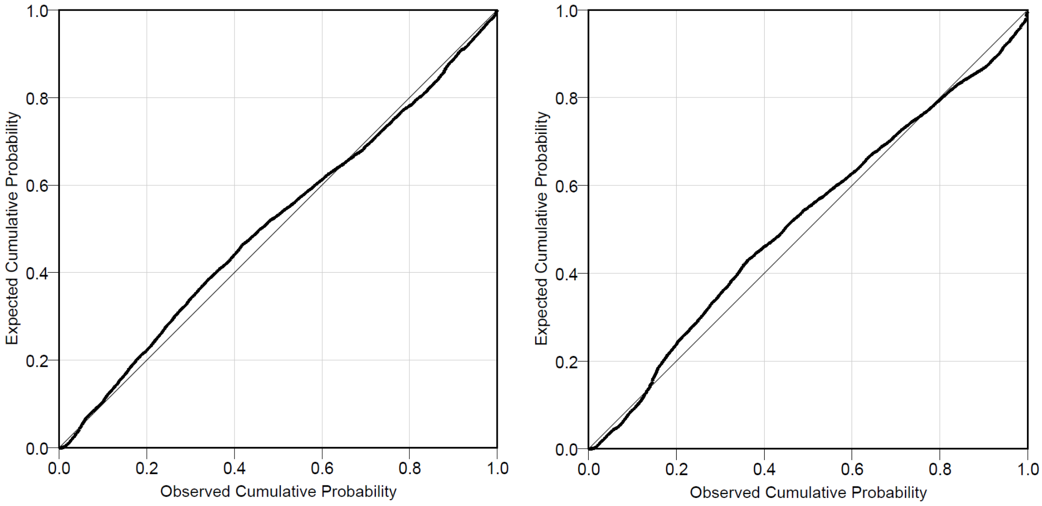

(c) linear-log Normal P-P Plot (d) linear-linear Normal P-P Plot

Fig. 7.5 Band 1 percentage frequency shift standardized residuals normality diagnostics linear-log model plots as compared to linear-linear model.

First, the estimated %FreqShift-Band1 standardized residual plots, comparing Linear-log transformed regression model to the previous linear model, in Section 7.3.1, are discussed such that the improvements in model fit and error reduction are highlighted. Comparing Fig. 7.5a and Fig. 7.5b the linear-log transformed regression model is clearly showing better normally distributed data as data of electrical substrate thickness and %BandSep data are log transformed. Also, linearity of residuals is improved which suggests a better model fit as Normal P-P plots are compared in Fig. 7.5c and Fig. 7.5d.

Output statistical tables of multiple linear regression analysed on SPSS for Band 1 linear-log transformed model are presented in Table 7.7, Table 7.8, and Table 7.9.

Table 7.7 Band 1 Linear-Log Multiple Regression - Model Summary

Model	R	R Square	Adjusted R Square	Std. Error of the Estimate
%FreqShift-Band1	0.887	0.786	0.786	2.21

Table 7.8 Band 1 Linear-Log Regression Model - ANOVA

Model		Sum of Squares	df	Mean Square	F	p value
%FreqShift-Band 1	Regression	84751.8	5	16950.4	3462.3	< 0.001
	Residual	23053.9	4709	4.9		
	Total	107805.7	4714			

Table 7.7 presents the model summary for the linear-log multiple regression output, which shows that the standard error is reduced as a consequence of improved model fit, where the residuals are normally distributed. Also, the linear-log transformed model has a higher percentage of 79% success that %FreqShift-Band1 is estimated with larger accuracy (**R Square** $=$ 0.79) , Table 7.7, as compared to the previous model of 76.5%, Table 7.1. Moreover, the transformed model is statistically significant (**p value** < 0.001) with all included independent variables of high importance as demonstrated in ANOVA, as detailed in Table 7.8.

Unstandardized multiple linear regression coefficients for the linear-log transformed model are detailed in Table 7.9. Independent variables are not correlated as expected (**Tolerance** $>$ 0.1). Each is statistically significant and contributes to the output (**p value** < 0.001). The model interprets the physical insights on coupling where variation in electrical substrate thickness and periodicity affects %FreqShift-Band 1 the most, when observing standardized coefficients. Also, a narrower 95% confidence interval is an advantage reflecting on better model fit.

Table 7.9 Band 1 Linear-Log Regression Model - Coefficients

	Unstandardized Coefficient		Standardized Coefficient		95% Confidence Interval of B		Collinearity Statistics
Model	B	Std. Error	Beta	p value	Lower Bound	Upper Bound	Tolerance
Intercept	34.01	0.438		< 0.001	33.16	34.87	
$\ln\frac{\mathrm{H}}{\lambda_\mathrm{N}}$	6.47	0.079	0.664	< 0.001	6.32	6.63	0.684
$\frac{\mathrm{P_T}}{\lambda_\mathrm{N}}$	-37.72	0.644	-0.413	< 0.001	-38.98	-36.46	0.915
$\frac{\mathrm{S_g}}{\mathrm{P_T}}$	-21.71	0.563	-0.275	< 0.001	-22.81	-20.61	0.895
ε_r	-0.24	0.015	-0.129	< 0.001	-0.269	-0.212	0.735
$\ln$ %BandSep	1.86	0.066	0.191	< 0.001	1.73	1.99	0.985

Therefore, %FreqShift-Band1 linear-log transformed model is:

$$\text{\%FreqShift-Band1} = 34 + 6.47\ln\frac{\mathrm{H}}{\lambda_\mathrm{N}} - 37.72\frac{\mathrm{P_T}}{\lambda_\mathrm{N}} - 21.71\frac{\mathrm{S_g}}{\mathrm{P_T}} - 0.24\varepsilon_r + 1.86\ln(\text{\%BandSep}) \tag{7.10}$$

where λ_N is the upper band wavelength. Table 7.9 detail IV unstandardized coefficients.

7.4.2 Band 2 log-linear transformed regression model

For the second band and upon observation of %FreqShift-Band2 proposed linear model to estimate frequency displacement due to mutual coupling, it was found that the model fit and linearity can be further improved by taking the natural log of the experimentally observed dependant variable data (%FreqShift-Band2). This has proved very effective as the second band percentage frequency shift due to coupling is very sensitive to all variables included in the model. Transformation of data has great advantage to correct any non-linearity issues between dependent and independent variable(s) where residuals divert from normality, margins of errors are larger and confidence interval is wider. An effective non-linear model is developed yet implementing multiple linear regression technique where log transformed dependent variable (%FreqShift-Band2) data is regressed over all independent variables. The general form of a log-linear transformed model is:

$$\ln(\mathrm{Y} + |\mathrm{Y}_{max(-ve)}| + 1) = \mathrm{B}_0 + \mathrm{B}_1\mathrm{X}_1 + \mathrm{B}_2\mathrm{X}_2 + \mathrm{B}_3\mathrm{X}_3 + \mathrm{B}_4\mathrm{X}_4 + \mathrm{B}_5\mathrm{X}_5 + \in \tag{7.11}$$

where $\mathrm{X_n}$ are independent variables referring to substrate electrical thickness, electrical periodicity, interelement spacing to periodicity ratio, substrate permittivity and %BandSep stated in order of $(\mathrm{n} = 1,2,3,4,5)$. And, $\mathrm{B_n}$ are coefficients associated with $\mathrm{X_n}$, which illustrates that a one unit increase in $\mathrm{X_n}$ will increase $\ln(\mathrm{Y} + |\mathrm{Y}_{max(-ve)}|+1)$ by $\mathrm{B_n}$ units.

Note that the dependant variable observed data is adjusted to account for any value that is zero or negative which invalidate the natural log calculations. Therefore, the term $(|\mathrm{Y}_{max(-ve)}|+1)$ is added to the observed dependant variable data prior to log-transformation. $(|\mathrm{Y}_{max(-ve)}|)$ is the absolute value of maximum negative data observed.

Therefore, the predicted log-linear Band 2 model in general form is:

$$\mathrm{Y} + |\mathrm{Y}_{max(-ve)}|+1 = \exp^{\mathrm{B_0+B_1X_1+B_2X_2+B_3X_3+B_4X_4+B_5X_5+\in}} \tag{7.12}$$

Results from applying the log-linear transformation ahead of multiple linear regression conducted on IBM SPSS Statistics software is discussed next. Model fit for %FreqShift-Band2 is assessed. A better estimate of %FreqShift-Band2, due to mutual coupling, is illustrated in log-linear as demonstrated in model summary, Table 7.10. **R Square** $= 0.912$, which means that the transformed model predicts the %FreqShift-Band2 with 91% chance of success as compared to 81% in the linear-linear model discussed in Table 7.4, Section 7.3.2; therefore, an improvement of 10%. ANOVA, Table 7.11, shows that the model is also statistically significant where (**p value** < 0.001) is maintained.

Table 7.10 Band 2 Log-Linear Multiple Regression - Model Summary

Model	R	R Square	Adjusted R Square	Std. Error of the Estimate
ln(%FreqShift-Band2 + 17)	0.955	0.912	0.912	0.195

Table 7.11 Band 2 Log-Linear Regression Model - ANOVA

Model		Sum of Squares	df	Mean Square	F	p value
ln(%FreqShift-Band2 + 17)	Regression	1841.2	5	368.3	9719.8	< 0.001
	Residual	178.4	4710	0.038		
	Total	2019.7	4715			

Improvement in implementing this technique is significantly obvious. Plots of standardized residuals for the log-linear model as compared to those of the linear-linear model are presented in Fig 7.6. Skewness in normality of standardized residuals is reduced for a log-linear transformed model comparing histogram plots in Fig 7.6a and Fig 7.6b. Also, Normal P-P plots of standardized residuals for log-linear and linear-linear regression models are compared against each other and shows that the residuals margin of error is reduced by applying the log-transformation to dependent variable data, as in Fig 7.6c and Fig 7.6d.

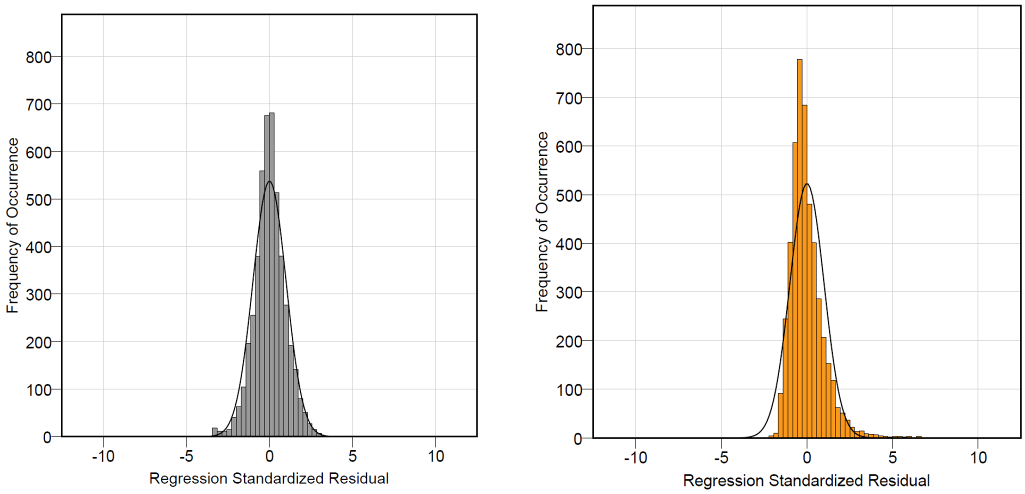

(a) log-linear Histogram (b) linear-linear Histogram

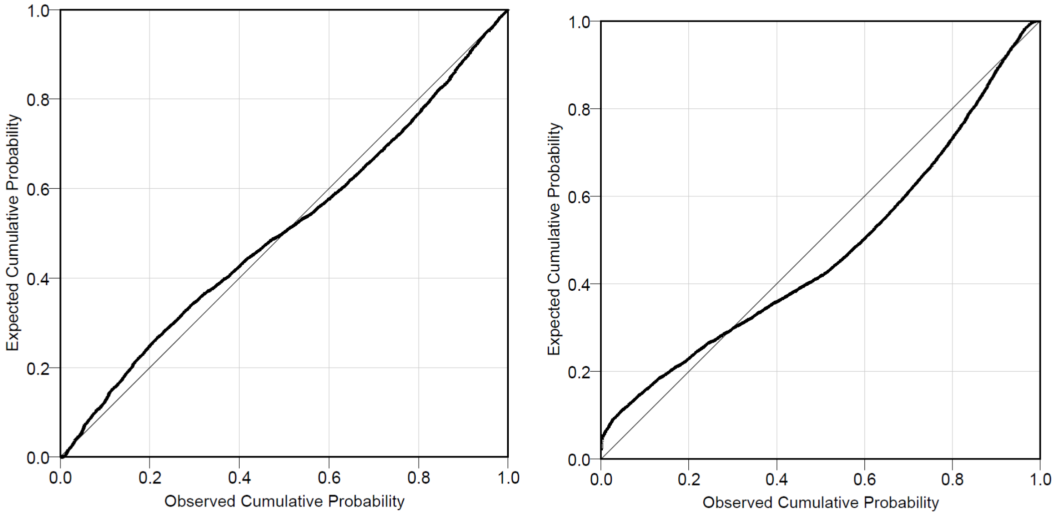

(c) log-linear Normal P-P Plot (d) linear-linear Normal P-P Plot

Fig. 7.6 Band 2 percentage frequency shift regression standardized residuals normality diagnostics log-linear model plots as compared to linear-linear model.

The most important aspects are the regression coefficients, which are essential to get the equation for model fit as detailed in Table 7.12. Input variables are independent where no multicollinearity is detected (**Tolerance** > 0.1) and they are significant to the model (**p value** < 0.001). Also The most important aspects are the regression coefficients, which are essential to get the equation for model fit as detailed in Table 7.12a 95% confidence interval range is narrower suggesting less room for error and reflecting on a better model estimate. Moreover, unstandardized coefficients demonstrates the significant effect of substrate thickness and unit cell periodicity on mutual coupling. Therefore, the model estimating percentage frequency shift in Band 2 is:

$$\%\text{FreqShift-Band2} + 17 = \exp^{4.3+35.5\frac{\mathrm{H}}{\lambda_\mathrm{N}}-8.6\frac{\mathrm{P_T}}{\lambda_\mathrm{N}}-1.5\frac{\mathrm{S_g}}{\mathrm{P_T}}-0.025\varepsilon_r+20.4\mathrm{e}^{-5}(\%\text{BandSep})} \tag{7.13}$$

Table 7.12 Band 2 Log-Linear Regression Model - Coefficients

	Unstandardized Coefficient		Standardized Coefficient		95% Confidence Interval of B		Collinearity Statistics
Model	B	Std. Error	Beta	p value	Lower Bound	Upper Bound	Tolerance
Intercept	4.31	0.015		< 0.001	4.28	4.34	
$\frac{\mathrm{H}}{\lambda_\mathrm{N}}$	35.53	0.312	0.568	< 0.001	34.91	36.14	0.752
$\frac{\mathrm{P_T}}{\lambda_\mathrm{N}}$	-8.57	0.056	-0.685	< 0.001	-8.68	-8.46	0.923
$\frac{\mathrm{S_g}}{\mathrm{P_T}}$	-1.48	0.048	-0.137	< 0.001	-1.58	-1.39	0.937
ε_r	-0.025	0.001	-0.100	< 0.001	-0.028	-0.023	0.777
%BandSep	$20.4\mathrm{e}^{-5}$	$6.8\mathrm{e}^{-5}$	0.013	0.003	$7.1\mathrm{e}^{-5}$	$33.7\mathrm{e}^{-5}$	0.983

7.5 Summary Of Design Methodology

Mutual coupling in dual band interdigital HIS design is treated analytically where models to predict percentage frequency shift in both Band 1 and Band 2 are developed based on regression analysis. These models are, therefore, very effective to estimate mutual coupling in advance for a reliable design methodology to realise miniaturised dual band interdigital HIS applicable to a generalised structure. Linear regression models provide good accuracy and simplicity where further improvement to model fit has been conducted by applying log-transformation techniques. Fig 7.7 presents a flow chart that summarizes design steps to efficiently realise a dual band interdigital high impedance surface as based on applying regression models, utilizing a simplified design approach and reduced iterative simulation steps.

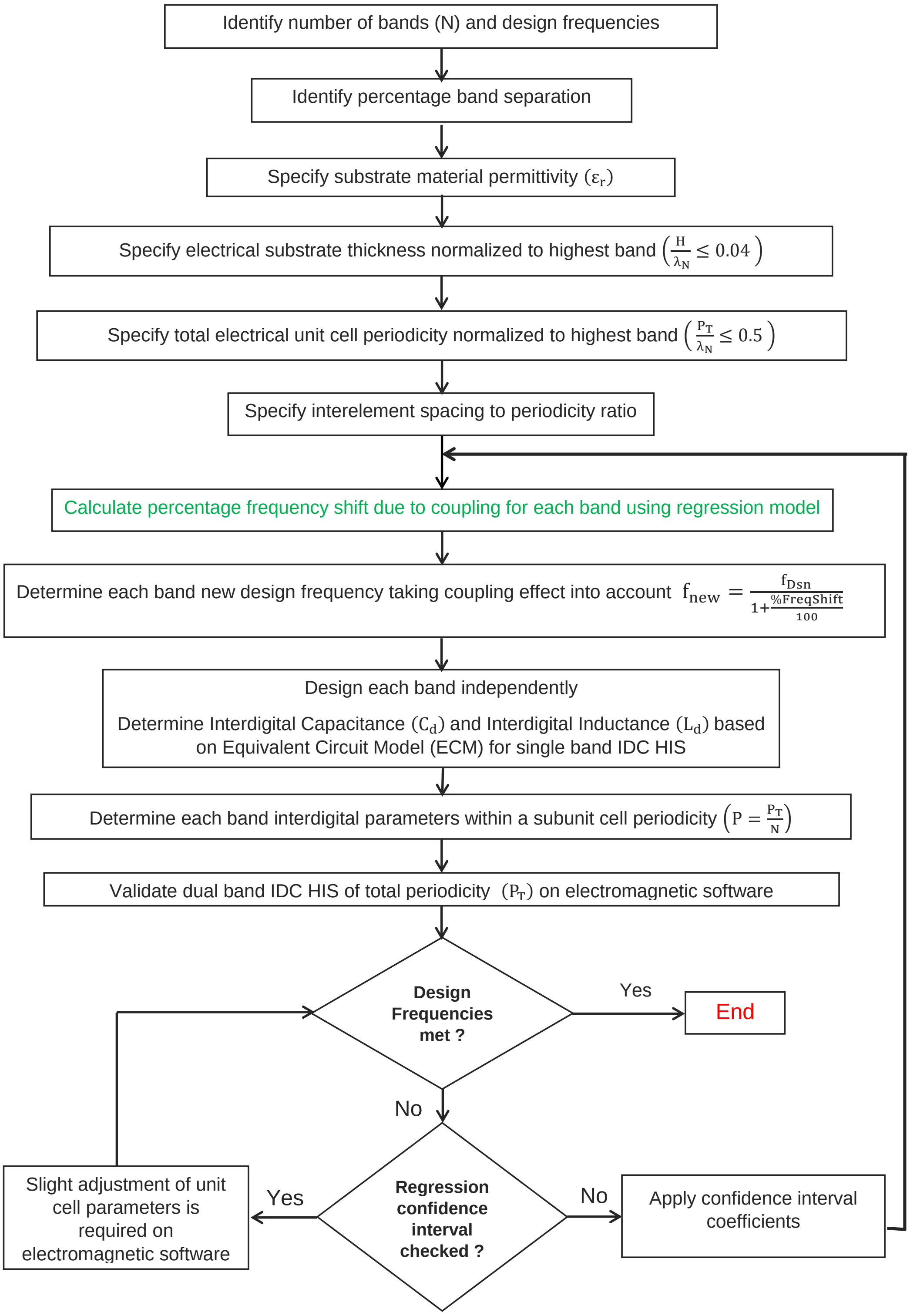

Fig. 7.7 Design procedure for miniaturised dual band interdigital HIS predicting inter unit cell mutual coupling level using multiple linear regression models.

7.6 Mutual Coupling Model Verification In Dual Band Interdigital HIS Design

Coupling models proposed for both Band 1 and Band 2 are experimentally validated in design and measurements of dual band interdigital HIS by applying design methodology that was discussed in Section 7.5. Three different designs are discussed in consequent subsections:
Design 1: miniaturised Dual Band Single Layer Single Polarized (DB-SLSP) interdigital HIS.
Design 2: miniaturised Dual Band Dual Layer Dual Polarized (DB-DLDP) interdigital HIS.
Design 3: miniaturised Dual Band Single Layer Dual Polarized (DB-SLDP) interdigital HIS.

7.6.1 Interdigital HIS Design 1 - Dual Band Single Layer Single Polarized (DB-SLSP)

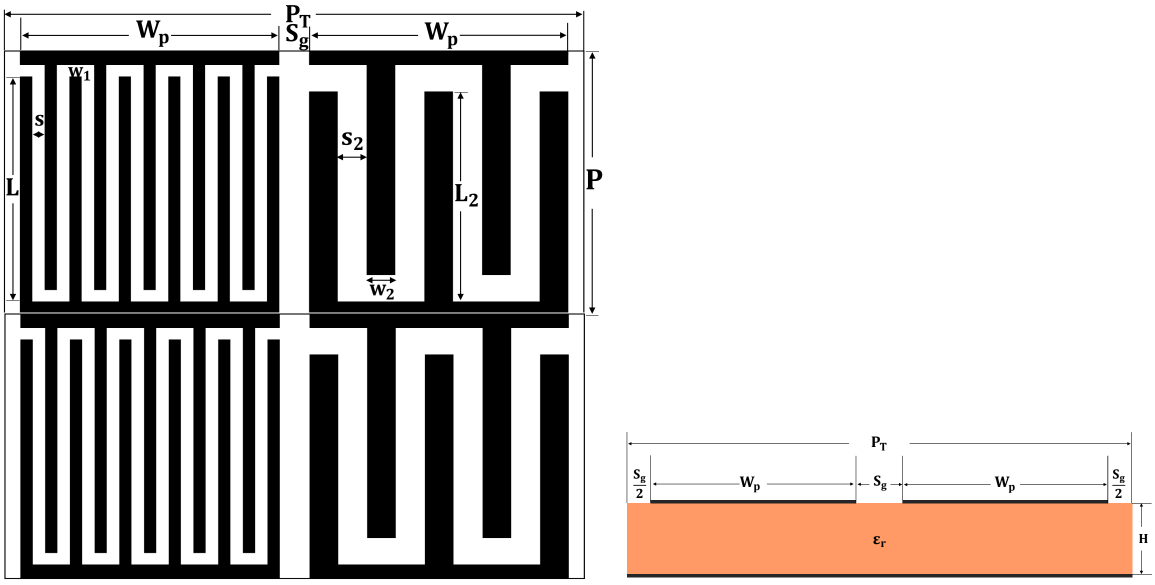

(a) Top View (b) Side View

Fig. 7.8 Miniaturised Dual Band Single Layer Single Polarized (DB-SLSP) interdigital HIS.

Dual band miniaturised interdigital HIS Design 1, shown in Fig. 7.8, feature a polarization dependent capacitive single layer structure, which is supported by a dielectric material and backed by a metal plane. The top layer, as in Fig. 7.8a, comprises of two concatenated subunit cells, loaded with unequal interdigital capacitance densities and where the design methodology is detailed in Chapter 6. Therefore, the terminology Dual Band Single Layer Single Polarized (DB-SLSP) is used. Design is based on predicting percentage frequency displacement, in each band, considering regression models developed in this chapter to verify the methodology summarized in Fig. 7.7.

Table 7.13 Design 1 Dual Band Single Layer Single Polarized (DB-SLSP) Interdigital HIS Unit Cell and Equivalent Circuit Parameters

IDC HIS Parameters	Band 1	Band 2
Substrate material	RO4003C	RO4003C
Substrate thickness $(\mathrm{H_d})$	0.4 mm	0.4 mm
Rohacell thickness $(\mathrm{H_v})$	3 mm	3 mm
Subunit cell periodicity (P)	10.8 mm	10.8 mm
Required design frequency $(\mathrm{f_{dsn}})$	1500 MHz	2500 MHz
%FreqShift dual band coupling	8%	20%
New design frequency $(\mathrm{f_{new}})$	1380 MHz	1940 MHz
Previous interdigital capacitance $(\mathrm{C_{d(dsn)}})$	2.4 pF	0.7 pF
New interdigital capacitance $(\mathrm{C_{d(new)}})$	2.8 pF	1.3 pF
Previous interdigital inductance $(\mathrm{L_{d(dsn)}})$	0.9 nH	1.9 nH
New interdigital inductance $(\mathrm{L_{d(new)}})$	0.8 nH	1.2 nH
Number of digits $(\mathrm{N_d})$	17	9
Digits gap/width (s=w)	0.32 mm	0.54 mm
Digits length (L)	8.9 mm	8.7 mm

A dual band interdigital HIS operating at 1500MHz and 2500MHz (%BandSep = 100%) is considered. The design is modelled on Rogers Substrate RO4003C ($\varepsilon_r = 3.38, \tan\delta = 0.0027$). Total electrical periodicity $0.18\lambda_\mathrm{N}$, electrical substrate thickness $0.028\lambda_\mathrm{N}$ and interelement spacing to periodicity ratio is 0.075. Applying proposed regression models, (%FreqShift-Band2 = 8%) and (%FreqShift-Band2 = 20%) in Band1 and Band2 respectively. Therefore, each subunit cell is modelled individually to operate at recalculated design frequencies of 1380MHz and 1940MHz such that mutual coupling is taken into account. Table 7.13 details unit cell design parameters as well as corresponding circuit interdigital elements comparing the previous and new calculated interdigital capacitance and inductance, based on design equations reported in Chapter 5. It can be observed that interdigital capacitance had to be increased to meet the required new design frequency especially for the high band where new capacitance is almost double what was previously required.

The HIS is fabricated as a periodic array of 10 by 10 unit cells printed on a 0.4 mm Rogers substrate PCB of total dimensions 210 mm by 210 mm, supported by a 3 mm Rohacell material and then backed by metal as shown in Fig. 7.9. Reflection phase characteristics of manufactured miniaturised dual band interdigital HIS, (DB-SLSP) Design 1, is measured at normal incidence using an NRL Arch setup within an anechoic chamber as in Fig. 7.10, calibrated with respect to a metal surface. Two horn antennas operating within bandwidth of 2-18 GHz were used and HIS board dimensions of $\lambda_{1.5\mathrm{GHz}} \times \lambda_{1.5\mathrm{GHz}}$ are adequate to avoid diffractions from edges and interference with the horn antennas beamwidth.

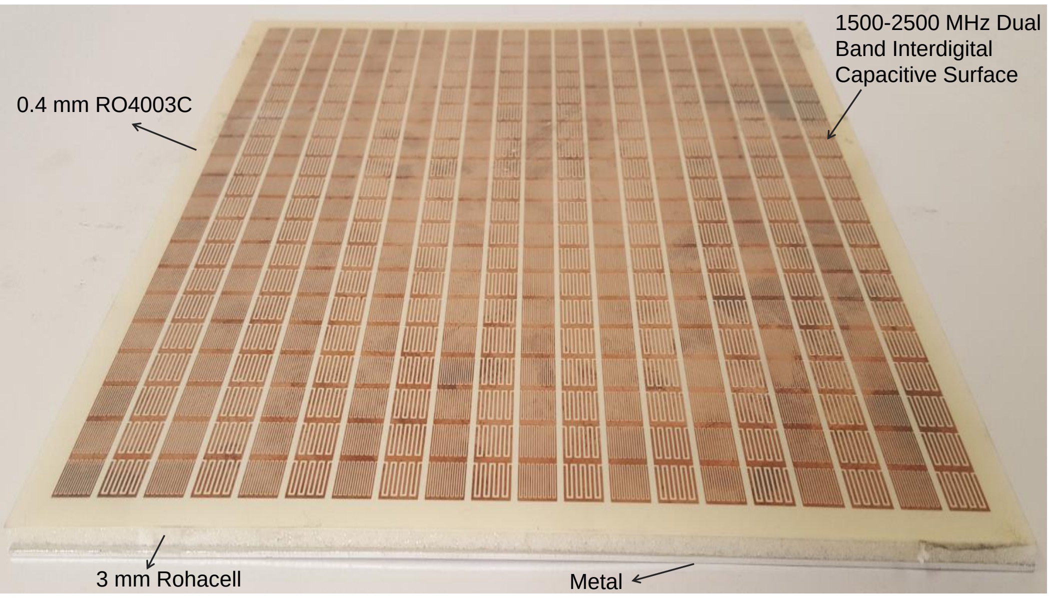

Fig. 7.9 Manufactured miniaturised interdigital dual band HIS Design 1 operating at 1500 MHz and 2500 MHz.

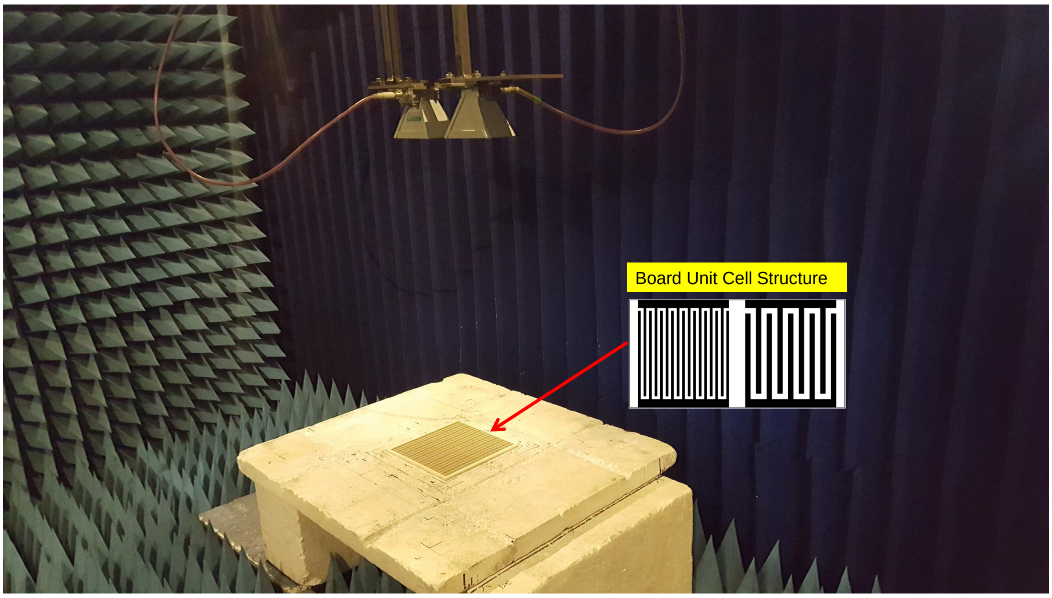

Fig. 7.10 NRL Arch normal incidence reflectivity measurement setup featuring manufactured Design 1 DB-SLSP interdigital HIS operated at 1500 MHz and 2500 MHz.

Simulated reflection coefficient of the dual band interdigital HIS is compared against reflectivity measurements where resonance frequencies shows reasonable agreement and a dual band interdigital HIS is realised at 1500MHz and 2500MHz, as in Fig. 7.11. The design proves the reliability of regression equations to predict %FreqShift in each of Band 1 and Band 2 as the result of expected mutual coupling. The first band measured and simulated ±90° bandwidth agrees to a great extent of around 9% as well as achieving design frequency requirement. However, the measured second band operating ±90° bandwidth is degraded as compared to simulated results which have predicted a fractional bandwidth of 2.5%, which explains the discrepancy in measured and simulated resonance frequency. Degradation of upper band measured bandwidth is due to system losses which was induced by manufacturing such as dielectric losses, copper losses and mismatch errors as well as inevitable mutual coupling where methods to improve upper band fractional bandwidth must be further researched.

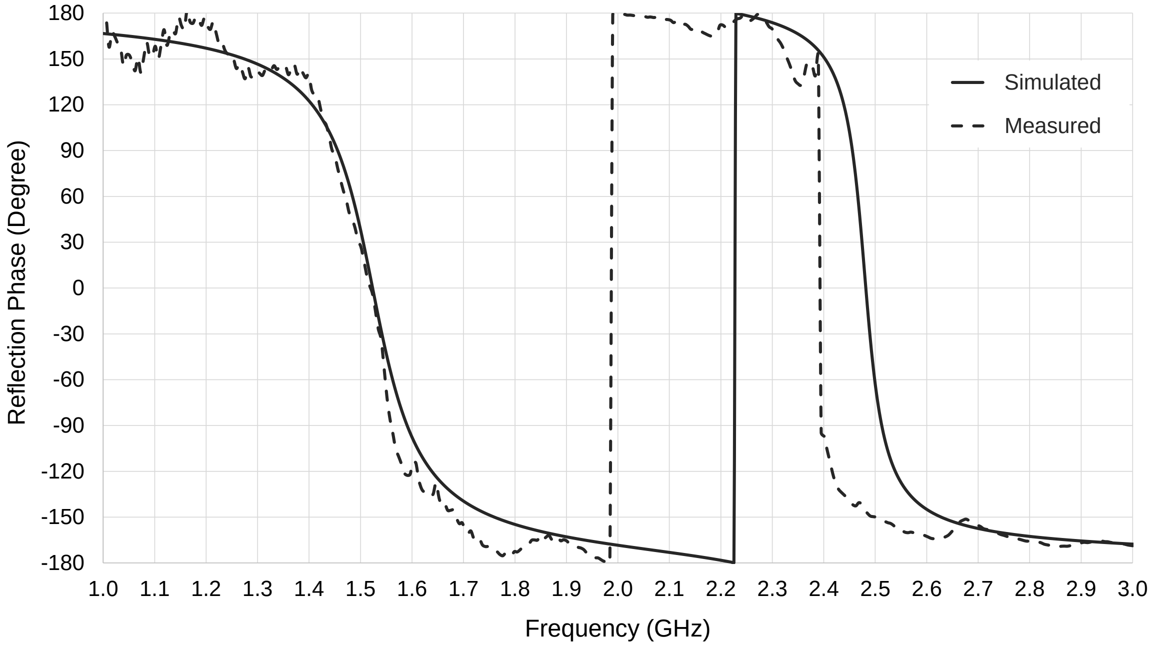

Fig. 7.11 Simulated and measured reflection phase for miniaturised DB-SLSP interdigital HIS (Design 1). Unit cell design parameters,Table 7.13.

7.6.2 Interdigital HIS Design 2 - Dual Band Dual Layer Dual Polarized (DB-DLDP)

In Section 7.6.1, a single polarized dual band interdigital HIS was characterized. An upgraded design prototype featuring a dual polarized structure is discussed in this section. Design 2; constitutes of the same unit structure as HIS Design 1; however, two identical dual band interdigital capacitive layers printed on both sides of a very thin dielectric substrate, but rotated 90° with respect to each other are considered. The two layer interdigital capacitive structure is then supported by a Rohacell material and backed by a metal surface. Therefore, a light weight miniaturised Dual Band Dual Layer Dual Polarized (DB-DLDP) interdigital HIS is realised, as shown in Fig.7.12. The top interdigital layer is excited by E_1 polarized wave and lower interdigital capacitive surface layer is excited by E_2 polarized wave.

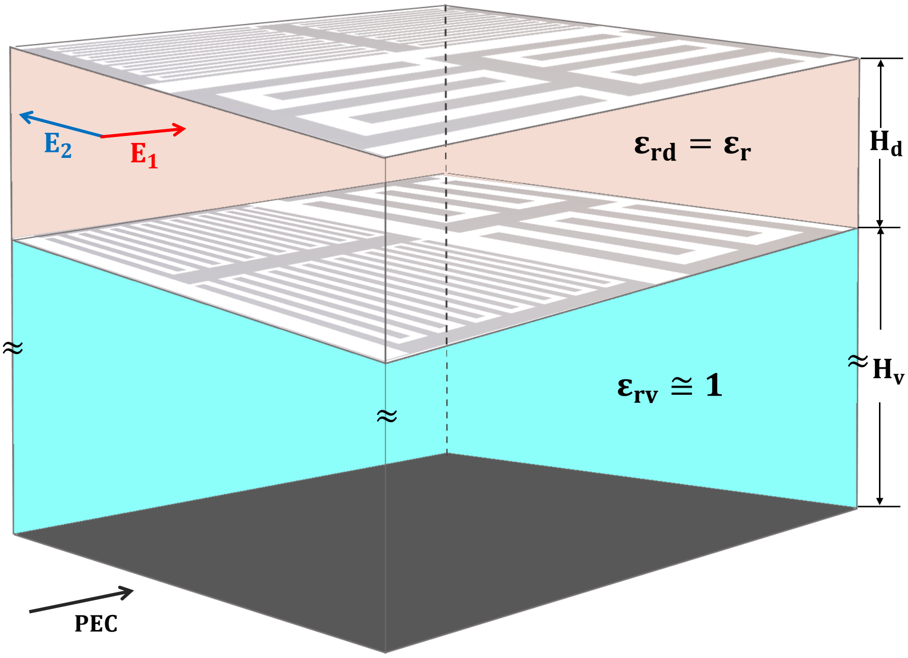

Fig. 7.12 Miniaturised interdigital HIS Design 2 - Dual Band Dual Layer Dual Polarized (DB-DLDP) 3D prospective view.

Nevertheless, closely spaced dual band interdigital layers are also mutually coupled and will interfere with inter unit cell mutual coupling expected within each layer of dual band system. Therefore, interlayer coupling and dual band inter unit cell mutual coupling are to be taken into account consecutively. Mutual coupling between subunit cell dual band structure is expected to induce an increase in resonance frequency and is determined using regression models developed for Band 1 and Band 2, which are illustrated by the quantitative term percentage frequency shift, "%FreqShift". Inter layer mutual coupling is anticipated and expected to reduce resonance frequency by a percentage frequency shift "%FreqShift(DLCplng)" which is interpolated from methodology discussed in Appendix B.

For the dual band interdigital HIS of concern, Fig. 7.12, it is believed that dual layer interaction and sustained unwanted interference will have a major effect on the high band resonance frequency but of less significance where the lower band is concerned. A miniaturised dual band dual polarized interdigital HIS, characterized by dual layer interdigital capacitive surfaces, is designed with prior information on mutual coupling between bands (regression models) as well as dual layer mutual coupling. New design resonance frequencies for Band 1 and Band 2 are defined in Eq. (7.14) and Eq. (7.15) respectively.

$$\mathrm{f_{new(Band1)}} = \frac{\mathrm{f_{dsn}}}{1+\dfrac{\%\mathrm{FreqShift\text{-}Band1}}{100}} \tag{7.14}$$

$$\mathrm{f_{new(Band2)}} = \frac{\mathrm{f_{dsn}}}{\left(1+\dfrac{\%\mathrm{FreqShift\text{-}Band2}}{100}\right)\left(1+\dfrac{\%\mathrm{FreqShift(DLCplng)}}{100}\right)} \tag{7.15}$$

Miniaturised DB-DLDP interdigital HIS Design 2 is modelled to operate at 1500 MHz and 2500 MHz and considered for the analysis, which is carried forward from dual band Design 1, Section 7.6.1, such that a comparison can be made. Having considered mutual coupling effects induced by dual band structure as well as two layer interdigital surfaces, Band 1 is designed at 1380 MHz while Band 2 is designed at 2380 MHz. Table 7.14 detail the Complete design parameters for the interdigital dual band dual layer HIS of interest.

Table 7.14 Design 2 Dual Band Dual Layer Dual Polarized (DB-DLDP) Interdigital HIS Unit Cell and Equivalent Circuit Parameters

IDC HIS Parameters	Band 1	Band 2
Substrate material	RO4003C	RO4003C
Substrate thickness (H_d)	0.4 mm	0.4 mm
Rohacell thickness (H_v)	3 mm	3 mm
Subunit cell periodicity (P)	10.8 mm	10.8 mm
Required design frequency (f_{dsn})	1500 MHz	2500 MHz
%FreqShift dual band coupling	8%	20%
%FreqShift(DLCplng)	–	-12%
New design frequency (f_{new})	1380 MHz	2380 MHz
Previous interdigital capacitance ($C_{d(dsn)}$)	2.4 pF	0.7 pF
New interdigital capacitance ($C_{d(new)}$)	2.8 pF	0.8 pF
Previous interdigital inductance ($L_{d(dsn)}$)	0.9 nH	1.9 nH
New interdigital inductance ($L_{d(new)}$)	0.8 nH	1.7 nH
Number of digits (N_d)	17	6
Digits gap/width (s=w)	0.32 mm	0.84 mm
Digits length (L)	8.9 mm	8.3 mm

The HIS, which is miniaturized at a periodicity of $0.18\lambda_{2.5\mathrm{GHz}}$ is modelled on 0.4 mm Rogers substrate material $(\varepsilon_r = 3.38, \tan\delta = 0.0027)$ and 3 mm Rohacell material equivalent to a total substrate electrical thickness of $0.028\lambda_{2.5\mathrm{GHz}}$. Fig. 7.13 presents CST Microwave Studio full wave simulations for the normal incidence reflection phase properties of the dual band dual layer HIS, which is observed at both E_1 and E_2 polarizations. For the lower band, of 1500 MHz, the E_1 polarization resonance frequency is slightly offset with respect to the E_2 polarization; while in the upper band, of 2500 MHz, both E_1 and E_2 polarizaions agree at the same resonance frequency, as shown in Fig. 7.13, and which is attributed to the sensitivity of the lower band to interlayer coupling. Band 1 and Band 2 fractional bandwidh is 8.5% and 2.5% respectively.

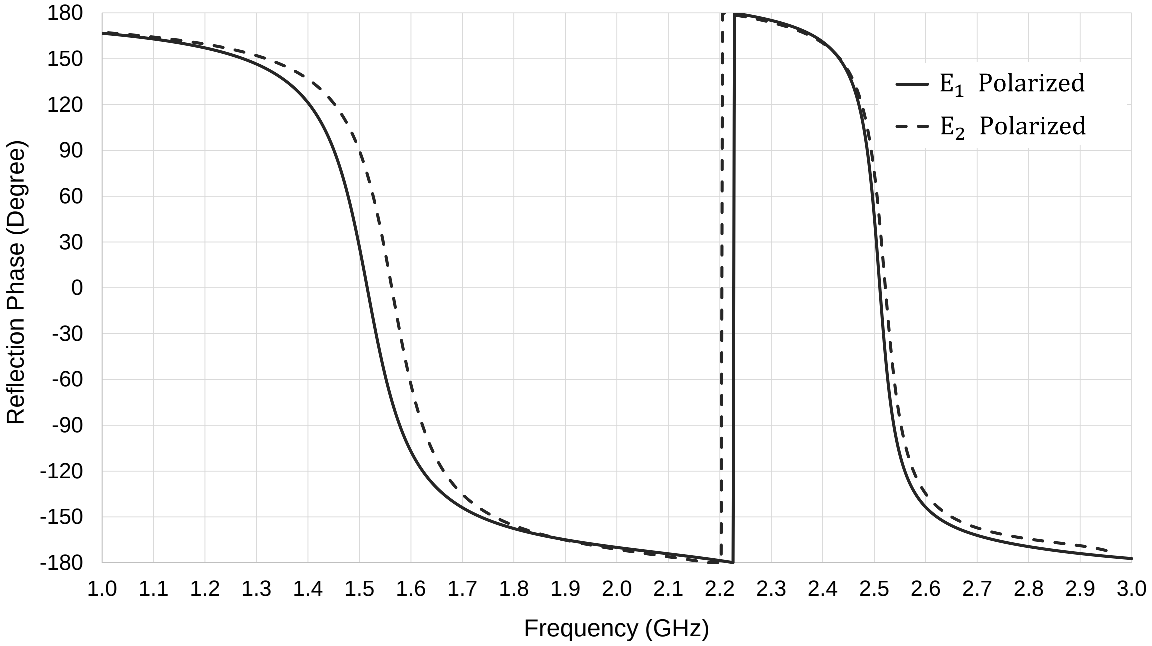

Fig. 7.13 Simulated reflection phase for miniaturised Dual Band Dual Layer Dual Polarized (DB-DLDP) interdigital HIS (Design 2). Unit cell parameters, Table 7.14.

7.6.3 Interdigital HIS Design 3 - Dual Band Single Layer Dual Polarized (DB-SLDP)

A novel dual band dual polarized miniaturised interdigital HIS top view model is presented in Fig 7.14. The design features a single layer interdigital capacitive surface supported by a dielectric material and backed by a metal plate such that a HIS is realised. As in the top view model, Fig 7.14, the unit cell comprises of square periodicity (P_T) within which four subunit cells are arranged, each of subunit cell periodicity (P). For dual band performance, two interdigital capacitance densities are engineered such that interdigital capacitance (C_{d1}) contributes to Band 1 resonance, while (C_{d2}) for resonance in Band 2. Each band is required to be individually designed and optimized incorporating the equivalent circuit model and applying design methodology of the single band dual polarized interdigital HIS (Design 3) detailed in Chapter 5. Nevertheless, inter unit cell mutual coupling must be taken into consideration for the proposed design technique to be successful. Both bands design resonance frequencies are expected to encounter a frequency shift due to mutual coupling. Consequently, regression models established earlier are implemented to determine coupling effects as illustrated by quantities %FreqShift-Band1 and %FreqShift-Band2 corresponding to Band 1 and Band 2 respectively. Therefore, the corresponding subunit cell in each band is individually designed at recalculated new design resonance frequencies and distributed to operated by E_1 and E_2 polarized waves.

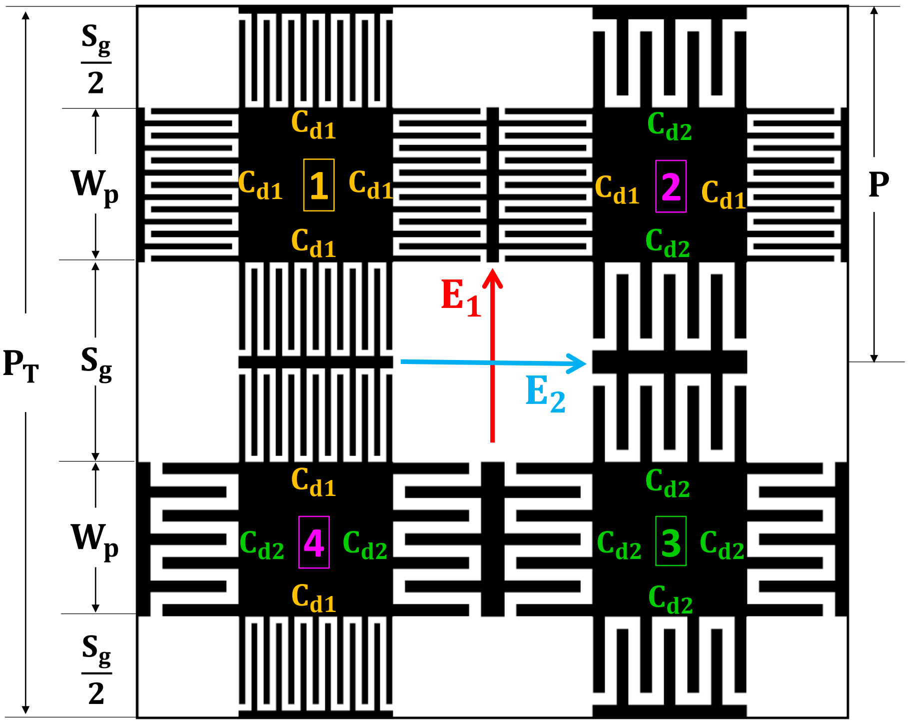

Fig. 7.14 Miniaturised interdigital HIS Design 3 - Dual Band Single Layer Dual Polarized (DB-SLDP) top view model.

Design concepts are verified in the following case study. A dual band interdigital HIS is designed to operate at 1000 MHz and 1500 MHz, therefore, a percentage band separation of 50%. Unit cell total electrical periodicity $0.13\lambda_N$ and interelement spacing to periodicity ratio $(\frac{S_g}{P_T} = 0.25)$ is considered. Light weight HIS substrate is comprised of 0.8 mm FR4 $(\varepsilon_r = 4.3, \tan\delta = 0.025)$ and 5.5 mm Rohacell material, therefore, an equivalent electrical thickness of $0.032\lambda_N$. Proposed regression coupling models to calculate frequency shift in Band 1 and Band 2 are implemented. As mutual coupling is concerned, Band 1 frequency is expected to increase by 5% while Band 2 undergoes an increase of 30% in frequency. Therefore, new design frequencies for Band 1 and Band 2 are 955 MHz and 1050 MHz respectively. Based on the equivalent circuit model approach, required interdigital capacitance in each band is calculated as well as associated unit cell physical dimensions to meet design requirements. Table 7.15 summarizes the design parameters with the final required interdigital number of digits and digits width /gap such that the HIS resonates at 1000 MHz and 1500 MHz. Where mutual coupling is predicted and taken into consideration for a dual band dual polarized performance, an increase in both band's interdigital capacitance density was required.

Table 7.15 Design 3 Dual Band Single Layer Dual Polarized (DB-SLDP) Interdigital HIS Unit Cell and Equivalent Circuit Parameters

IDC HIS Parameters	Band 1	Band 2
Substrate material	FR4	FR4
Substrate thickness (H_d)	0.8 mm	0.8 mm
Rohacell thickness (H_v)	5.5 mm	5.5 mm
Subunit cell periodicity (P)	13 mm	13 mm
Required design frequency (f_{dsn})	1000 MHz	1500 MHz
%FreqShift dual band coupling	5%	30%
New design frequency (f_{new})	955 MHz	1050 MHz
Design interdigital capacitance $(C_{d(dsn)})$	5 pF	2.2 pF
New interdigital capacitance $(C_{d(new)})$	5.5 pF	3.8 pF
Design total interdigital inductance $(L_{d1(dsn)} + L_{d2(dsn)})$	2 nH	2 nH
New total interdigital inductance $(L_{d1(new)} + L_{d2(new)})$	2 nH	2 nH
Number of digits (N_d)	72	49
Digits gap/width $(s{=}w)$	0.045 mm	0.067 mm
Digits length (L)	3.2 mm	3.2 mm

Dual band dual polarized interdigital HIS Design 3 is modelled on CST Microwave Studio such that reflection phase characteristics are validated numerically through simulations as observed at normal incidence in both E_1 and E_2 polarizations. Simulated reflection phase plots are presented in Fig 7.15 which prove credibility of the proposed approach where design resonance frequencies of 1000 MHz and 1500 MHz are achieved with good accuracy. Operating ±90° bandwidth for Band 1 and Band 2 are 9.5% and 2% respectively. Dual band dual polarized HIS Design 3 provides more robust dual polarization as compared with dual band dual polarized interdigital HIS Design 2 based on dual layer technique for the later reflection phase characteristics strongly agree in both polarizations.

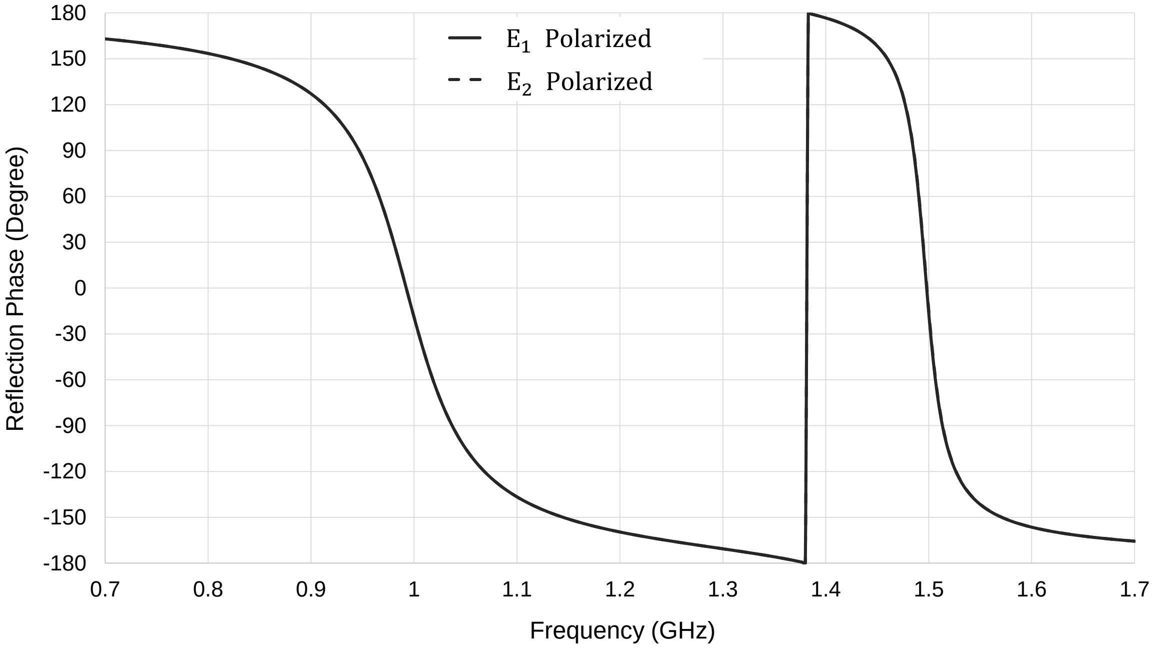

Fig. 7.15 Simulated reflection phase for miniaturised Dual Band Single Layer Dual Polarized (DB-SLDP) interdigital HIS (Design 3). Unit cell parameters, Table 7.15.

7.7 Conclusion

In this chapter, a mathematical solution to dual band mutual coupling has been proposed. With the aim to maintain a simplified design methodology, a dual band interdigital HIS has been realised by concatenating two single band subunit cells each individually designed. However, this method is governed by inter unit cell mutual coupling and is a major constraint where a simplified design technique would not be possible unless side effects of mutual coupling are taken into consideration in advance. Inter unit cell mutual coupling will cause an undesired frequency shift in both bands and is a function of HIS unit cell parameters which induce both capacitive and inductive coupling effects. Unit cell parameters of interest in order of significance are: substrate thickness, unit cell periodicity, interelement spacing, permittivity and percentage band separation.

In order to generalise the methodology, a comprehensive study of unit cell parameters that affect dual band HIS mutual coupling has been conducted where percentage frequency shift in each band was recorded. Data collected for this study was then implemented into a regression model. A multiple linear regression analysis technique has been considered in this study, being a very robust method that enables to predict a given response from one or more input(s). Being able to calculate the effects of inter unit cell mutual coupling renders the design methodology straight forward. Therefore, while physical constraints and limitations concerning HIS design are considered, it has been possible to efficiently design dual band miniaturised interdigital HIS using the method summarized in Fig 7.7.

Furthermore, while multiple linear regression analysis is a highly reputed statistical technique errors are inevitable and model prediction can fail if the design limits are violated. Initially, multiple linear regression had been used on collected data to realise linear-linear models that predict %FreqShift-Band1 and %FreqShift-Band2 respectively, therefore, it predicted 76.5% and 81% success to accurately estimate percentage displacement in Band 1 and Band 2 respectively. However, normal distribution plots also suggested that there is some non-linearity in the data which has been improved by applying transformation techniques. Therefore, logarithmic transformation to observed data was implemented and provided better accuracy in the regression model fit. Where Band 1 is concerned, log transformation has been applied to input variables data (electrical substrate thickness and %BandSep) and %FreqShift-Band1 model fit was improved to 79%, also reflecting on normal distribution plots. On the other hand, where Band 2 is concerned, log transformation to output variable data has been applied improving the model fit to 91% success in predicting %FreqShift-Band2.

In the last part of this chapter, the multiple linear regression technique implemented to model the effects of mutual coupling in a miniaturised dual band interdigital HIS has been validated in three original high impedance surfaces prototypes.

First, is the proposed miniaturised interdigital HIS Design 1 which is a Dual Band Single Layer Single Polarized (DB-SLSP) structure. The surface constitutes of a capacitive interdigital layer printed on a thin dielectric, supported by Rohacell and backed by metal. The mutual coupling level has been estimated and resonance frequencies of Band 1 and Band 2 were recalculated using the corresponding multiple linear regression models. Miniaturised HIS has been validated numerically and experimentally through measurements showing good agreement in realising design frequencies. However, degradation of upper band bandwidth in measurements was significant and is required to be investigated further and requires improvement.

Subsequently, miniaturised interdigital HIS Design 2 has been proposed next. Characterized as a Dual Band Dual Layer Dual Polarized (DB-DLDP) structure; the interdigital HIS is an upgraded version of dual band interdigital HIS Design 1 for two identical layers incorporated closely spaced and orthogonal to each other to feature dual polarization. Dual band interdigital capacitive layers, separated by a very thin dielectric, are then supported by Rohacell and backed by metal. Therefore, miniaturised light weight compact HIS has been achieved. Inter unit cell mutual coupling as well as interlayer mutual coupling has been taken into consideration as part of the design process. A case study has been considered and validated through numerical analysis for a DB-DLDP interdigital HIS operating at 1500 MHz and 2500 MHz. Detailed design steps provided high accuracy and reliability of regression models developed and methodology implemented.

Finally, reliability of mutual coupling models developed by regression technique has been further assessed as a novel dual band interdigital HIS design that has been proposed. Miniaturised interdigital HIS Design 3 features a Dual Band Single Layer Dual Polarized (DB-SLDP) structure designed with prior knowledge to expected percentage frequency shift in both Band 1 and Band 2. Interdigital structure has been engineered such that a dual polarized dual band single layer capacitive surface is printed on a thin dielectric material supported by a Rohacell layer and backed by metal. Numerical simulation analysis provided excellent reflection phase characteristics results meeting resonance frequency design requirements and acceptable fractional bandwidth.

Chapter 8

Conclusion And Future Work

8.1 Research Project Conclusions

This research project has investigated miniaturisation techniques to realise dual band high impedance surfaces. Dual band has been achieved by concatenation of individually designed subunit cell HIS structures such that the design process is straightforward. The methodology incorporated in miniaturisation has been focused on increasing effective sheet capacitance of the capacitive HIS FSS-based layer which was accomplished by either implementing surface mount lumped capacitor loading or by engineering interdigital capacitors within the HIS unit cell. Each approach has its design challenges and limitations which has been successfully dealt with within the thesis. Inter unit cell mutual coupling was a consequential issue and occupied remarkable attention throughout the thesis leading to a novel technique to effectively encounter mutual coupling. Nevertheless, within all the thesis chapters the project objective in realising a miniaturised dual band HIS unit cell of periodicity less than one tenth of the wavelength is generally achieved. Achievements, critiques and project limitations, where each technical chapter is concerned, are summarized below.

In Chapter 3, a miniaturised dual band high impedance surface within a unit cell periodicity of 0.03λ and total electrical thickness of 0.01λ has been realised by incorporating two different surface mount capacitors loaded within adjacent subunit cells. Excessively reduced unit cell size and mutual coupling restricted the fractional bandwidth to 2.4% and 0.6% in Band 1 (430 MHz) and Band 2 (900 MHz) respectively. This chapter provided comprehensive analysis and conclusions on inter unit cell mutual coupling being significant enough to limit tuning capability of each band whose resonance frequency is desired to be merely determined by the choice of lumped capacitor, also, limiting the fractional bandwidth.

In Chapter 4, a technical robust solution to inter unit cell mutual coupling has been proposed while utilizing surface mount capacitor loading as the desired miniaturisation technique. By implementing guard conductors around each miniaturised HIS subunit cell band isolation was possible for each band to be mechanically tuned by the sole variation of loaded capacitor value. Analytical investigation as well as an empirical circuit model has been proposed to explain the structure's mechanism. Parametric analysis conducted suggests that a thick conductor width is preferable for effective band isolation. A miniaturised dual band gridded lumped capacitor loaded HIS has been presented operating at 430 MHz and 900 MHz as modelled on 0.09λ periodicity, and total electrical thickness of 0.02λ realising a fractional bandwidth of 1.4% and 2.2% in lower and upper bands respectively. Moreover, lumped capacitor resistive losses has been highlighted to increase system losses and possess design limitation degrading the fractional bandwidth. This has been demonstrated in a practical design case study for a planar monopole antenna integrated with miniaturised dual band gridded lumped capacitor loaded HIS. A low profile antenna/HIS system was possible; however, gain was hindered by component and system losses.

To overcome lumped capacitor resistive losses and realise improved fractional bandwidth while maintaining miniaturisation, lumped capacitors were replaced by interdigital capacitors. Nevertheless, design of interdigital structures were governed by the choice of geometrical properties such as number of digits, digits length, digits width and gap for the required effective capacitance to be fulfilled and HIS resonance frequency realised. Therefore, it was expected that HIS unit cell periodicity and substrate properties were to have significant influence on the design process. In order to avoid time consuming, non methodological and inefficient multiple iterations governed by numerical simulations that are required to tune unit cell interdigital HIS parameters for design reflection phase requirements, a robust technique has been developed in this research study allowing effective and efficient characterization of miniaturised interdigital high impedance surfaces. Methodology started by considering a single band interdigital HIS structure. Thereafter, to maintain an uncomplicated design process, a dual band interdigital HIS system is generated from two individually designed single band structures. The design process is extended through a novel approach to manage inter unit cell mutual coupling and offer comprehensive design strategy to realise miniaturised dual band interdigital HIS has also been discussed.

Therefore subsequent technical chapters on interdigital HIS design were concluded as:

Chapter 5, design of miniaturised single band interdigital HIS has been analytically discussed based on an equivalent circuit model approach presenting an original design methodology especially in modelling interdigital inductance. This method has been proven very efficient to determine interdigital HIS unit cell parameters that realise design frequency with least simulation time effort. To model and optimize the interdigital capacitor effectively within a given HIS unit cell periodicity, design parameters that are involved have been discussed and addressed where a comprehensive parametric study has been conducted. Therefore, optimum miniaturised single band interdigital HIS within a unit cell periodicity of 0.03λ, total electrical thickness 0.03λ and a generous fractional bandwidth of 20% was demonstrated. The later structure was polarization dependent and comprises the basic interdigital HIS denoted as Single Band Single Layer Single Polarized (SB-SLSP) interdigital HIS Design 1. Furthermore, the work has been extended to integrate single band interdigital HIS Design 1 for dual polarization. A Single Band Dual Layer Dual Polarized (SB-DLDP) interdigital HIS Design 2 has been discussed operating at 900 MHz as modelled on a unit cell periodicity of 0.037λ and total electrical thickness 0.02λ where a fractional bandwidth of 15% was realised. Finally, a novel Single Band Single Layer Dual Polarized (SB-SLDP) interdigital HIS Design 3 has been proposed associated with a robust equivalent circuit model and original design equations. Design 3 was optimized within periodicity of 0.13λ and total electrical thickness 0.03λ operating at 1.5 GHz, and a fractional bandwidth of 15%. Single band interdigital HIS Design 1 and Design 3 have been verified experimentally performing as a ground plane for an ultra wideband monopole antenna. A low profile platform tolerant antenna/HIS system has been realised for the antenna gain to improve by an average of 4 dB as single band interdigital HIS Design 1 and Design 3 are concerned.

In Chapter 6, miniaturised dual band interdigital HIS has been discussed. In order to sustain a simple straightforward design process which does not rely on simulation iterations, dual band interdigital HIS was realised by combining two single band miniaturised interdigital HIS subunit cells, individually optimized according to the methodology discussed in Chapter 5. Nevertheless, the design was notably limited by inter unit cell mutual coupling resulting in displacing resonance frequencies, in both bands, from design requirements. A process to reverse engineer the design has been addressed, but, it necessitated prior knowledge of expected resonance frequency shift as a result to inter unit cell mutual coupling. Therefore, a 900 MHz and 1800 MHz dual band case study was analysed as realised on a 0.15λ periodicity and 0.046λ total electrical thickness where a 13.4% and 2% $\pm 90^\circ$ bandwidth was observed in lower and upper bands respectively, and proved the technique reliable. However, a generalised solution was required otherwise the design method renders inefficient. For these purposes a comprehensive detailed parametric study has been conducted, within this chapter, such that design parameters and factors that induce inter unit cell mutual coupling are assessed. Therefore, it was concluded that mutual coupling is of an inductive and capacitive nature and very much related to unit cell parameters, band separation and design specification.

Consequently, in Chapter 7, a generalised solution to predict percentage frequency displacement induced by inter unit cell mutual coupling has been developed. Having defined the unit cell parameters and factors that contributed to mutual coupling, multiple linear regression analysis has been implemented proposing a mathematical model to estimate percentage frequency shift in each of the lower and upper bands. Observed from a statistical point of view, optimized percentage frequency shift regression models for improved model fit were discussed as transformation techniques were applied, which have improved accuracy and reliability of the analysis. Three novel dual band miniaturised interdigital HIS design prototypes were considered to validate regression mathematical models, define and consolidate proposed simplified design methodology and discuss polarization dependency in HIS along with miniaturisation level and fractional bandwidth. Dual Band Single Layer Single Polarized (DB-SLSP) miniaturised interdigital HIS Design 1 was first discussed as modelled and measured to operate at 1.5 GHz and 2.5 GHz within a periodicity of 0.18λ, and total electrical thickness 0.028λ realising a fractional bandwidth of 9.4% and 3% in lower and upper bands respectively. Design frequencies were realised; however, degradation in measured upper band bandwidth was observed. Then, Dual Band Dual Layer Dual Polarized (DB-DLDP) miniaturised interdigital HIS Design 2 was discussed where regression models proved great accuracy in realising resonance frequencies for the design modelled at 1.5 GHz and 2.5 GHz within a periodicity of 0.18λ, and total electrical thickness 0.028λ realising a fractional bandwidth of 8.5% and 2.5% in lower and upper bands respectively. Finally, the proposed Design 3 Dual Band Single Layer Dual Polarized (DB-SLDP) miniaturised interdigital HIS. The structure has been designed analytically implementing equivalent circuit model and regression models which proved very reliable as a case study was considered. Design 3 modelled at 1 GHz and 1.5 GHz within a unit cell periodicity of 0.13λ and total electrical thickness of 0.031λ, has been numerically analysed realising a fractional bandwidth of 9.5% and 2% in lower and upper bands respectively.

In conclusion, this work enables a miniaturized dual band high impedance surface to be realised, which can be achieved by incorporating lumped capacitor loading or interdigital capacitances. This technique can be used with the constraints of taking mutual coupling into account and will be useful in many applications, where a dual band HIS is implemented to realise low profile antenna systems.

8.2 Future Work

This thesis has investigated miniaturisation of dual band high impedance surfaces utilizing two different miniaturisation techniques exemplified by incorporating lumped capacitor loading and using interdigital capacitors, both significantly increase the HIS effective surface capacitance. Each miniaturisation method had its design challenges and limitations and considerable attention on inter unit cell mutual coupling occupied major part of the work within the thesis. Methods proposed were successful to meet the requirements of miniaturisation, uncomplicated design process and managing mutual coupling where several HIS prototypes have been discussed, all observed at normal incidence. Nevertheless, additional work is required for HIS design improvement which is expected to be under particular research attention for many years to come. Therefore, recommended future work would include:

- Work presented within the thesis has only investigated high impedance surface reflection phase properties as observed at normal incidence. Therefore, it will be of great benefit to examine the stability of each design prototype with respect to the different angle of incidences.

- High impedance surface design and validation throughout the thesis has considered applications as related to observing the surface reflection phase characteristics, therefore, realised as an artificial magnetic conductor. It is very important to consider research on bandgap properties of design prototypes addressed. Therefore, looking into dispersion diagrams, where more than one band is concerned, for the surface operating as an electromagnetic bandgap structure.

- Exploring options to upgrade high impedance surface design into a multiband system would be another challange. It has been shown that it would be possible to realise triple band high impedance surface in gridded lumped capacitor loaded design. This structure has the potential to upgrade into a quad band for example. Also, dual band interdigital high impedance surface discussing the effectiveness of the regression models to realise a multiband miniaturised structure should be investigated.

- Throughout the thesis, passive high impedance surface designs have been discussed. Considering work on upgrading designs to be actively tunable would be of great advantage. For example, lumped capacitors can be replaced by varactor diodes and options to tune interdigital capacitors is to be investigated. This would give the surface great potential of design flexibility.

- Non-periodic, high impedance surface is a topic increasing in popularity. Therefore, exploring this option into proposed high impedance surface designs is recommended.

- Finally, degradation in HIS operational bandwidth was observed especially in the upper band in both lumped component loaded and interdigital HIS designs where this is attributed to mutual coupling and system losses. Therefore, further research into factors that contribute to increasing high impedance surface fractional bandwidth is required. Suggestions would include reducing losses in the system by opting for a lossless substrate, overcome conductor losses, lumped component losses and increasing inductance effect of the structure aiming for increased bandwidth.

References

[1] George Gabriel Stokes. I. On a remarkable phenomenon of crystalline reflection. *Proceedings of the Royal Society of London*, 38(235-238):174–185, 1885.

[2] Lord Rayleigh. On the remarkable phenomenon of crystalline reflexion described by Prof. Stokes. *The London, Edinburgh, and Dublin Philosophical Magazine and Journal of Science*, 26(160):256–265, 1888.

[3] D Sievenpiper, Zhang Lijun, R F J Broas, N G Alexopolous, and E Yablonovitch. High-impedance electromagnetic surfaces with a forbidden frequency band. *Microwave Theory and Techniques, IEEE Transactions on*, 47(11):2059–2074, 1999.

[4] F Hopkinson and David Rittenhouse. An Optical Problem, Proposed by Mr. Hopkinson, and Solved by Mr. Rittenhouse. *Transactions of the American Philosophical Society*, 2:201–206, 1786.

[5] Jagadis Chunder Bose. On Polarisation of Electric Rays by Double Refracting Crystals. *Journal of the Asiatic Society of Bengal*, 64(2):146–152, 1895.

[6] Jagadis Chunder Bose. On the Rotation of Plane of Polarisation of Electric Waves by a Twisted Structure. *Proceedings of the Royal Society of London*, 63:146–152, 1898.

[7] V Veselago. The electrodynamics of substances with simultaneosly negative values of epsilon and mue. *Soviet Phsics Uspekhi*, 10(4):509–514, 1968.

[8] J B Pendry, A J Holden, D J Robbins, and W J Stewart. Low frequency plasmons in thin-wire structures. *Journal of Physics: Condensed Matter*, 10(22):4785–4809, 1998.

[9] J B Pendry, A J Holden, W J Stewart, and I Youngs. Extremely Low Frequency Plasmons in Metallic Mesostructures. *Physical Review Letters*, 76(25):4773–4776, 1996.

[10] J B Pendry, A J Holden, D J Robbins, and W J Stewart. Magnetism from conductors and enhanced nonlinear phenomena. *Microwave Theory and Techniques, IEEE Transactions on*, 47(11):2075–2084, 1999.

[11] D C Vier D. R. Smith N. Kroll, and S. Schultz. Direct calculation of permeability and permittivity for a left-handed metamaterial. *Applied Physics Letters*, 77(14):2246–2248, 2000.

[12] Willie J Padilla D. R. Smith D. C. Vier, S. C. Nemat-Nasser, and S. Schultz. Composite Medium with Simultaneously Negative Permeability and Permittivity. *Phys. Rev. Lett.*, 84(18):4184–4187, 2000.

[13] J B Pendry. Negative Refraction Makes a Perfect Lens. *Physical Review Letters*, 85(18):3966–3969, 2000.

[14] K Buell, H Mosallaei, and K Sarabandi. A substrate for small patch antennas providing tunable miniaturization factors. *IEEE Transactions on Microwave Theory and Techniques*, 54(1):135–146, 2006.

[15] D Schurig, J J Mock, B J Justice, S A Cummer, J B Pendry, A F Starr, and D R Smith. Metamaterial Electromagnetic Cloak at Microwave Frequencies. *Science*, 314(5801):977, 2006.

[16] X Wang, F Chen, and E Semouchkina. Implementation of Low Scattering Microwave Cloaking by All-Dielectric Metamaterials. *IEEE Microwave and Wireless Components Letters*, 23(2):63–65, 2013.

[17] J Li, Q Zeng, R Liu, and T A Denidni. Beam-Tilting Antenna With Negative Refractive Index Metamaterial Loading. *IEEE Antennas and Wireless Propagation Letters*, 16:2030–2033, 2017.

[18] Eli Yablonovitch. Inhibited Spontaneous Emission in Solid-State Physics and Electronics. *Physical Review Letters*, 58(20):2059–2062, 1987.

[19] E Yablonovitch and T J Gmitter. Photonic band structure: The face-centered-cubic case. *Physical Review Letters*, 63(18):1950–1953, 1989.

[20] Sajeev John. Strong localization of photons in certain disordered dielectric superlattices. *Physical Review Letters*, 58(23):2486–2489, 1987.

[21] E Yablonovitch, T J Gmitter, and K M Leung. Photonic band structure: The face-centered-cubic case employing nonspherical atoms. *Physical Review Letters*, 67(17):2295–2298, 1991.

[22] E Özbay, A Abeyta, G Tuttle, M Tringides, R Biswas, C T Chan, C M Soukoulis, and K M Ho. Measurement of a three-dimensional photonic band gap in a crystal structure made of dielectric rods. *Physical Review B*, 50(3):1945–1948, 1994.

[23] C T Chan, K M Ho, and C M Soukoulis. Photonic Band Gaps in Experimentally Realizable Periodic Dielectric Structures. *EUROPHYSICS LETTERS*, 16(6):563–568, 1991.

[24] D F Sievenpiper, M E Sickmiller, and E Yablonovitch. 3D Wire Mesh Photonic Crystals. *Physical Review Letters*, 76(14):2480–2483, 1996.

[25] N. Engheta and R. W. Ziolkowski. *Metamaterials: Physics and Engineering Explorations*. Wiley-Blackwell, 2006.

[26] Christophe Caloz and Tatsuo Itoh. *Electromagnetic Metamaterials: Transmission Line Theory and Microwave Applications*. Wiley-IEEE Press, 2005.

[27] Guglielmo Marconi and Charles Samuel Franklin. Reflector for use in wireless telegraphy and telephony, 1919.

[28] G G Macfarlane. Quasi-stationary field theory and its application to diaphragms and junctions in transmission lines and wave guides. *Electrical Engineers - Part IIIA: Radiolocation, Journal of the Institution of*, 93(4):703–719, 1946.

[29] H G Booker. Slot aerials and their relation to complementary wire aerials (Babinet's principle). *Electrical Engineers - Part IIIA: Radiolocation, Journal of the Institution of*, 93(4):620–626, 1946.

[30] R Ulrich. Far-infrared properties of metallic mesh and its complementary structure. *Infrared Physics*, 7(1):37–55, 1967.

[31] Shung-Wu Lee, G Zarrillo, and Chak-Lam Law. Simple formulas for transmission through periodic metal grids or plates. *Antennas and Propagation, IEEE Transactions on*, 30(5):904–909, 1982.

[32] T K WU. *Frequency Selective Surface and Grid Array*. John Wiley & Sons, Inc., 1995.

[33] Ben A Munk. *Frequency Selective Surfaces: Theory and Design*. Wiley-Blackwell, 2000.

[34] Herbert Goldstein. *Cavity resonators and wave guides containing periodic elements*. PhD thesis, Massachusetts Institute of Technology, 1943.

[35] A L Cullen. The excitation of plane surface waves. *Proceedings of the IEE - Part IV: Institution Monographs*, 101(7):225–234, 1954.

[36] W Rotman. A Study of Single-Surface Corrugated Guides. *Proceedings of the IRE*, 39(8):952–959, 1951.

[37] F Yang and Y Rahmat-Samii. *Electromagnetic Band Gap Structures in Antenna Engineering*. Cambridge University Press, 2009.

[38] C Chang and Y Qian. Analysis and applications of uniplanar compact photonic bandgap structures. *Progress In Electromagnetics Research, PIER*, 41:211–235, 2003.

[39] S Clavijo, R E Diaz, and W E McKinzie III. Design methodology for Sievenpiper high-impedance surfaces: an artificial magnetic conductor for positive gain electrically small antennas. *Antennas and Propagation, IEEE Transactions on*, 51(10):2678–2690, 2003.

[40] M Wilhelm, R Taylor, K Church, and D Werner. Meta-materials concepts in high-frequency applications. In *The 2002 45th Midwest Symposium on Circuits and Systems, 2002. MWSCAS-2002.*, volume 2, pages II–II, 2002.

[41] R Gonzalo, P De Maagt, and M Sorolla. Enhanced patch-antenna performance by suppressing surface waves using photonic-bandgap substrates. *Microwave Theory and Techniques, IEEE Transactions on*, 47(11):2131–2138, 1999.

[42] R Coccioli, Yang Fei-Ran, Ma Kuang-Ping, and T Itoh. Aperture-coupled patch antenna on UC-PBG substrate. *Microwave Theory and Techniques, IEEE Transactions on*, 47(11):2123–2130, 1999.

[43] R Abhari and G V Eleftheriades. Metallo-dielectric electromagnetic bandgap structures for suppression and isolation of the parallel-plate noise in high-speed circuits. *Microwave Theory and Techniques, IEEE Transactions on*, 51(6):1629–1639, 2003.

[44] C Ning, J Jin, K Yang, H Xie, D W Wang, Y Liao, L D Wang, H S Chen, E P Li, and W Yin. A Novel Electromagnetic Bandgap Power Plane Etched With Multiring CSRRs for Suppressing Simultaneous Switching Noise. *IEEE Transactions on Electromagnetic Compatibility*, 60(3):733–737, 2018.

[45] D Rano and M S Hashmi. A New Miniaturized Slot-loaded EBG Cell for Cancelling Surface Waves in PCBs. In *2018 IEEE Asia-Pacific Conference on Antennas and Propagation (APCAP)*, pages 349–350, 2018.

[46] B Mohamadzade and M Afsahi. Mutual coupling reduction and gain enhancement in patch array antenna using a planar compact electromagnetic bandgap structure. *IET Microwaves, Antennas & Propagation*, 11(12):1719–1725, 2017.

[47] F Yang and Y Rahmat-Samii. Microstrip antennas integrated with electromagnetic band-gap (EBG) structures: a low mutual coupling design for array applications. *Antennas and Propagation, IEEE Transactions on*, 51(10):2936–2946, 2003.

[48] Y Fan, J Huang, T Chang, and X Liu. A Miniaturized Four-Element MIMO Antenna With EBG for Implantable Medical Devices. *IEEE Journal of Electromagnetics, RF and Microwaves in Medicine and Biology*, 2(4):226–233, 2018.

[49] G Goussetis, A P Feresidis, and J C Vardaxoglou. Tailoring the AMC and EBG characteristics of periodic metallic arrays printed on grounded dielectric substrate. *Antennas and Propagation, IEEE Transactions on*, 54(1):82–89, 2006.

[50] H Ouassal, J Shaker, L Roy, K Hettak, and R E Amaya. A Novel Multifunctional EBG-Based Coupled-Line-Defect Directional Coupler Based on Layered Dielectric Substrates. *IEEE Transactions on Components, Packaging and Manufacturing Technology*, 8(12):2140–2151, 2018.

[51] Yang Li, Fan Mingyan, Chen Fanglu, She Jingzhao, and Feng Zhenghe. A novel compact electromagnetic-bandgap (EBG) structure and its applications for microwave circuits. *Microwave Theory and Techniques, IEEE Transactions on*, 53(1):183–190, 2005.

[52] Zheng Qiu-Rong, Fu Yun-Qi, and Yuan Nai-Chang. A Novel Compact Spiral Electromagnetic Band-Gap (EBG) Structure. *Antennas and Propagation, IEEE Transactions on*, 56(6):1656–1660, 2008.

[53] F Costa, O Luukkonen, C R Simovski, A Monorchio, S A Tretyakov, and P M de Maagt. TE Surface Wave Resonances on High-Impedance Surface Based Antennas: Analysis and Modeling. *Antennas and Propagation, IEEE Transactions on*, 59(10):3588–3596, 2011.

[54] Zhang Ying, J von Hagen, M Younis, C Fischer, and W Wiesbeck. Planar artificial magnetic conductors and patch antennas. *Antennas and Propagation, IEEE Transactions on*, 51(10):2704–2712, 2003.

[55] C R Simovski, P de Maagt, and I V Melchakova. High-impedance surfaces having stable resonance with respect to polarization and incidence angle. *Antennas and Propagation, IEEE Transactions on*, 53(3):908–914, 2005.

[56] A Bellion and M Cable. A new wideband and compact High Impedance Surface. In *Antenna Technology and Applied Electromagnetics (ANTEM), 2012 15th International Symposium on*, pages 1–5, 2012.

[57] A Foroozesh and L Shafai. Investigation Into the Application of Artificial Magnetic Conductors to Bandwidth Broadening, Gain Enhancement and Beam Shaping of Low Profile and Conventional Monopole Antennas. *Ieee Transactions on Antennas and Propagation*, 59(1):4–20, 2011.

[58] M Hosseinipanah and Q Wu. Equivalent Circuit Model for Designing of Jerusalem Cross-Based Artificial Magnetic Conductors. *Radioengineering*, 2009.

[59] J Li, H Huo, J Chen, S Zhu, H Shi, and A Zhang. Miniaturised artificial magnetic conductor and its application in unidirectional circularly polarised slot antenna design. *IET Microwaves, Antennas & Propagation*, 12(12):1885–1889, 2018.

[60] Z Chen, K Solbach, D Erni, and A Rennings. Improving B1 Efficiency and Signal-to-Noise-Ratio of a Surface Coil by a High-Impedance-Surface RF Shield for 7-T Magnetic Resonance Imaging. *IEEE Transactions on Microwave Theory and Techniques*, 65(3):988–997, 2017.

[61] I Issa, K L Ford, M Rao, and J Wild. Enhancement of radio frequency magnetic field for a 1.5 T magnetic resonance system using a high impedance surface. *IET Microwaves, Antennas & Propagation*, 10(13):1378–1383, 2016.

[62] H R Raad, A I Abbosh, H M Al-Rizzo, and D G Rucker. Flexible and Compact AMC Based Antenna for Telemedicine Applications. *Ieee Transactions on Antennas and Propagation*, 61(2):524–531, 2013.

[63] A Y Modi, C A Balanis, C R Birtcher, and H N Shaman. Novel Design of Ultrabroadband Radar Cross Section Reduction Surfaces Using Artificial Magnetic Conductors. *Ieee Transactions on Antennas and Propagation*, 65(10):5406–5417, 2017.

[64] F Costa and A Monorchio. Multiband electromagnetic wave absorber based on reactive impedance ground planes. *Microwaves, Antennas & Propagation, IET*, 4(11):1720–1727, 2010.

[65] F Costa, A Monorchio, and G Manara. Analysis and Design of Ultra Thin Electromagnetic Absorbers Comprising Resistively Loaded High Impedance Surfaces. *Antennas and Propagation, IEEE Transactions on*, 58(5):1551–1558, 2010.

[66] M Yoo and S Lim. Polarization-Independent and Ultrawideband Metamaterial Absorber Using a Hexagonal Artificial Impedance Surface and a Resistor-Capacitor Layer. *Ieee Transactions on Antennas and Propagation*, 62(5):2652–2658, 2014.

[67] B Munk, R Kouyoumjian, and L Peters Jr. Reflection properties of periodic surfaces of loaded dipoles. *Antennas and Propagation, IEEE Transactions on*, 19(5):612–617, 1971.

[68] F Yang and Y Rahmat-Samii. Reflection phase characterizations of the EBG ground plane for low profile wire antenna applications. *Antennas and Propagation, IEEE Transactions on*, 51(10):2691–2703, 2003.

[69] Y Toyota, A E Engin, Kim Tae Hong, M Swaminathan, and S Bhattacharya. Size reduction of electromagnetic bandgap (EBG) structures with new geometries and materials. In *Electronic Components and Technology Conference, 2006. Proceedings. 56th*, page 6 pp., 2006.

[70] L Yousefi, B Mohajer-Iravani, and O M Ramahi. Enhanced Bandwidth Artificial Magnetic Ground Plane for Low-Profile Antennas. *Antennas and Wireless Propagation Letters, IEEE*, 6:289–292, 2007.

[71] S Tse, B Sanz Izquierdo, J C Batchelor, and R J Langley. Reduced sized cells for electromagnetic bandgap structures. In *Metamaterials for Microwave and (Sub) Millimetre Wave Applications: Photonic Bandgap and Double Negative Designs, Components and Experiments, 2003. IEE Seminar on*, pages 8/1–8/8, 2003.

[72] E A Parker and A N A El Sheikh. Convoluted dipole array elements. *Electronics Letters*, 27(4):322–323, 1991.

[73] E Rajo-Iglesias, L Inclan-Sanchez, J L Vazquez-Roy, and E Garcia-Munoz. Size Reduction of Mushroom-Type EBG Surfaces by Using Edge-Located Vias. *IEEE Microwave and Wireless Components Letters*, 17(9):670–672, 2007.

[74] R B Waterhouse and D Novak. A Small Electromagnetic Bandgap Structure. In *Microwave Symposium Digest, 2006. IEEE MTT-S International*, pages 602–605, 2006.

[75] M Hosseinipanah and Q Wu. Miniaturised high-impedance surface with high angular stability of resonant frequency. *Electronics Letters*, 45(24):1204–1206, 2009.

[76] H Oraizi and R Tirandaz. Design of a novel miniaturized planar structure for the realization of artificial magnetic conductors. In *2015 23rd Iranian Conference on Electrical Engineering*, pages 489–492, 2015.

[77] J C Vardaxoglou, G Gousetis, and A P Feresidis. Miniaturisation schemes for metallodielectric electromagnetic bandgap structures. *Microwaves, Antennas & Propagation, IET*, 1(1):234–239, 2007.

[78] F Grange, C Delaveaud, and K Madhjoubi. Miniaturization of artificial magnetic conductors. In *Antennas and Propagation Society International Symposium (APSURSI), 2010 IEEE*, pages 1–4, 2010.

[79] C Mias. Frequency selective surfaces loaded with surface-mount reactive components. *Electronics Letters*, 39(9):724–726, 2003.

[80] Xu Rong Rong, Zhao Huai Cheng, Zong Zhi Yuan, and Wu Wen. Loaded frequency selective surfaces using substrate integrated waveguide technology. In *Microwave and Millimeter Wave Technology, 2008. ICMMT 2008. International Conference on*, volume 4, pages 2051–2054, 2008.

[81] H Liu, K L Ford, and R J Langley. Design Methodology for a Miniaturized Frequency Selective Surface Using Lumped Reactive Components. *Antennas and Propagation, IEEE Transactions on*, 57(9):2732–2738, 2009.

[82] H Liu, K L Ford, and R J Langley. Miniaturised artificial magnetic conductor design using lumped reactive components. *Electronics Letters*, 45(6):294–295, 2009.

[83] G D Alley. Interdigital Capacitors and Their Application to Lumped-Element Microwave Integrated Circuits. *Microwave Theory and Techniques, IEEE Transactions on*, 18(12):1028–1033, 1970.

[84] S Rogers, W McKinzie, and G Mendolia. AMCs comprised of interdigital capacitor FSS layers enable lower cost applications. In *IEEE Antennas and Propagation Society International Symposium. Digest. Held in conjunction with: USNC/CNC/URSI North American Radio Sci. Meeting (Cat. No.03CH37450)*, volume 2, pages 411–414 vol.2, 2003.

[85] Y Fu, N Yuan, and G Zhang. Compact high-impedance surfaces incorporated with interdigital structure. *Electronics Letters*, 40(5):310–311, 2004.

[86] R C Hadarig, M E de Cos, and F Las-Heras. Novel Miniaturized Artificial Magnetic Conductor. *Antennas and Wireless Propagation Letters, IEEE*, 12:174–177, 2013.

[87] B Lin, X Cao, Y Yang, and X Wen. Compact high-impedance surfaces integrated with rhombic interdigital structure. *Electronics Letters*, 43(20):1100–1101, 2007.

[88] Bao-Qin Lin and Xi Wen. A novel uniplanar compact EBG incorporated with interdigital structure. *Microwave and Optical Technology Letters*, 50(3):555–557, 2008.

[89] S Sheikh. Miniaturized-Element Frequency-Selective Surfaces Based on the Transparent Element to a Specific Polarization. *IEEE Antennas and Wireless Propagation Letters*, 15:1661–1664, 2016.

[90] D Rano and M Hashmi. Interdigital based EBG: Compact and polarization stable for MBAN and Wi-Fi. In *12th European Conference on Antennas and Propagation (EuCAP 2018)*, pages 1–5, 2018.

[91] J H Yoon, Y J Yoon, W Lee, and J So. Miniaturised artificial magnetic conductors with wide split ring resonators and interdigital structures. *Electronics Letters*, 48(22):1411–1412, 2012.

[92] A Presse, X Zhang, M Mantash, A C Tarot, and J M Floc'h. Miniaturization of an artificial magnetic conductor with interdigital capacitances. In *2015 Loughborough Antennas & Propagation Conference (LAPC)*, pages 1–4, 2015.

[93] L Lanuzza, A Monorchio, D J Kern, and D H Werner. A robust GA-FSS technique for the synthesis of optimal multiband AMCs with angular stability. In *Antennas and Propagation Society International Symposium, 2003. IEEE*, volume 2, pages 419–422 vol.2, 2003.

[94] D J Kern, D H Werner, and P L Werner. Optimization of multi-band AMC surfaces with magnetic loading. In *IEEE Antennas and Propagation Society Symposium, 2004.*, volume 1, pages 823–826 Vol.1, 2004.

[95] D J Kern, D H Werner, A Monorchio, L Lanuzza, and M J Wilhelm. The design synthesis of multiband artificial magnetic conductors using high impedance frequency selective surfaces. *Antennas and Propagation, IEEE Transactions on*, 53(1):8–17, 2005.

[96] W McKinzie and S Rogers. A multi-band artificial magnetic conductor comprised of multiple FSS layers. In *Antennas and Propagation Society International Symposium, 2003. IEEE*, volume 2, pages 423–426 vol.2, 2003.

[97] J H Yoon, Kim Eun Young, Lim Yohan, and Y J Yoon. Equivalent circuit model and reflection phase control methods for dual-band AMC. In *Proceedings of the 5th European Conference on Antennas and Propagation (EUCAP)*, pages 1222–1226, 2011.

[98] R J Langley and E A Parker. Double-square frequency-selective surfaces and their equivalent circuit. *Electronics Letters*, 19(17):675–677, 1983.

[99] Wu Te-Kao. Four-band frequency selective surface with double-square-loop patch elements. *Antennas and Propagation, IEEE Transactions on*, 42(12):1659–1663, 1994.

[100] C K Lee and R J Langley. Equivalent-circuit models for frequency-selective surfaces at oblique angles of incidence. *Microwaves, Antennas and Propagation, IEE Proceedings H*, 132(6):395–399, 1985.

[101] Wu Te-Kao and Lee Shung-Wu. Multiband frequency selective surface with multiring patch elements. *Antennas and Propagation, IEEE Transactions on*, 42(11):1484–1490, 1994.

[102] S Zhu and R Langley. Dual-Band Wearable Textile Antenna on an EBG Substrate. *Antennas and Propagation, IEEE Transactions on*, 57(4):926–935, 2009.

[103] A Ahmad, F Faisal, S Khan, S Ullah, and U Ali. Performance analysis of a wearable and dual band planar antenna using a mushroom-like electromagentic bandgap (EBG) ground plane. In *2015 International Conference on Open Source Systems & Technologies (ICOSST)*, pages 24–29, 2015.

[104] R A Hill and B A Munk. The effect of perturbating a frequency-selective surface and its relation to the design of a dual-band surface. *Antennas and Propagation, IEEE Transactions on*, 44(3):368–374, 1996.

[105] A P Feresidis, A Chauraya, G Goussetis, J C Vardaxoglou, and P DeMaagt. Multiband artificial magnetic conductor surfaces. In *Metamaterials for Microwave and (Sub) Millimetre Wave Applications: Photonic Bandgap and Double Negative Designs, Components and Experiments, 2003. IEE Seminar on*, pages 2/1–2/6, 2003.

[106] M A Hiranandani, A B Yakovlev, and A A Kishk. Artificial magnetic conductors realised by frequency-selective surfaces on a grounded dielectric slab for antenna applications. *Microwaves, Antennas and Propagation, IEE Proceedings -*, 153(5):487–493, 2006.

[107] G Goussetis and A P Feresidis. Perturbed frequency selective surfaces for multiband high impedance surfaces. *Microwaves, Antennas & Propagation, IET*, 4(8):1105–1110, 2010.

[108] C Yang and L Chen. A dual-band antenna integrated with EBG structure. In *2016 5th International Symposium on Next-Generation Electronics (ISNE)*, pages 1–2, 2016.

[109] O Folayan and R J Langley. Wideband reduced size electromagnetic bandgap structure. *Electronics Letters*, 41(20):1099–1100, 2005.

[110] O Folayan and R Langley. Dual frequency band antenna combined with a high impedance band gap surface. *Microwaves, Antennas & Propagation, IET*, 3(7):1118–1126, 2009.

[111] N Chahat, M Zhadobov, R Sauleau, and K Mahdjoubi. Improvement of the on-body performance of a dual-band textile antenna using an EBG structure. In *2010 Loughborough Antennas & Propagation Conference*, pages 465–468, 2010.

[112] M E de Cos, Y Alvarez, and F Las-Heras. Novel Broadband Artificial Magnetic Conductor With Hexagonal Unit Cell. *Antennas and Wireless Propagation Letters, IEEE*, 10:615–618, 2011.

[113] W Chen, C A Balanis, and C R Birtcher. Dual Wide-Band Checkerboard Surfaces for Radar Cross Section Reduction. *Ieee Transactions on Antennas and Propagation*, 64(9):4133–4138, 2016.

[114] A Ghosh, V Kumar, G Sen, and S Das. Gain enhancement of triple-band patch antenna by using triple-band artificial magnetic conductor. *IET Microwaves, Antennas & Propagation*, 12(8):1400–1406, 2018.

[115] X Chen, L Li, C H Liang, Z J Su, and C Zhu. Dual-Band High Impedance Surface With Mushroom-Type Cells Loaded by Symmetric Meandered Slots. *Ieee Transactions on Antennas and Propagation*, 60(10):4677–4687, 2012.

[116] K Zhang, X Zhou, Z Wei, and H Zhai. A low-profile dual-band antenna loaded with the AMC surface. In *2017 Sixth Asia-Pacific Conference on Antennas and Propagation (APCAP)*, pages 1–3, 2017.

[117] S Ghosh and K V Srivastava. An Equivalent Circuit Model of FSS-Based Metamaterial Absorber Using Coupled Line Theory. *IEEE Antennas and Wireless Propagation Letters*, 14:511–514, 2015.

[118] R Garg and I J Bahl. Characteristics of Coupled Microstriplines. *IEEE Transactions on Microwave Theory and Techniques*, 27(7):700–705, 1979.

[119] Michael Hiebel. *Fundementals of Vector Network Analysis*. Rohde and Schwarz GmbH & Co. KG, fifth edition, 2011.

[120] Eugene F. Knott, John F. Shaeffer, and Michael T Tuley. *Radar cross section*. Scitech Publishing, second edition, 2004.

[121] K Sarabandi and N Behdad. A Frequency Selective Surface With Miniaturized Elements. *Antennas and Propagation, IEEE Transactions on*, 55(5):1239–1245, 2007.

[122] D Ferreira, R F S Caldeirinha, I Cuiñas, and T R Fernandes. Square Loop and Slot Frequency Selective Surfaces Study for Equivalent Circuit Model Optimization. *Ieee Transactions on Antennas and Propagation*, 63(9):3947–3955, 2015.

[123] E A Parker. *The gentleman's guide to frequency selective surfaces*. 1991.

[124] Inder J Bahl. *Lumped Elements for RF and Microwave Circuits*. Artech House, 2003.

[125] Brian C Wadell. Transmission line design handbook, 1991.

[126] Qi Xiaoning, Wang Gaofeng, Yu Zhiping, R W Dutton, Young Tak, and N Chang. On-chip inductance modeling and RLC extraction of VLSI interconnects for circuit simulation. In *Proceedings of the IEEE 2000 Custom Integrated Circuits Conference (Cat. No.00CH37044)*, pages 487–490, 2000.

[127] R Hosono, N Guan, H Tayama, and H Furuya. An equivalent circuit model for meander-line monopole antenna attached to metallic plate. In *2012 International Symposium on Antennas and Propagation (ISAP)*, pages 1421–1424, 2012.

[128] David M Pozar. *Microwave Engineering*. John Wiley and Sons, third edition, 2004.

[129] Rola Saad and Kenneth L. Ford. A miniaturised dual band artificial magnetic conductor using interdigital capacitance. In *8th European Conference on Antennas and Propagation, EuCAP 2014*, pages 25–26. IEEE, apr 2014.

[130] D G Kleinbaum, L Kupper, K E Muller, and A Nizam. *Applied Regression Analysis and Other Multivariable Methods*. Duxburry Press, fourth edition, 2008.

[131] Barbara G Tabachnick and Linda S Fidell. *Using Multivariate Statistics*. Pearson Education, fifth edition, 2007.

[132] CST. CST Software Support Pages (https://www.cst.com), 2015.

[133] T Weiland, M Timm, and I Munteanu. A practical guide to 3-D simulation. *IEEE Microwave Magazine*, 9(6):62–75, 2008.

[134] F Bayatpur and K Sarabandi. Multipole Spatial Filters Using Metamaterial-Based Miniaturized-Element Frequency-Selective Surfaces. *Microwave Theory and Techniques, IEEE Transactions on*, 56(12):2742–2747, 2008.

[135] G Xu, S V Hum, and G V Eleftheriades. A Technique for Designing Multilayer Multistopband Frequency Selective Surfaces. *Ieee Transactions on Antennas and Propagation*, 66(2):780–789, 2018.

[136] J Pallant. *SPSS Survival Manual: A step by step guide to data analysis using IBM SPSS*. McGraw Hill, fifth edition, 2013.

Appendix A

CST Microwave Studio

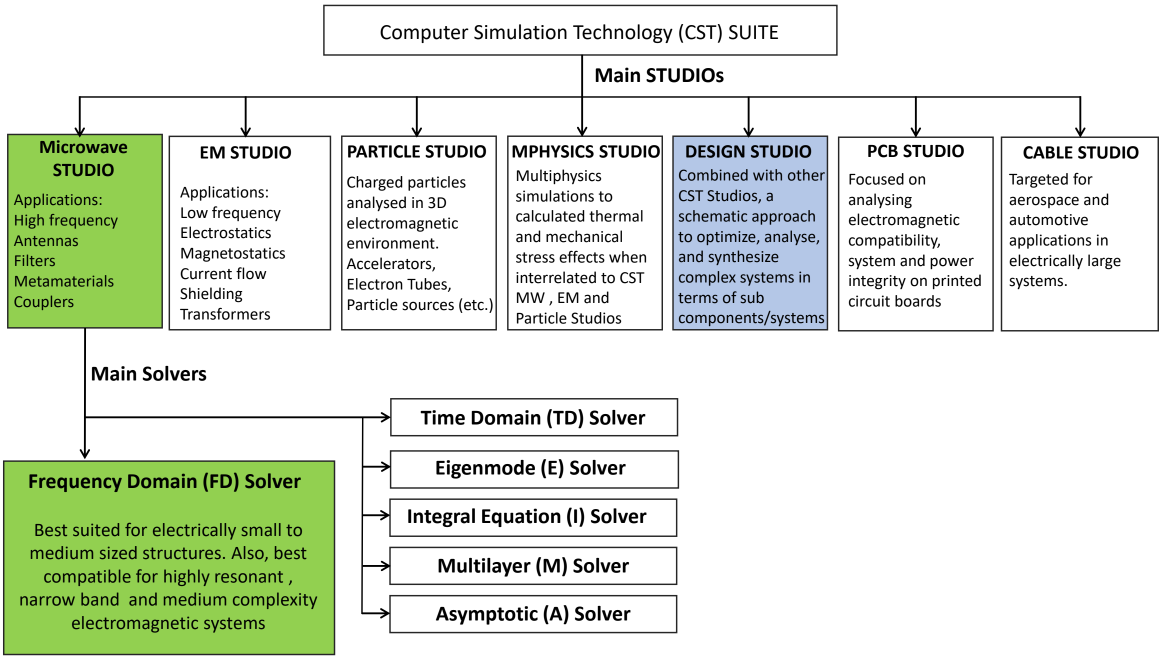

Fig. A.1 Overview of Computer Simulation Technology (CST) software.

CST SUITE is a commercial simulation software, stands for Computer Simulation Technology. It provide engineers with a tool to design and predict performance of various systems with applications to Microwave, Aerospace, Automotive, RF, Electrostatics and Magnetostatics for more reliable manufacturing. Fig. A.1 presents a general schematic overview for CST Suite detailing main studios available and general outline to their applications. Detailed information about CST SUITE Studios can be found in [132]. However, this Appendix is focused on CST Microwave Studio, detailing important concepts of Time Domain(TD) and Frequency Domain (FD) solvers being best suited as the thesis is concerned.

A.1 CST Microwave Studio Concepts

CST Microwave Studio (MWS) software is an integrated part within CST SUITE and characterized as a robust tool dedicated for 3D electromagnetic modelling enabling fast design and efficient analysis to solve high frequency problems. Main areas of applications include periodic structures, metamaterials, antennas, filters, couplers, waveguides, transmission lines stated as an example. The software provides user friendly graphical user interface where models are constructed, parametrized, and optimized using wide range of available functions and material prototypes which are essential to be accurately utilized for a successful simulation run such as including material losses and setting compatible boundary conditions. Based on numerical techniques, CST MWS is capable of performing fast and accurate calculations of parameters that characterize system behaviour which is of high interest to engineers such as calculations of S-parameters, dispersion diagrams, 2D and 3D Farfield, Gain, efficiency and extraction of network parameters.

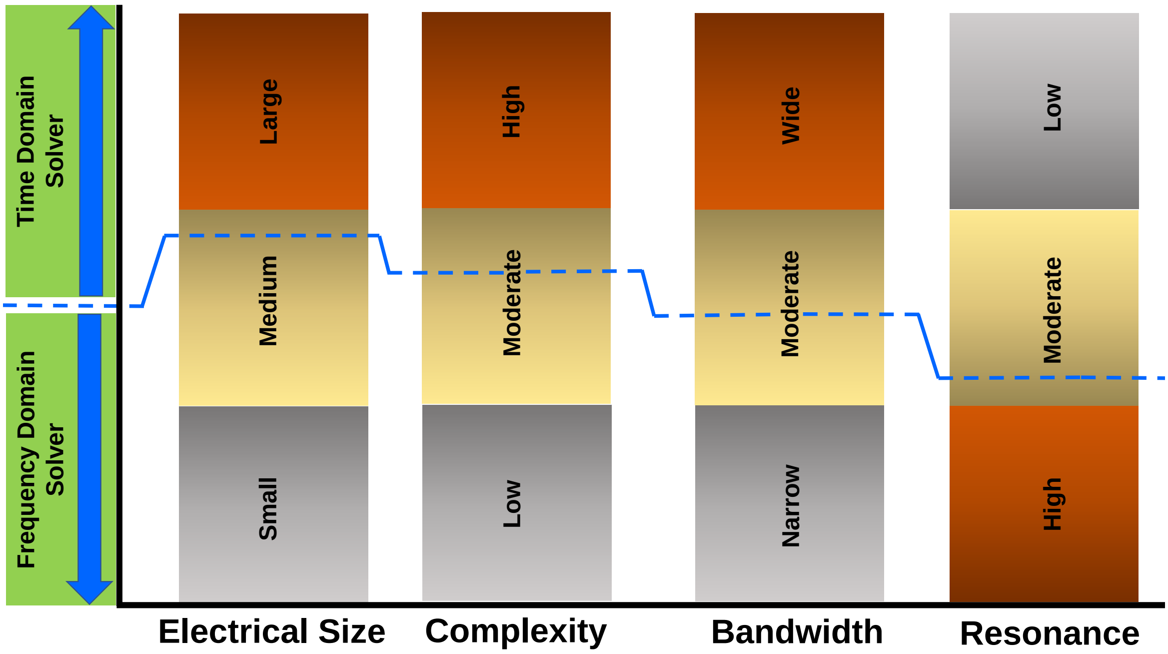

Fig. A.2 Time Domain (TD) and Frequency Domain (FD) solvers suitability.

As any available Studios within the CST SUITE environment, CST Microwave Studio is accompanied with various solvers which are; Frequency Domain (FD) solver, Time Domain (TD) solver, Integral Equation (IE) solver, Eigenmode solver, Multilayer solver, and Asymptotic solver. All solvers utilize numerical methods to predict electromagnetic properties of simulated models and the choice of solver depends on the area of application and design characteristics. As this thesis is concerned, only Time Domain and Frequency

Domain solvers are discussed being best suited for high impedance surfaces and antenna characterizations. All other mentioned solvers fall outside the scope of this thesis and more information can be found in [132]. Fig. A.2 compares Time Domain (TD) and Frequency Domain (FD) solvers within CST MWS as with respect to where most applicable such that simulation time, computational memory, accuracy and efficiency are best optimized. For structures which are complex, electrically large, medium to low resonance and broadband; TD solver is best suited. However for electrically small, narrowband, strongly resonant structures of medium to low complexity; FD solver is the adequate choice.

A.2 CST Microwave Studio Meshing Technique

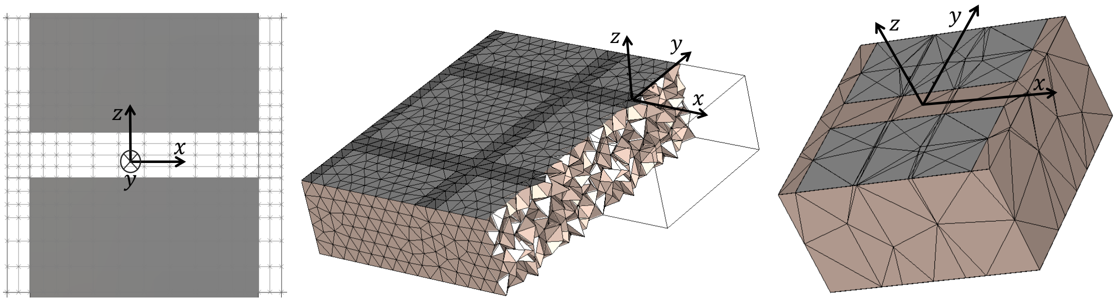

(a) Hexahedral Mesh (b) Tetrahedral Mesh (c) Surface Mesh

Fig. A.3 CST Suite supported mesh types.

The response of modelled electromagnetic structures in CST 3D environment is characterised by available solvers upon discretization of the structure in the so called "Mesh" where Maxwell's equations are solved using numerical methods chosen based on the type of mesh applied and consequently the solver involved in the simulation. Therefore, it is vital that appropriate meshing configuration is defined in order to accurately model the design where a trade off can be made between simulation running time and accuracy. In general, densely meshed structures require large computational resources and long time to complete irrespective of solver type chosen. Nevertheless efficient meshing is realised by understanding the physicality of the design where localized mesh refinement is applied in areas of significant energy change such as input ports, bends and gaps, therefore, improving the quality of the mesh as well as solver's accuracy. Three types of mesh configurations are available which are supported by various solvers accordingly. First, Hexahedral Mesh demonstrated for a patch HIS unit cell structure, Fig. A.3a. The unit cell is discretized using mesh lines in xz-plane, as shown, but Hexahedral lines are also applied xy and yz planes within the 3D model. Hexahedral mesh is available to both TD and FD solvers within CST MSW.

However, Hexahedral mesh does not support material jumps and discontinuity, therefore, it is associated with Perfect Boundary Approximation (PBA) as well as Thin Sheet Technology (TST) which significantly enhances the quality of Hexahedral mesh. PBA allows efficient modelling of curved elements while TST efficiently models thin elements with perfect electrical properties [132]. Second, Tetrahedral mesh, Fig. A.3b, is shown for a simple patch HIS unit cell structure. The unit cell is discretized into tetrahedrons in 3-dimensional configuration. Frequency Domain (FD) solver utilizes Tetrahedral mesh very efficiently. Finally, Surface mesh, Fig. A.3c, is also available within CST MWS and mainly dedicated to Integral Equation Solver which is broadly outside the scope of this thesis being most applicable to significantly electrically large structures with mainly metallic surfaces.

A.3 Time Domain (TD) Solver

Transient Solver is one of available calculation methods within Time Domain (TD) solver which is applicable to work within the thesis. It is a very efficient and robust tool that calculates electromagnetic field development and progress for structures modelled within appropriate boundary conditions and input/output ports. TD solver is strongly supported by Hexahedral mesh where attention is made to optimize the mesh such that all elements of the structure is efficiently discretized to improve the solver's accuracy. Only single run is required over a broadband range where discrete time samples are considered as associated with discrete time locations. Time and frequency domain calculations can be obtained such as S-parameter, field distributions and farfield radiation patterns. Full solver details can be found in [132, 133]

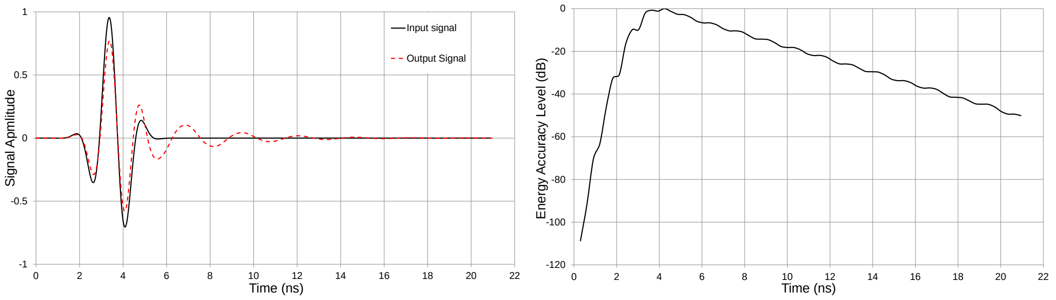

(a) Signal Amplitude (b) Energy Plot

Fig. A.4 Transient Solver Accuracy Checks.

In Transient solver, the structure is initially excited by a Guasian pulse where field propagation is monitored at discrete time. Time signals are desired to decay to zero such that the fields are accurately estimated. Therefore, input energy to the system is expected to totally dissipate before the simulation stops. However, this is not practically possible due to numerical errors, also called "numerical noise". To achieve reasonable results, convergence analysis is conducted while initially setting system's accuracy level to a certain threshold such that the energy is allowed to decay where the noise within the structure is reduced. A threshold of at least -40 dB indicates the level which the remaining energy within the system falls with respect to the maximum energy. Two plots give indication on simulation run performance. First, input and output signal amplitude plots are observed. An example is shown for a half wavelength dipole antenna in Fig. A.4 where confidence in S-parameter results can be achieved as output signal is negligible after 16 ns. Accuracy level was set to -50 dB which is illustrated by associated energy graph presented in Fig. A.4. It is observed that the resonant nature of the structure is within the solver's capacity and output energy level is reduced to -50 dB within 22 ns where all input energy exist the system with minimum residual numerical noise. For electromagnetic structures of highly resonant nature, output signals experience significant ripples and could be trapped within the system which invalidate the S-parameter calculations. Frequency Domain (FD) Solver is the better alternative and is discussed next.

A.4 Frequency Domain (FD) Solver

Frequency Domain (FD) solver is supported by both Hexahedral and Tetrahedral mesh. Tetrahedral mesh is discussed in this section being the most efficient way to analyse highly resonant, narrowband and complex systems as related to thesis work covered for high impedance surface design. FD solver analyse a given structure in the frequency domain by calculating fields at discrete frequency points (samples) where a full simulation run is required for each frequency sample considered. Thereafter, frequency samples are used to calculate S–parameters within a broader spectrum. Accuracy of the solver is enhanced by considering narrower bandwidth in contrary to TD solver. Furthermore, due to the complexity of tetrahedral mesh, it is difficult to predict the mesh size required such that numerical simulation renders accurate field and S - parameters estimates. Therefore, efficient use of FD solver is achieved by incorporating adaptive mesh refinement feature which enhances tetrahedral mesh quality resulting in optimum discretization of the model. Full information on solver is detailed in [132, 133]. In general, FD solver is memory and time consuming since mesh size and calculation time increases with the system's complexity. Success of the FD solver simulation run is governed by defining adequate frequency range and boundary conditions being initial steps to take.

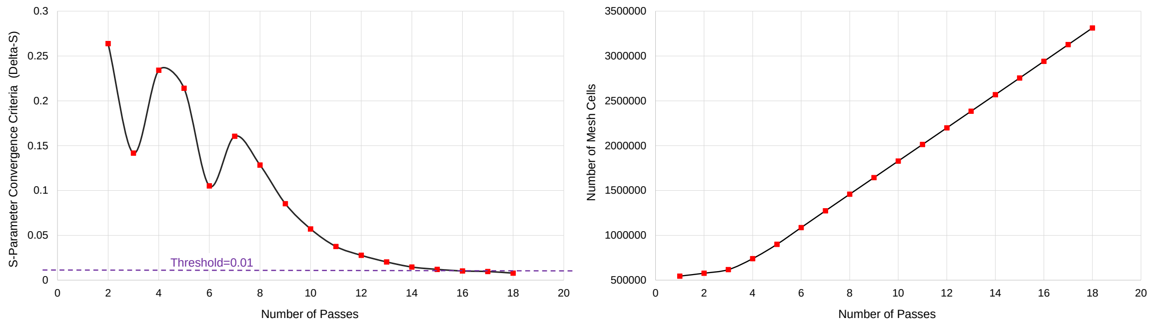

(a) Delta-S

(b) Mesh size

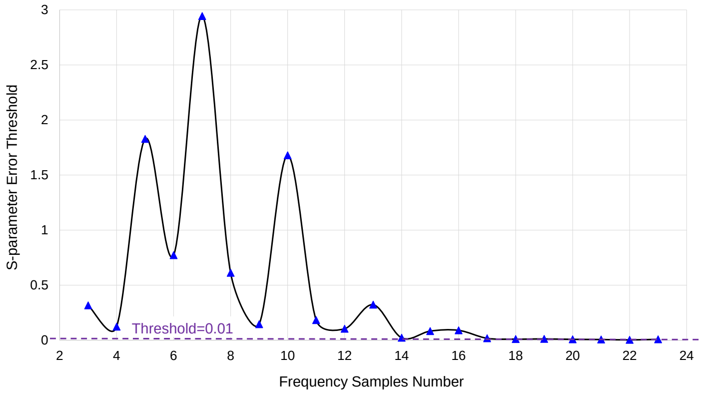

(c) S-parameters Progression

Fig. A.5 Frequency Domain Solver Accuracy Checks.

Nevertheless, insights on the mesh quality and accuracy of S-parameters calculations is obtained from convergence check on Delta-S, progression of samples and total mesh size which are presented at end of simulation run. First, information obtained about density and quality of tetrahedral mesh is observed from the S-parameters convergence criteria plot (Delta-S) which is related to adaptive mesh refinement. Delta-S defines the maximal variation in absolute value of complex S-parameters, as calculated for a given adaptive frequency sample, among two successive simulation runs. A threshold of 0.01 is considered. When Delta-S $<$ 0.01, adaptive mesh refinement stops where tetrahedral mesh is considered adequate and frequency sampling follows. The quality of Delta-S $<$ 0.01 graph is an indication of system complexity. If the threshold is not met, the structure is not appropriately discretized for the numerical technique to give reasonable results. An example is shown in Fig. A.5a for the case when a planar monopole antenna is modelled with miniaturised interdigital HIS and simulated using FD solver. The system converged to an acceptable mesh after 18 passes but resulting in very large mesh size of 3,312,610 tetrahedrons which is demonstrated in the associated plot of number of mesh cells versus number of adaptive mesh passes, Fig. A.5b. Second, Interpolation error estimate plot is of significant importance to assess the validity of simulation run as defines S-parameters progression reflecting on total number of samples required such that the S-parameters are reasonably accurate within the frequency range defined. This is obtained once mesh refinement is complete, where number of frequency samples required to interpolate the S-parameters within a given spectrum is increased until the "S-parameter error threshold" is achieved, 0.01 is the default value. "S-parameter error threshold" is defined as the utmost divergence of linear S-parameters calculated among two consecutive runs. Regarding the later case of monopole antenna above interdigital HIS, Fig. A.5c shows that 23 frequency samples were required for the S-parameters to converge.

A.5 Concluding Remarks

CST SUITE has been briefly addressed with focused discussion on TD and FD solvers within CST Microwave Studio. As this thesis is concerned, numerical simulations were very helpful in modelling and designing highly resonant miniaturised high impedance surfaces. Most work was conducted using FD solver being best suited for the applications within the thesis where TD solver is used to compare frequency domain results providing added confidence prior to manufacturing. However, computer simulations introduce numerical errors within the results and this is being taken into account while designs are compared to manufactured prototypes. Numerical errors are mainly introduced due to different factors such as:

- Geometrical errors where structure's details are not modelled accurately or neglected.
- Materials and components tolerances are not included in the simulations especially for cases when materials properties depend on frequency such as permittivity and loss tangent of some dielectrics stated as an example.
- Mismatch errors not included within the software.
- Models are modelled in an ideal environment which is not practically possible.
- Models which are not meshed properly will invalidate numerical methods applied by the solver resulting in huge inaccuracies.
- Solver convergence criteria are not met.

Appendix B

Single Band Design 2 - Dual Layer Dual Polarized IDC HIS Coupling Model

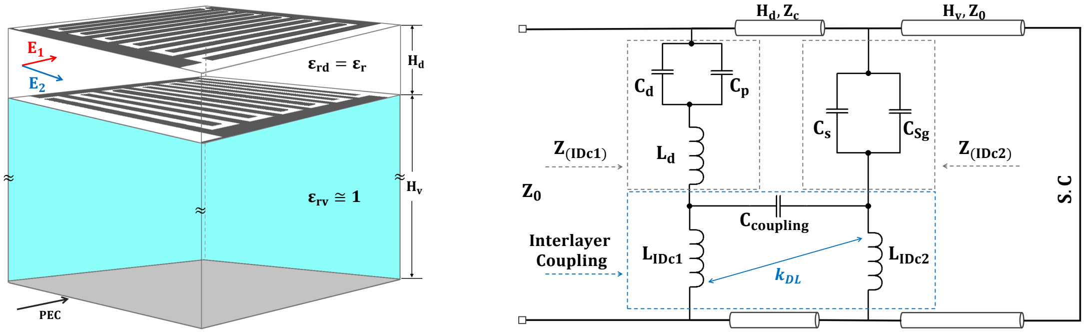

(a) 3D View (b) Equivalent Circuit Model

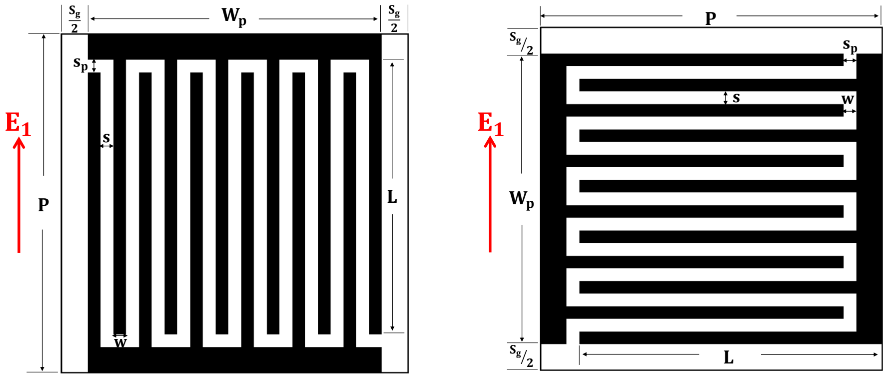

(c) Upper Layer Top View (d) Lower Layer Top View

Fig. B.1 Single Band Dual Layer Dual Polarized (SB-DLDP) Interdigital HIS.

Single Band Dual Layer Dual Polarized (SB-DLDP) Interdigital Capacitor (IDC) HIS is presented in Fig. B.1a. Dual polarization is realised by incorporating dual layer capacitive interdigital surfaces orthogonal to each other, printed as rotated 90° on both sides of a dielectric material of thickness ($\mathrm{H_d}$). The two layer structure is supported by a rohacell material of thickness ($\mathrm{H_v}$) which permittivity is close to unity and then backed by metallic plane to realise a light weight dual polarized HIS. For a normal incident plane wave, top interdigital surface, Fig. B.1c, is operated by $\mathrm{E_1}$ polarized wave while the lower interdigital surface, Fig. B.1d, is operated by $\mathrm{E_2}$ polarized wave. The top and lower interdigital capacitive surfaces are identical and closely spaced where interlayer coupling is a design constraint which is addressed in this Appendix.

B.1 Equivalent Circuit Model

Multilayer coupling in FSS has been previously reported in the literature such as in [134, 135] were interlayer coupling results from capacitive and inductive factors, all structure specific. Also, a similar configuration as capacitive interdigital dual layer, Fig. B.1a, was reported in [89] for an FSS structure. However, this Appendix will detail interlayer coupling as HIS is concerned dealing with new set of design equations that is utilized to include HIS ground plane effect. Interlayer interdigital HIS surface coupling is analysed through Equivalent Circuit Model (ECM) to explain the mechanism of the structure. The case when HIS is governed by $\mathrm{E_1}$ polarized field is considered to describe the principle of operation.

Referring to ECM, Fig. B.1b. Top interdigital surface, Fig. B.1c, of interdigital impedance ($\mathrm{Z_{IDC1}}$) interacts with lower interdigital surface, Fig. B.1d, of capacitive impedance ($\mathrm{Z_{IDC2}}$) through a transmission line section representing the thin dielectric substrate of thickness ($\mathrm{H_d}$) and permittivity (ε_r). Lower interdigital surface impedance is expected of a very small capacitance generated by polarization $\mathrm{E_1}$ as it illuminates the digits orthogonal to the field and will be insignificant if interlayer coupling does not exist. However, surface currents and H fields were observed to circulate within the outer digits and strips of both interdigital layers forming a rectangular ring-like structure which contributes to inductive coupling. Inductors $\mathrm{L_{IDC1}}$ and $\mathrm{L_{IDC2}}$ are therefore included in circuit model, Fig. B.1b, and mutually coupled through coupling factor (k_{DL}).

Furthermore, dual layer interdigital surface, of high capacitance density illustrated by densely packed digits, being closely spaced will generate parasitic coupling capacitance ($\mathrm{C_{coupling}}$) which contribute to interlayer capacitive coupling and defined as [124]:

$$\mathrm{C_{coupling}} = \varepsilon_0 \varepsilon_{eff} \frac{\mathrm{area}}{\mathrm{H_d}} \tag{B.1}$$

where area = $W_p \times W_p$ for a square interdigital unit cell structure. H_d and $\varepsilon_{eff} = \dfrac{\varepsilon_r + 1}{2}$ are the dielectric substrate thickness and effective permittivity respectively.

Finally, a transmission line section of length (H_v) and permittivity close to free space, terminated by a Short Circuit (S.C) is added in ECM to represent the supporting rohacell substrate and HIS metal plane, Fig. B.1b.

Analysis on interlayer coupling is conducted investigating the effect of substrate thickness (H_d) and considering proposed circuit model, Fig. B.1b. The surface is modelled on FR4 substrate ($\varepsilon_r = 4.3, \tan\delta = 0.025$), designed to operate at 900 MHz within a unit cell periodicity of 12.5 mm where a total of 12 digits were implemented each of thickness and gap of 0.5 mm. Circuit model elements are calculated according to equations proposed in Section B.2 and Section B.3. Dual layer interdigital HIS structure dielectric separation distance is varied from 0.05 mm to 1.6 mm where the circuit model elements are calculated and resonance frequency is compared to simulated reflection phase plot when modelled on CST Microwave Studio. Table B.1 presents the circuit model parameters where it can be observed that, for the case of (H_d = 0.05 mm), interlayer coupling is at its maximum where resonance frequency is reduced from 900 MHz to 537 MHz. As H_d increases interlayer coupling is reduced and the resonance frequency approaches the required design value.

Table B.1 Circuit Model Parameters of Single Band Dual Layer Dual Polarized Interdigital HIS. $\mathbf{f}_{dsn}$ = 900 MHz $\mathbf{C}_d$ = 2.8 pF $\mathbf{L}_d$ = 1.7 nH $\mathbf{C}_p$ = 1.5e^{-3} pF $\mathbf{C}_{Sg}$ = 0.4 pF $\mathbf{C}_s$ = 0.05 pF

H_d (mm)	H_v (mm)	$C_{coupling}$ (pF)	L_{IDC1} (nH)	L_{IDC2} (nH)	k_{DL}	f (MHz) ECM	f (MHz) Simulated
0.05	7.55	62	25.5	23.7	0.32	537	537
0.1	7.5	31	25.5	23.7	-0.4	657	659
0.2	7.4	15.5	25.5	23.6	-0.77	765	765
0.4	7.2	7.75	25.5	23.5	-0.93	842	843
0.6	7	5.2	25.5	23.4	-0.94	863	864
0.8	6.8	3.88	25.5	23.3	-0.92	870	870
1.6	6	1.94	25.5	23.2	-0.76	867	868

Next two sections will detail design equations implemented in the circuit model as dual layer dual polarized single band interdigital HIS is considered. Nevertheless, the above analysis is not conclusive. The circuit model defines and explains the mechanism of the structure, however, the reflection phase observed is as the upper layer is concerned. It is expected that as H_d is increased , H_v reduces to maintain a total effective substrate thickness constant and this reflects on increased resonance frequency of the lower layer if observed for polarization E_2. This will be discussed in Section B.4 where full wave simulations will discuss interlayer coupling influence in both polarizations. Conclusive solution to take interlayer coupling into account is proposed towards the end of this Appendix.

B.2 Top Layer Interdigital Surface Explained

Top interdigital layer, Fig. B.1c, E_1 polarized, uncoupled impedance (Z_{IDC1}):

$$Z_{IDC1} = j\omega L_d + \frac{1}{j\omega(C_d + C_p)} \tag{B.2}$$

where L_d, C_d and C_p are the top layer interdigital capacitive surface interdigital inductance, interdigital capacitance, mutual capacitance as extensively discussed in Chapter 5.
Due to interlayer coupling, top layer inductance (L_{IDC1}) resulted. It is the series combination of inductances generated by side digits and interdigital plate strip-line:

$$L_{IDC1} = 2L_1 + L_2 \tag{B.3}$$

L_1 is the inductance of a strip line of length (L), width (w) and copper thickness (t), generated in first/last digit of interdigital top capacitive surface, Fig. B.1c, defined as [124]:

$$L_1 = 0.2L\left[\ln\left(\frac{L}{w+t}\right) + 1.193 + \frac{w+t}{3L}\right]K_1 \tag{B.4}$$

L_1 is in (nH). L, w, t are in (mm). K_1 is the correction factor which takes HIS total substrate thickness (H) effect into account when $\left(\frac{w}{H} > 0.05\right)$, defined as [124]:

$$K_1 = 0.57 - \ln\left(\frac{w}{H}\right) \tag{B.5}$$

L_2 is the inductance of a strip line of length (W_p), width (S_g) and copper thickness (t) representing top and lower strips connecting interdigital digits, Fig. B.1c, defined as [124]:

$$L_2 = 0.2W_p\left[\ln\left(\frac{W_p}{S_g+t}\right) + 1.193 + \frac{S_g+t}{3W_p}\right]K_2 \tag{B.6}$$

L_2 is in (nH). W_p, S_g and t are in (mm). K_2 is the correction factor which takes HIS total substrate thickness (H) effect into account when $\left(\frac{S_g}{H} > 0.05\right)$, defined as [124]:

$$K_1 = 0.57 - \ln\left(\frac{S_g}{H}\right) \tag{B.7}$$

B.3 Lower Layer Interdigital Surface Explained

Lower interdigital layer, Fig. B.1d, E_1 polarized, uncoupled interdigital impedance (Z_{IDC2}) is purely capacitive and is the parallel combinations of capacitances C_{S_g} and C_s:

$$Z_{IDC2} = \frac{1}{j\omega(C_s + C_{Sg})} \tag{B.8}$$

C_{S_g} is the lower layer capacitance generated between interelement spacing (S_g) [123, 121]:

$$C_{S_g} = \varepsilon_0 \varepsilon_{eff} \frac{2P}{\pi} \log \frac{1}{\sin\left[\frac{\pi}{2}\frac{S_g}{P}\right]} \tag{B.9}$$

Where C_s is the lower layer equivalent capacitance of multiple elementary capacitance (C_{s_i}) developed in series between adjacent interdigital digits separated by gap (s) and excited by E_1 polarization, Fig. B.1d. Therefore C_s is function of digits number (N_d):

$$C_s = \frac{C_{s_i}}{N_d - 1} \tag{B.10}$$

C_{s_i} is the elementary capacitance developed within gap (s) and periodicity (P) [123, 121]:

$$C_{s_i} = \varepsilon_0 \varepsilon_{eff} \frac{2P}{\pi} \log \frac{1}{\sin\left[\frac{\pi}{2}\frac{s}{P}\right]} \tag{B.11}$$

Lower interdigital layer inductance (L_{IDC2}), induced due to interlayer coupling, is the series equivalence of inductances observed in end top/bottom digits and interdigital plate strip-line:

$$L_{IDC2} = L_3 + 2L_4 \tag{B.12}$$

L_3 is the inductance of right and left strips of length (W_p) , total width (S_g) and copper thickness (t), Fig. B.1d, defined as [124]:

$$L_3 = 0.2W_p \left[\ln\left(\frac{W_p}{S_g + t}\right) + 1.193 + \frac{S_g + t}{3W_p}\right] K_3 \tag{B.13}$$

L_3 is in (nH). W_p, S_g and t are in (mm). K_3, correction factor which takes HIS rohacell substrate thickness (H_v) effect into account when $\left(\frac{S_g}{H_v} > 0.05\right)$, defined as [124]:

$$K_3 = 0.57 - \ln\left(\frac{S_g}{H_v}\right) \tag{B.14}$$

L_4 is the inductance of lower interdigital layer top and bottom digits of a strip line of length (L), width (w) and copper thickness (t), Fig. B.1d, defined as [124]:

$$L_4 = 0.2L\left[\ln\left(\frac{L}{w+t}\right)+1.193+\frac{w+t}{3L}\right]K_4 \tag{B.15}$$

L_4 is in (nH). L, w and t are in (mm). K_4 is the correction factor which takes HIS rohacell substrate thickness (H_v) effect into account when $\left(\frac{w}{H} > 0.05\right)$, defined as [124]:

$$K_4 = 0.57 - \ln\left(\frac{w}{H_v}\right) \tag{B.16}$$

B.4 Parametric Analysis

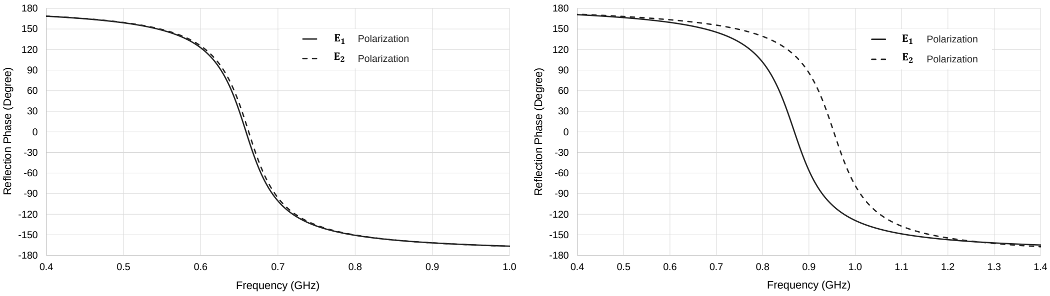

(a) $H_d = 0.1$ mm, $H_v = 7.5$ mm (b) $H_d = 1.6$ mm, $H_v = 6$ mm

Fig. B.2 Simulated reflection phase plot for SB-DLDP interdigital HIS observed at E_1 and E_2 polarizations and compared at dielectric separation thickness $(H_d = 0.1 \text{ mm} \ ,\ 1.6 \text{ mm})$.

Interlayer coupling is discussed using full wave simulations on CST Microwave Studio investigating dual layer separation thickness (H_d) effect. The surface, Fig. B.1a, is modelled on FR4 substrate $(\varepsilon_r = 4.3, \tan\delta = 0.025)$, designed to operate at 900 MHz within a unit cell periodicity of 12.5 mm where a total of 12 digits were implemented each of thickness and gap 0.5 mm. Resonance frequency at normal incidence is observed for both E_1 and E_2 polarizations considering the case of dielectric thickness $(H_d = 0.1 \text{ mm})$ and $(H_d = 1.6 \text{ mm})$ while maintaining total substrate thickness $(H = 7.6 \text{ mm})$, Fig. (B.2). It can be observed that for $(H_d = 0.1 \text{ mm})$, both polarizations resonance are identical but at the expense of reduced resonance frequency to around 660 MHz, Fig. B.2a. This is due to interlayer coupling and a reduction in resonance frequency is an illustration of increased overall capacitance or reduced equivalent interdigital capacitive layer impedance. On the other hand, for $(H_d = 1.6 \text{ mm})$, E_1 resonance frequency is increased close to its design value while E_2 resonance is increased above the design frequency, Fig. B.2b. While interlayer coupling is reduced as H_d increases,

E_1 and E_2 polarizations sustain different resonances due to the fact that lower surface, operated by E_2 polarization, is now supported by a reduced substrate thickness which diverts the structure from its design objectives.

B.5 Interlayer Coupling Factor (CF)

Single Band Dual Layer Dual Polarized (SB-DLDP) interdigital HIS, Fig. B.1a, is an upgraded version of Single Band Single Layer Single Polarized (SB-SLSP) interdigital HIS design, Chapter 5, with the main purpose to realise dual polarization implementing a simplified practical design procedure. Nevertheless, interlayer coupling exists as the two interdigital surfaces are closely spaced which imposes design constraints. Circuit model presented does not provide conclusive results to estimate the coupling in advance. Furthermore, parametric analysis conducted demonstrates that interlayer coupling reduces the resonance frequency indicating a consequent increase in dual layer effective capacitance $(\mathrm{C_{IDC(DL)}})$ which signifies a reduction of dual layer effective interdigital capacitive impedance $(\mathrm{Z_{IDC(DL)}})$.

Presented, a new approach to predict interlayer coupling by defining factor (CF) which is deduced from dual layer effective impedance $(\mathrm{Z_{IDC(DL)}})$ extracted when interdigital dual layer structure is simulated as a capacitive sheet, neglecting the HIS ground plane, and then compared against single layer interdigital capacitive sheet impedance $(\mathrm{Z_{IDC(SL)}})$ simulated under same conditions. Therefore, interlayer coupling factor (CF), Eq. (B.17), defines the factor that effective Dual Layer (DL) sheet capacitance $(\mathrm{C_{IDC(DL)}})$ is increased with respect to Single Layer (SL) sheet capacitance $(\mathrm{C_{IDC(SL)}})$. Moreover, in both SL and DL cases, HIS is regarded as a resonator where the interdigital sheet impedance is connected to equivalent substrate inductance of supporting substrate of thickness $(\mathrm{H_v})$ backed by metal plate. Consequently, Factor (CF) is related to DL and SL HIS substrate inductances and resonance frequencies $(\mathrm{L_{s(DL)}},\ \mathrm{L_{s(SL)}},\ \mathrm{f_{DL}}$ and $\mathrm{f_{SL}})$ as of Eq. (B.17).

$$\mathrm{CF} = \frac{\mathrm{C_{IDC(DL)}}}{\mathrm{C_{IDC(SL)}}} = \left(\frac{\mathrm{L_{s(SL)}}}{\mathrm{L_{s(DL)}}}\right)\left(\frac{\mathrm{f_{SL}}}{\mathrm{f_{DL}}}\right)^2 \tag{B.17}$$

where it is expected that $\mathrm{L_{s(SL)}} \backsimeq \mathrm{L_{s(DL)}}$.

Fig. B.3, presents design graph for interlayer coupling factor (CF) which estimates the dual layer interdigital capacitance increase with respect to single layer interdigital capacitance as plotted versus variation in dielectric thickness $(\mathrm{H_d})$. It can be observed that total equivalent capacitance of a dual layer structure is significantly increased, by a factor of 5.7, for a separation distance as close as 0.05 mm. As substrate thickness $(\mathrm{H_d})$ is increased, a steady state is achieved and coupling between layers is not an issue when $(\mathrm{H_d} > 0.6\ \mathrm{mm})$.

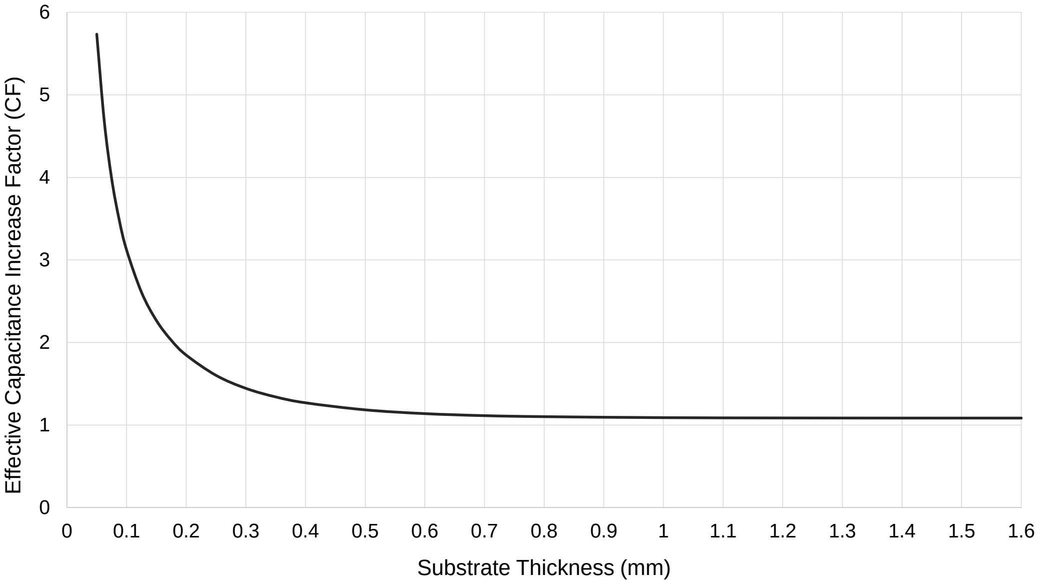

Fig. B.3 Interlayer coupling factor as function of varying dielectric thickness $(\mathrm{H_d})$.

However, the main focus is to maintain the two layers as intact as possible. Therefore, coupling factor (CF), Fig. B.3, is of significant importance. Dual layer dual polarized interdigital HIS can be designed based on methodology of single layer single polarized interdigital HIS, Chapter 5, but with prior knowledge to interlayer coupling such that the resonance frequency is recalculated to take the expected frequency decrease into account depending on the choice of dielectric thickness separating the two layers. Percentage frequency shift due to dual layer coupling $(\mathrm{\%FreqShift(DLCplng)})$ is deduced from Eq. (B.18). Where new design frequency $(\mathrm{f_{DL(new)}})$ can be interpolated using Eq. (B.19).

$$\mathrm{\%FreqShift(DLCplng)} = \frac{\mathrm{f_{DL}} - \mathrm{f_{SL}}}{\mathrm{f_{SL}}} = \frac{1}{\sqrt{\mathrm{CF}}} - 1 \tag{B.18}$$

$$\mathrm{f_{DL(new)}} = \frac{\mathrm{f_{SL}}}{1 + \dfrac{\mathrm{\%FreqShift(DLCplng)}}{100}} \tag{B.19}$$

Appendix C

Introduction To Multiple Linear Regression Analysis

Regression analysis is a powerful statistical tool to determine a mathematical model that assess the relationship between a Dependent Variable (DV), Y, and one or more Independent Variable(s) (IV), $\mathrm{X_1, X_2, ..., X_n}$. Therefore, called a multivariable technique that enables to predict a response, in a quantitative format, as the result of a given input(s). Where graphical representation is not possible when number of variables exceeds 3 dimensional prospect.

Multiple linear regression models the response into a linear mathematical model called surface equation, defined as [130]:

$$\mathrm{Y = B_0 + B_1X_1 + B_2X_2 + ... + B}_k\mathrm{X_n} + \in \tag{C.1}$$

where n is the number of Independent Variables (IV).
$\mathrm{B_0}$ is the intercept. $\mathrm{B_n}$ is the regression coefficient, also referred to as slope of model associated with each of independent variables $(\mathrm{X_n})$.
$\in$ is the error term

"Least Square Method" is the most popular technique to estimate the regression coefficients where error terms are minimized such that the model has best line fit.
For a quick review of the "Least Square Method" linear regression with one dependent variable and one independent variable will be discussed first.

C.1 Simple Linear Regression

Equation to fit a response dependent variable (Y) with respect to a set of observations made on independent variable (X), knowing there is a linear relationship, can be mathematically written as [130]:

$$Y = B_0 + B_1 X + \in \tag{C.2}$$

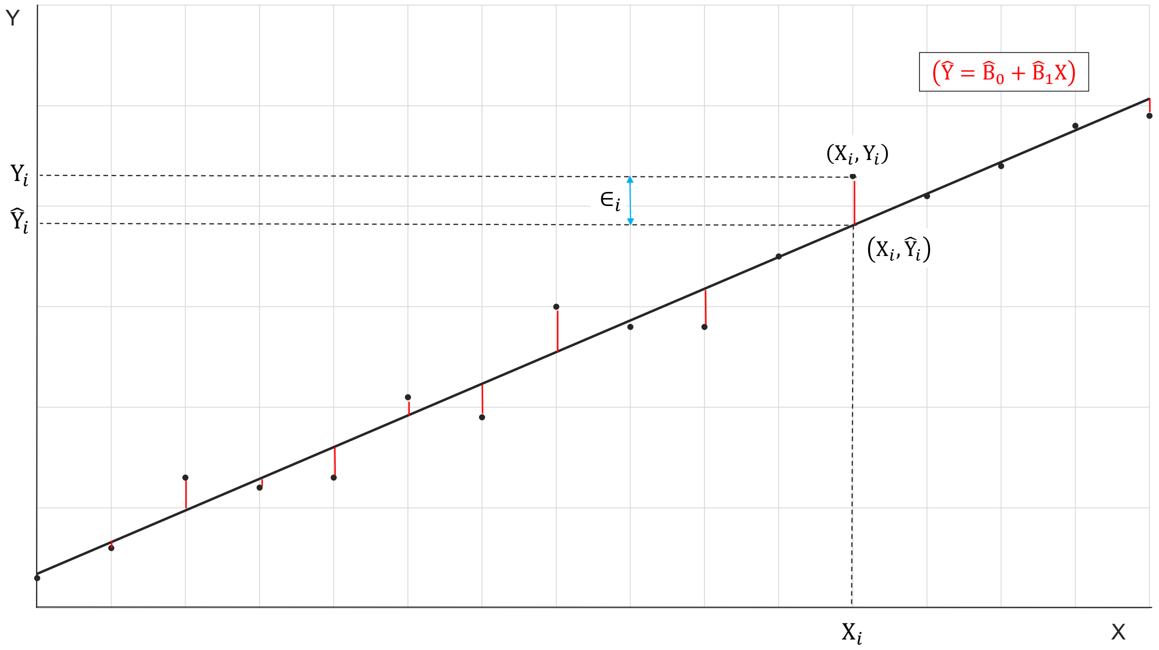

Fig. C.1 Simple linear regression model best fit line.

The m odel has best fit when the regression coefficients B_0 and B_1 are accurately determined such that the errors are minimum. Residuals of estimates or errors are defined as the difference between observed value and estimated value. As of Fig. C.1, sum of squares of the residual between each observed point (X_i, Y_i) and estimated point $(X_i, \hat{Y}_i)$ is defined as Sum of Square due to error (SSE), also called Residual Sum of Squares (SS_{res}) [130, 131]:

$$SS_{res} = \sum_{i=1}^{m} (Y_i - \hat{Y}_i)^2 = \sum_{i=1}^{m} (Y_i - \hat{B}_0 - \hat{B}_1 X_i)^2 \tag{C.3}$$

where m is the number of observations

Estimated dependent variable, $\hat{Y}_i = \hat{B}_0 + \hat{B}_1 X_i$, is the mathematical representation of a simple straight line fitted within the observed data.

Solution to find best fit model by estimating the coefficients that has minimum residual sum of square error SS_{res} is possible where $\hat{B}_0$ and $\hat{B}_1$ are defined as [130]:

$$\hat{B}_1 = \frac{\sum_{i=1}^{m} (X_i - \overline{X})(Y_i - \overline{Y})}{\sum_{i=1}^{m} (X_i - \overline{X})} \quad \text{and} \quad \hat{B}_0 = \overline{Y} - \hat{B}_1 \overline{X} \tag{C.4}$$

where $\overline{X}$ and $\overline{Y}$ are the sample mean of observed data X and Y respectively.
However, as number of observations (m) is always large, regression is done using computer software packages such are SPSS, SAS, R and MATLAB; due to the complexity of equations.

C.2 Multiple Linear Regression

To estimate the relationship between a given dependent variable and more than one independent variable Multiple Linear Regression is implemented and the least square method is used to estimate the regression coefficients that best approximate the model.Multiple linear regression equation is defined in Eq. (C.2).

Residual Sum of Squares (SS_{res}), is the difference between observed value (Y_i) and predicted value $(\hat{Y}_i)$, defined as [130, 131]:

$$SS_{res} = \sum_{i=1}^{m} (Y_i - \hat{Y}_i)^2 = \sum_{i=1}^{m} (Y_i - \hat{B}_0 - \hat{B}_1 X_{i1} - ... - \hat{B}_n X_{in})^2 \tag{C.5}$$

where m and n are the number of observations and number of independent variables respectively. Least square estimates of coefficients $(\hat{B}_0, \hat{B}_1, \hat{B}_2, ..., \hat{B}_n)$ are determined by finding the best values which minimizes residual sum of squares. Therefore, the regression model has linear relationship between each of independent variable represented in n-dimensions.

C.3 Multiple Linear Regression assumptions

In order to apply the above technique and obtain linear mathematical modelling of a given output with respect to observed inputs, assumptions discussed here should be met such that the model is fitted accurately [130, 131, 136].

- **Assumption # 1: Size of Sample (m)** Number of observations (m) dependant on the number of independent variables (n). It is recommended that $(m \geqslant 104 + n)$ [131].

- **Assumption # 2: No Singularity and Multicollinearity** Variables that contribute to predicting the output are expected to be completely independent where none depends on the other. Therefore, they are called Independent Variables (IV), non-singular and no correlation exists.

- **Assumption # 3: No Outliers** Observation which gives un-realistic outcome or value that is very high or very low such that it is offset from other observations should be excluded from the analysis unless they are of physical significance.
- **Assumption # 4: Collinearity between DV and IVs** Dependent Variable (DV) should be strongly related with each of Independent Variable (IV) where correlation coefficient is high. This means that each of IV contribute to the predicted outcome.
- **Assumption # 5: Normality and Linearity of Residuals** Sum of squares of residuals $(\mathrm{SS_{res}})$, Eq. (C.5), is expected to be normally distributed around mean value of zero as well as to possess a linear relationship with predicted values.
- **Assumption # 6: Homoscedasticity** Residuals as they are expected to be independent where the variation of residuals around the predicted values is balanced and consistent.

C.4 Squared Correlation Coefficient - R Square

Squared correlation coefficient **R Square** estimates the strength of linear relationship between the Dependent Variable (DV) and Independent Variable (IV) defined as [130, 131]:

$$\mathrm{R\ Sqaure} = \frac{\mathrm{SS_{reg}}}{\mathrm{SS_Y}} \tag{C.6}$$

where Sum of Squares (SS), over number of observations (m), are defined to estimate the variability between observed dependent variable (Y), mean of observed dependent variable $(\overline{\mathrm{Y}})$, and predicted (estimated) value of the dependent variable $(\hat{\mathrm{Y}})$ as defined in [130, 131]:
Total Sum of Squares $(\mathrm{SS_Y})$:

$$\mathrm{SS_Y} = \sum_{i=1}^{\mathrm{m}} (\mathrm{Y}_i - \overline{\mathrm{Y}})^2 \tag{C.7}$$

Regression Sum of Squares $(\mathrm{SS_{reg}})$:

$$\mathrm{SS_{reg}} = \sum_{i=1}^{\mathrm{m}} (\hat{\mathrm{Y}}_i - \overline{\mathrm{Y}})^2 \tag{C.8}$$

Residual Sum of Square $(\mathrm{SS_{res}})$:

$$\mathrm{SS_{res}} = \sum_{i=1}^{\mathrm{m}} (\mathrm{Y}_i - \hat{\mathrm{Y}}_i)^2 \tag{C.9}$$

Therefore, the Sum of Squares are related as follows [130, 131]:

$$\mathrm{SS_Y} = \mathrm{SS_{reg}} + \mathrm{SS_{res}} \tag{C.10}$$

For a perfect linear regression model fit, (**R Square** $= 1$), which means that the sum of squares due to error is negligible ($\mathrm{SS_{res}} = 0$).

C.5 Analysis Of Variance (ANOVA) Table

Table C.1 Multiple Linear Regression ANOVA - Explained

Model	Sum of Squares (SS)	df	Mean Square (MS)	F	p-value
Regression	$\mathrm{SS_{reg}}$	n	$\mathrm{MS_{reg}} = \dfrac{\mathrm{SS_{reg}}}{\mathrm{n}}$	$\dfrac{\mathrm{MS_{reg}}}{\mathrm{MS_{res}}}$	< 0.001
Residual	$\mathrm{SS_{res}}$	$\mathrm{m-n-1}$	$\mathrm{MS_{res}} = \dfrac{\mathrm{SS_{res}}}{\mathrm{m-n-1}}$		
Total	$\mathrm{SS_Y}$	$\mathrm{m-1}$			

Analysis Of Variance (ANOVA) Table presents a summary that examines the quality of fit of the linear regression model , dependent variable (Y), with respect to n independent variables $(\mathrm{X_1, X_2, \ldots, X_n})$, as observed for m occurrences. The output ANOVA table is detailed in Table C.1. The focus in ANOVA table would be on F-Statistic test which is a test of variation between means to test the quality of Sum of Squares (SS) and therefore the regression model. If the linear model is estimated to a good accuracy and all independent variables included are statistically significant, then F would be very large which means that the Mean Square of Residuals $(\mathrm{MS_{res}})$ is minimum and the errors are insignificant.

Moreover, since regression analysis is a statistical method, the main aim is to validate the significance of independent variables included in the model where the null hypothesis is to be neglected. Null hypothesis is where there is a possibility that the regression coefficients in the model could be zero and thus the independent variables are insignificant. This is examined by observing the (**p value**) in the ANOVA table where (**p value** < 0.001) reflects that the probability of occurrence of the null hypothesis is very small and therefore the present analysis is statistically significant.